
Electronic Thesis and Dissertation Repository

12-12-2017 10:00 AM

Proteomic Characterization of Human Multipotent Stromal Cells Secreted Proteins with Therapeutic Potential for β -cell Regeneration

Miljan Kuljanin, *The University of Western Ontario*

Supervisor: Lajoie, Gilles A., *The University of Western Ontario*

Co-Supervisor: Hess, David A., *The University of Western Ontario*

A thesis submitted in partial fulfillment of the requirements for the Doctor of Philosophy degree in Biochemistry

© Miljan Kuljanin 2017

Follow this and additional works at: <https://ir.lib.uwo.ca/etd>



Part of the [Disease Modeling Commons](#), [Medical Biochemistry Commons](#), and the [Medical Cell Biology Commons](#)

Recommended Citation

Kuljanin, Miljan, "Proteomic Characterization of Human Multipotent Stromal Cells Secreted Proteins with Therapeutic Potential for β -cell Regeneration" (2017). *Electronic Thesis and Dissertation Repository*. 5082.

<https://ir.lib.uwo.ca/etd/5082>

This Dissertation/Thesis is brought to you for free and open access by Scholarship@Western. It has been accepted for inclusion in Electronic Thesis and Dissertation Repository by an authorized administrator of Scholarship@Western. For more information, please contact wlsadmin@uwo.ca.

ABSTRACT

Novel strategies to stimulate the expansion of β -cell mass *in situ* are warranted for diabetes therapy. Cell-replacement therapies for the treatment of diabetes have become a focal point in recent years. Endogenous regeneration of β -cell mass has been demonstrated using human multipotent stromal cells (hMSC). However, the secretory factors responsible for initiating endogenous regeneration remain unknown. Successful large-scale proteomic applications to address these questions have been limited in part by difficulties in correctly selecting the appropriate methodologies. Thus the goal of this thesis was a combination of assessing different proteomic workflows to facilitate investigation into hMSC biology, applying these methods to identify important factors secreted by hMSC for β -cell regeneration, as well as functionally investigating candidate proteins and refining current models of hMSC mediated β -cell regeneration.

In working towards these goals, we first assessed the advantages and disadvantages of multiple fractionation techniques to help guide future experimental designs in general proteomic workflows. By applying these methodologies, we probed the secretome of hMSC and identified candidate regulators responsible for regeneration of β -cell mass. In particular, Wnt-signaling we identified as an important contributor for islet regenerative capacity. In addition, we recognized the clinical applicability of determining protein signatures that could be used to screen hMSC that possessed islet regenerative capacity. Therefore, a robust quantitative proteomics method was developed to screen hMSC that could be used in downstream clinical

applications for β -cell regeneration. Taking cues from these proteomic screens, we demonstrate that intrapancreatic-delivery of concentrated hMSC conditioned media (CM) can independently mediate endogenous islet regeneration, without injecting cells. The therapeutic effect was augmented by increasing protein dose and by the activation of Wnt-signaling during CM generation. The mechanisms of islet regeneration were multi-factorial, with evidence of glucagon⁺ cells emerging from the ductal niche within one day of CM injection, followed by α - β -cell conversion with NKX6.1-expression in transitioning β -cells, and augmented β -cell proliferation to generate functionally mature neoislet that respond to glucose. Altogether, these studies provide an extraordinary view of how this dynamic cell type can be used in clinical settings, to stimulate the expansion of β -cell mass and tip the balance in favor of islet regeneration versus destruction during diabetes.

KEY WORDS: human multipotent stromal cells, proteomics, islet regeneration, conditioned media, effectors, mass spectrometry, Wnt-signaling, β -cell mass, quantitative proteomics, SILAC, regenerative medicine, diabetes

CO-AUTHORSHIP STATEMENT

Chapter 2

Kuljanin M*, Dieters-Castator DZ*, Hess DA, Postovit LM, Lajoie GA. (2017) "Comparison of Sample Preparative Techniques for Large-Scale Proteomics". *Proteomics*. 17:1-9.

*MK and *DZDC contributed equally to this manuscript. MK designed and performed experiments, interpreted data, and wrote the manuscript. DZDC also designed and performed experiments, interpreted data and wrote the manuscript. DAH, LMP and GAL helped design experiments, refine concepts and revised the manuscript.

Chapter 3

Kuljanin M, Bell GI, Sherman SE, Lajoie GA, Hess DA. (2017) "Proteomic Characterization Reveals Active Wnt-signaling by Human Multipotent Stromal Cells as a Key Regulator of β -cell Survival and Proliferation ". *Diabetologia*. 10: 1987-1998.

MK designed and performed experiments, interpreted data, and wrote the initial draft of the manuscript. GIB performed *in vivo* transplantation experiments, collected and assembled data, and provided critical revision of the manuscript. SES performed confocal microscopy, collected and assembled data. GAL and DAH helped design experiments, refine concepts and revised the final version of the manuscript.

Chapter 4

Kuljanin M, Bell GI, Hess DA, Lajoie GA. (2017) “Predicting the Therapeutic Potential of Human Multipotent Stromal Cells Conditioned Media using Quantitative Proteomics”. (In preparation)

MK designed and performed experiments, interpreted data, and wrote the initial draft of the manuscript. GIB performed *in vivo* characterization experiments, collected and assembled data, and provided critical revision of the manuscript. DAH and GAL helped design experiments, refine concepts and revised the final version of the manuscript.

Chapter 5

Kuljanin M, Elgamal RM, Bell GI, Lajoie GA, Hess DA. (2017) “Wnt-pathway stimulated MSC-secreted effectors mediate islet regeneration”. Cell Stem Cell. (Submitted, November 2017)

MK designed and performed experiments, interpreted data, and wrote the initial draft of the manuscript. RME performed IHC and confocal microscopy experiments, interpreted data, and provided critical revision of the manuscript. GIB performed *in vivo* characterization experiments, collected and assembled data, and provided critical revision of the manuscript. GAL and DAH helped design experiments, refine concepts and revised the final version of the manuscript.

ACKNOWLEDGEMENT

Foremost, I would like to express my sincere gratitude to my supervisors Dr. Gilles A. Lajoie and Dr. David A. Hess for their continuous support throughout my PhD study and research, for their patience, motivation and enthusiasm. You both have provided me a project that was both challenging and rewarding to say the least. Thank you for always listening, respecting, and guiding me at all times throughout my research and writing of this thesis. My experiences with each of you have been truly memorable and have shaped me into the scientist I am today.

To the members of the Hess lab past and present, I appreciate all of the support and guidance I have received from everyone. Gillian, Dave and Ayesh thank you for teaching me about cell culture, helping me grow and maintain my cultures and always making sure all reagents were ordered. A special thank you to Gillian for performing all my mouse work so I could keep my hands clean. Stephen, Tyler and Ruth thank you for always providing me with answers to questions inside and outside of the lab, and providing experimental guidance.

To the member of the Lajoie lab past and present, thank you for always supporting and guiding me. Dylan and Adam, you have challenged me to think outside the box and have always helped me with anything science/life related. Paula, thank you for always fighting the never ending MS instrument battle and for always stepping in when I needed your help and advice.

TABLE OF CONTENTS

ABSTRACT	i
CO-AUTHORSHIP STATEMENT	iii
ACKNOWLEDGEMENT	v
TABLE OF CONTENTS	vi
LIST OF TABLES	xi
LIST OF FIGURES	xii
LIST OF APPENDICES	xv
LIST OF ABBREVIATIONS, SYMBOLS, AND NOMENCLATURE	xvi
Chapter 1 Introduction	1
1.1 Diabetes Mellitus	1
1.2 Architecture of the pancreas.....	2
1.3 Treatments for diabetes.....	3
1.3.1 Cell-replacement therapies for diabetes	4
1.3.2 Endogenous islet regeneration	6
1.4 Multipotent stromal cells	8
1.4.1 MSC in clinical trials.....	9
1.4.2 Differentiation of MSC into insulin producing cells	10
1.4.3 Endogenous β -cell regeneration using MSC.....	11
1.5 Overview of the Wnt-Signaling Pathway.....	13
1.5.1 Modulation of Wnt-signaling.....	16
1.6 Mass spectrometry-based proteomics.....	18
1.6.1 General MS-based proteomics workflow	19
1.6.2 Fractionation strategies for MS-based proteomics.....	21
1.7 Quantitative MS-based proteomics	22
1.7.1 Targeted Proteomics.....	23
1.8 Scope of thesis.....	25
1.9 References.....	28

Chapter 2	Evaluation of Sample Fractionation Techniques for Large-Scale In-depth Proteomic Analysis	39
2.1	Introduction	39
2.2	Results	41
2.2.1	Proteome coverage of different workflows on a Q Exactive mass spectrometer	41
2.2.2	Comparison of fractionation efficiency	44
2.2.3	Distribution of proteins and peptides	47
2.2.4	Evaluating peptide characteristics	50
2.2.5	Sample preparation time	53
2.3	Discussion	54
2.4	Experimental Methods	55
2.4.1	Cell culture and protein extraction	55
2.4.2	Chloroform/methanol protein precipitation	56
2.4.3	Unfractionated on-pellet in-solution digestion	56
2.4.4	SDS-PAGE followed by in-gel digestion	57
2.4.5	GELFrEE fractionation followed by in-solution digestion	57
2.4.7	High pH reversed phase peptide fractionation	58
2.4.8	LC-MS/MS	59
2.4.9	Data Analysis	59
2.5	References	61
Chapter 3	Proteomic Characterization of Paracrine Signals Secreted by Multipotent Stromal Cells that Augment Blood Glucose	66
3.1	Introduction	66
3.2	Results	68
3.2.1	Regenerative capacity of human MSCs was donor specific	68
3.2.2	MSC ^R exclusively secreted proteins associated with active Wnt signaling	69
3.2.3	Quantification of Wnt, matrix remodeling and pro-angiogenic proteins	76
3.2.4	MSC ^R increased expression of Wnt pathway mRNA	77
3.2.5	MSCs show activation of Wnt signaling via accumulation of nuclear β -catenin	80
3.2.6	GSK3 inhibition in MSC ^{NR} generates CM that improves human β -cell survival in vitro	82

3.3	Discussion	87
3.4	Experimental Methods.....	92
3.4.1	Transplantation of human derived MSCs.....	92
3.4.2	MSC culture and SILAC labeling.....	92
3.4.3	Generation of labeled CM and proteomic workflows.....	92
3.4.4	SDS-PAGE Fractionation and mass spectrometry	93
3.4.5	Proteomic data analysis.....	94
3.4.6	HMVEC tubule forming assay.....	94
3.4.7	qRT-PCR of the Wnt signaling pathway.....	95
3.4.8	Confocal microscopy for total β -catenin.....	95
3.4.9	Flow cytometry for total β -catenin	96
3.4.10	Human islet culture with MSC CM	96
3.4.11	Statistical analysis.....	97
3.5	References.....	98
Chapter 4	Predicting the Therapeutic Potential of Human Multipotent Stromal Cells Using Quantitative Proteomics.....	103
4.1	Introduction.....	103
4.2	Results	108
4.2.1	Angiogenic capacity of hMSC CM.....	108
4.2.2	β -cell regenerative capacity of hMSC CM.....	111
4.2.3	Validation of regenerative signature using targeted proteomics	114
4.2.4	Characterization of unknown hMSC lines using proteomic classifier	117
4.2.5	Biological validation of unknown hMSC lines.....	122
4.3	Discussion	125
4.4	Experimental Methods.....	130
4.4.1	Generation of CM for co-culture and proteomic analysis	130
4.4.2	HMVEC tubule forming assay	130
4.4.3	Human islet culture with hMSC CM	131
4.4.4	Chloroform/Methanol Precipitation and Protein Digestion.....	131
4.4.5	Liquid Chromatography-Tandem Mass Spectrometry (LC-MS/MS)	132
4.4.6	Label-free proteomic data analysis	133

4.4.7	Support vector machine learning	133
4.4.8	Peptide Synthesis	134
4.4.9	Targeted proteomic data analysis	134
4.4.10	Transplantation of hMSC	135
4.4.11	Statistical analysis.....	135
4.5	References	136
Chapter 5 Wnt-Activated hMSC Conditioned Media Mediates Islet Cell Regeneration in vivo		141
5.1	Introduction.....	141
5.2	Results	145
5.2.1	Intrapancreatic hMSC injection induced emergence of single insulin ⁺ cells	145
5.2.2	Intrapancreatic hMSC CM injection reduced hyperglycemia....	150
5.2.3	Active Wnt-signaling generated CM with augmented glucose lowering capacity.....	151
5.2.4	hMSC CM loses glucose lowering capacity after heat denaturing	157
5.2.5	Islet regeneration resulted in increased β -cell mass	160
5.2.6	Regenerated islets showed increased vascularization.....	164
5.2.7	Regenerative CM increased islet association with the ductal epithelium.....	164
5.2.8	Regenerative CM stimulated β -cell proliferation	165
5.2.9	hMSC CM induce α - β -cell conversion and maturation of new β - cells.....	171
5.2.10	Proteomic analyses of WNT+ CM identified pro-islet regenerative proteins	178
5.4	Experimental Methods.....	186
5.4.1	Animal Maintenance and Manipulations	186
5.4.2	Human Subjects.....	187
5.4.3	Generation of hMSC CM for injection and proteomics	188
5.4.4	Glucose Tolerance Test.....	188
5.4.5	Serum insulin and glucagon ELISA.....	189
5.4.5	RNA isolation, qPCR and integrity analysis	189
5.4.6	Immunohistochemistry and Immunofluorescent analysis.....	190
5.4.7	Quantification of islet blood vessel density	190

5.4.8	Quantification of proliferating cells and ductal association.....	191
5.4.9	Quantification of transcription factor expression	191
5.4.10	Quantification of glucagon+ cells with NKX6.1.....	191
5.4.11	Confocal Microscopy.....	192
5.4.12	Chloroform/methanol precipitation and protein digestion	192
5.4.13	Liquid Chromatography-Tandem Mass Spectrometry (LC-... MS/MS).....	193
5.4.14	Label-free proteomic data analysis	194
5.4.15	Human islet culture with hMSC CM and recombinant ligands	194
5.4.16	Cell Counts	195
5.4.17	Statistical analysis.....	195
5.5	References	196
Chapter 6	Discussion	202
6.1	Summary	202
6.2	A new model for hMSC regulated β -cell regeneration	203
6.2.1	Insulin like growth factors (IGFs) and β -cell mass	204
6.2.2	Transforming growth factor β and β -cell mass.....	206
6.2.3	Wnt-signals formulate a regenerative niche.....	207
6.3	α -to- β -cell conversion.....	210
6.4	Clinical Applications.....	211
6.4.1	Directed delivery of hMSC CM.....	212
6.4.2	Autoimmunity after regeneration.....	213
6.5	Future Directions	214
6.6	References	217
Appendix I	222
Appendix II	233
Appendix III	240
Curriculum Vitae	242

LIST OF TABLES

Table 3.1	Exclusively detected proteins in CM from hMSC ^R	74
Table 3.2	Exclusively detected proteins in CM from hMSC ^{NR}	74
Table 4.1	Score metric for regenerative capacity of unknown hMSC lines	120
Table 4.2	Support vector machine scoring metric for regenerative capacity of unknown hMSC lines	121
Table A2.1	Proteomic performance across different fractionation workflows	223
Table A2.2	Acquisition parameters for the Q Exactive.	224
Table A3.1	Acquisition parameters for the Q Exactive	225
Table A4.1	Posterior probabilities generated using SVM.	226
Table A4.2	Proteins and peptides used for targeted proteomics	228
Table A4.3	Acquisition parameters for the Q Exactive Plus	229
Table A5.1	Fold change of proteins during Wnt-modulation	230
Table A5.2	Antibody concentration and manufacture information	232

Electronic Supplemental Material

Table ESM 3.1	Exclusively detected proteins in islet regenerative hMSC ^R	
Table ESM 3.2	Exclusively detected proteins in non-regenerative hMSC ^{NR}	
Table ESM 3.3	Proteins detected in bothh MSC ^R and hMSC ^{NR}	
Table ESM 3.4	Quantitative proteomics for differentially expressed proteins	
Table ESM 5.1	Secreted proteins detected after manipulation of Wnt-signaling	

LIST OF FIGURES

Figure 1.1	The basic elements involved in canonical Wnt-signaling.....	15
Figure 1.2	General proteomics workflow.	20
Figure 2.1	High confidence identification and large overlap between proteomes from different techniques	43
Figure 2.2	Fractionation efficiency varies between proteins and peptide separation techniques.....	45
Figure 2.3	Fractionation efficiency comparison between protein based separation techniques.....	46
Figure 2.4	Peptide and protein distribution profiles deviate for each separation technique.	48
Figure 2.5	Comparison of orthogonality at the peptide level between each fractionation technique.....	49
Figure 2.6	Different fractionation techniques provide complementary sequence coverage.	51
Figure 2.7	All workflows preferentially enrich for hydrophilic peptides.....	52
Figure 3.1	Functional characterization of islet hMSC ^R and hMSC ^{NR}	71
Figure 3.2	Qualitative analyses of proteins exclusively secreted by hMSC ^R or hMSC ^{NR}	72
Figure 3.3	Quantitative analyses of proteins secreted by both hMSC ^R and hMSC ^{NR}	78
Figure 3.4	hMSC treatment with GSK3 inhibitor induced nuclear β -catenin localization.....	81
Figure 3.5	Culture of human islets in GSK-inhibited CM increased β -cell number.	83
Figure 3.6	Culture of human islets in GSK-inhibited CM increased β -cell proliferation.....	86
Figure 4.1	Predictive assay workflow.	112

Figure 4.2	Angiogenic potential of hMSC CM.....	110
Figure 4.3	Predictive protein signatures for β -cell regenerative hMSC.....	113
Figure 4.4	Quantitative validation of regenerative hMSC protein signature.....	116
Figure 4.5	Quantitative proteomic validations of unknown hMSC lines.	124
Figure 4.6	Biological validation of the predictive assay.	129
Figure 5.1	Intrapancreatic delivery of ex vivo expanded MSC cells does not augment the recovery of blood glucose in STZ-treatenNOD/SCID mice	147
Figure 5.2	Intrapancreatic transplanted MSC are present in the pancreas at D42 and give rise to single insulin positive murine cells.	149
Figure 5.3	Intrapancreatic-injection of Wnt-activated hMSC CM improved glucose control.....	154
Figure 5.4	hMSC show robustly stimulation and inhibition of Wnt-signaling by CHIR99201 and IWR-1, respectfully.	156
Figure 5.5	Islet Regenerative CM loses capacity to lower blood glucose levels after heating.....	159
Figure 5.6	Intrapancreatic-injection of Wnt-activated hMSC CM increased islet number, size, and β -cell mass.....	162
Figure 5.7	Intrapancreatic-injection of Wnt-activated hMSC CM increased islet ductal association.....	167
Figure 5.8	Intrapancreatic-injection of Wnt-Activated hMSC CM increased β -cell proliferation.....	169
Figure 5.9	Intrapancreatic-injection of Wnt-activated hMSC CM increased β -cell maturation.	173
Figure 5.10	Intrapancreatic-injection of Wnt-activated hMSC CM increased α - β -cell conversion.....	175
Figure 5.11	Intrapancreatic-injection of Wnt-activated hMSC CM displays α - β -cell transition.	175
Figure 5.12	Proteomic analyses of WNT+ CM identified pro-islet regenerative proteins.	180
Figure 6.1	New model for hMSC induced β -cell regeneration.	209

Figure A3.1	Condition media generated by hMSC ^R augments spontaneous HMVEC tube formation after 24 hrs in vitro	234
Figure A3.2	Total β -catenin levels in hMSC treated with CHIR99201 quantified using flow cytometry.....	235
Figure A3.3	Culture conditions for human pancreatic islets using condition media generated by hMSC ^{NR} samples.	236
Figure A3.4	Flow cytometry analysis of human pancreatic islets for β -cell content and survival.....	237
Figure A5.1	hMSC conditioned media transplanted increased islet vascularization	238
Figure A5.2	Intrapancreatic-injection of Wnt-activated hMSC CM shown no difference in endocrine marker NKX2.2	239

LIST OF APPENDICES

Appendix I	Supporting datasets for proteomic characterization of conditioned media generated from human multipotent stromal cells (hMSC).....	222
Appendix II	Supporting figures for proteomic characterization of conditioned media generated from human multipotent stromal cells (hMSC).....	233
Appendix III	Copyright Permission.....	240

LIST OF ABBREVIATIONS, SYMBOLS, AND NOMENCLATURE

7AAD	7-aminoactinomycin D
ABC	Ammonium bicarbonate
ACN	Acetonitrile
ADAMTS	A disintegrin and metalloproteinase with thrombospondin motifs
ANG	Angiogenin
ANGPT	Angiopoietin
ANOVA	Analysis of variance
APC	Adenomatous polyposis coli
AUC	Area under the curve
BCA	Bicinchoninic acid assay
BM	Bone marrow
BMI	Body mass index
BMP	Bone morphogenetic protein
bRP	Basic reverse phase
CAB	Citric acid buffer
CD	Cluster of differentiation
CK1	Casein kinase 1
CK19	Cytokeratin 19
CM	Conditioned media
CTGF	Connective tissue growth factor
CV	Coefficient of variance

CXCL	Chemokine ligand
DAB	Diaminobenzidine
DIVAA	Directed <i>in vivo</i> angiogenesis assay
DKK1	Dickkopf 1
DMEM	Dulbecco's Modified Eagle Medium
DMSO	Dimethyl sulfoxide
DTT	Dithiothreitol
dWNT+	Denatured Wnt activated conditioned media
EBM	Endothelial basal medium
ECM	Extracellular matrix
EdU	5-ethynyl-2'-deoxyuridine
EGF	Endothelial growth factor
EGM	Endothelial growth medium
ELISA	Enzyme linked immunosorbent assay
EMT	Epithelial to mesenchymal transition
ES	Embryonic Stem Cells
FA	Formic acid
FDR	False discovery rate
FGF	Fibroblast growth factor
FITC	Fluorescein isothiocyanate
FLT4	Endothelial growth factor receptor 4
Flz3	FluoZin-3
GABA	Gamma-aminobutyric acid

GDF	Growth differentiated factor 15
GELFrEE	Gel elution liquid fraction entrapment
GLUT	Glucose transporter
GOCC	Gene ontology cellular component
GSEA	Gene set enrichment analysis
GSK3	Glycogen synthase kinase
HLA	Human leukocyte antigen
hMSC	Human multipotent stromal cells
HMVEC	Human microvascular endothelial cells
HpH	High reverse phase chromatography
HPLC	High-performance liquid chromatography
I.P.	Intraperitoneal
IAA	Iodoacetamide
iCAT	Isotope-coded affinity tags
IDF	International Diabetes Federation
IEF	Isoelectric focusing
IFCB	International Federation for Cell Biology
IIDP	Integrated Islet Distribution Program
iPan	Intrapancreatically
iPSC	Induced pluripotent stem cells
iTRAQ	Isobaric tags for relative and absolute quantification
IV	Intravenous
kDA	Kilodaltons

KDR	Vascular endothelial growth factor
KITLG	Mast cell growth factor
LC	Liquid chromatography
LFQ	Label free quantification
LiCl	Lithium chloride
MMP	Matrix metalloproteinase
MRM	Multiple reactions monitoring
MS	Mass spectrometry
MSC	Multipotent stromal cells
MSC ^{NR}	Non-regenerative multipotent stromal cells
MSC ^R	Regenerative multipotent stromal cells
MSMS	Tandem mass spectrometry
MudPIT	Multidimensional protein identification technology
MW	Molecular weight
NEFA	Non-essential fatty acids
NKX2.2	Homeobox protein Nkx2.2
NKX6.1	Homeobox protein Nkx6.1
NOD/SCID	Non-obese diabetic/ severe combined immunodeficiency
NPTX1	Neuronal pentraxin 1
PBS	Phosphate buffered saline
PDGFR	Platelet derived growth factor receptor
PDX1	Pancreatic duodenal homeobox protein 1
PE	Phycoerythrin

PF4V1	Platelet factor 4 variant
PRM	Parallel reaction monitoring
PSM	Peptide-spectrum match
PTM	Post-translational modifications
RPMI	Roswell Park Memorial Institute
SAX	Strong anion exchange
SCX	Strong cation exchange
SDS-PAGE	Sodium-dodecyl sulfate poly-acrylamide gel electrophoresis
SEC	Size exclusion chromatography
SEM	Standard error of the mean
SFRP1	Secreted frizzled-related protein 1
SILAC	Stable isotopic labelling in cell culture by amino acids
Spondins	Secreted potentiators of Wnt signaling
SRM	Selected reaction monitoring
STZ	Streptozotocin
SVM	Support vector machine
T1D	Type 1 diabetes
T2D	Type 2 diabetes
TFA	Trifluoroacetic acid
THBS	Thrombospondin
TIMP	Metalloproteinase inhibitor
TMT	Tandem mass tags

UPLC	Ultra performance liquid chromatography
VEGF	Vascular endothelial growth factor
vWF	von Willebrand factor
WIF-1	Wnt-inhibitory factor 1
WISP2/CCN5	Wnt-inducible signalling pathway protein 2
WNT-	Wnt inhibited
WNT+	Wnt activated

Ala	(A)	Alanine
Arg	(R)	Arginine
Asn	(N)	Asparagine
Asp	(D)	Aspartic acid
Cys	(C)	Cysteine
Gln	(Q)	Glutamine
Glu	(E)	Glutamic acid
Gly	(G)	Glycine
His	(H)	Histidine
Ile	(I)	Isoleucine
Leu	(L)	Leucine
Lys	(K)	Lysine
Met	(M)	Methionine
Phe	(F)	Phenylalanine
Pro	(P)	Proline

Ser	(S)	Serine
Thr	(T)	Threonine
Trp	(W)	Tryptophan
Tyr	(Y)	Tyrosine
Val	(V)	Valine

Chapter 1

Introduction

1.1 Diabetes Mellitus

Diabetes mellitus encompasses a group of metabolic diseases characterized by high blood glucose [1], caused by the inability of the pancreas to produce enough insulin, or by the body to respond effectively to the insulin produced [2]. Diabetes can be further sub-classified into two main types: (1) type one diabetes (T1D), also known as juvenile diabetes, which results from autoimmune destruction of insulin producing β -cells within the islets of Langerhans, and (2) type two diabetes (T2D), also known as adult-onset diabetes, is characterized by insulin resistance in peripheral tissues, often leading to improper insulin production by β -cells [3]. T2D is the most prevalent form of diabetes and accounts for approximately 90% of all diabetes cases worldwide. The World Health Organization estimates that more than 300 million people have been diagnosed with diabetes, and this number is projected to increase to 550 million by 2030 [4]. The International Diabetes Federation (IDF) has reported that annual health care spending to treat diabetes was upwards of 650 billion dollars in 2015, and that diabetes results in 5 million deaths per year, making diabetes a worldwide epidemic [5]. Currently there is no accepted cure for diabetes. However, there are various treatments and strategies that can help manage living with diabetes. In T2D, management mostly focuses on controlling circulating blood glucose levels by adapting diets to less carbohydrate rich foods, as well as increasing energy

expenditure through daily exercise. However, in cases where insulin resistance is high, or insulin secretion is exhausted, exogenous administration of insulin is ultimately required [6]. T1D is a multi-factorial disease with contributions from genetics and environmental stimuli, and unlike T2D is not caused by poor management of diet and exercise. T1D occurs through auto immune destruction of β -cells mediated by T-helper and cytotoxic T-lymphocytes and auto-antibodies generated towards epitomes present specifically on β -cells [7,8]. Patients diagnosed with T1D must also alter their diets, and exogenous administration of insulin is mandatory. The amount of insulin and the timing of insulin injections, in both types of diabetes, are determined by residual islet function, age, lifestyle, meal plans and general health of the patient [9].

1.2 Architecture of the pancreas

The pancreas is an important glandular organ that is located in the abdominal cavity behind the stomach which participates in the digestive and endocrine systems in vertebrates [10]. The majority of the pancreas is comprised of exocrine cells (98%), which secrete products through ducts; the remaining 2% is composed of endocrine cells, which secrete endocrine hormones directly into the blood stream [11]. The primary role of the endocrine pancreas is regulation of blood glucose levels. Highly organized structures called islets of Langerhans are present in the pancreas. Within these islets exists at least five main cell types that are involved in the regulation of blood glucose levels through the secretion of various hormones. These five main types are as follows: (1) α -cells, which are responsible for increasing blood glucose levels through the secretion of glucagon, (2) β -cells,

which are responsible for decreasing blood glucose through the secretion of insulin, (3) delta-cells, which regulate both α and β -cell function through the secretion of somatostatin, (4) gamma-cells, which regulates both pancreatic secretion activities as well as hepatic glycogen levels through the secretion of pancreatic polypeptide, and (5) epsilon-cells, which secrete ghrelin, one of the main hormone involved in hunger stimuli [12]. Insulin is a protein hormone that is secreted as a prohormone, and contains a cleavable connecting peptide, called C-peptide. Therefore, the functional form of insulin and C-peptide are found in equimolar amounts during insulin secretion, and the amount of C-peptide secreted into the serum has showed great clinical utility in assessing residual insulin secretion in patients with diabetes [13]. Glucose homeostasis is tightly controlled by the secretion of insulin and the function of glucose transporters. Adipose and muscles cells are largely responsible for the uptake of glucose from the blood stream via the highly specialized glucose receptor (GLUT4). When insulin binds its receptor, a downstream phosphorylation cascade occurs, signaling the synthesis and recruitment of GLUT4 to the cell surface for glucose uptake. In contrast, β -cells function primarily through a bidirectional glucose transporter (GLUT2). GLUT2 is a free flowing glucose receptor and is required so that β -cells can accurately gauge serum glucose levels and secrete insulin accordingly [14]. These two highly conserved signaling events occur in unison to help achieve glucose homeostasis in vertebrates.

1.3 Treatments for diabetes

Islet replacement therapy via the Edmonton Protocol has provided proof-of-concept that islet transplantation can temporarily reduce insulin

dependence in severe T1D patients [15]. Briefly, cadaveric pancreata are harvested and the islets are isolated using a mixture of enzymes called Liberase. Islets are then infused into the patient via the hepatic portal vein, and secrete insulin after engraftment in the liver [16]. Although this is an attractive strategy to combat diabetes, there are two main drawbacks preventing the widespread use of this therapy: (1) a critical shortage of cadaveric donor islet cells, and (2) eventual rejection of the implanted cells by the body's immune system [16]. Patients treated with transplanted islet cells are administered immunosuppressive drugs to prevent allogenic islet rejections, but these drugs are known to have serious side effects and the use of exogenous insulin is ultimately required in most recipients after one year post transplantation [17]. Safer ways to control rejection and autoimmunity as well as the development of a renewable source of β -cells needs to be achieved before islet replacement therapies can become a widespread cure.

1.3.1 Cell-replacement therapies for diabetes

Cell-replacement therapies for the treatment of diabetes have become a focal point for researchers in recent years. Many different potential sources of cells exist, such as pluripotent human embryonic stem cells or adult stem cells, all of which focus on generating enormous quantities of transplantable β -cells [12]. Embryonic stem (ES) cells are pluripotent meaning they can undergo differentiation into the three main germ layers: ectoderm, endoderm and mesoderm, and therefore human ES cells can potentially differentiate into insulin secreting beta-like cells [18]. Mouse ES cells have been successfully induced to differentiate into insulin-producing cells that self-assemble to form three-dimensional pancreatic islets. Although at a low frequency, these beta-

like cells can secrete insulin in response to glucose [19]. Subsequently, a similar approach was taken using human ES cells that produced insulin secreting beta-like cells at a much higher frequency [20]. The efficiency of differentiating human ES cells into β -cells has been met with many challenges. One of the main drawbacks with this approach is that direct differentiation into β -cells cannot be achieved, instead long, strict multistage differentiation regimes are needed [21]. As a result, generated cells often resemble immature β -cells, and fail to perform insulin secretion *in vitro*. In addition, human ES cell-derived beta-like cells often do not express appropriate β -cell-specific markers or transcription factors, and are often found to be poly-hormonal, ultimately leading to delayed or limited insulin secretion when transplanted *in vivo* [22,23]. As proof-of-concept, in 2014 the approval for phase I/II clinical trials involving differentiated human ES cells was conducted. ViaCyte Inc. used a device that provided immunoprotection from the recipient's immune system, that also contained pores big enough for the insulin to be released [24]. Although this trial is still ongoing, many challenges have surfaced: rejection of human ES cells, inefficient maturation of insulin producing β -cells and lack of vascularization within the device to allow for adequate insulin transport to periphery [25].

An alternative approach to generate β -cells is the use of induced pluripotent stem cells (iPSCs), which have the potential to be an unlimited source of human insulin secreting cells that can be generated efficiently using allogenic and autologous sources [26]. Induced pluripotent stem cells were first introduced in 2006 from mouse somatic cells by using a mixture of four transcription factors, now termed the "Yamanaka factors", to generate cells

with gene expression profiles and development potential similar to ES cells [27]. In addition, iPSCs have also been generated using approaches involving small molecules [28]. Since then, many groups have demonstrated the vast potential of iPSCs to generate human disease-in-a-dish models and the development of patient specific transplantable cell sources for regenerative medicine [29]. The direct differentiation of multiple human iPSCs, using small molecules, has been shown to produce insulin secreting cells that co-express transcription factors of mature β -cells, and have been successfully used in mouse models to revert hyperglycemia [23,30]. Lastly, modulation of several key signaling pathways and the use of three-dimensional culture system has generated glucose responsive, mono-hormonal insulin-producing cells that mimic the function of human islets both *in vitro* and *in vivo* [22]. Although these techniques generate a large number of transplantable cells, they do so with the risk of tumorigenicity. Since the starting population of cells is pluripotent, benign growths, or teratomas, are possible due to undifferentiated cells that are still present after differentiated cultures [31]. All the aforementioned strategies rely on the generation of cells that can secrete insulin and do not harness the innate endogenous regenerative potential of the pancreas.

1.3.2 *Endogenous islet regeneration*

β -cell mass under normal healthy conditions has been shown to be very dynamic throughout the life span of several mammalian species [32]. For example, β -cell are capable of undergoing self replication during obesity and pregnancy [33]. Therefore, the potential for endogenous restoration of islet function is theoretically possible. Two mechanisms for β -cell expansion

have been proposed: (1) pre-existing β -cells undergo proliferation to generate more β -cell mass [34,35], and (2) β -cell regeneration is initiated at the ductal epithelium through islet neogenesis [36–38]. During pancreatic development, ductal cells show great plasticity and can give rise to both endocrine and exocrine cells types [39]. After 10 weeks of gestation, a large increase in cell proliferation and differentiation occurs, accompanied by the budding/shedding of the terminal duct cells that give rise to pancreatic islets [40]. After pancreatic damage, either surgical or chemical, the emergence of small islet clusters that line the ductal epithelium has argued that this is indirect evidence for islet neogenesis in the adult organism [41]. Alternatively, a large body of literature suggests that multipotent differentiation can occur from progenitor cells that give rise to new islet clusters [42–44]. Multi-lineage differentiation has been observed from endocrine progenitors that share common regulatory factors such as pancreatic duodenal homeobox protein 1 (PDX1) and homeobox protein Nkx2.2 (NKX2.2), both of which are present in every cell that forms the islet [45]. Therefore, it has been proposed that α - β -cell trans-differentiation may be responsible for regeneration of β -cell mass after STZ-mediated β -cell ablation [46]. Although, many possible avenues exist, the factors responsible for initiating regeneration have not yet been determined. It is unlikely that a single effectors could be responsible for endogenous pancreas regeneration, but instead, the mechanisms mentioned above may act synergistically to increase β -cell mass and alleviate hyperglycemia.

The most compelling evidence of endogenous pancreas regeneration was presented during the Joslin Medalist Study. This study involved the evaluation of pancreatic β -cell function in a large number of insulin-dependent

patients that have had the disease for more than 50 years [47]. Random serum C-peptide levels were monitored and showed that 67.4% of all participants had minimal or sustained ranges. Moreover, post-mortem examination of pancreata from multiple Medalists showed that islets contained proliferating β -cells as well as β -cells undergoing apoptosis, suggesting residual β -cell mass experienced steady-state turnover in the face of ongoing autoimmune destruction [47].

1.4 Multipotent stromal cells

Multipotent stromal cells (MSC), also referred to as mesenchymal stromal cells or mesenchymal stem cells, were first identified by A. J. Friedenstein in 1976 [48,49]. These cell types were initially identified by their ability to adhere to tissue culture plastic, and differentiate into several mesodermal tissue types [50]. Multipotent stromal cells are adult stem cells and are multipotent, meaning they can differentiate into restricted lineages such as adipocytes, osteoblasts and chondrocytes [51–53]. Although, there is no single cell surface epitope that can selectively identify MSC, the International Society for Cellular Therapy has provided criteria that all cells must meet to be considered MSC [54]. To be classified as MSC, cells must express CD105, CD73 and CD90 and must lack the expression of hematopoietic markers CD45, CD34, CD14 and CD19 [52]. In addition to being routinely generated from bone marrow, MSC can also be expanded from adipose tissue, cord blood, placenta, amniotic fluid, as well as feta blood, liver, kidney, lung and spleen tissue (reviewed in [55]). MSC are considered good candidates for cellular therapies for several reasons: (1) they are easily obtained and isolated from bone marrow aspirates from either autologous or

allogenic donors, (2) can be efficiently expanded under normal culture conditions, (3) they are multipotent and non-tumorigenic [56] , (4) they are part of the body's natural repair mechanisms and have been shown to home to sites of injury, and lastly (5) secrete a plethora of trophic factors that mediate cell differentiation, migrations and survival [57]. Therefore, MSC have become one of the most predominant cell types used in clinical trials worldwide.

1.4.1 MSC in clinical trials

Clinical grade manufacturing of MSC is a routine and simple procedure that can be performed in normal tissue culture flasks or expanded for large-scale applications using bioreactors [58]. MSC have been used in clinical trials for approximately 15 years now to treat a variety of diseases, mainly involved in tissue injury or immune disorders [59]. MSC have been clinically used in diseases that include, osteogenesis imperfect, cartilage defects, hematopoietic stem cell transplants, graft-versus-host disease, multiple sclerosis, Crohns disease as well as diabetes (reviewed in [60]). In 2014, the International Federation for Cell Biology (IFCB) identified 313 clinical trials that involved MSC, majority of which were in phase I/II (41.7%), with only a small percentage in phase III (4.2%). A more recent investigation using data from the United States of America based registry (ClinicalTrials.gov) returned 493 clinical studies that involved the use of MSC. Geographical assessment of MSC clinical trials show that China, Europe and the United States of America account for approximately 73% of all trials worldwide (www.BioInformant.com). As mentioned previously, MSC have the ability to home to sites of injury and secrete a wide variety of bio-active factors that

influence the surrounding microenvironment. Although it is widely accepted that the regenerative and therapeutic effect elicited by MSC is largely due to secreted factors, the breadth of factors involved in initiating regeneration have not been fully elucidated.

1.4.2 Differentiation of MSC into insulin producing cells

Like embryonic stem (ES) cells and inducible pluripotent stem cell (iPSCs), it has been reported that MSC can be differentiated into insulin producing cells, after endocrine specific transcription factor over expression [61]. Under physiological conditions, MSC are restricted to the production of cells of the mesoderm (bone, cartilage, fat, muscle), and the insulin producing cells derived from MSC do not respond correctly to increased glucose levels, and do not show increases in C-peptide levels [62]. Furthermore, differentiation of MSC isolated from rats into insulin producing cells has been demonstrated using protein mixtures obtained from pancreatic extracts. Rat MSC were bathed in media that was supplemented with pancreatic extract and after one week of culture, MSC spontaneously assembled into islet-like structures [63]. In addition, the use of more defined culture media, spontaneous differentiation of MSC into insulin contained cells was also demonstrated, although at a very low frequency (1/200 cell) [64]. Lastly, MSC harvested from rats were trans-differentiated into insulin secreting cells that eventually aggregated to form islet-like clusters using complete media supplemented with high glucose. Interestingly, these clusters showed pancreatic gene expression profiles that were similar to mature β -cells and possessed the ability to revert hyperglycemia in hyperglycemic mouse models [65]. Although a promising avenue for the treatment of diabetes, the frequency

at which MSC differentiate into insulin producing cell is very low, and does not meet the requirements needed for human therapies.

1.4.3 Endogenous β -cell regeneration using MSC

Since MSC have been shown to have immunomodulatory and tissue microenvironment modifying properties, direct infusion of MSC has been reported to promote the survival and regeneration of endogenous β -cells [66,67]. In fact, using a mouse model of chemically induced pancreatic damage that caused hyperglycemia, direct intravenous (IV) transplantation of bone marrow-derived murine cells containing MSC initiated endogenous pancreatic regeneration [68]. More importantly, it has been shown that human MSC (hMSC) derived from adult bone marrow can potentially initiate endogenous pancreatic regeneration. Briefly, hMSC were intravenously transplanted into chemically-induced hyperglycemic mice and were able to recover glucose control within 7 days of treatment. Serum insulin levels increased in mice reverting hypoinsulinemia. It is also important to note that transplanted hMSC did not differentiate into β -cells *in vivo*, but activated the regeneration of recipient islets in the murine pancreas [69]. Interestingly, transplantation of regenerative MSC samples increased the number of small islets that were associated with the ductal regions. Collectively, these data suggested that hMSC stimulate a putative islet neogenic mechanism [70]. However, of the different donor-derived hMSC lines transplanted, only approximately 25% could revert hyperglycemia after transplantation, suggesting regenerative capacity was cell line and donor specific [70]. It was hypothesized that hMSC with regenerative capacity secrete unique islet neogenic proteins into the microenvironment that form a niche permitting

endogenous islet formation. Lastly, the use of autologous hMSC has been evaluated in a clinical setting with newly diagnosed T1D patients. Twenty adult patients 10 of which received only insulin treatment, and 10 which received hMSC treatment, were assessed for C-peptide levels for up to one year [71]. Patients that received hMSC treatment showed stable or elevated C-peptide levels compared to insulin only treated patients, showing that hMSC treatment had no adverse affects and could effectively delay the severity of disease progression [71].

Preliminary global mRNA microarray analyses revealed Wnt-signaling to be elevated at the transcript level in regenerative MSC [70]. As part of this study, detailed proteomic analysis of secretory factors deposited into the regenerative niche by hMSC was performed to confirm these findings. However, activation of Wnt-signaling has been shown to increase the proliferation rate of adult human β -cells and more than double the β -cell mass in rodent models [72,73]. The use of protein factors or media conditioned by hMSC to treat diabetes has recently gained traction in pre-clinical studies. Multiple intravenous injection of conditioned media (CM) in T2D rats effectively reduced systemic blood glucose levels, through the induction of proliferation of residual β -cells [74]. In addition, Gao *et. al.* demonstrated the CM could initiate recovery of T1D mice through the activation of the pAKT survival pathway in β -cells, and successfully showed that harvested islets bathed in CM can undergo β -cell proliferation *in vitro* [75]. Both the above mentioned studies used IV injections their mode of delivery and did not investigate whether more directed delivery to the site of injury would increase the islet regenerative effect of the CM. Other modes of delivery have been

investigated. Intraperitoneal injection of periostin, a protein secreted at high levels in hMSC, resulted in an increased number of islets and improvement of long-term glucose homeostasis *in vivo*, which was also shown to have potent islet regenerative effects via delivery through the common bile duct [76]. These findings suggested for the first time that activation of endogenous regenerative mechanisms could be achieved via protein-based therapies based on secreted effectors derived from hMSC.

1.5 Overview of the Wnt-Signaling Pathway

Wnt-signaling is an evolutionarily conserved pathway that regulates aspects of cell migration, cell fate determination, proliferation, cell polarity, neural patterning, organogenesis as well as stem cell differentiation and self renewal [77]. Extracellular Wnt-ligands are responsible for stimulating several intra-cellular signal transduction cascades that include both canonical Wnt-signaling, dependent on β -catenin signaling, and non-canonical Wnt-signaling, which is independent of β -catenin signaling [78]. The canonical Wnt-signaling pathways can be broken down into three major components (Figure 1.1): (1) extracellular region that contains Wnt ligands which are secreted glycoproteins that bind the cysteine-rich domain of the corresponding receptor called Frizzled and co-receptor LRP5/6 [79], (2) intracellular region where signal transduction is regulated by a protein complex that is referred to as the “destruction complex” [80], and lastly (3) the nuclear region, where dynamic nuclear shuttling of β -catenin and eventual transcription of downstream products of Wnt-signaling occur [81]. In an inactive cell (Figure 1.1a); most of the endogenous β -catenin that is presented is found interacting with E-cadherin. Excess β -catenin that is produced is rapidly turned over by the

destruction complex. The destruction complex consists of multiple subunits that include the scaffolding protein Axin, adenomatous polyposis coli (APC) protein, disheveled, and serine threonine kinases glycogen synthase kinase (GSK3) and casein kinase 1 (CK1) [80]. Degradation of β -catenin occurs in two steps. The first involves two phosphorylation events by CK1 and GSK3. CK1 phosphorylation on serine 45 occurs first, which is a primer for the main phosphorylation even by GSK3 at threonine 41 and serine 37 and 33 [82]. The second involves recruitment of an E3-ubiquitin ligase which poly-ubiquitinates β -catenin, marking it for degradation by the proteasome, rendering Wnt-signaling inactive. In the active state (Figure 1.1b), Wnt ligands bind the frizzled receptor, which recruits the cytoplasmic effector disheveled to the receptor. Disheveled is responsible for interacting with Axin and recruitment of the destruction complex to the frizzled receptor [83]. Once in close proximity, phosphorylation mediated by CK1 and GSK3 occurs on LRP5/6, binding it to Axin. In this state, the destruction complex cannot interact with excess β -catenin; therefore no phosphorylation and no degradation can occur [84].

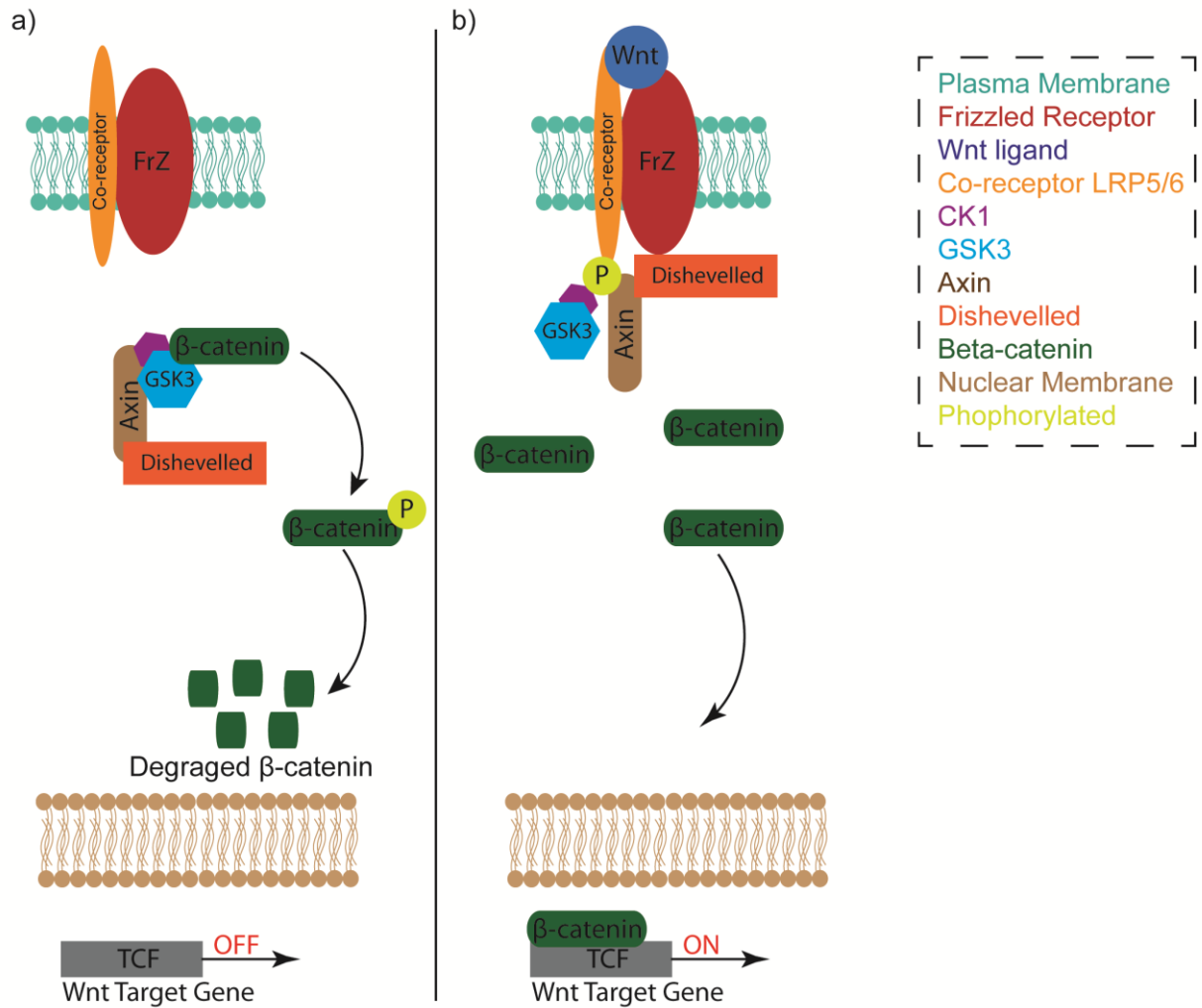


Figure 1.1 The basic elements involved in canonical Wnt-signaling. In its simplest form, Wnt-signaling can be broken down into two states. (a) With no presence of Wnt ligands, free β -catenin is bound to the destruction complex. The destruction complex is comprised of Axin, Dishevelled, CK1 and GSK3 subunits. Once bound to the destruction complex, phosphorylation of β -catenin occurs, marking it for degradation by the proteasome. (b) In the active state, Wnt ligands bind to their corresponding receptor called frizzled and its co-receptor LRP5/6. Recruitment of dishevelled to the receptor occurs placing Axin in close proximity to LRP5/6. Phosphorylation of Axin binds it to the LRP, preventing beta catenin degradation and allowing accumulation on free β -catenin. Beta catenin can then translocate across the nuclear membrane and turn on transcription of downstream Wnt target genes.

1.5.1 *Modulation of Wnt-signaling*

Modulation of Wnt-signaling can occur using a variety of Wnt ligand as well as a plethora of small molecules. One feature common to all cells that are activated by Wnt-signaling is increases in the intracellular levels of β -catenin. One of the most common ways of activating Wnt using ligands is by over expression of WNT3A or WNT1. Over expression of these ligands have been demonstrated in gliomas and glioma stem cells that rapidly increased tumor progression [85]. Interestingly, activation of Wnt signaling by WNT3A or by WNT5A has also been demonstrated by bathing cultured cells in conditioned medium generated from enteroendocrine L-cells. Human hematopoietic stem cells were exposed to conditioned media that contained WNT3A and over 7 days the frequency of proliferating cells increased drastically [86]. A common problem with activating cells with Wnt ligands is that there are 19 known mammalian Wnt ligands that are cross-reactive with 10 frizzled receptors, making it very difficult to correctly choose a single ligand that will activate your cell type [87]. Furthermore, Wnt ligands undergo heavy post-translational modification, making them difficult to produce using bacterial expression systems. Palmitoylation, the attachment of fatty acids such as palmitic acid to cysteine residue, is essential for the secretion of Wnt ligands, making them extremely hydrophobic and difficult to purify [88]. Ultimately, whether or not cells will respond to Wnt signals largely depends on if they have the appropriate receptors present on their surfaces. Since full receptor profiling is very time consuming and not routinely performed, many have turned to alternative methods, such as small molecules, in an attempt to recapitulate active Wnt-signaling. The most common way of activating Wnt-signaling is by

modulation of the subunits that make up the destruction complex. The use of lithium chloride (LiCl) has been known to activate Wnt-signaling for over two decades. Lithium chloride exerts its effect on Wnt-signaling by inhibiting the activity of the enzyme GSK3, which as mentioned before, phosphorylates β -catenin leading to degradation by the proteasome [89]. Since then, over 30 different inhibitors of GSK3 that have IC_{50} values in the nanomolar ranges have been described, (reviewed in [90]). Of these small molecules, CHIR99201 has been widely used to activate Wnt-signaling in cells, and of particular interest, stem cells [91].

Upregulated Wnt-signaling is often found in cancers [92]. Therefore, inhibition of Wnt-signaling is seen as a therapy to arrest the growth or proliferation of tumors. Inhibition of Wnt-signaling can also be achieved through antagonistic ligands. A potent inhibitor of Wnt-signaling is a small ligand called dickkopf-1 (DKK1) that has been shown to bind to the co-receptor of frizzled, LRP5/6, and leads to removal of this complex via endocytosis [93]. Wnt-inhibitory factor 1 (WIF-1) also inhibits Wnt-signaling although through a different mechanism. WIF-1 contains a lipid binding pocket that can interact with the palmitoyl moiety that is commonly found on Wnt ligand, decreasing their availability and binding to frizzled receptors [94]. Alternatively, inhibition of Wnt-signaling can also be achieved using small molecules. Through screening of a diverse synthetic chemical library, two new classes of small molecules that disrupt Wnt-signaling have been identified. The first class of molecules called IWP, inhibit Wnt-signaling by targeting the acyltransferase Porcupine, which is responsible for Wnt ligand Palmitoylation. The second class of molecules called IWR, inhibit Wnt-signaling by

abrogating Axin protein turnover, which is responsible for assembly of the destruction complex [95,96]. As described in chapters 3 and 5 of this thesis, modulation of Wnt-signaling can be recapitulated *in vitro* effectively using various small molecules or ligands.

1.6 Mass spectrometry-based proteomics

Proteomic analysis of biological samples generally deals with identification of genes and cellular mRNA products at the protein level [97]. Largely, proteomic analyses are performed using three techniques: (1) Western blotting, which involves the use of specific antibodies to detect a single or few proteins of interest, (2) protein arrays, which include enzyme-linked immunosorbent assays (ELISA), which can identify many proteins of interests using specific antibodies, and finally (3) mass spectrometry (MS)-based proteomics, which measures thousands of proteins directly using mass derived from their peptides and fragments. What limits the first two techniques mentioned is that the direct measurement of the proteins of interest does not occur and throughput is often low. Instead measurement of a secondary signal, often the production of a light signal (fluorescence, chemiluminescence) occurs. Not subject to these limitations, mass spectrometry-based proteomics has become one of the most powerful tools for identifying the presence and quantitative abundance of expressed proteins, providing unprecedented insight into the molecular language of cellular biology [98,99].

1.6.1 General MS-based proteomics workflow

Modern day analysis of complete proteomes has been facilitated by combining many analytical techniques. MS based proteomic analysis can be broken down into four general steps (Figure 1.2). The first involves enzymatic digestion of proteins into peptides using a site-specific protease which is termed “bottom-up” proteomics [100]. Trypsin, the gold standard for proteolysis of biological samples, generates multiply charged (≥ 2 charge state) peptides ~14 amino acids long making it highly suitable for bottom-up mass spectrometry applications [101]. The complexity of the sample determines how much useful information can be obtained from a single MS experiment. Depending on the desired depth of analysis, the second step often involves some form of pre-fractionation. Generally, fractionation techniques can be broken down into two main categories, fractionation at the protein level or at the peptide level. The third step involves separation of the complex peptide mixture via liquid chromatography (LC) coupled to a mass spectrometer. Liquid chromatography (most often reverse phase) is used to provide an additional depth of separation based on hydrophobic character of the peptides. This step also includes data acquisition using peptide fragment information generated by tandem mass spectrometry (MSMS). The last step in the proteomics pipeline is interpretation of data using fragmentation information generated by sequencing/matching of MSMS spectra [102]. Each peptide spectrum is matched to known databases or *in silico* digests of a sequenced database and statistical cut-offs are applied to ensure proper and accurate identification of their corresponding proteins [103].

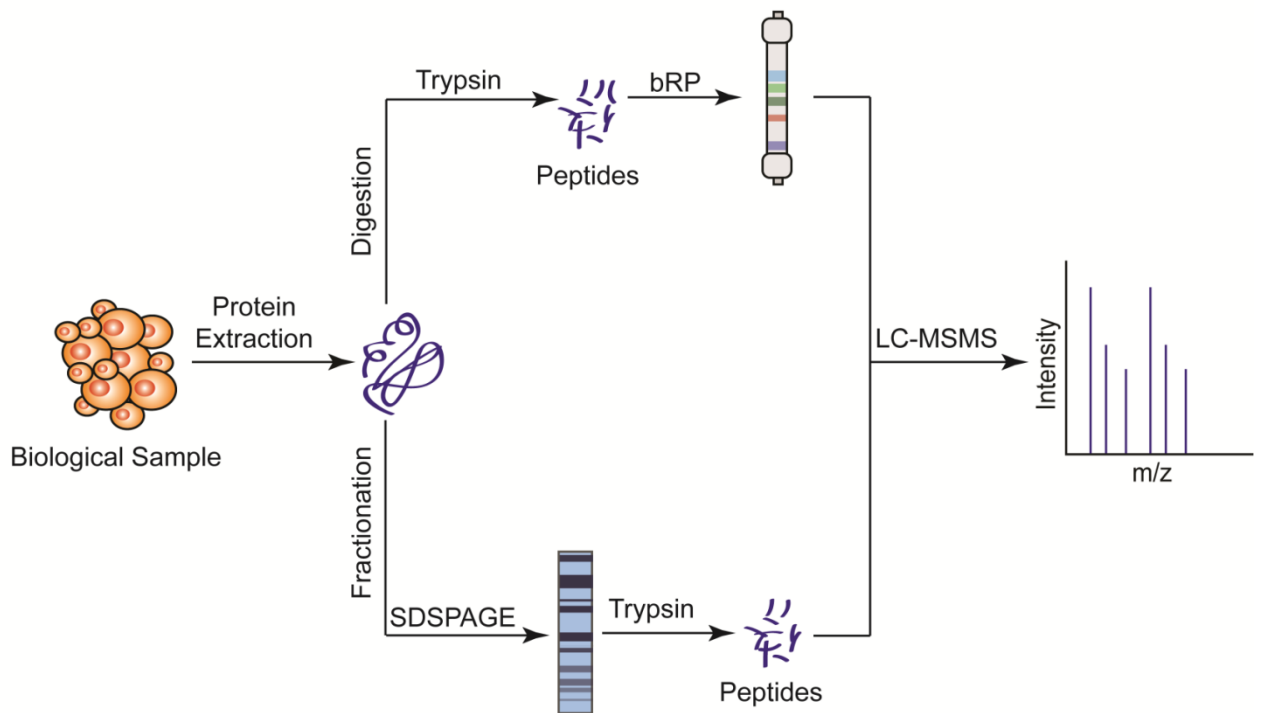


Figure 1.2 General proteomics workflow. For general protein identification in MS-based proteomics biological samples can be analyzed in two different ways. The first step involves extraction of the proteins from the biological sample. Next, the proteins can be fractionated, for example with SDS-PAGE. Protein bands are excised out of the gel and digested into peptide using trypsin. Alternatively, proteins can be digested using trypsin prior to fractionation. After digestion, the total peptide pool is fractionated, for example with basic reverse phase chromatography. The last step involves separation of the peptide by liquid chromatography (LC) that is coupled to mass spectrometry (MS). Peptides are fragmented by tandem MSMS analysis and the corresponding spectras are analyzed using matching to in silico databases

1.6.2 Fractionation strategies for MS-based proteomics

The most commonly used protein based fractionation method is sodium-dodecyl sulfate poly-acrylamide gel electrophoresis (SDS-PAGE). SDS-PAGE separates proteins based on molecular size. Protein bands can be easily excised out of the gel and subsequent trypsin digestions can be performed [104]. However, due to poor extraction of peptides from the acrylamide gels, other techniques that harness the resolution of PAGE separation have been investigated. One such method that has alleviated poor sample recovery from SDS-PAGE is termed Gel Elution Liquid Fraction Entrapment Electrophoresis (GELFrEE). GELFrEE fractionation also utilizes an acrylamide gel to separate proteins, but fully elutes them into a liquid collection chamber, that allows for in-solution digestion of proteins into peptides [105]. Another less popular separation technique is called size exclusion chromatography (SEC) which utilizes porous beads to separate proteins based on size [106]. Peptide based fractionation techniques occur after the initial proteolytic digest. Peptides can be separated into sequential fractions based on their physiochemical properties. Peptides are often fractionated by exploiting their inherent charges using strong cation exchange (SCX) or strong anion exchange (SAX) [107]. SCX fractionation relies on the affinity that peptides have for a solid support that is negatively charged, and SAX contains solid supports that are positively charged [108]. Peptides are eluted off the solid supports by changes in buffer pH or increases in salt concentrations. Most recently, the use of basic reverse phase (bRP) chromatography prior to MS-analysis has been implemented [109,110]. The pH difference in bRP causes the hydrophobicity of certain amino acids to

change, resulting in a shift in retention times that is orthogonal to low pH reverse phase. Choosing the most appropriate fractionation technique will depend on time availability, amount of sample, complexity of the sample and the required proteomic depth needed to answer the biological question at hand.

1.7 Quantitative MS-based proteomics

The accurate and quantitative assessment of protein or peptide levels in biological samples is one of the most challenging areas still being improved upon in MS-based proteomics. Quantification relies on the ability to assess minute changes in the abundance of proteins upon alterations of steady-states [111]. In addition to assessing changes in biology, quantitative proteomics can also be used to account for technical variability at various stages of sample handling and preparation [112]. Quantitative proteomic applications have relied mostly on isotopic labels to distinguish the relative abundance levels between samples. Applications of isotopic labeling can be performed at the protein or peptide level, and samples can be mixed in pre-defined ratios, prior to LC-MSMS analysis. Label-based approaches are still the most widely accepted ways of making proteomics quantitative, but in recent years label-free approaches have become more popular, due to their simpler experimental design and lower overhead costs [113,114].

The most popular isotopic labeling strategy used to study dynamic changes in biology is termed stable isotopic labeling in cell culture by amino acids (SILAC). SILAC relies on metabolic incorporation of amino acids with substituted stable isotopic nuclei, ^{13}C and ^{15}N , most commonly present on

arginine and lysine. This technique relies on cells prolonged exposure to the label, to ensure that the endogenous amino acids are replaced completely by the heavy amino acid [115]. In this fashion, the relative abundance of proteins within two samples can be measured by looking at the mass spectral signals that are obtained from heavy samples (labeled with ^{13}C , ^{15}N) compared to signals obtained from the light samples (labeled with ^{12}C , ^{14}N). One major hurdle to SILAC experiments is that the samples must be labeled at the cellular level. To overcome this, many isotopic labeling reagents have been developed that target primary amines and can be used post protein harvesting and digestion. Examples of these include isotope-coded affinity tags (iCAT) [116], isobaric tags for relative and absolute quantification (iTRAQ) [117] and tandem mass tags (TMT) [118]. In each method, an isotopic reporter ion is analyzed by MS that infers relative abundance levels for each sample they originated from.

1.7.1 Targeted Proteomics

Targeted proteomics can be performed in two different ways: (1) selected reaction monitoring (SRM), also known as multiple reactions monitoring (MRM) [119], or (2) by parallel reaction monitoring (PRM) [120]. Targeted proteomics has been widely used in drug screening, environmental toxicology and to identify metabolites as well as biomarkers for disease diagnostics [121]. SRM is performed by using MSMS fragment ion pairs that are known as transitions to identify peptide and their corresponding proteins. The biggest advantage SRM has over traditional data driven MS-based proteomic approaches is that only a few proteins are selected for quantification, and thus this affords greater selectivity and sensitivity [122]. A

selected list of fragment ions, called transitions, is selected and the MS only targets those peptides for subsequent MSMS analysis. A disadvantage of SRM is inherent in the experimental set up. Targeted lists must be generated prior to MS-analysis; therefore the investigator must know what they are looking for ahead of time. In addition, a retention time generated by LC separation is required to avoid co-isolation and fragmentation of equivalent masses. Lastly, the size of the targeted list is limited, and one fragment ion is monitored at a time, making it difficult to choose the correct transitions prior to MS-analysis. Recently, PRM has been introduced to overcome some of the challenges faced with SRM experiments [123]. Like SRM, PRM also utilizes a pre-defined set of targets. However, PRM methods are capable of monitoring all fragment ions from a single peptide. Thus peptides are selected for monitoring instead of transitions, eliminating the need for transition optimization normally found in SRM approaches. Another advantage that PRM approaches afford is that they are performed on high-resolution high mass accuracy instruments. Higher resolution instruments allow for less co-isolation and therefore selected targets are easily distinguished from peptides of similar mass [124]. In general, targeted MS-based proteomic approach can be broken down into four steps: (1) selection of the targeted list of peptides that will be monitored, (2) MS-selection of the corresponding mass by isolation, (3) fragmentation of the selected ion, and (4) analysis of the fragment ions. In addition, the use of isotopically labeled “spiked-in” standards can be used for absolute quantification (reviewed in [125]).

1.8 Scope of thesis

Human multipotent stromal cells (hMSC) have been identified as extremely versatile cells for clinical use in regenerative medicine. Therefore, pre-clinical studies directed at large-scale proteomic analyses to determine the therapeutic potential of hMSC need to be undertaken. Understanding how hMSC exert their therapeutic effect through the secretion of bioactive molecules has not been studied in therapies aimed at endogenous β -cell regeneration. To date, large scale MS-based proteomic applications have not been successfully applied to hMSC biology. One potential reason for this is the difficulty in correctly selecting the appropriate methodologies to maximize complete proteome depth without sacrificing precious instrument time. In light of this, the goal of this thesis was to develop a combination of proteomic methods to assess queries into hMSC biology, as well as applying these techniques to identify specific therapeutic functions of hMSC, and to functionally validate candidate proteins of interest in application of β -cell regeneration.

Working towards these objectives, we first assessed the advantages and disadvantages of multiple fractionation techniques to help guide future experimental designs in general proteomic workflows (Chapter 2). By repeating four of the most common ways to perform fractionation, using a very complex sample (cell lysate), we identified the tradeoffs of each method in terms of cost, proteomic depth, instrument time and sample handling time. In light of this, using fractionation and proteomic techniques, we investigated what proteins are secreted by hMSC that possess islet regenerative potential compared to hMSC that show no improvement in systemic blood glucose,

after transplantation into immunodeficient mice rendered hyperglycemic by streptozotocin (STZ) treatment (Chapter 3). We discovered that hMSC signaled through several dynamic and complementary pathways that formulate a regenerative microenvironment applicable to the development of islet expansion therapies for diabetes. In addition to the discovery of key secretory hMSC regenerative pathways, active Wnt-signaling, was validated as playing a central role in hMSC-induction of β -cell survival and proliferation. Since the regenerative potential of hMSC was previously cell line-specific [70], lengthy *in vivo* characterization methods to identify hMSC lines useful in regenerative applications of diabetes. Faster and higher throughput methods for screening hMSC potency for β -cell regeneration are needed. To address this need, we performed a targeted MS-based proteomic approach designed to predict the therapeutic potential of hMSC, in context of β -cell regeneration (Chapter 4). Using simple *in vitro* characterization assays in conjunction with secreted conditioned media generated from hMSC, we are able to identify subsets that possess β -cell regenerative and angiogenic potential. With our proteomic screen we successfully identified over 10 proteins that can be used reliably to classify hMSC based on their therapeutic potential and successfully classify 16 previously uncharacterized hMSC lines. Lastly combining our findings that regenerative hMSC secrete active Wnt products (Chapter 3), we demonstrated that Wnt-signaling could be modulated in non-regenerative hMSC to increase their regenerative secretory potential, and validated the importance of Wnt-signaling using direct injection of CM into STZ-treated diabetic mouse models *in vivo* (Chapter 5). Herein, we showed for the first time that media conditioned by hMSC had the ability to induce endogenous β -

cell regeneration, free of cells. In addition we found hyperglycemia-reducing effect correlated directly with protein concentration, and after activation of Wnt-signaling during CM generation, this therapeutic effect could be greatly enhanced. Lastly, we investigated secretory changes upon modulation of Wnt-signaling using MS-based proteomic approaches and identified key pro- β -cell survival proteins that increase during activation of Wnt-signaling. Taken together, our studies improved the understanding of proteins secreted by hMSC capable of stimulating islet regeneration. We developed screening techniques to identify regenerative hMSC secretory patterns, and identified factors present in CM generated from hMSC that mediate endogenous β -cell regeneration. Altogether, these studies provide an extraordinary view of how this dynamic cell type can be used in clinical settings, to stimulate the expansion of β -cell mass and tip the balance in favor of islet regeneration versus destruction during diabetes.

1.9 References

- [1] A.B. Olokoba, O.A. Obateru, L.B. Olokoba, Type 2 Diabetes Mellitus: A Review of Current Trends, *Oman Med. J.* 27 (2012) 269–273. doi:10.5001/omj.2012.68.
- [2] S. Wild, G. Roglic, A. Green, R. Sicree, H. King, Global prevalence of diabetes: estimates for the year 2000 and projections for 2030., *Diabetes Care.* 27 (2004) 1047–53.
- [3] E. Hathout, Islet transplant: an option for childhood diabetes?, *Arch. Dis. Child.* 88 (2003) 591–594. doi:10.1136/adc.88.7.591.
- [4] G. Danaei, M.M. Finucane, Y. Lu, G.M. Singh, M.J. Cowan, C.J. Paciorek, J.K. Lin, F. Farzadfar, Y.H. Khang, G. a. Stevens, M. Rao, M.K. Ali, L.M. Riley, C. a. Robinson, M. Ezzati, National, regional, and global trends in fasting plasma glucose and diabetes prevalence since 1980: Systematic analysis of health examination surveys and epidemiological studies with 370 country-years and 2??7 million participants, *Lancet.* 378 (2011) 31–40. doi:10.1016/S0140-6736(11)60679-X.
- [5] IDF, IDF Diabetes Atlas, 2015. doi:10.1289/image.ehp.v119.i03.
- [6] L. Chen, D.J. Magliano, P.Z. Zimmet, The worldwide epidemiology of type 2 diabetes mellitus—present and future perspectives, *Nat. Rev. Endocrinol.* 8 (2011) 228–236. doi:10.1038/nrendo.2011.183.
- [7] H. Skarstrand, E. Krupinska, T.J.K. Haataja, F. Vaziri-Sani, J.O. Lagerstedt, A. Lernmark, Zinc transporter 8 (ZnT8) autoantibody epitope specificity and affinity examined with recombinant ZnT8 variant proteins in specific ZnT8R and ZnT8W autoantibody-positive type 1 diabetes patients, *Clin. Exp. Immunol.* 179 (2015) 220–229. doi:10.1111/cei.12448.
- [8] V. Öling, H. Reijonen, O. Simell, M. Knip, J. Ilonen, Autoantigen-specific memory CD4 + T cells are prevalent early in progression to Type 1 diabetes, *Cell. Immunol.* 273 (2012) 133–139. doi:10.1016/j.cellimm.2011.12.008.
- [9] L.C. Rogers, R.G. Frykberg, D.G. Armstrong, A.J.M. Boulton, M. Edmonds, G. Ha Van, A. Hartemann, F. Game, W. Jeffcoate, A. Jirkovska, E. Jude, S. Morbach, W.B. Morrison, M. Pinzur, D. Pitocco, L. Sanders, D.K. Wukich, L. Uccioli, The Charcot foot in diabetes, *Diabetes Care.* 34 (2011) 2123–2129. doi:10.2337/dc11-0844.
- [10] J. Keller, P. Layer, Human pancreatic exocrine response to nutrients in health and disease., *Gut.* 54 (2005) 1–28. doi:10.1136/gut.2005.065946.
- [11] J. Dolensek, M.S. Rupnik, A. Stozar, Structural similarities and differences between the human and the mouse pancreas, *Islets.* 7 (2015) 2–9. doi:10.1080/19382014.2015.1024405.

- [12] P. Itkin-Ansari, I. Geron, E. Hao, C. Demeterco, B. Tyrberg, F. Levine, Cell-Based Therapies for Diabetes: Progress towards a Transplantable Human β Cell Line, *Ann. N. Y. Acad. Sci.* 1005 (2003) 138–147. doi:10.1196/annals.1288.015.
- [13] A.G. Jones, A.T. Hattersley, The clinical utility of C-peptide measurement in the care of patients with diabetes, *Diabet. Med.* 30 (2013) 803–817. doi:10.1111/dme.12159.
- [14] B. Thorens, Glucose transporters in the regulation of intestinal, renal, and liver glucose fluxes., *Am. J. Physiol.* 270 (1996) G541–G553.
- [15] E. a. Ryan, B.W. Paty, P. a. Senior, D. Bigam, E. Alfadhli, N.M. Kneteman, J.R.T. Lakey, a. M.J. Shapiro, Five-year follow-up after clinical islet transplantation, *Diabetes.* 54 (2005) 2060–2069. doi:10.2337/diabetes.54.7.2060.
- [16] a. M.J. Shapiro, E. a. Ryan, J.R.T. Lakey, Islet cell transplantation, *Lancet.* 358 (2001) S21. doi:10.1016/S0140-6736(01)07034-9.
- [17] P.A. Halban, M.S. German, S.E. Kahn, G.C. Weir, Current status of islet cell replacement and regeneration therapy, *J. Clin. Endocrinol. Metab.* 95 (2010) 1034–1043. doi:10.1210/jc.2009-1819.
- [18] J.A. Thomson, J. Itskovitz-eldor, S.S. Shapiro, M.A. Waknitz, J.J. Swiergiel, V.S. Marshall, J.M. Jones, Embryonic Stem Cell Lines Derived from Human Blastocysts, *Science (80-.)*. 1145 (2007) 1145–1148. doi:10.1126/science.282.5391.1145.
- [19] N. Lumelsky, Differentiation of Embryonic Stem Cells to Insulin-Secreting Structures Similar to Pancreatic Islets, *Science (80-.)*. 292 (2001) 1389–1394. doi:10.1126/science.1058866.
- [20] S. Assady, G. Maor, M. Amit, J. Itskovitz-Eldor, K.L. Skorecki, M. Tzukerman, Insulin Production by Human Embryonic Stem Cells, *Diabetes.* 50 (2001) 1691–1697. doi:10.2337/diabetes.50.8.1691.
- [21] K. a D'Amour, A.G. Bang, S. Eliazer, O.G. Kelly, A.D. Agulnick, N.G. Smart, M.A. Moorman, E. Kroon, M.K. Carpenter, E.E. Baetge, Production of pancreatic hormone-expressing endocrine cells from human embryonic stem cells., *Nat. Biotechnol.* 24 (2006) 1392–401. doi:10.1038/nbt1259.
- [22] F.W. Pagliuca, J.R. Millman, M. Gürtler, M. Segel, A. Van Dervort, J.H. Ryu, Q.P. Peterson, D. Greiner, D.A. Melton, Generation of functional human pancreatic β cells *in vitro*, *Cell.* 159 (2014) 428–439. doi:10.1016/j.cell.2014.09.040.
- [23] M.C. Nostro, F. Sarangi, C. Yang, A. Holland, A.G. Elefanty, E.G. Stanley, D.L. Greiner, G. Keller, Efficient generation of NKX6-1+ pancreatic progenitors from multiple human pluripotent stem cell lines, *Stem Cell Reports.* 4 (2015) 591–604. doi:10.1016/j.stemcr.2015.02.017.

- [24] A. Trounson, C. McDonald, Stem Cell Therapies in Clinical Trials: Progress and Challenges, *Cell Stem Cell*. 17 (2015) 11–22. doi:10.1016/j.stem.2015.06.007.
- [25] V. Sordi, S. Pellegrini, L. Piemonti, Immunological Issues After Stem Cell-Based β Cell Replacement, *Curr. Diab. Rep.* 17 (2017). doi:10.1007/s11892-017-0901-4.
- [26] C.N. Mayhew, J.M. Wells, Converting human pluripotent stem cells into β -cells: recent advances and future challenges, *Curr. Opin. Organ Transplant*. 15 (2010) 54–60. doi:10.1097/MOT.0b013e3283337e1c.
- [27] K. Takahashi, K. Tanabe, M. Ohnuki, M. Narita, T. Ichisaka, K. Tomoda, S. Yamanaka, Induction of Pluripotent Stem Cells from Adult Human Fibroblasts by Defined Factors, *Cell*. 131 (2007) 861–872. doi:10.1016/j.cell.2007.11.019.
- [28] Y. Shi, C. Desponts, J.T. Do, H.S. Hahm, H.R. Schöler, S. Ding, Induction of Pluripotent Stem Cells from Mouse Embryonic Fibroblasts by Oct4 and Klf4 with Small-Molecule Compounds, *Cell Stem Cell*. 3 (2008) 568–574. doi:10.1016/j.stem.2008.10.004.
- [29] Y. Shi, H. Inoue, J.C. Wu, S. Yamanaka, Induced pluripotent stem cell technology: a decade of progress, *Nat. Rev. Drug Discov.* 16 (2016) 115–130. doi:10.1038/nrd.2016.245.
- [30] M.P. Walczak, A.M. Drozd, E. Stoczynska-Fidelus, P. Rieske, D.P. Grzela, Directed differentiation of human iPSC into insulin producing cells is improved by induced expression of PDX1 and NKX6.1 factors in IPC progenitors, *J. Transl. Med.* 14 (2016) 341. doi:10.1186/s12967-016-1097-0.
- [31] X. Fu, Y. Xu, Challenges to the clinical application of pluripotent stem cells: towards genomic and functional stability., *Genome Med.* 4 (2012) 55. doi:10.1186/gm354.
- [32] M. Banerjee, M. Kanitkar, R.R. Bhonde, Approaches Towards Endogenous Pancreatic Regeneration, *Rev. Diabet. Stud.* 2 (2005) 165–165. doi:10.1900/RDS.2005.2.165.
- [33] A.E. Butler, J. Janson, W.C. Soeller, P.C. Butler, Increased Beta -Cell Apoptosis Prevents Adaptive Increase in Beta -Cell Mass in Mouse Model of Type 2 Diabetes, *Diabetes*. 52 (2003) 2304–2314. doi:10.2337/diabetes.52.9.2304.
- [34] Y. Dor, J. Brown, O.I. Martinez, D. a Melton, Adult pancreatic β -cells are formed by self-duplication rather than stem-cell differentiation., *Nature*. 429 (2004) 41–46. doi:10.1038/nature02520.
- [35] L. Bouwens, D.G. Pipeleers, Extra-insular β -cells associated with ductules are frequent in adult human pancreas, *Diabetologia*. 41 (1998) 629–633. doi:10.1007/s001250050960.

- [36] F. Delaspre, R.L. Beer, M. Rovira, W. Huang, G. Wang, S. Gee, M. Del Carmen Vitery, S.J. Wheelan, M.J. Parsons, Centroacinar cells are progenitors that contribute to endocrine pancreas regeneration, *Diabetes*. 64 (2015) 3499–3509. doi:10.2337/db15-0153.
- [37] R.L. Beer, M.J. Parsons, M. Rovira, Centroacinar cells: At the center of pancreas regeneration, *Dev. Biol.* 413 (2016) 8–15. doi:10.1016/j.ydbio.2016.02.027.
- [38] S. Afelik, M. Rovira, Pancreas β -cell regeneration: Facultative or dedicated progenitors?, *Mol. Cell. Endocrinol.* 445 (2016). doi:http://dx.doi.org/10.1016/j.mce.2016.11.008.
- [39] S. Puri, M. Hebrok, Cellular Plasticity within the Pancreas— Lessons Learned from Development, *Dev. Cell.* 18 (2010) 342–356. doi:10.1016/j.devcel.2010.02.005.
- [40] G.K. Gittes, Developmental biology of the pancreas: A comprehensive review, *Dev. Biol.* 326 (2009) 4–35. doi:10.1016/j.ydbio.2008.10.024.
- [41] M. Chintinne, G. Stangé, B. Denys, P. In 'T Veld, K. Hellemans, M. Pipeleers-Marichal, Z. Ling, D. Pipeleers, Contribution of postnatally formed small β -cell aggregates to functional β -cell mass in adult rat pancreas, *Diabetologia*. 53 (2010) 2380–2388. doi:10.1007/s00125-010-1851-4.
- [42] K.H. Song, S.H. Ko, Y.B. Ahn, S.J. Yoo, H.M. Chin, H. Kaneto, K.H. Yoon, B.Y. Cha, K.W. Lee, H.Y. Son, *In vitro* transdifferentiation of adult pancreatic acinar cells into insulin-expressing cells, *Biochem. Biophys. Res. Commun.* 316 (2004) 1094–1100. doi:10.1016/j.bbrc.2004.02.153.
- [43] K. Minami, M. Okuno, K. Miyawaki, A. Okumachi, K. Ishizaki, K. Oyama, M. Kawaguchi, N. Ishizuka, T. Iwanaga, S. Seino, Lineage tracing and characterization of insulin-secreting cells generated from adult pancreatic acinar cells., *Proc. Natl. Acad. Sci. U. S. A.* 102 (2005) 15116–15121. doi:10.1073/pnas.0507567102.
- [44] S.R. Smukler, M.E. Arntfield, R. Razavi, G. Bikopoulos, P. Karpowicz, R. Seaberg, F. Dai, S. Lee, R. Ahrens, P.E. Fraser, M.B. Wheeler, D. Van Der Kooy, The adult mouse and human pancreas contain rare multipotent stem cells that express insulin, *Cell Stem Cell.* 8 (2011) 281–293. doi:10.1016/j.stem.2011.01.015.
- [45] B. Taylor, F.F. Liu, M. Sander, Nkx6.1 Is Essential for Maintaining the Functional State of Pancreatic B-cells, *Cell Rep.* 4 (2013) 1262–1275. doi:10.1016/j.celrep.2013.08.010.
- [46] G.C. Weir, S. Bonner-Weir, GABA Signaling Stimulates β Cell Regeneration in Diabetic Mice, *Cell.* 168 (2017) 7–9. doi:10.1016/j.cell.2016.12.006.
- [47] H. a Keenan, J.K. Sun, J. Levine, A. Doria, L.P. Aie, Residual Insulin Production and Pancreatic [Beta] -Cell Turnover After 50 Year ...,

Diabetes. 59 (2010) 2846–2853. doi:10.2337/db10-0676.

- [48] R.F. Pereira, K.W. Halford, M.D. O'Hara, D.B. Leeper, B.P. Sokolov, M.D. Pollard, O. Bagasra, D.J. Prockop, Cultured adherent cells from marrow can serve as long-lasting precursor cells for bone, cartilage, and lung in irradiated mice., *Proc. Natl. Acad. Sci. U. S. A.* 92 (1995) 4857–61. doi:10.1073/pnas.92.11.4857.
- [49] M.F. Pittenger, Multilineage Potential of Adult Human Mesenchymal Stem Cells, *Science* (80-.). 284 (1999) 143–147. doi:10.1126/science.284.5411.143.
- [50] D.J. Prockop, I. Sekiya, D.C. Colter, Isolation and characterization of rapidly self-renewing stem cells from cultures of human marrow stromal cells., *Cytotherapy*. 3 (2001) 393–6. doi:10.1080/146532401753277229.
- [51] J. Sanchez-Ramos, S. Song, F. Cardozo-Pelaez, C. Hazzi, T. Stedeford, A. Willing, T.B. Freeman, S. Saporta, W. Janssen, N. Patel, D.R. Cooper, P.R. Sanberg, Adult Bone Marrow Stromal Cells Differentiate into Neural Cells *in vitro*, *Exp. Neurol.* 164 (2000) 247–256. doi:10.1006/exnr.2000.7389.
- [52] D. Woodbury, E.J. Schwarz, D.J. Prockop, I.B. Black, Adult rat and human bone marrow stromal cells differentiate into neurons, *J. Neurosci. Res.* 61 (2000) 364–370. doi:10.1002/1097-4547(20000815)61:4<364::AID-JNR2>3.0.CO;2-C.
- [53] S. Wakitani, T. Saito, A.I. Caplan, Myogenic cells derived from rat bone marrow mesenchymal stem cells exposed to 5-azacytidine., *Muscle Nerve*. 18 (1995) 1417–26. doi:10.1002/mus.880181212.
- [54] M. Dominici, K. Le Blanc, I. Mueller, I. Slaper-Cortenbach, F.. Marini, D.S. Krause, R.J. Deans, A. Keating, D.J. Prockop, E.M. Horwitz, Minimal criteria for defining multipotent mesenchymal stromal cells. The International Society for Cellular Therapy position statement, *Cytotherapy*. 8 (2006) 315–317. doi:10.1080/14653240600855905.
- [55] A.G. Via, A. Frizziero, F. Oliva, Biological properties of mesenchymal Stem Cells from different sources., *Muscles. Ligaments Tendons J.* 2 (2012) 154–62. <http://www.ncbi.nlm.nih.gov/pubmed/23738292%5Cnhttp://www.pubmedcentral.nih.gov/articlerender.fcgi?artid=PMC3666517>.
- [56] D. Rubio, J. Garcia-Castro, M.C. Martín, R. de la Fuente, J.C. Cigudosa, A.C. Lloyd, A. Bernad, Spontaneous Human Adult Stem Cell Transformation, *Cancer Res.* 65 (2005) 3035–3039. doi:10.1158/0008-5472.CAN-04-4194.
- [57] R. Henschler, E. Deak, E. Seifried, Homing of mesenchymal stem cells, *Transfus. Med. Hemotherapy*. 35 (2008) 306–312. doi:10.1159/000143110.
- [58] P.J. Hanley, Z. Mei, M.G. Cabreira-hansen, M. Klis, W. Li,

- Manufacturing mesenchymal stromal cells for phase I clinical trials, 15 (2014) 416–422. doi:10.1016/j.jcyt.2012.09.007.Manufacturing.
- [59] X. Wei, X. Yang, Z. Han, F. Qu, L. Shao, Y. Shi, Mesenchymal stem cells: a new trend for cell therapy, *Acta Pharmacol. Sin.* 34 (2013) 747–754. doi:10.1038/aps.2013.50.
- [60] N. Kim, S.-G. Cho, Clinical applications of mesenchymal stem cells, *Korean J. Intern. Med.* 28 (2013) 387. doi:10.3904/kjim.2013.28.4.387.
- [61] R.S.Y. Wong, Extrinsic factors involved in the differentiation of stem cells into insulin-producing cells: An overview, *Exp. Diabetes Res.* 2011 (2011). doi:10.1155/2011/406182.
- [62] M.M. Gabr, M.M. Zakaria, A.F. Refaie, S.M. Khater, S.A. Ashamallah, A.M. Ismail, N. El-Badri, M.A. Ghoneim, Generation of insulin-producing cells from human bone marrow-derived mesenchymal stem cells: Comparison of three differentiation protocols, *Biomed Res. Int.* 2014 (2014). doi:10.1155/2014/832736.
- [63] K.S. Choi, J.S. Shin, J.J. Lee, Y.S. Kim, S.B. Kim, C.W. Kim, *In vitro* trans-differentiation of rat mesenchymal cells into insulin-producing cells by rat pancreatic extract, *Biochem. Biophys. Res. Commun.* 330 (2005) 1299–1305. doi:10.1016/j.bbrc.2005.03.111.
- [64] H. Jahr, R.G. Bretzel, Insulin-positive cells *in vitro* generated from rat bone marrow stromal cells, *Transpl. Proc.* 35 (2003) 2140–2141. doi:10.1016/S0041-1345(03)00747-4.
- [65] S.-H. Oh, T.M. Muzzonigro, S.-H. Bae, J.M. LaPlante, H.M. Hatch, B.E. Petersen, Adult bone marrow-derived cells trans-differentiating into insulin-producing cells for the treatment of type I diabetes., *Lab. Invest.* 84 (2004) 607–617. doi:10.1038/labinvest.3700074.
- [66] D. Gerace, R. Martiniello-Wilks, N.T. Nassif, S. Lal, R. Steptoe, A.M. Simpson, CRISPR-targeted genome editing of mesenchymal stem cell-derived therapies for type 1 diabetes: a path to clinical success?, *Stem Cell Res. Ther.* 8 (2017) 62. doi:10.1186/s13287-017-0511-8.
- [67] R.H. Lee, M.J. Seo, R.L. Reger, J.L. Spees, A. Pulin, S.D. Olson, D.J. Prockop, Multipotent stromal cells from human marrow home to and promote repair of pancreatic islets and renal glomeruli in diabetic NOD/scid mice, *Proc. Natl. Acad. Sci.* 103 (2006) 17438–17443. doi:10.1073/pnas.0608249103.
- [68] D. Hess, L. Li, M. Martin, S. Sakano, D. Hill, B. Strutt, S. Thyssen, D. Gray, M. Bhatia, Bone marrow-derived stem cells initiate pancreatic regeneration., *Nat. Biotechnol.* 21 (2003) 763–770. doi:10.1038/nbt841.
- [69] G.I. Bell, M.T. Meschino, J.M. Hughes-Large, H.C. Broughton, A. Xenocostas, D.A. Hess, Combinatorial Human Progenitor Cell Transplantation Optimizes Islet Regeneration Through Secretion of Paracrine Factors, *Stem Cells Dev.* 21 (2012) 1863–1876.

doi:10.1089/scd.2011.0634.

- [70] G.I. Bell, H.C. Broughton, K.D. Levac, D.A. Allan, A. Xenocostas, D.A. Hess, Transplanted Human Bone Marrow Progenitor Subtypes Stimulate Endogenous Islet Regeneration and Revascularization, *Stem Cells Dev.* 21 (2012) 97–109. doi:10.1089/scd.2010.0583.
- [71] P.-O. Carlsson, E. Schwarcz, O. Korsgren, K. Le Blanc, Preserved b-Cell Function in Type 1 Diabetes by Mesenchymal Stromal Cells, *Diabetes.* 64 (2015) 587–592. doi:10.2337/db14-0656.
- [72] H. Aly, N. Rohatgi, C.A. Marshall, T.C. Grossenheider, H. Miyoshi, T.S. Stappenbeck, S.J. Matkovich, M.L. McDaniel, A Novel Strategy to Increase the Proliferative Potential of Adult Human β -Cells While Maintaining Their Differentiated Phenotype, *PLoS One.* 8 (2013). doi:10.1371/journal.pone.0066131.
- [73] R. Mussmann, M. Geese, F. Harder, S. Kegel, U. Andag, A. Lomow, U. Burk, D. Onichtchouk, C. Dohrmann, M. Austen, Inhibition of GSK3 promotes replication and survival of pancreatic β -cells, *J. Biol. Chem.* 282 (2007) 12030–12037. doi:10.1074/jbc.M609637200.
- [74] H. Hao, J. Liu, J. Shen, Y. Zhao, H. Liu, Q. Hou, C. Tong, D. Ti, L. Dong, Y. Cheng, Y. Mu, J. Liu, X. Fu, W. Han, Multiple intravenous infusions of bone marrow mesenchymal stem cells reverse hyperglycemia in experimental type 2 diabetes rats, *Biochem. Biophys. Res. Commun.* 436 (2013) 418–423. doi:10.1016/j.bbrc.2013.05.117.
- [75] X. Gao, L. Song, K. Shen, H. Wang, M. Qian, W. Niu, X. Qin, Bone marrow mesenchymal stem cells promote the repair of islets from diabetic mice through paracrine actions, *Mol. Cell. Endocrinol.* 388 (2014) 41–50. doi:10.1016/j.mce.2014.03.004.
- [76] J.K. Smid, S. Faulkes, M.A. Rudnicki, Periostin induces pancreatic regeneration, *Endocrinology.* 156 (2015) 824–836. doi:10.1210/en.2014-1637.
- [77] A. Wodarz, R. Nusse, Mechanisms of Wnt Signaling in Development, *Annu. Rev. Cell Dev. Biol.* 14 (1998) 59–88. doi:10.1146/annurev.cellbio.14.1.59.
- [78] R. Habas, I.B. Dawid, Dishevelled and Wnt signaling: is the nucleus the final frontier?, *J. Biol.* 4 (2005) 2. doi:10.1186/jbiol22.
- [79] Y. Komiyama, R. Habas, Wnt signal transduction pathways, *Organogenesis.* 4 (2008) 68–75. doi:10.4161/org.4.2.5851.
- [80] J.L. Stamos, W.I. Weis, The β -catenin destruction complex, *Cold Spring Harb. Perspect. Biol.* 5 (2013) 1–16. doi:10.1101/cshperspect.a007898.
- [81] K. Willert, K.A. Jones, K. Willert, K.A. Jones, Wnt signaling : is the party in the nucleus ? Wnt signaling : is the party in the nucleus ?, (2006) 1394–1404. doi:10.1101/gad.1424006.

- [82] E.M. Verheyen, C.J. Gottardi, Regulation of Wnt/ β -catenin signaling by protein kinases, *Dev. Dyn.* 239 (2009) NA-NA. doi:10.1002/dvdy.22019.
- [83] N.S. Tolwinski, M. Wehrli, A. Rives, N. Erdeniz, S. DiNardo, E. Wieschaus, Wg/Wnt signal can be transmitted through arrow/LRP5,6 and axin independently of Zw3/Gsk3 β activity, *Dev. Cell.* 4 (2003) 407–418. doi:10.1016/S1534-5807(03)00063-7.
- [84] H. Yamamoto, S. Kishida, M. Kishida, S. Ikeda, S. Takada, A. Kikuchi, Phosphorylation of axin, a Wnt signal negative regulator, by glycogen synthase kinase-3 β regulates its stability, *J. Biol. Chem.* 274 (1999) 10681–10684. doi:10.1074/jbc.274.16.10681.
- [85] N. Kaur, S. Chettiar, S. Rathod, P. Rath, D. Muzumdar, M.L. Shaikh, A. Shiras, Wnt3a mediated activation of Wnt/ β -catenin signaling promotes tumor progression in glioblastoma., *Mol. Cell. Neurosci.* 54 (2013) 44–57. doi:10.1016/j.mcn.2013.01.001.
- [86] K. Willert, J.D. Brown, E. Danenberg, A.W. Duncan, I.L. Weissman, T. Reya, J.R. Yates, R. Nusse, Wnt proteins are lipid-modified and can act as stem cell growth factors, *Nature.* 423 (2003) 448–452. doi:10.1038/nature01611.
- [87] C.Y. Janda, L.T. Dang, C. You, J. Chang, W. de Lau, Z.A. Zhong, K.S. Yan, O. Marecic, D. Siepe, X. Li, J.D. Moody, B.O. Williams, H. Clevers, J. Piehler, D. Baker, C.J. Kuo, K.C. Garcia, Surrogate Wnt agonists that phenocopy canonical Wnt and β -catenin signalling, *Nature.* 545 (2017) 234–237. doi:10.1038/nature22306.
- [88] R. Takada, Y. Satomi, T. Kurata, N. Ueno, S. Norioka, H. Kondoh, T. Takao, S. Takada, Monounsaturated Fatty Acid Modification of Wnt Protein: Its Role in Wnt Secretion, *Dev. Cell.* 11 (2006) 791–801. doi:10.1016/j.devcel.2006.10.003.
- [89] P.S. Klein, D.A. Melton, A molecular mechanism for the effect of lithium on development., *Proc. Natl. Acad. Sci. U. S. A.* 93 (1996) 8455–8459. doi:10.1073/pnas.93.16.8455.
- [90] L. Meijer, M. Flajolet, P. Greengard, Pharmacological inhibitors of glycogen synthase kinase 3, *Trends Pharmacol. Sci.* 25 (2004) 471–480. doi:10.1016/j.tips.2004.07.006.
- [91] J. Silva, O. Barrandon, J. Nichols, J. Kawaguchi, T.W. Theunissen, A. Smith, Promotion of reprogramming to ground state pluripotency by signal inhibition, *PLoS Biol.* 6 (2008) 2237–2247. doi:10.1371/journal.pbio.0060253.
- [92] P. Polakis, Wnt signaling in cancer, *Cold Spring Harb. Perspect. Biol.* 4 (2012) 9. doi:10.1101/cshperspect.a008052.
- [93] A. Niida, T. Hiroko, M. Kasai, Y. Furukawa, Y. Nakamura, Y. Suzuki, S. Sugano, T. Akiyama, DKK1, a negative regulator of Wnt signaling, is a target of the β -catenin/TCF pathway., *Oncogene.* 23 (2004) 8520–8526.

doi:10.1038/sj.onc.1207892.

- [94] T. Malinauskas, A.R. Aricescu, W. Lu, C. Siebold, E.Y. Jones, Modular mechanism of Wnt signaling inhibition by Wnt inhibitory factor 1, *Nat. Struct. Mol. Biol.* 18 (2011) 886–893. doi:10.1038/nsmb.2081.
- [95] B. Chen, M.E. Dodge, W. Tang, J. Lu, Z. Ma, C.-W. Fan, S. Wei, W. Hao, J. Kilgore, N.S. Williams, M.G. Roth, J.F. Amatruda, C. Chen, L. Lum, Small molecule-mediated disruption of Wnt-dependent signaling in tissue regeneration and cancer, *Nat. Chem. Biol.* 5 (2009) 100–107. doi:10.1038/nchembio.137.
- [96] O. Kulak, H. Chen, B. Holohan, X. Wu, H. He, D. Borek, Z. Otwinowski, K. Yamaguchi, L.A. Garofalo, Z. Ma, W. Wright, C. Chen, J.W. Shay, X. Zhang, L. Lum, Disruption of Wnt/ β -Catenin Signaling and Telomeric Shortening Are Inextricable Consequences of Tankyrase Inhibition in Human Cells, *Mol. Cell. Biol.* 35 (2015) 2425–2435. doi:10.1128/MCB.00392-15.
- [97] R. Aebersold, M. Mann, Mass spectrometry-based proteomics., *Nature.* 422 (2003) 198–207. doi:10.1038/nature01511.
- [98] H. Steen, M. Mann, The abc's (and xyz's) of peptide sequencing, *Nat. Rev. Mol. Cell Biol.* 5 (2004) 699–711. doi:10.1038/nrm1468.
- [99] B. Domon, Mass Spectrometry and Protein Analysis, *Science* (80-.). 312 (2006) 212–217. doi:10.1126/science.1124619.
- [100] Y. Zhang, B.R. Fonslow, B. Shan, M. Baek, J.R. Yates, Protein Analysis by Shotgun / Bottom-up Proteomics, (2013).
- [101] J.M. Burkhardt, C. Schumbrutzki, S. Wortelkamp, A. Sickmann, R.P. Zahedi, Systematic and quantitative comparison of digest efficiency and specificity reveals the impact of trypsin quality on MS-based proteomics, *J. Proteomics.* 75 (2012) 1454–1462. doi:10.1016/j.jprot.2011.11.016.
- [102] A. Schmidt, I. Forne, A. Imhof, Bioinformatic analysis of proteomics data, *BMC Syst. Biol.* 8 (2014) S3. doi:10.1186/1752-0509-8-S2-S3.
- [103] H. Lam, E.W. Deutsch, J.S. Eddes, J.K. Eng, S.E. Stein, R. Aebersold, Building consensus spectral libraries for peptide identification in proteomics, *Nat. Methods.* 5 (2008) 873–875. doi:10.1038/nmeth.1254.
- [104] S.C. Bendall, A.T. Booy, G. Lajoie, Proteomic Analysis of Pluripotent Stem Cells, in: *Curr. Protoc. Stem Cell Biol.*, John Wiley & Sons, Inc., Hoboken, NJ, USA, 2007. doi:10.1002/9780470151808.sc01b01s2.
- [105] C. Witkowski, J. Harkins, Using the GELFREE 8100 Fractionation System for Molecular Weight-Based Fractionation with Liquid Phase Recovery, *J. Vis. Exp.* (2009) 3–5. doi:10.3791/1842.
- [106] P. Lecchi, A.R. Gupte, R.E. Perez, L. V. Stockert, F.P. Abramson, Size-exclusion chromatography in multidimensional separation schemes for proteome analysis, *J. Biochem. Biophys. Methods.* 56 (2003) 141–152.

doi:10.1016/S0165-022X(03)00055-1.

- [107] N.A. Kulak, G. Pichler, I. Paron, N. Nagaraj, M. Mann, Minimal, encapsulated proteomic-sample processing applied to copy-number estimation in eukaryotic cells., *Nat. Methods.* 11 (2014) 319–24. doi:10.1038/nmeth.2834.
- [108] X. Zhang, A. Fang, C.P. Riley, M. Wang, F.E. Regnier, C. Buck, Multi-dimensional liquid chromatography in proteomics—A review, *Anal. Chim. Acta.* 664 (2010) 101–113. doi:10.1016/j.aca.2010.02.001.
- [109] F. Yang, Y. Shen, D.G. Camp, R.D. Smith, High-pH reversed-phase chromatography with fraction concatenation for 2D proteomic analysis, *Expert Rev. Proteomics.* 9 (2012) 129–134. doi:10.1586/epr.12.15.
- [110] C.D. Kelstrup, R.R. Jersie-Christensen, T.S. Batth, T.N. Arrey, A. Kuehn, M. Kellmann, J. V. Olsen, Rapid and deep proteomes by faster sequencing on a benchtop quadrupole ultra-high-field orbitrap mass spectrometer, *J. Proteome Res.* 13 (2014) 6187–6195. doi:10.1021/pr500985w.
- [111] V.C. Wasinger, M. Zeng, Y. Yau, Current Status and Advances in Quantitative Proteomic Mass Spectrometry, *Int. J. Proteomics.* 2013 (2013) 1–12. doi:10.1155/2013/180605.
- [112] O.T. Schubert, H.L. Röst, B.C. Collins, G. Rosenberger, R. Aebersold, Quantitative proteomics: challenges and opportunities in basic and applied research, *Nat. Protoc.* 12 (2017) 1289–1294. doi:10.1038/nprot.2017.040.
- [113] J. Cox, M. Mann, MaxQuant enables high peptide identification rates, individualized p.p.b.-range mass accuracies and proteome-wide protein quantification, *Nat. Biotechnol.* 26 (2008) 1367–1372. doi:10.1038/nbt.1511.
- [114] H. Weisser, S. Nahnsen, J. Grossmann, L. Nilse, A. Quandt, H. Brauer, M. Sturm, E. Kenar, O. Kohlbacher, R. Aebersold, L. Malmström, An automated pipeline for high-throughput label-free quantitative proteomics, *J. Proteome Res.* 12 (2013) 1628–1644. doi:10.1021/pr300992u.
- [115] S.-E. Ong, Stable Isotope Labeling by Amino Acids in Cell Culture, SILAC, as a Simple and Accurate Approach to Expression Proteomics, *Mol. Cell. Proteomics.* 1 (2002) 376–386. doi:10.1074/mcp.M200025-MCP200.
- [116] Y. Shiio, R. Aebersold, Quantitative proteome analysis using isotope-coded affinity tags and mass spectrometry, *Nat. Protoc.* 1 (2006) 139–145. doi:10.1038/nprot.2006.22.
- [117] S. Wiese, K.A. Reidegeld, H.E. Meyer, B. Warscheid, Protein labeling by iTRAQ: A new tool for quantitative mass spectrometry in proteome research, *Proteomics.* 7 (2007) 340–350. doi:10.1002/pmic.200600422.

- [118] A. Thompson, J. Scheifer, K. Kuhn, S. Kienle, J. Schwarz, G. Schmidt, T. Neumann, C. Hamon, Tandem mass tags: A novel quantification strategy for comparative analysis of complex protein mixtures by MS/MS, *Anal. Chem.* 75 (2003) 1895–1904. doi:10.1021/ac0262560.
- [119] V. Lange, P. Picotti, B. Domon, R. Aebersold, Selected reaction monitoring for quantitative proteomics: a tutorial, *Mol. Syst. Biol.* 4 (2008). doi:10.1038/msb.2008.61.
- [120] S. Gallien, E. Duriez, C. Crone, M. Kellmann, T. Moehring, B. Domon, Targeted Proteomic Quantification on Quadrupole-Orbitrap Mass Spectrometer, *Mol. Cell. Proteomics.* (2012) 1709–1723. doi:10.1074/mcp.O112.019802.
- [121] P. Picotti, R. Aebersold, Selected reaction monitoring–based proteomics: workflows, potential, pitfalls and future directions, *Nat. Methods.* 9 (2012) 555–566. doi:10.1038/nmeth.2015.
- [122] R. Kiyonami, A. Schoen, A. Prakash, S. Peterman, V. Zabrouskov, P. Picotti, R. Aebersold, A. Huhmer, B. Domon, Increased Selectivity, Analytical Precision, and Throughput in Targeted Proteomics, *Mol. Cell. Proteomics.* 10 (2011) M110.002931. doi:10.1074/mcp.M110.002931.
- [123] A.C. Peterson, J.D. Russell, D.J. Bailey, M.S. Westphall, J.J. Coon, Parallel Reaction Monitoring for High Resolution and High Mass Accuracy Quantitative, Targeted Proteomics, *Mol. Cell. Proteomics.* 11 (2012) 1475–1488. doi:10.1074/mcp.O112.020131.
- [124] R.A. Zubarev, A. Makarov, Orbitrap mass spectrometry, *Anal. Chem.* 85 (2013) 5288–5296. doi:10.1021/ac4001223.
- [125] N. Rauniyar, Parallel reaction monitoring: A targeted experiment performed using high resolution and high mass accuracy mass spectrometry, *Int. J. Mol. Sci.* 16 (2015) 28566–28581. doi:10.3390/ijms161226120.

Chapter 2

Evaluation of Sample Fractionation Techniques for Large-Scale In-depth Proteomic Analysis¹

2.1 Introduction

Sample preparation strategies employed in bottom-up proteomics can be broadly categorized into workflows which omit or implement fractionation at the protein or peptide level prior to LC-MSMS [1]. Prior limitations in mass spectrometry hardware and high pressure liquid chromatography rendered unfractionated preparations ineffective, necessitating the need for extensive fractionation to achieve deep proteome coverage [2]. Recent advances in instrumentation speed and sensitivity in conjunction with UPLC systems utilizing longer columns and smaller particles sizes has substantially improved characterization of complex, unfractionated proteomes [3]. This is exemplified by Nagaraj and colleagues and Pirmoradian *et al.*, who detected over 3900 yeast and 4800 HeLa proteins, respectively, by employing long gradients and 50 cm reversed phase columns coupled to a high resolution Q Exactive mass spectrometer [3,4]. In fact, it is now possible to detect ~4000 yeast and ~4400 HeLa proteins in approximately 1h with current state-of-the-art Orbitrap-based mass spectrometers (Orbitrap Fusion and Q Exactive High Field) [5,6].

¹ This chapter contains excerpts with permission from the following paper:

Kuljanin M*, Dieters-Castator DZ*, Hess DA, Postovit LM, Lajoie GA. (2017) "Comparison of Sample Preparative Techniques for Large-Scale Proteomics". *Proteomics*. 17:1-9.

* Denotes equal author contribution

In contrast, fractionation approaches based on molecular weight (MW), charge, pI, or hydrophobicity require substantially more acquisition time and sample handling. Nonetheless, these workflows contribute to our understanding of biological systems by characterizing PTMs, enriching for low abundance species and quantifying expression for thousands of proteins [7–10]

SDS-PAGE protein separation coupled with in-gel digestion was commonly used in mass spectrometry-based proteomics [11,12]. Its robustness, low cost, high resolution and ability to handle detergent containing samples make it amenable to many workflows. Two recently published drafts of the human proteome utilized SDS-PAGE to obtain unprecedented protein expression profiles across several tissue types (84–92% human proteome) [13,14]. However, SDS-PAGE is time consuming, manually intensive and subject to variable peptide extraction efficiencies [11]. Gel Eluted Liquid Fractionation Entrapment Electrophoresis (GELFrEE) technology, in part, overcomes these issues by combining gel-based separation with solution phase recovery to enable reproducible, semi-automated fractionation with reduced sample handling and loss [15]. Moreover, several techniques utilizing peptide based fractionation have achieved exceptional proteome coverage which include multidimensional protein identification technology (MudPIT) [16], isoelectric focusing (IEF) [17,18], and more recently High-/Low-pH reversed phase chromatography (HpH or bRP) [6,19]. Alternatively, small scale peptide fractionation (C18, SCX, and SAX) can be readily performed in StageTips without requiring dedicated fractionation equipment [20–22].

Many large scale proteomic studies employ methodologies such as those listed but few have extensively compared their performance relative to one another [23–25]. In light of this, we compared HeLa proteomes obtained from unfractionated, SDS-PAGE, GELFrEE, SCX StageTip and HpH sample preparations across several parameters. With identical material and LC-MS time (except unfractionated samples), our findings reveal most workflows perform well but HpH consistently displayed the best overall performance.

2.2 Results

2.2.1 Proteome coverage of different workflows on a Q Exactive mass spectrometer

HeLa proteomes obtained from unfractionated, SDS-PAGE, GELFrEE, SCX StageTip and high pH reverse phase (HpH) sample preparations were systematically compared. Several modifications were made to each technique from its original protocol in order to allow for equal comparisons. In total, 10 fractions were analyzed by LC-MS (~1ug per fraction) for each technique in biological triplicate. All fractions were run on a 4h gradient plus washing and re-equilibration. Replicates were searched both individually and grouped using the match between runs feature in MaxQuant. Where applicable, protein identifications containing ≥ 1 unique peptide in 2 out of 3 biological replicates was used for analysis [26]. In general, each method tested received more instrument time compared to previous reports and when necessary, utilized chloroform/methanol precipitation to remove SDS coupled with on-pellet, in solution digestion.

Within each replicate for different workflows, ~7.1% of the total proteome was “matched-between-runs” and >95% was present in all

biological replicates suggesting high reproducibility for each technique. Moreover, only a small fraction of proteins were identified by one unique peptide (Figure 2.1a). In total, 5189, 6959, 5919, 7655, 8470 proteins were detected with unfractionated, SDS-PAGE, GELFrEE, SCX and HpH workflows, respectively.

In terms of proteomic depth, nearly 5200 proteins were detected in unfractionated HeLa digests which is on par with previous reports [4,26]. Proteomic coverage with SDS-PAGE was also comparable to reports from other groups [27,28]. While Botelho *et al.* previously reported similar performance between GELFrEE and SDS-PAGE using an LTQ ion trap, SDS-PAGE detected ~1,000 more proteins than GELFrEE [25]. We identified a respectable number of proteins with SCX StageTips (7655), which were less than that obtained by Kulak *et al.* by using a similar technique [22]. Differences in sample preparation (lysis buffer and digestion) as well as column size may be contributing factors. The number of proteins identified with HpH was similar to Kelstrup *et al.* (8470 vs. 8500 IDs) and the highest out of all workflows tested [6]. Several proteomic studies reported increased proteome depth by incorporating data from multiple workflows and/or instrumentation [29–31]. Combining all sample preparative techniques yielded over 8700 unique proteins. This was an increase of ~3% over HpH, which alone had nearly 700 exclusive proteins (Figure 2.1b).

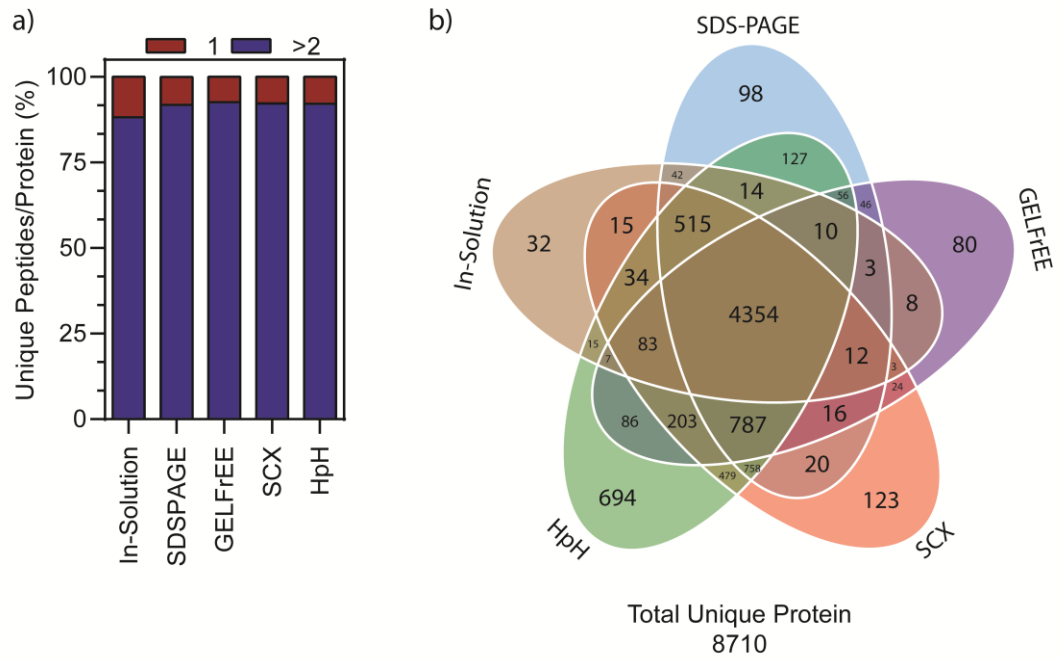


Figure 2.1 High confidence identification and large overlap between proteomes from different techniques. (a) Majority of the proteins (95%) were identified with high confidences (2 or more unique peptides, blue) for each technique. (b) Total proteins exclusive (11%) and common (50%) to five different preparative techniques analyzed on a Q Exactive. Gene symbols were used for analysis and proteins exclusive to one biological replicate were omitted.

2.2.2 Comparison of fractionation efficiency

The capacity of pre-fractionation to resolve unique proteins or peptides into discrete packets reduces sample complexity and improves peptide detection and identification by MS [32]. To assess fractionation efficiency for each technique, we examined how many unique peptides, and proteins where applicable, were exclusive to 1, 2 or 3 or more fractions. For this analysis, biological replicates were searched individually without matching.

In principle, SDS-PAGE displays good protein separation and resolution over a wide range of MWs, generally within a few kilo Daltons (kDa). Surprisingly, we found with SDS-PAGE that only 27.7% and 59.5% of proteins identified were exclusive to 1 or 2 fractions, respectively (Figure 2.2a). However, at the peptide level, 58.2% and 82.8% were exclusive to 1 or 2 fractions, respectively (Figure 2.2c). Of note, the GELFrEE protocol was less efficient at separating proteins than SDS-PAGE (Figure 2.2b, d). Silver stained GELFrEE fractions ran on 1D SDS-PAGE revealed moderate overlap between adjacent lanes (Figure 2.3a, b). Moreover, Box-and-Whisker plots of median fraction MW further illustrate limited separation with GELFrEE compared to SDS-PAGE (Figure 2.2c). In contrast, other studies utilizing SDS-PAGE or GELFrEE found 64-67% of proteins identified were exclusive to a single fraction [25,27]. Peptide fractionation efficiency with SCX StageTips was similar to Kulak *et al.* with 53.8% and 77.4% exclusive to 1 or 2 SCX fractions, respectively (Figure 2.2e) [22]. However, the HpH method gave the best fractionation performance with 80.1% and 94.5% of all peptides exclusive to 1 or 2 fractions, respectively (Figure 2.2f).

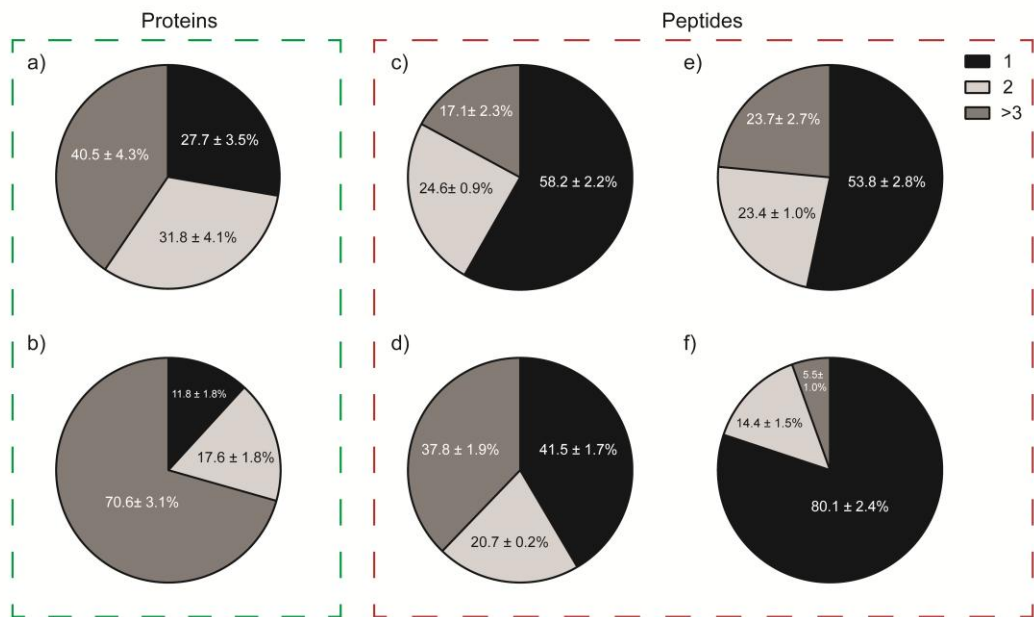


Figure 2.2 Fractionation efficiency varies between proteins and peptide separation techniques. Pie chart displaying percentage of unique proteins and peptides (mean \pm S.D) exclusive to one (black), 2 (light grey) and three of more (grey) fractions for (a) SDS-PAGE (protein level), (b) GELFrEE (protein level), (c) SDS-PAGE (peptide level), (d) GELFrEE (peptide level), (e) SCX and (f) HpH. SDS-PAGE and HpH exhibited the greatest fractionation efficiency for protein and peptide-based separation techniques, respectively.

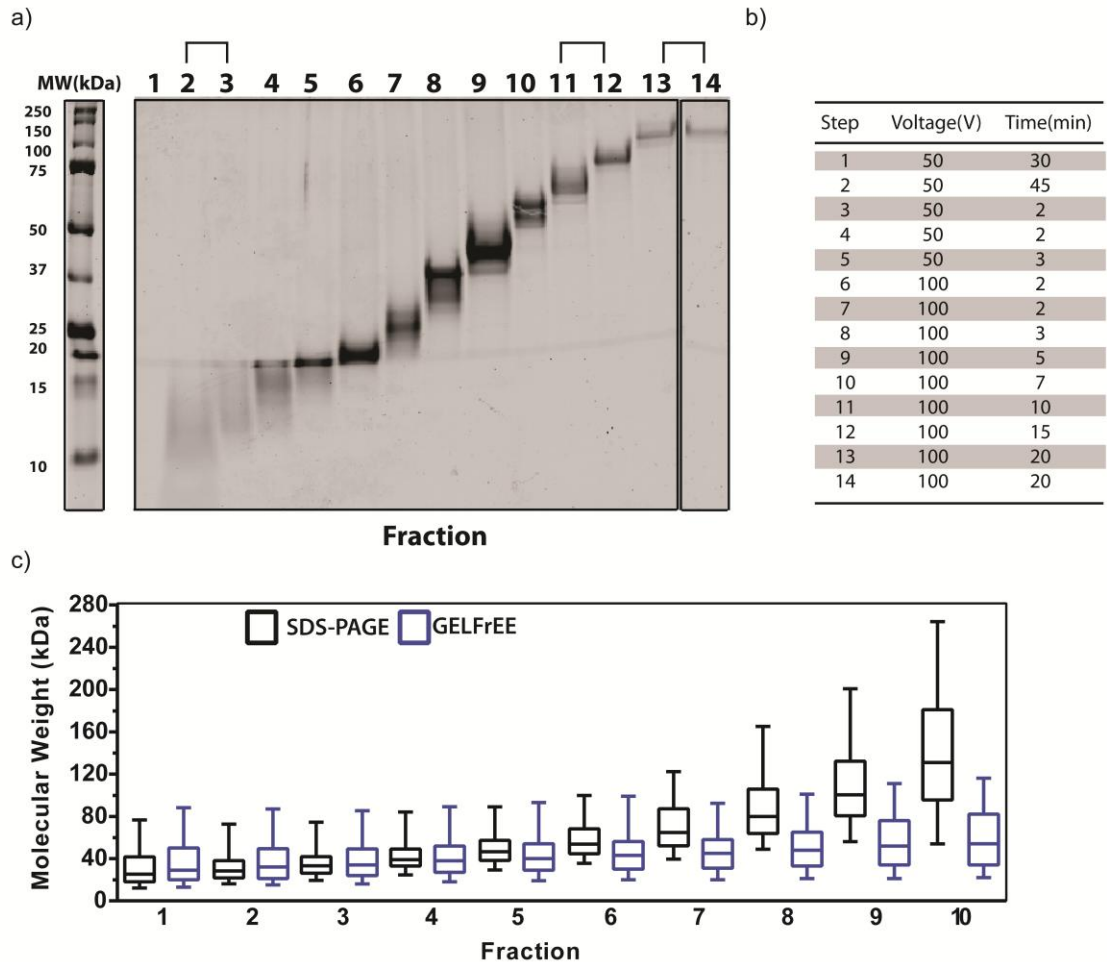


Figure 2.3 Fractionation efficiency comparison between protein based separation techniques. (a) Silver stained 1D SDS-PAGE of fractions collected on an 8% Tris-acetate GELFrEE cartridge starting with 100 ug of HeLa lysate. Fraction 14 was run on the same gel. (B) Gradient was slightly modified to allow leading dye front to be eluted in the first fraction. Fraction 1 was discarded and fractions 2 and 3, 11 and 12, and 13 and 14 were combined to produce a total of 10 fractions. (C) Box-and-Whisker plot of median protein MW detected in each fraction for SDS-PAGE (black) and GELFrEE (blue). Boxes represent 75% and 25% percentiles and Whiskers indicate 90% and 10% percentiles.

2.2.3 *Distribution of proteins and peptides*

Fractionation techniques which exhibit orthogonal separations are more efficient at maximizing MS/MS time across the entire gradient space [32]. Unique peptides and proteins per fraction were correlated for each preparative technique (Figure 2.4). For SDS-PAGE, peptides and proteins increased slightly with MW before declining in later fractions (higher MW) (Figure 2.4a). Peptides and proteins per fraction with GELFrEE decreased until fraction 5 before recovering (Figure 2.4b). SCX displayed a sharp increase in peptides/proteins detected in early fractions before plateauing while HpH numbers decreased only slightly with fraction number (Figure 2.4c, d). Retention time and peptide density plots illustrate a similar trend observed for peptides and proteins per fraction (Figure 2.5). For example, SDS-PAGE and GELFrEE exhibited higher peptide density with increasing fraction number (MW). Alternatively, peptide density remained even across all HpH fractions due to its concatenation scheme.

We next examined peptides: protein ratios for each technique and found gel-based methods had approximately one less peptide identified per protein compared to peptide fractionation even though gel-based approaches generated roughly 300K more MS2 scans (Table A2.1). As expected, in-solution digests had the lowest peptides: protein ratio (10.1:1) but identified the greatest proteins/hour (1298/hour). While total unique peptides were indicative of proteins identified for each technique, this was not the case with peptide spectral matches (PSMs). For example, GELFrEE had the greatest number of PSMs but the fewest unique peptides and proteins.

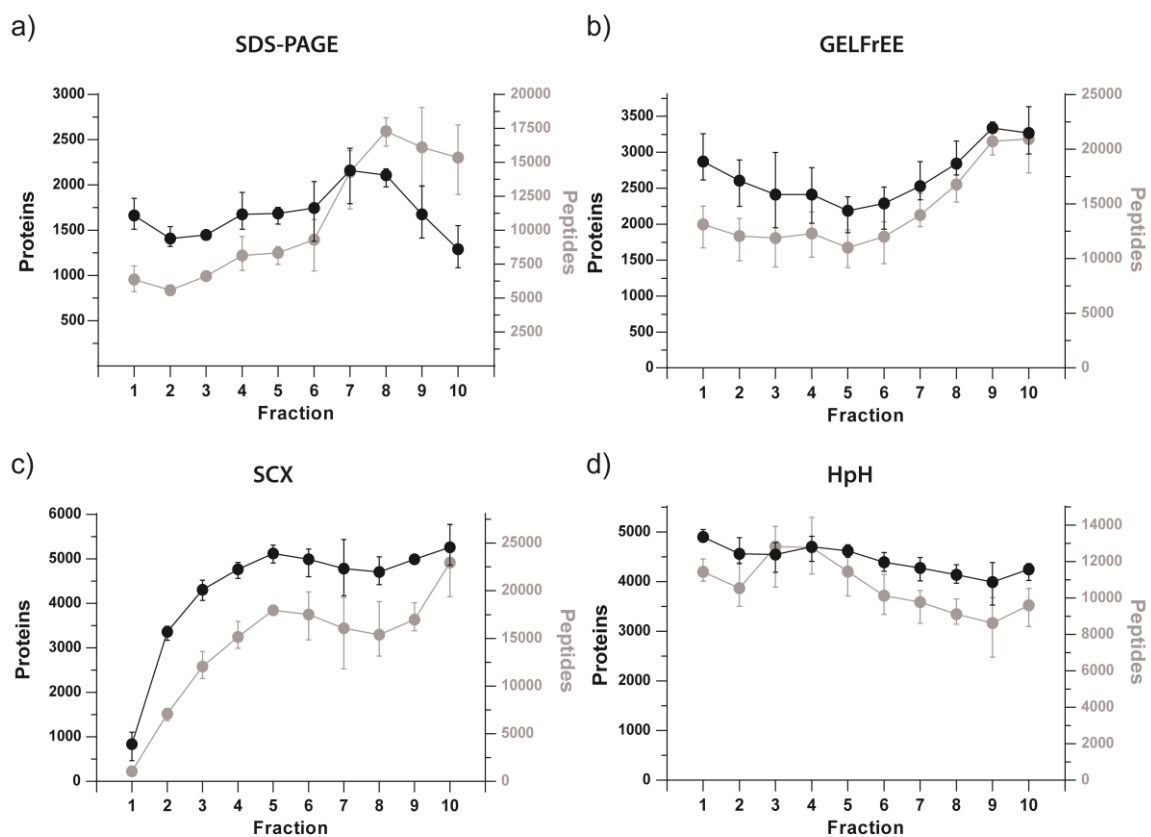


Figure 2.4 Peptide and protein distribution profiles deviate for each separation technique. Distribution of unique peptides (right y-axis, grey) and proteins (left y-axis, black) identified per fraction for (a) SDS-PAGE, (b) GELFrEE, (c) SCX and (d) HpH.

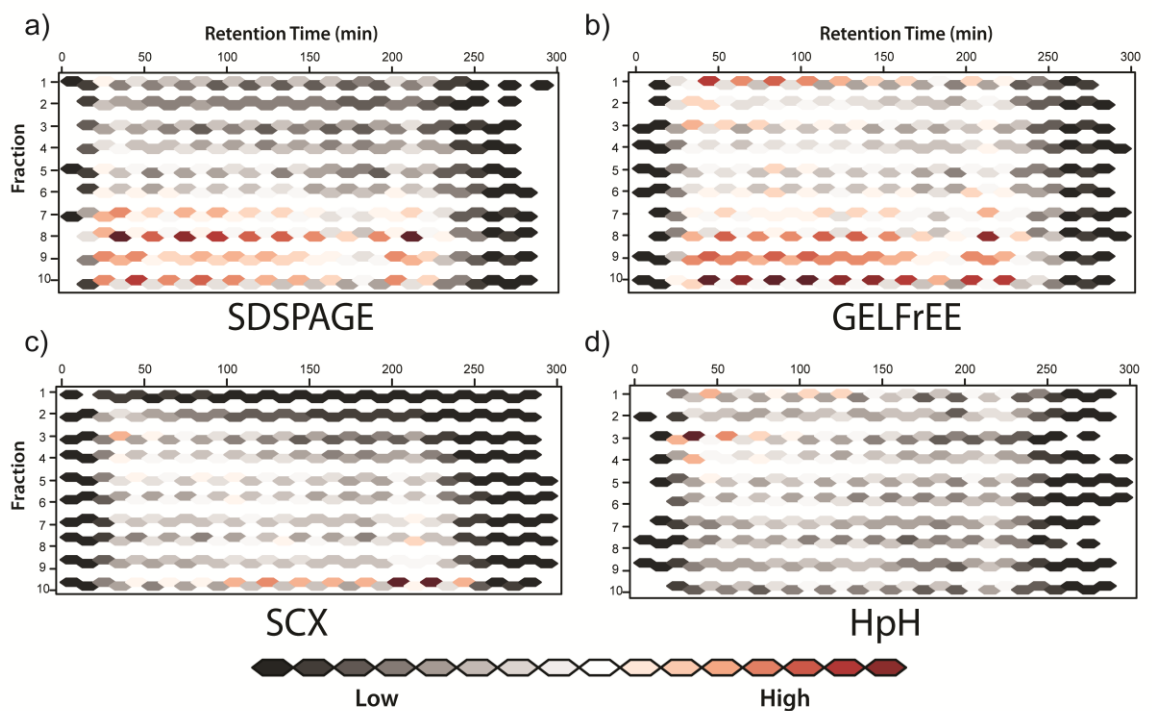


Figure 2.5 Comparison of orthogonality at the peptide level between each fractionation technique. Peptide density distribution was assessed using the hexbin package in R; each hexagon represents 500 peptides with red indicating the highest density. (a) Orthogonality is poor at later fractions for both (a) SDS-PAGE and (b) GELFrEE. (c) SCX fractionation shows high orthogonality but high peptide density in later fractions. (d) HpH fractionation shows evenly distributed peptide throughout each fraction and highest orthogonality.

2.2.4 Evaluating peptide characteristics

Examining the median sequence coverage achieved for each method revealed a peak in peptide density between 10% and 15% before tailing off (Figure 2.6a). For gel-based workflows, the median sequence coverage with GELFrEE (~27%) was higher than SDS-PAGE (22.6%) (Figure 2.6b). SCX and HpH peptide fractionation improved median sequence coverage to ~27% and 24.4%, respectively, over the unfractionated in-solution digest (22.8%) (Figure 2.6b). Combining sequence information from all methods improved median sequence coverage of the HeLa proteome to 38.0%. This can be attributed to a 48.6% increase in total unique peptides (165K) over HpH, which had the second highest number of unique peptides (111K) (Table A2.1). For comparison, Kelstrup *et al.* achieved a median sequence coverage of >40% with HeLa digests fractionated by HpH (14 fractions) using the latest generation Q Exactive HF [6].

Next, we calculated the grand average of hydropathy (GRAVY) scores for unique peptides detected by each workflow to determine whether any bias towards hydrophobic or hydrophilic species existed (Figure 2.7a). All methods displayed a propensity to enrich for hydrophilic peptides as indicated by negative GRAVY scores. Dunn's multiple comparison, post hoc analysis revealed a significantly higher ($P < 0.001$) median GRAVY score with unfractionated in-solution digests compared to all other techniques (Figure 2.7b). These findings are in line with previous groups which found cellular digests to be primarily hydrophilic and also suggested a proportion of hydrophobic peptides are lost during sample handling [33,34].

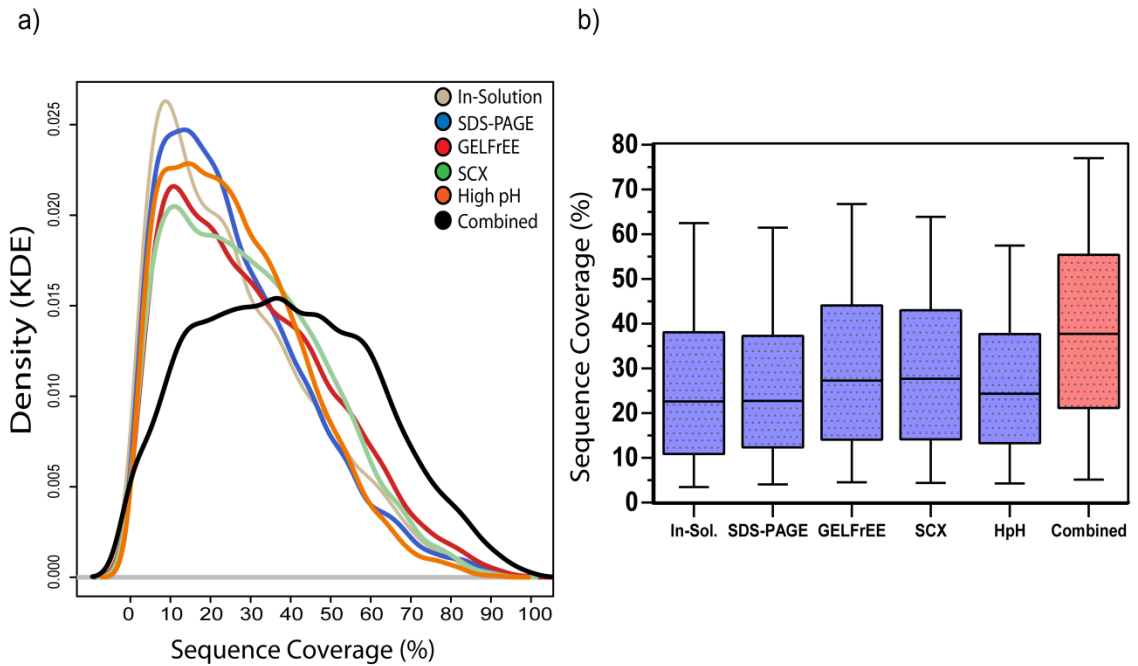


Figure 2.6 Different fractionation techniques provide complementary sequence coverage. (a) Kernel density estimation comparing percent sequence coverage for each technique. A slight maxima is observed near 40% (black line) when combining sequence information from all methods. (b) Box-and-Whisker plots displaying median percent sequence coverage for individual techniques (blue). Box-and-Whisker indicates 75 and 25% percentiles, and 95 and 5% percentiles, respectively. On-way ANOVA was performed using Kruskal-Wallis test to assess differences in mean sequence coverage distribution between methods. Combined Data set is show in red. All methods were significantly different from each other ($p < 0.05$), with the exception of GELFrEE and SCX.

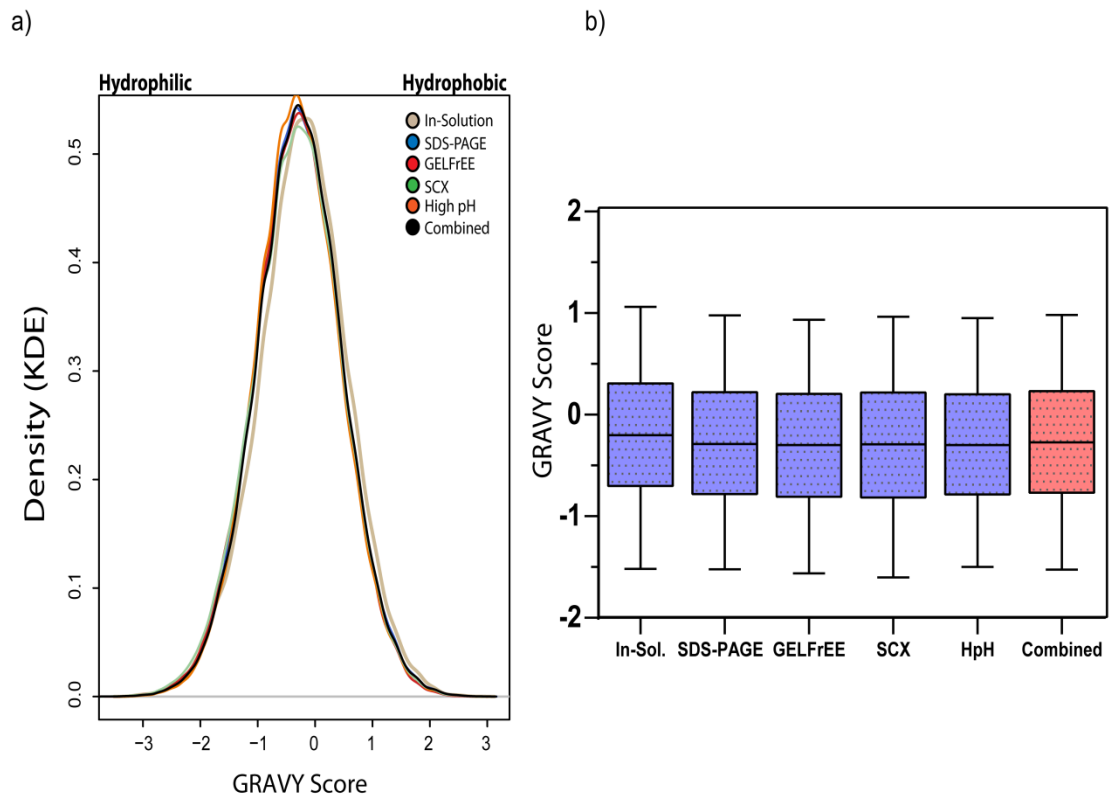


Figure 2.7 All workflows preferentially enrich for hydrophilic peptides. (a) Kernel density estimation was performed using GRAVY scores from each method. GRAVY scores <0 indicate the presence and relative abundance of hydrophilic species. (b) Box-and-Whisker plot displaying mean GRAVY scores. Boxes represent 75% and 25% percentiles and whiskers indicate 95% and 5% percentiles. One-way ANOVA was performed using the Kruskal-Wallis test to assess differences in mean GRAVY score distribution between methods. Combined dataset is shown in red. In-solution was significantly from different from all other methods (p -value <0.0001).

Analysis of missed cleavages revealed that a large number were present in most sample preparations although many (~70%) were restricted to one. As expected, SDS-PAGE was the highest (44.5%) which may be explained by poor absorption and diffusion of trypsin into the gel pieces. Missed cleavages with GELFrEE was relatively high (34.8%) compared to unfractionated in-solution samples (25.6%) even though digestion was performed essentially the same for both techniques. SCX fractionation exhibited the least missed cleavages (15.9%) followed by HpH (22.1%). We also investigated peptides with missed cleavages from HpH preparations which contained internal lysine (K) and/or arginine (R) residues. Notably, we found the frequency of internal K residues to be ~2 fold higher than R even though their abundance in the human proteome (Uniprot) is approximately even (~5.8% for K and ~5.6% for R). Hence, future sample preparations may benefit by utilizing Trypsin and endoproteinase Lys-C (LysC) in combination to minimize the number of missed cleavages occurring at lysine.

2.2.5 Sample preparation time

Reproducibility, feasibility/cost and throughput are important parameters to consider when choosing a sample preparation to employ in bottom-up proteomics. Although it is difficult to objectively quantify these parameters for each technique, SCX StageTip fractionation was by far the most efficient and straightforward method due to the capacity to process samples in parallel and short elution times. HpH fraction collection was automated but is limited to processing one sample at a time. In addition, HpH requires a dedicated fractionation system as well as additional time for concatenation, drying and column cleaning between replicates. GELFrEE can

be multiplexed up to 8 samples but needs ~3 hours to run plus chloroform/methanol precipitation of each fraction. It also requires a dedicated unit and custom cartridges. SDS-PAGE, as expected, was the most labour intensive technique and required an additional day for de-staining. However, SDS-PAGE as well as SCX StageTips, were the most cost-effective and accessible methods.

2.3 Discussion

In this study, we compared the performance of several commonly used sample preparative techniques for bottom-up proteomics. As expected, fractionation yielded more protein identifications, and in most cases, greater sequence coverage, than unfractionated in-solution digests. Peptide-based fractionation outperformed gel-based workflows in terms of protein IDs and fractionation efficiency but not necessarily sequence coverage. However, differences in digestion efficiency between in-gel and in-solution preparations is likely a contributing factor and warrants further investigation. Interestingly, we did not achieve similar proteome depth with GELFrEE compared to SDS-PAGE. This may be a consequence of the low 8% tris-acetate cartridges and short resolving gel (1cm) used as a prerequisite for eluting high MW proteins within a reasonable time frame. In addition, the GELFrEE collection chamber was not rinsed between cycles to maximize sample recovery. Hence, carry over between fractions from residual sample in the GELFrEE collection chamber could have led to an under representation of separation. Regardless, we believe that proteoforms (isoforms, PTMs and cleaved/fragmented proteins) migrating at different MWs are recorded as single entries during database searching, thereby underestimating the true fractionation efficiency

of SDS-PAGE and GELFrEE. For example, Titin, a 3.6 MDa protein was detected in low, intermediate and high MW SDS-PAGE and GELFrEE fractions. Nonetheless, GELFrEE remains an invaluable tool for top-down proteomics [35].

Although combining multiple techniques improved protein identifications and sequence coverage, the additional acquisition time needed is not feasible for the majority of medium to large scale proteomic studies (≥ 1 proteome/day of instrument time). It is doubtful that faster mass spectrometers with increased sensitivity and dynamic range will bypass the need for some form of sample fractionation to achieve maximum proteome coverage. Utilizing multiple enzyme digestion strategies or iterative exclusion in tandem with techniques like HpH fractionation may be more appropriate for achieving optimal sequence coverage [7,36,37]. Additional improvements to protein extraction/handling, column technology and instrumentation could also yield increased proteome depth. In summary, the findings reported here illustrate the benefits and limitations of different techniques for analyzing a complex cellular proteome and should help aid in the design of future bottom-up proteomics studies. Ultimately, the degree of fractionation needed is determined by how much data is needed to answer the biological question at hand.

2.4 Experimental Methods

2.4.1 Cell culture and protein extraction

HeLa cells (obtained from the ATCC) were maintained in DMEM F12 media supplemented with 10% FBS (Life Technologies). Confluent 15 cm plates of HeLa cells were rinsed with PBS, trypsinized and then centrifuged at

400 xg for 5 minutes to pellet cells. Cell pellets were re-suspended in PBS, pelleted again and stored at -80°C. To prepare lysates for LC-MS, frozen cell pellets were incubated in 8M Urea, 50 mM ammonium bicarbonate (ABC), 10mM DTT, 2% SDS and sonicated with a probe sonicator (20 X 0.5 second pulses; Level 1) (ThermoFisher Scientific) to shear DNA. Lysates were quantified using a Pierce™ 660 nm Protein Assay (ThermoFisher Scientific) and stored at -80°C until future use.

2.4.2 Chloroform/methanol protein precipitation

HeLa lysates were reduced in 10 mM DTT for 30 minutes and alkylated in 100 mM Iodoacetamide (IAA) for 30 minutes at room temperature in the dark. Next, lysates were precipitated in chloroform/methanol in 1.5 mL microfuge tubes according to Wessel and Flügge [38]. Briefly, 100 µg aliquots of HeLa lysates were topped up to 150 µL with 50mM ABC. To each sample, 600 µL of cold methanol was added followed by 150 µL of chloroform and thorough vortexing. A volume of 450 µL of water was added before additional vortexing and centrifugation at 14,000 x g for 5 min. The upper aqueous/methanol phase was carefully removed to avoid disturbing the precipitated protein interphase. A second 450 µL volume of cold methanol was added to each sample followed by vigorous vortexing and centrifugation at 14, 000 x g for 5 min. Remaining chloroform/methanol was discarded and the precipitated protein pellet air dried in a fume hood.

2.4.3 Unfractionated on-pellet in-solution digestion

On-pellet protein digestion was performed using a modified protocol described by Duan et al. [39]. Briefly, 150 µL of 50 mM ABC (pH 8) trypsin

solution was added to precipitated protein pellets (1:50 ratio) and incubated overnight at 37°C in a water bath shaker. An additional aliquot of trypsin was added the next day (1:100 ratio) for ~4 hours before acidifying (pH 3-4) with 10% formic acid (FA). Digests were centrifuged at 14,000 x g to pellet insoluble material before LC-MS or peptide fractionation.

2.4.4 SDS-PAGE followed by in-gel digestion

HeLa lysates were fractionated by SDS-PAGE as previously described [40]. Briefly, 100 µg of lysate was separated on a 12% acrylamide tris-glycine gel followed by fixing, staining with Coomassie blue and de-staining overnight on a horizontal shaker. Each lane was divided into 10 equal gel fractions which were manually processed into ~1x1 mm³ cubes using a razor blade. Gel pieces were reduced in 10 mM DTT for 30 minutes and alkylated in 100 mM IAA for 30 minutes at room temperature in the dark. After dehydration with ACN, gel pieces were swelled in 100 µL of 50 mM ABC (pH 8) trypsin solution (1:25 ratio distributed evenly across 10 fractions) and incubated overnight in a water bath shaker at 37°C. Peptides were extracted from gel pieces in the presence of a water bath sonicator by adding a small volume of 10% FA followed by dehydration in 300 µL ACN for 10 minutes, two times. Samples were dried in a SpeedVac (ThermoFisher Scientific) and re-suspended in 0.1% FA prior to LC-MS.

2.4.5 GELFrEE fractionation followed by in-solution digestion

HeLa lysates (100 µg/chamber) were fractionated on an 8% tris-acetate cartridge using the GELFrEE system according to the manufacturer (Expedeon). Sample collection was not started until blue loading dye was

visible in the collection chamber after which 150-200 μ L of liquid was removed and replaced following each time interval. Running buffer was changed every hour or half hour when using 50 or 100 V, respectively. Fractions 2 and 3, 11 and 12, and 13 and 14 were concatenated to generate a total of 10 fractions that were processed using chloroform/methanol and in-solution digestion as described above.

2.4.6 SCX peptide fractionation

Tryptic peptides recovered from chloroform/methanol precipitated, in-solution digests of HeLa lysate (100 μ g) were fractionated using SCX StageTips similarly to Kulak *et. al* [22]. Approximately 100 μ g of peptides, acidified with 1% TFA, were distributed evenly between four 12-plug SCX StageTips. In total, 10 SCX fractions were collected by eluting in 75, 100, 125, 150, 175, 200, 225, 250 and 300 mM ammonium acetate/20% ACN solutions followed by a final elution with 5mM ammonium hydroxide/80% ACN. Fractions eluted with identical buffers from quadruplicate StageTips were combined, dried in a SpeedVac, resuspended in ddH₂O and dried again to evaporate residual ammonium acetate. All samples were resuspended in 0.1% FA prior to LC-MS analysis.

2.4.7 High pH reversed phase peptide fractionation

Proteins (100 μ g) obtained from chloroform/methanol precipitation were digested in-solution with trypsin as described above. Next, tryptic peptides were fractionated on a Waters XBridge BEH130 C18 5 μ m 4.6 mm x 250 mm column connected to an Agilent 1100 HPLC system at a flow rate of 1 mL/min at 20°C. Buffer A (100% water) and buffer B (10% water/90% ACN) were

maintained at pH 10.0 by the addition of ammonium hydroxide immediately prior to fractionation. The gradient consisted of 5% to 35% B over 55 minutes, 70% B over 8 min, hold at 70% B for 2 minutes, return to 5% B over 5 min and then hold for 15 minutes. A total of 50 fractions were collected during the first 75 minutes of the gradient (1.5 mL per fraction) using an automated fraction collector. The volume of each fraction was reduced using a SpeedVac and every 10th fraction was concatenated. The final 10 fractions were dried completely using a SpeedVac and resuspended 0.1% FA prior to LC-MS.

2.4.8 LC-MS/MS

All fractions/digests were analyzed using an M-class nanoAcquity UHPLC system (Waters) connected to a Q Exactive mass spectrometer (ThermoFisher Scientific). Buffer A consisted of Water/0.1% FA and Buffer B consisted of ACN/0.1%FA. Peptides (~1 µg measured by BCA) were initially loaded onto an ACQUITY UPLC M-Class Symmetry C18 Trap Column, 5 µm, 180 µm x 20 mm and trapped for 4 minutes at a flow rate of 10 µl/min at 99% A/1% B. Peptides were separated on an ACQUITY UPLC M-Class Peptide BEH C18 Column, 130 Å, 1.7 µm, 75 µm X 250 mm operating at a flow rate of 300 nL/min at 35°C using a non-linear gradient consisting of 1-7% B over 7 minutes, 7-19% B over 173 minutes and 19-30% B over 60 minutes before increasing to 95% B and washing. Settings for data acquisition on the Q Exactive are outlined in the appendix (Table A2.2).

2.4.9 Data Analysis

All raw MS files were searched in MaxQuant version 1.5.2.8 using the Human Uniprot database (reviewed only; updated May 2014 with 40,550

entries) [41,42]. Missed cleavages were set to 3 and I=L. Cysteine carbamidomethylation was set as a fixed modification. Oxidation (M), N-terminal Acetylation (protein), and Deamidation (NQ) were set as a variable modifications (max. number of modifications per peptide = 5) and all other settings were left as default. Precursor mass deviation was left at 20 ppm and 4.5 ppm for first and main search, respectively. Fragment mass deviation was left at 20 ppm. Protein and peptide FDR was set to 0.01 (1%) and the decoy database was set to revert. Match between runs was enabled where specified in main text. Bioinformatics analysis was performed using Perseus version 1.5.5.3. Briefly, protein lists were loaded into Perseus and proteins identified by site, reverse and contaminants were removed [43]. When using the match between runs feature, datasets were filtered for proteins containing a minimum of one unique peptide in at least 2 out of 3 biological replicates. Kernel density estimation was performed using R statistical software version 3.2.3. Graphpad Prism version 6.01 was used to conduct nonparametric Kruskal-Wallis test coupled with Dunn's multiple comparison, along with the Mann-Whitney test to assess significance.

2.5 References

- [1] L. Ly, V.C. Wasinger, Protein and peptide fractionation, enrichment and depletion: Tools for the complex proteome, *Proteomics*. 11 (2011) 513–534. doi:10.1002/pmic.201000394.
- [2] M. Mann, N.A. Kulak, N. Nagaraj, J. Cox, The Coming Age of Complete, Accurate, and Ubiquitous Proteomes, *Mol. Cell*. 49 (2013) 583–590. doi:10.1016/j.molcel.2013.01.029.
- [3] N. Nagaraj, N. Alexander Kulak, J. Cox, N. Neuhauser, K. Mayr, O. Hoerning, O. Vorm, M. Mann, System-wide Perturbation Analysis with Nearly Complete Coverage of the Yeast Proteome by Single-shot Ultra HPLC Runs on a Bench Top Orbitrap, *Mol. Cell. Proteomics*. 11 (2012) M111.013722. doi:10.1074/mcp.M111.013722.
- [4] M. Pirmoradian, H. Budamgunta, K. Chingin, B. Zhang, J. Astorga-Wells, R.A. Zubarev, Rapid and Deep Human Proteome Analysis by Single-dimension Shotgun Proteomics, *Mol. Cell. Proteomics*. 12 (2013) 3330–3338. doi:10.1074/mcp.O113.028787.
- [5] A.S. Hebert, A.L. Richards, D.J. Bailey, A. Ulbrich, E.E. Coughlin, M.S. Westphall, J.J. Coon, The One Hour Yeast Proteome, *Mol. Cell. Proteomics*. 13 (2014) 339–347. doi:10.1074/mcp.M113.034769.
- [6] C.D. Kelstrup, R.R. Jersie-Christensen, T.S. Batth, T.N. Arrey, A. Kuehn, M. Kellmann, J. V. Olsen, Rapid and deep proteomes by faster sequencing on a benchtop quadrupole ultra-high-field orbitrap mass spectrometer, *J. Proteome Res.* 13 (2014) 6187–6195. doi:10.1021/pr500985w.
- [7] S.C. Bendall, C. Hughes, J.L. Campbell, M.H. Stewart, P. Pittock, S. Liu, E. Bonneil, P. Thibault, M. Bhatia, G. a Lajoie, An enhanced mass spectrometry approach reveals human embryonic stem cell growth factors in culture., *Mol. Cell. Proteomics*. 8 (2009) 421–432. doi:10.1074/mcp.M800190-MCP200.
- [8] H. Wang, T. Chang-wong, H. Tang, D.W. Speicher, Comparison of Extensive Protein Fractionation and Repetitive LC-MS / MS Analyses on Depth of Analysis for Complex Proteomes research articles, (2010) 1032–1040.
- [9] T.S. Batth, C. Francavilla, J. V. Olsen, Off-line high-pH reversed-phase fractionation for in-depth phosphoproteomics, *J. Proteome Res.* 13 (2014) 6176–6186. doi:10.1021/pr500893m.
- [10] J. Mayne, A.E. Starr, Z. Ning, R. Chen, C.K. Chiang, D. Figeys, Fine tuning of proteomic technologies to improve biological findings: Advancements in 2011-2013, *Anal. Chem.* 86 (2014) 176–195. doi:10.1021/ac403551f.

- [11] K.D. Speicher, O. Kolbas, S. Harper, D.W. Speicher, Systematic analysis of peptide recoveries from in-gel digestions for protein identifications in proteome studies, *J. Biomol. Tech.* 11 (2000) 74–86.
- [12] A. Shevchenko, H. Tomas, J. Havlis, J. V Olsen, M. Mann, In-gel digestion for mass spectrometric characterization of proteins and proteomes., *Nat. Protoc.* 1 (2006) 2856–2860. doi:10.1038/nprot.2006.468.
- [13] M.-S. Kim, S.M. Pinto, D. Getnet, R.S. Nirujogi, S.S. Manda, R. Chaerkady, A.K. Madugundu, D.S. Kelkar, R. Isserlin, S. Jain, J.K. Thomas, B. Muthusamy, P. Leal-Rojas, P. Kumar, N.A. Sahasrabudde, L. Balakrishnan, J. Advani, B. George, S. Renuse, L.D.N. Selvan, A.H. Patil, V. Nanjappa, A. Radhakrishnan, S. Prasad, T. Subbannayya, R. Raju, M. Kumar, S.K. Sreenivasamurthy, A. Marimuthu, G.J. Sathe, S. Chavan, K.K. Datta, Y. Subbannayya, A. Sahu, S.D. Yelamanchi, S. Jayaram, P. Rajagopalan, J. Sharma, K.R. Murthy, N. Syed, R. Goel, A.A. Khan, S. Ahmad, G. Dey, K. Mudgal, A. Chatterjee, T.-C. Huang, J. Zhong, X. Wu, P.G. Shaw, D. Freed, M.S. Zahari, K.K. Mukherjee, S. Shankar, A. Mahadevan, H. Lam, C.J. Mitchell, S.K. Shankar, P. Satishchandra, J.T. Schroeder, R. Sirdeshmukh, A. Maitra, S.D. Leach, C.G. Drake, M.K. Halushka, K. Prasad, R.H. Hruban, C.L. Kerr, G.D. Bader, C.A. Iacobuzio-Donahue, H. Gowda, A. Pandey, A draft map of the human proteome A, *Nature*. 509 (2014) 575–581. doi:10.1038/nature13302.A.
- [14] M. Wilhelm, J. Schlegl, H. Hahne, A.M. Gholami, M. Lieberenz, M.M. Savitski, E. Ziegler, L. Butzmann, S. Gessulat, H. Marx, T. Mathieson, S. Lemeer, K. Schnatbaum, U. Reimer, H. Wenschuh, M. Mollenhauer, J. Slotta-Huspenina, J.-H. Boese, M. Bantscheff, A. Gerstmair, F. Faerber, B. Kuster, Mass-spectrometry-based draft of the human proteome, *Nature*. 509 (2014) 582–587. doi:10.1038/nature13319.
- [15] J.C. Tran, A.A. Doucette, Gel-eluted liquid fraction entrapment electrophoresis: An electrophoretic method for broad molecular weight range proteome separation, *Anal. Chem.* 80 (2008) 1568–1573. doi:10.1021/ac702197w.
- [16] M.P. Washburn, D. Wolters, J.R. Yates, Large-scale analysis of the yeast proteome by multidimensional protein identification technology., *Nat. Biotechnol.* 19 (2001) 242–7. doi:10.1038/85686.
- [17] D.R. Stein, X. Hu, S.J. Mccorrister, G.R. Westmacott, F.A. Plummer, T.B. Ball, M.S. Carpenter, High pH reversed-phase chromatography as a superior fractionation scheme compared to off-gel isoelectric focusing for complex proteome analysis, *Proteomics*. 13 (2013) 2956–2966. doi:10.1002/pmic.201300079.
- [18] R.M.M. Branca, L.M. Orre, H.J. Johansson, V. Granholm, M. Huss, Å. Pérez-Bercoff, J. Forshed, L. Käll, J. Lehtiö, HiRIEF LC-MS enables deep proteome coverage and unbiased proteogenomics, *Nat. Methods*.

11 (2013) 59–62. doi:10.1038/nmeth.2732.

- [19] P. McQueen, O. Krokhin, Optimal selection of 2D reversed-phase–reversed-phase HPLC separation techniques in bottom-up proteomics, *Expert Rev. Proteomics*. 9 (2012) 125–128. doi:10.1586/epr.12.8.
- [20] J. Rappsilber, Y. Ishihama, M. Mann, Stop And Go Extraction tips for matrix-assisted laser desorption/ionization, nanoelectrospray, and LC/MS sample pretreatment in proteomics, *Anal. Chem.* 75 (2003) 663–670. doi:10.1021/ac026117i.
- [21] Y. Ishihama, J. Rappsilber, M. Mann, Modular stop and go extraction tips with stacked disks for parallel and multidimensional peptide fractionation in proteomics, *J. Proteome Res.* 5 (2006) 988–994. doi:10.1021/pr050385q.
- [22] N.A. Kulak, G. Pichler, I. Paron, N. Nagaraj, M. Mann, Minimal, encapsulated proteomic-sample processing applied to copy-number estimation in eukaryotic cells., *Nat. Methods*. 11 (2014) 319–24. doi:10.1038/nmeth.2834.
- [23] H. Wang, S. Sun, Y. Zhang, S. Chen, P. Liu, B. Liu, An off-line high pH reversed-phase fractionation and nano-liquid chromatography-mass spectrometry method for global proteomic profiling of cell lines, *J. Chromatogr. B Anal. Technol. Biomed. Life Sci.* 974 (2015) 90–95. doi:10.1016/j.jchromb.2014.10.031.
- [24] X. Yin, Y. Zhang, X. Liu, C. Chen, H. Lu, H. Shen, P. Yang, Systematic comparison between SDS-PAGE/RPLC and high-/low-pH RPLC coupled tandem mass spectrometry strategies in a whole proteome analysis, *Analyst*. 140 (2015) 1314–1322. doi:10.1039/C4AN02119C.
- [25] D. Botelho, M.J. Wall, D.B. Vieira, S. Fitzsimmons, F. Liu, A. Doucette, Top-Down and Bottom-Up Proteomics of SDS-Containing Solutions Following Mass-Based Separation research articles, (2010) 2863–2870.
- [26] S.S. Thakur, T. Geiger, B. Chatterjee, P. Bandilla, F. Fröhlich, J. Cox, M. Mann, Deep and highly sensitive proteome coverage by LC-MS/MS without prefractionation., *Mol. Cell. Proteomics*. 10 (2011) M110.003699. doi:10.1074/mcp.M110.003699.
- [27] L.A. Weston, K.M. Bauer, A.B. Hummon, Comparison of bottom-up proteomic approaches for LC-MS analysis of complex proteomes, *Anal. Methods*. 5 (2013) 4615. doi:10.1039/c3ay40853a.
- [28] M.S. Heroux, M. a Chesnik, B.D. Halligan, M. Al-Gizawiy, J.M. Connelly, W.M. Mueller, S.D. Rand, E.J. Cochran, P.S. LaViolette, M.G. Malkin, K.M. Schmainda, S.P. Mirza, Comprehensive Characterization of Glioblastoma Tumor Tissues for Biomarker Identification using Mass Spectrometry-based Label-free Quantitative Proteomics., *Physiol. Genomics*. 46 (2014) physiolgenomics.00034.2014-.

doi:10.1152/physiolgenomics.00034.2014.

- [29] L.N.F. Darville, B.H.A. Sokolowski, In-depth proteomic analysis of mouse cochlear sensory epithelium by mass spectrometry, *J. Proteome Res.* 12 (2013) 3620–3630. doi:10.1021/pr4001338.
- [30] K.A. Jones, P.D. Kim, B.B. Patel, S.G. Kelsen, A. Braverman, D.J. Swinton, P.R. Gafken, L.A. Jones, W.S. Lane, J.M. Neveu, H.C.E. Leung, S.A. Shaffer, J.D. Leszyk, B.A. Stanley, T.E. Fox, A. Stanley, M.J. Hall, H. Hampel, C.D. South, A. De La Chapelle, R.W. Burt, D.A. Jones, L. Kopelovich, A.T. Yeung, Immunodepletion plasma proteomics by TripleTOF 5600 and Orbitrap Elite/LTQ-Orbitrap Velos/Q Exactive mass spectrometers, *J. Proteome Res.* 12 (2013) 4351–4365. doi:10.1021/pr400307u.
- [31] E. Mostovenko, C. Hassan, J. Rattke, A.M. Deelder, P.A. van Veelen, M. Palmblad, Comparison of peptide and protein fractionation methods in proteomics, *EuPA Open Proteomics.* 1 (2013) 30–37. doi:10.1016/j.euprot.2013.09.001.
- [32] Y. Wang, F. Yang, M.A. Gritsenko, Y. Wang, T. Clauss, T. Liu, Y. Shen, M.E. Monroe, D. Lopez-Ferrer, T. Reno, R.J. Moore, R.L. Klemke, D.G. Camp, R.D. Smith, Reversed-phase chromatography with multiple fraction concatenation strategy for proteome profiling of human MCF10A cells, *Proteomics.* 11 (2011) 2019–2026. doi:10.1002/pmic.201000722.
- [33] B. Manadas, J.A. English, K.J. Wynne, D.R. Cotter, M.J. Dunn, Comparative analysis of OFFGel, strong cation exchange with pH gradient, and RP at high pH for first-dimensional separation of peptides from a membrane-enriched protein fraction, *Proteomics.* 9 (2009) 5194–5198. doi:10.1002/pmic.200900349.
- [34] S. Magdeldin, K. Yamamoto, Y. Yoshida, B. Xu, Y. Zhang, H. Fujinaka, E. Yaoita, J.R. Yates, T. Yamamoto, Deep proteome mapping of mouse kidney based on OFFGel prefractionation reveals remarkable protein post-translational modifications, *J. Proteome Res.* 13 (2014) 1636–1646. doi:10.1021/pr401122m.
- [35] A.D. Catherman, K.R. Durbin, D.R. Ahlf, B.P. Early, R.T. Fellers, J.C. Tran, P.M. Thomas, N.L. Kelleher, Large-scale Top-down Proteomics of the Human Proteome: Membrane Proteins, Mitochondria, and Senescence, *Mol. Cell. Proteomics.* 12 (2013) 3465–3473. doi:10.1074/mcp.M113.030114.
- [36] T. Glatter, C. Ludwig, E. Ahrné, R. Aebersold, A.J.R. Heck, A. Schmidt, Large-scale quantitative assessment of different in-solution protein digestion protocols reveals superior cleavage efficiency of tandem Lys-C/trypsin proteolysis over trypsin digestion, *J. Proteome Res.* 11 (2012) 5145–5156. doi:10.1021/pr300273g.

- [37] X. Guo, D.C. Trudgian, A. Lemoff, S. Yadavalli, H. Mirzaei, Confetti : A Multiprotease Map of the HeLa Proteome for Comprehensive Proteomics * □, (2014) 1573–1584. doi:10.1074/mcp.M113.035170.
- [38] D. Wessel, U.I. Flügge, A method for the quantitative recovery of protein in dilute solution in the presence of detergents and lipids, *Anal. Biochem.* 138 (1984) 141–143. doi:10.1016/0003-2697(84)90782-6.
- [39] X. Duan, R. Young, R.M. Straubinger, B. Page, J. Cao, H. Wang, H. Yu, J.M. Canty, J. Qu, A straightforward and highly efficient precipitation/on-pellet digestion procedure coupled with a long gradient nano-LC separation and orbitrap mass spectrometry for label-free expression profiling of the swine heart mitochondrial proteome, *J. Proteome Res.* 8 (2009) 2838–2850. doi:10.1021/pr900001t.
- [40] S.C. Bendall, A.T. Booy, G. Lajoie, Proteomic Analysis of Pluripotent Stem Cells, in: *Curr. Protoc. Stem Cell Biol.*, John Wiley & Sons, Inc., Hoboken, NJ, USA, 2007. doi:10.1002/9780470151808.sc01b01s2.
- [41] J. Cox, M. Mann, MaxQuant enables high peptide identification rates, individualized p.p.b.-range mass accuracies and proteome-wide protein quantification, *Nat. Biotechnol.* 26 (2008) 1367–1372. doi:10.1038/nbt.1511.
- [42] T.U. Consortium, UniProt: a hub for protein information, *Nucleic Acids Res.* 43 (2014) D204–D212. doi:10.1093/nar/gku989.
- [43] S. Tyanova, T. Temu, P. Sinitcyn, A. Carlson, M.Y. Hein, T. Geiger, M. Mann, J. Cox, The Perseus computational platform for comprehensive analysis of (prote)omics data., *Nat. Methods.* 13 (2016) 731–40. doi:10.1038/nmeth.3901.

Chapter 3

Proteomic Characterization of Paracrine Signals Secreted by Multipotent Stromal Cells that Augment Blood Glucose¹

3.1 Introduction

In 2013, WHO reported that over 347 million people worldwide lived with diabetes, and estimated that this number will increase to 552 million by 2030, making diabetes a worldwide epidemic [1]. The Edmonton Protocol provided proof-of-concept that islet transplantation can temporarily reduce insulin dependence in individuals with type 1 diabetes [2]. Although islet replacement is an attractive strategy to combat diabetes, a critical shortage of donor islets and eventual rejection by continuing autoimmunity prevent the widespread application of this approach [3]. Bone marrow (BM)-derived stem cell transplantation has also been reported to promote endogenous islet regeneration in preclinical models, and represents a promising alternative strategy to combat diabetes [4].

Human multipotent stromal cells (hMSC) have become a focal point in recent clinical trials for tissue repair [5]. hMSC are readily available from autologous or allogenic donors, they are efficiently expanded in culture and they home to damaged tissues to initiate innate repair mechanisms [6].

¹ This chapter contains excerpts with permission from the following paper:

Kuljanin M, Bell GI, Sherman SE, Lajoie GA, Hess DA. (2017) "Proteomic Characterization Reveals Active Wnt-signaling by Human Multipotent Stromal Cells as a Key Regulator of B-cell Survival and Proliferation ". *Diabetologia*. 10: 1987-1998.

hMSC exert their therapeutic effects primarily through the secretion of trophic signals within damaged organs, or impact tissue repair from distant sites by secretion of regenerative effectors into the circulation within exosomes or microvesicles [7]. Exosomes harvested from hMSC contain pro-angiogenic proteins and promote the healing of ischemic tissue [8,9]. hMSC also secrete a wide variety of immunomodulatory molecules that dampen autoimmunity via modulation of immune cell functions [10,11]. Currently, the mechanisms underlying the regenerative and immunomodulatory effects of hMSC remain poorly understood, and better understanding of MSC protein secretion is required to harness the true regenerative capacity of hMSC.

In the context of diabetes, transplanted human BM-derived hMSC have been shown to promote repair of pancreatic islets and renal glomeruli in non-obese diabetic (NOD)/severe combined immunodeficiency (SCID) mice after β -cell ablation [6]. Although hMSC conversion into insulin-expressing beta-like cells has been demonstrated after stable induction of PDX1 [12], minimally manipulated hMSC did not adopt a β -cell phenotype after transplantation *in vivo*. In contrast, transplanted hMSC initiated endogenous islet recovery via paracrine stimulation [13]. In a series of publications, we have shown that human BM-derived hMSC stimulated the emergence of small, recipient-derived islet-like structures associated with the ductal epithelial niche within 7 days of injection into streptozotocin (STZ)-treated hyperglycemic NOD/SCID mice [14,15]. Unfortunately, hMSC samples showed donor-dependent variability in the capacity to improve glycemia and prolonged expansion *ex vivo* reduced islet regenerative prowess [14]. Thus, detailed proteomic

analyses of the islet regenerative hMSC secretome remain the key to understanding which protein signals promote islet regeneration in situ.

We compared the secretory protein profile of human BM-derived hMSC with or without islet regenerative capacity by performing global proteomic analysis of conditioned culture media (CM) after stable isotope labeling with amino acids in cell culture (SILAC) [16]. We hypothesized that islet regenerative hMSC will secrete a combination of unique protein factors that augment islet regeneration. In order to confirm our findings we also examined the effects of exogenous stimulation of Wnt signaling in hMSC for the survival and proliferation of human islet-derived β -cells *in vitro*. To our knowledge, this is the first proteomic study linking the human hMSC secretome profile with β -cell regenerative function and it highlights the importance of active Wnt signaling in the maintenance of hMSC-induced islet regeneration.

3.2 Results

3.2.1 Regenerative capacity of human hMSC was donor specific

Hyperglycemic (15–25 mmol/l), STZ-treated (35 mg/kg per day, days 1–5) NOD/SCID mice were i.v. injected on day 10 with hMSC (5×10^5) [14,17], and blood glucose levels were monitored for 42 days. Compared with PBS-injected control mice, hMSC samples ($N=3$) that showed significant reduction in systemic blood glucose from days 17–42 were termed hMSC^R and hMSC samples ($n=3$) that did not show blood glucose reduction (>25 mmol/l) were termed hMSC^{NR} (Figure 3.1a). There was a significant reduction in blood glucose AUC for hMSC^R vs. hMSC^{NR} samples (Figure 3.1b). Out of a total of 18 hMSC lines tested, six (~33%) were characterized as hMSC^R, four (~22%) demonstrated intermediate regenerative capacity and eight (~44%) were

characterized as hMSC^{NR}. hMSC lines with intermediate regenerative capacity were not used in this study. All hMSC^R and hMSC^{NR} lines possessed multipotent differentiation potential into adipogenic and osteogenic lineages *in vitro* [14, 15]. Cell surface phenotype showed that both hMSC^R and hMSC^{NR} expressed the stromal markers CD90 and CD105 (>95%) without expression of the pan-leukocyte marker CD45. hMSC donor information, including age, sex, weight and body mass index (BMI), is shown in Figure 3.1c.

3.2.2 *hMSC^R exclusively secreted proteins associated with active Wnt signaling*

We have previously shown that hMSC^R demonstrated increased transcription of matrix metalloproteases, EGF-family ligands and downstream products of Wnt-signaling [15]. Here, we sought to confirm and identify secreted protein targets that contribute to islet regeneration by comparing the secretome of hMSC^R and hMSC^{NR} samples using global MS-based proteomics coupled with SILAC. CM was harvested from each hMSC line (24 hrs) and analyzed in biological and technical duplicates. The total number of proteins detected for each hMSC sample is shown in Figure 3.2a. Proteins from each hMSC line were combined based on regenerative capacity and complete lists of secreted proteins detected exclusively in CM from hMSC^R or hMSC^{NR}, or proteins common to both groups, were generated (ESM Tables 3.1–3.3). Of 4665 total proteins detected (false discovery rate 1%), 3023 (~65%) were produced by both hMSC^R and hMSC^{NR}, 850 (~18%) were produced by hMSC^R exclusively, while 792 (~17%) were produced by hMSC^{NR} exclusively (Figure 3.2b). Gene ontology using cellular component analysis revealed that hMSC^R CM contained qualitatively more proteins with

extracellular localization (21% vs. 14%), while hMSC^{NR} CM contained more membrane-bound proteins (23% vs. 19%) (Figure 3.2c). Moving forward, protein lists were filtered to include only extracellular (secreted) and membrane-bound proteins, and were further analyzed for known biological functions and signaling family association.

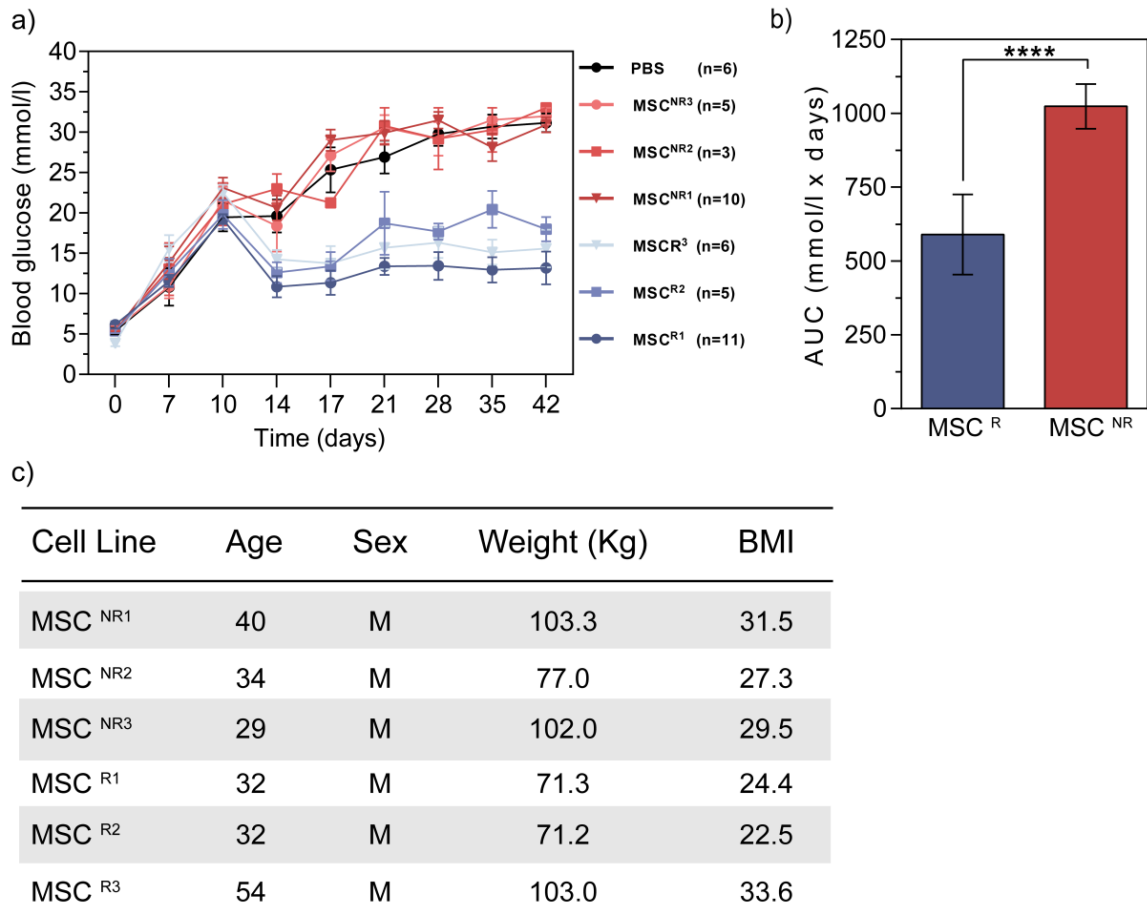


Figure 3.1 Functional characterization of islet hMSC^R and hMSC^{NR}. (a) MSCs from six donors were injected into STZ-treated (35 mg/kg per day, days 1–5) NOD/SCID mice on day 10, and blood glucose was monitored weekly until 42 days to segregate hMSC^R (blue) vs. hMSC^{NR} (red) samples compared with PBS-injected control mice (black). Blood glucose concentrations were lower after injection of hMSC^R compared with hMSC^{NR} samples. (b) Blood glucose AUC was significantly reduced with hMSC^R (n = 3) (blue) vs. hMSC^{NR} (n = 3) (red) samples. (c) Donor characteristics were similar between hMSC^{NR} and hMSC^R samples. Data are presented as mean \pm SEM. *** $p < 0.001$

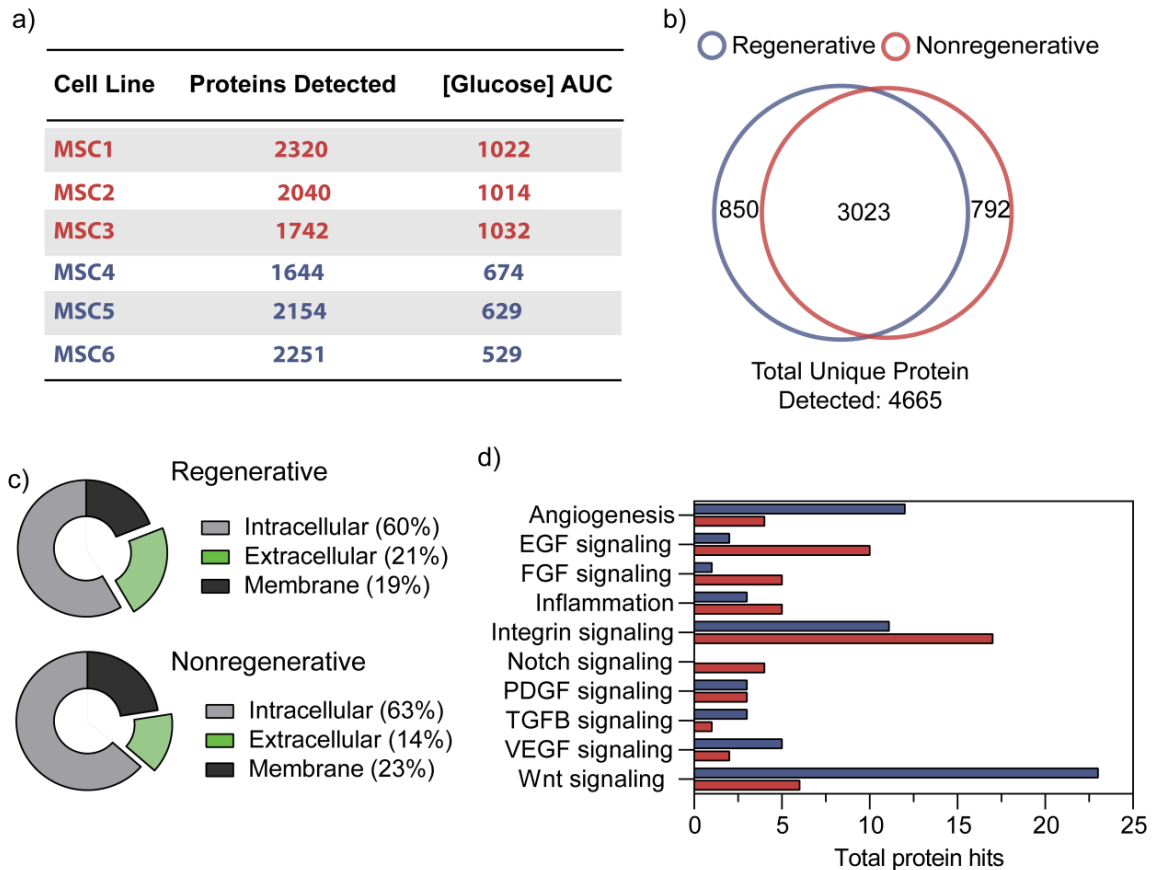


Figure 3.2 Qualitative analyses of proteins exclusively secreted by hMSC^R or hMSC^{NR}. (a) Total proteins identified for hMSC^R (blue) and hMSC^{NR} (red) lines using SILAC. (b) Venn diagram showing that out of the 4665 total proteins detected, 850 were unique to hMSC^R (blue) and 792 were unique to hMSC^{NR} (red). (c) hMSC^R demonstrated a higher proportion of proteins with extracellular (secreted) localization compared with hMSC^{NR}. (d) hMSC^R secreted more proteins associated with the activation of Wnt signaling and angiogenesis. hMSC^{NR} secreted more proteins associated with EGF, FGF and Notch signaling.

hMSC^R demonstrated increased representation of secreted proteins associated with angiogenesis and activation of the Wnt-signaling pathway, while hMSC^{NR} showed increased secretion of proteins associated with EGF, FGF and Notch signaling pathways (Figure 3.2d). hMSC^R exclusively secreted several proteins associated with cell survival and growth, such as FGF7 and bone morphogenetic protein (BMP) 4. Pro-angiogenic factors vascular endothelial growth factor receptor 2 (KDR), vascular endothelial growth factor receptor 4 (FLT4) and regulators of angiogenesis A disintegrin and metalloproteinase with thrombospondin motifs (ADAMTS)13 and 18 were also unique to the hMSC^R secretome [18]. Notably, hMSC^R secreted potentiators of Wnt signaling (spondins), ligand activators of Wnt-signaling (WNT5B) and downstream products of Wnt-signaling that modify the extracellular matrix (ECM) (Wnt-inducible signaling pathway protein 2 [WISP2/CCN5]) (Table 3.1) [19–21]. In contrast, proteins exclusively detected in hMSC^{NR} CM included positive and negative regulators of angiogenesis (FGF receptor (FGFR) 4, FLT1) [18,22], and an abundance of pro-inflammatory cytokines (IL-6, IL-8) and C-X-C motif chemokines (CXCL2, 3, 5) (Table 3.2) [23]. Collectively, these findings suggested hMSC^R actively secreted cell growth supportive factors with reduced secretion of common pro-inflammatory signals, and only hMSC^R showed production of multiple effectors associated with active Wnt signaling.

Table 3.1 Exclusively detected proteins in CM from hMSC^R. A table outlining highly confidence protein secreted factors that are involved in angiogenesis, inflammation, matrix remodeling and Wnt-signaling.

Gene Symbol	Protein Name	Biological Function
ADAMTS13	A disintegrin and metalloproteinase with thrombospondin motifs 13	Matrix metalloproteinase
ADAMTS18	A disintegrin and metalloproteinase with thrombospondin motifs 18	Matrix metalloproteinase
EGF	Epidermal growth factor	Regulator of cell growth, proliferation and differentiation
FGF7	Fibroblast growth factor 7	Tissue repair, mitogenic cell survival
FLT4	Vascular endothelial growth factor receptor 3	Secretion of VEGFA/C
IGF2	Insulin-like growth factor 2	Growth promoting hormone
KIT	Mast/stem cell growth factor receptor Kit	Migration, survival and proliferation of stem cells
KDR	Vascular endothelial growth factor receptor 2	Regulation of angiogenesis and vascular development
MMP10	Stromelysin-2	Matrix metalloproteinase
MMP12	Macrophage metalloelastase	Matrix metalloproteinase
MMP3	Stromelysin-1	Matrix metalloproteinase
PDGFD	Platelet-derived growth factor D	Regulation of cell proliferation, migration and chemotaxis
SPON2	Spondin 2	Activator of Wnt signaling
TIMP4	Metalloproteinase inhibitor 4	Matrix metalloproteinase inhibitor
WISP2	Wnt1-inducible-signalling pathways protein 2	CCN5, regulator of cell growth
WNT5A	Protein Wnt5b	Activator of Wnt signaling

Table 3.2 Exclusively detected proteins in CM from hMSC^{NR}. A table outlining highly confidence protein secreted factors that are involved in angiogenesis, inflammation, matrix remodeling and Wnt-signaling

Gene Symbol	Protein Name	Biological Function
CXCL2	C-X-C motif chemokine 2	Inflammatory response
CXCL3	C-X-C motif chemokine 3	Inflammatory response
CXCL5	C-X-C motif chemokine 5	Inflammatory response
GDF15	Growth/differentiation factor 15	Regulator of inflammation and apoptosis
FLT1	Vascular endothelial growth factor receptor 1	Negative regulator of vascular growth factor A signaling
FGFR4	Fibroblast growth factor receptor 4	Regulation of angiogenesis and vascular development
FZD1	Frizzled-1	Wnt-signaling receptor
FZD2	Frizzled-2	Wnt-signaling receptor
FZD7	Frizzled-7	Wnt-signaling receptor
IL-1 β	Interleukin-1 beta	Inflammatory response
IL-6	Interleukin-6	Inflammatory response
IL-8	Interleukin-8	Inflammatory response
MMP11	Stromelysin-3	Matrix metalloproteinase
NOV	Protein NOV homologue	CCN3, promoter of cell differentiation
TGFBR2	Transforming growth factor beta receptor type-2	Regulator of cell growth, proliferation and differentiation

3.2.3 Quantification of Wnt, matrix remodeling and pro-angiogenic proteins

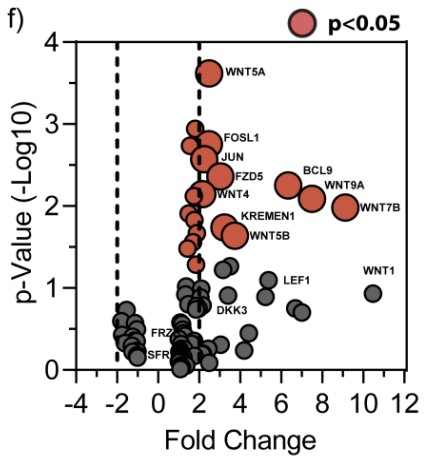
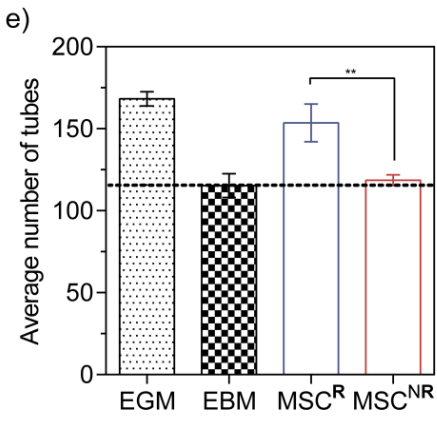
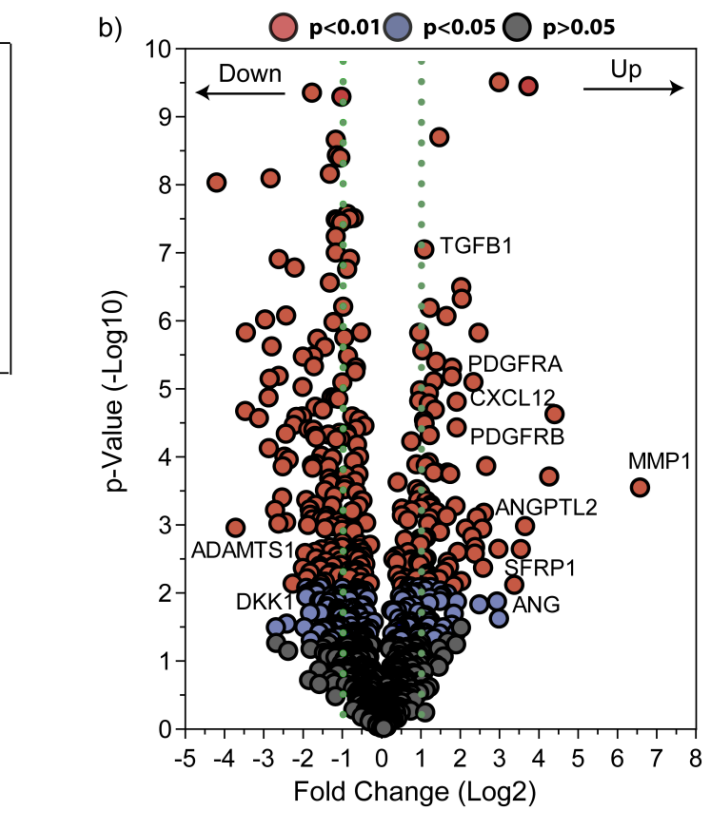
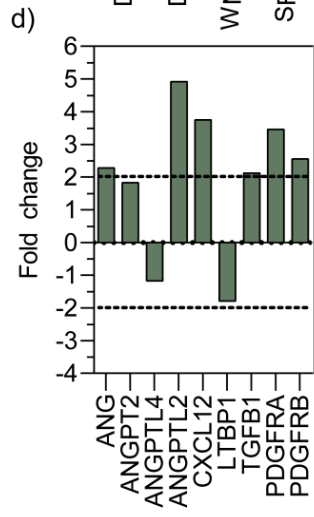
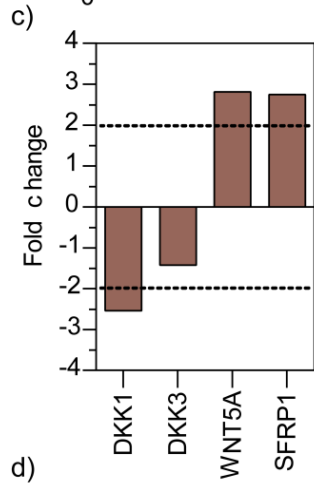
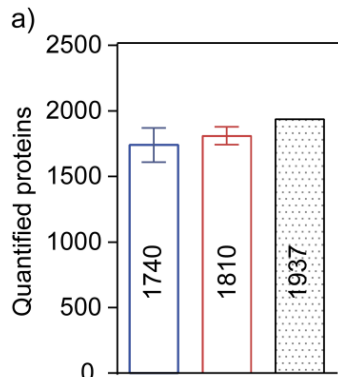
To quantify proteins secreted by both hMSC^R and hMSC^{NR}, quantitative proteomics was performed using label-free quantification [16,24] to identify proteins differentially secreted into serum-containing media. Lists were filtered to include only secreted and membrane-bound proteins, and 1038 common proteins were quantified to generate lists of differentially expressed proteins (ESM Table 3.4). We did not observe any significant difference in the total number of proteins quantified between samples (Figure 3.3a), and 468 proteins were differentially expressed between hMSC^R vs. hMSC^{NR} samples ($p < 0.05$, Figure 3.3b). Upregulated proteins in hMSC^R CM included matrix remodeling proteins (matrix metalloproteinase (MMP)1, MMP3, ADAMs and BMPs) [25,26], effectors of Wnt-signaling (WNT5A, secreted frizzled-related protein 1 [SFRP1]) (Figure 3.3c) [20], additional targets implicated in angiogenesis (angiogenin [ANG], angiopoietin [ANGPT]1, ANGPTL2, TGFB1, TGFB2, platelet-derived growth factor receptor [PDGFR] A, B) [22,27] and chemokines involved in cell recruitment (CXCL12) (Figure 3.3d) [21,28]. Thus, the activation of Wnt and pro-angiogenic signaling again correlated with islet regenerative potency. Conversely, the negative regulator of Wnt-signaling Dickkopf-related protein (DKK)1 was increased ~2.5-fold in hMSC^{NR} CM, and negative regulators of angiogenesis (ADAMTSs, thrombospondin [THBS] 1 and THBS2) and inhibitors of matrix remodeling proteins (metalloproteinase inhibitor [TIMP] 3) were increased in hMSC^{NR} CM [29]. HMVECs were cultured on growth factor-reduced Geltrex to assess the angiogenic potential of hMSC CM *in vitro* (Figure 3.3e). A significant increase in the tubule formation was observed

when HMVECs were cultured using CM from hMSC^R compared with hMSC^{NR}. Representative photomicrographs of tube formation after 24 hrs are shown in Figure A3.1. Finally, we identified that pro-differentiation proteins associated with Notch signaling were upregulated in hMSC^{NR} (NOTCH2, JAG-1) [30], suggesting that inhibited Wnt and angiogenic signaling and activated Notch signaling was associated with diminished islet regenerative capacity.

3.2.4 hMSC^R increased expression of Wnt pathway mRNA

To confirm the activation of Wnt-signaling in hMSC^R, we assessed mRNA expression of 84 genes related to Wnt-pathway signal transduction, using three hMSC^R and three hMSC^{NR} lines performed in duplicate. Transcripts with differential expression greater than two fold between hMSC^R vs. hMSC^{NR} revealed 18 significantly changing genes (Figure 3.3f), normalized to the geometric mean of three housekeeping genes: ACTB, B2M and HPRT1, that did not show significant variation across samples. Notably, all differentially expressed mRNAs (18 genes) were upregulated in hMSC^R, and no significantly changing genes were down regulated. Upregulation of WNT5A/B in hMSC^R was confirmed at the mRNA level. Other upregulated mRNA in hMSC^R included transcription factors (FOSL1, JUN) and receptors associated with Wnt-signaling (FZD5) [19,31]. Taken together, upregulation of Wnt-signaling at the mRNA and protein level strongly suggests active Wnt-signaling during expansion was a unique and conserved characteristic that correlated with the reduction of hyperglycemia after transplantation of hMSC^R *in vivo*.

Figure 3.3 Quantitative analyses of proteins secreted by both hMSC^R and hMSC^{NR}. (a) Total number of proteins quantified within all three hMSC^R (blue), hMSC^{NR} (red) samples and total number of quantified proteins (grey). (b) Representative volcano plot of differentially expressed secreted proteins. A change greater than twofold is represented outside the green boundaries. (c) hMSC^R showed increased secretion of Wnt activators (Wnt5A), while hMSC^{NR} showed increased secretion of Wnt inhibitors (DKK1). (d) hMSC^R demonstrated increased secretion of pro-angiogenic proteins, TGFB1 and SDF-1 (CXCL12). (e) Spontaneous tubule formation of HMVECs on growth factor-reduced Geltrex was increased when cultured using CM generated from hMSC^R compared with hMSC^{NR}. (f) Quantitative PCR for Wnt-signaling related transcripts in hMSC^R compared to hMSC^{NR}. Data are presented as mean \pm SD. **p < 0.01



3.2.5 *hMSC show activation of Wnt-signaling via accumulation of nuclear β -catenin*

Canonical Wnt-signaling converges on the actions of β -catenin, a transcription factor that increases the expression of downstream effectors of Wnt signals [32]. We mimicked Wnt-signaling in hMSC^{NR} and hMSC^R using a small molecule (CHIR99201) inhibitor of GSK3. GSK3 actively phosphorylates β -catenin, which marks it for ubiquitination and degradation. Therefore, inhibition of GSK3 leads to stabilization and accumulation of free β -catenin [19]. hMSC samples showed maximal increases in total β -catenin using 5–10 μ mol/l CHIR99201 for 24–48 h. We then used confocal microscopy to visualize the accumulation of nuclear β -catenin (Figure 3.4). Compared with DMSO control cells (Figure 3.4a), hMSC^{NR} and hMSC^R stimulated with 10 μ mol/l CHIR99201 showed increased nuclear β -catenin localization (Figure 3.4b, c). Next, hMSC^{NR} and hMSC^R samples were analyzed in quadruplicate to quantify total β -catenin levels by flow cytometry (Figure 3.5d). Representative dot plots are shown in Figure A3.2. Compared with DMSO control cells, both hMSC subtypes treated with CHIR99201 showed significantly increased total β -catenin. Thus, inhibition of GSK3 with CHIR99201 mimicked activated Wnt signaling in hMSC^R and hMSC^{NR}.

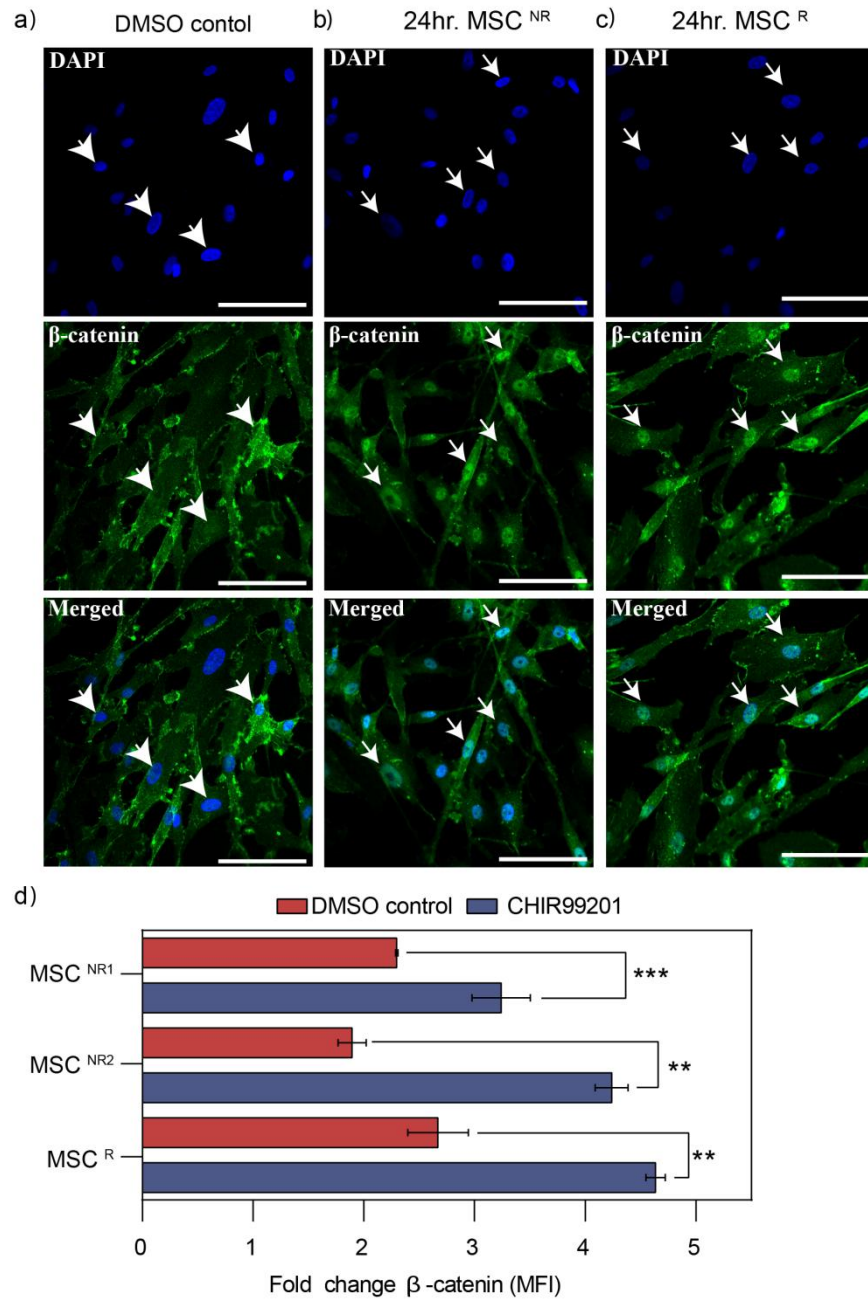
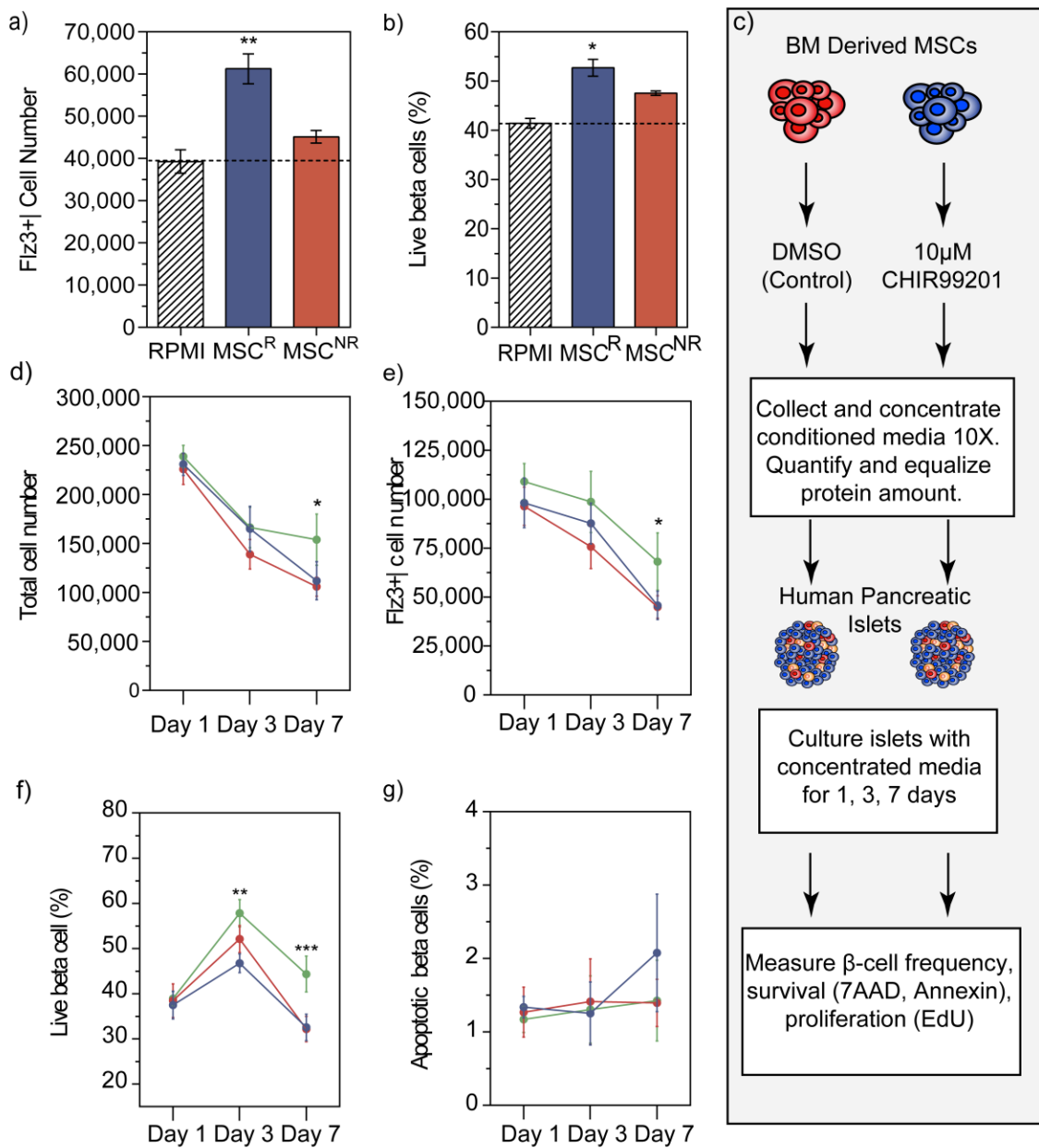


Figure 3.4 hMSC treatment with GSK3 inhibitor induced nuclear β -catenin localization. Representative photomicrographs showing hMSC^R and hMSC^{NR} stained for β -catenin (green) and DAPI (blue) after treatment with (a) DMSO vehicle, (b) CHIR99201 (24 h) hMSC^{NR}, (c) CHIR99201 (24 h) hMSC^R. White arrows indicate examined nuclei with nuclear staining and arrowheads indicate examined nuclei without nuclear staining. Scale bars, 50 μ m. (d) Intracellular β -catenin was increased in both hMSC^R and hMSC^{NR} treated with CHIR99201 (grey bars) or DMSO control (white bars). Data are presented as mean \pm SEM. ** $p < 0.01$, *** $p < 0.001$

3.2.6 GSK3 inhibition in hMSC^{NR} generates CM that improves human β -cell survival *in vitro*

To assess whether hMSC^R CM could improve β -cell survival *in vitro*, we cultured primary human islet preparations for up to 7 days in CM from hMSC^R and hMSC^{NR}, and performed multiparametric flow cytometry to analyze β -cell survival and proliferation. Human islets were obtained through the Integrated Islet Distribution Program (IIDP). Compared with hMSC^{NR} CM, human islets grown in hMSC^R CM showed increased total number of β -cells (Figure 3.5a) and an increased frequency of live β -cells (Figure 3.5b) after 7 days of culture. To further assess the influence of active Wnt-signaling on islet regenerative paracrine function, we also assessed whether CM generated by hMSC^{NR} treated with a GSK3 inhibitor (CHIR99201) during expansion could promote human β -cell survival or proliferation in cultured human islets. CM recovered from hMSC^{NR} cultured with vehicle control (DMSO) only (basal CM) was compared with CM recovered from hMSC^{NR} treated with 10 μ mol/l CHIR99201 (GSK3i CM) (Figure 3.5c). Five independent human islet samples were cultured as indicated in Figure A3.3. At each time point, human islets were harvested, dissociated with trypsin, and stained using Fl3 to estimate β -cell frequency, 7AAD to determine cell viability and Annexin-V to determine apoptosis rates by multiparametric flow cytometry. Representative dot plots are shown in Figure A3.4. Compared with basal CM, human islets grown in CM generated by GSK3-inhibited hMSC^{NR} showed increased total cell numbers (Figure 3.5d), β -cell numbers (Figure 3.5e) and the proportion of live (7AAD) β -cells at 7 days culture (Figure 3.5f). However, no significant changes in the frequency of apoptotic β -cells were observed (Figure 3.5g).

Figure 3.5 Culture of human islets in GSK-inhibited CM increased β -cell number. Human islets cultured in CM generated from hMSC^R showed (a) increased β -cell number and (b) increased proportion of live β -cells after 7 days of culture. (c) Human islets were cultured in CM generated by hMSC^{NR} treated with DMSO (basal CM) or CHIR99201 (GSK3i CM). Compared with human islets cultured in basal CM (red) and RPMI (blue), islets cultured in GSK3-inhibited CM (green) showed increased (d) cell number, (e) β -cell number and (f) proportion of live β -cells at day 7. (g) Human islets cultured in hMSC^{NR} CM did not alter apoptotic β -cell frequency. Data are presented as mean \pm SEM. *p < 0.05, **p < 0.01, ***p < 0.001



To determine whether increased β -cell number was augmented by increased β -cell proliferation *in vitro*, we measured EdU incorporation in insulin⁺ β -cells. At each time point, human islets were harvested, permeabilized, stained for intracellular insulin and proliferation was detected by EdU incorporation using the Click-It system. Compared with basal CM, islet exposure to CM generated by GSK3-inhibited hMSC^{NR} increased the overall frequency of proliferating cells (Figure 3.6a) and proportion of total proliferating β -cells (Figure 3.6b). Finally, islet donor variability was documented by donor information including age, sex, BMI and average blood glucose levels (Figure 3.6c). Collectively, these data suggest that CM generated from hMSC^{NR} treated with CHIR99201 promoted β -cell survival and induced β -cell proliferation *in vitro*.

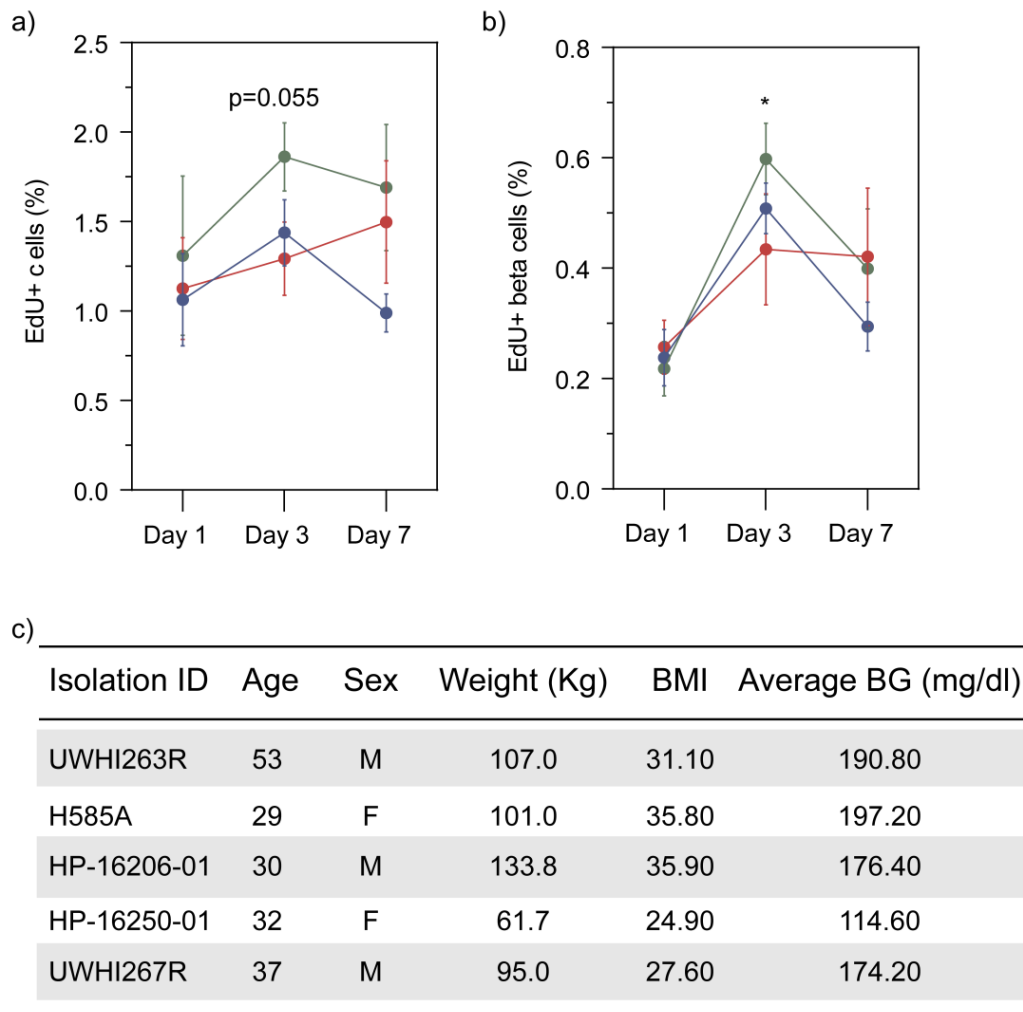


Figure 3.6 Culture of human islets in GSK-inhibited CM increased β -cell proliferation. (a, b) Compared with human islets cultured in basal CM (red) and RPMI (blue), islets cultured in GSK3i CM (green) showed increased proportion of insulin⁺/EdU⁺ β -cells at day 3. (c) Islets were obtained through the IIDP from five independent donors with variable weight, BMI and average blood glucose (Avg.BG) values. Data are presented as mean \pm SEM. *p < 0.05

3.3 Discussion

We used comprehensive SILAC-based proteomic analyses to identify hMSC-secreted factors that correlated with the capacity to lower circulating blood glucose after transplantation into STZ-treated NOD/SCID mice. hMSC^R, demonstrated with glucose-lowering capacity after transplantation, secreted proteins associated with cell growth, matrix remodeling, immunosuppressive and pro-angiogenic properties. In contrast, hMSC^{NR}, which lacked islet regenerative functions, secreted proteins involved in the initiation of inflammation and the negative regulation of angiogenesis. Notably, hMSC^R consistently demonstrated mRNA and protein expression associated with active Wnt-signaling, a novel signature that correlated with islet regenerative capacity. Inhibition of GSK3 activity with CHIR99201 mimicked Wnt-signaling in hMSC^{NR} and resulted in the generation of CM that supported β -cell survival and proliferation within cultured human islets *in vitro*. Thus, we report a central role for Wnt-signaling in the establishment of an islet regenerative secretory profile in hMSC^R, and improve our understanding of hMSC-secreted signals governing islet regeneration. We predict this data set will aid in the development of future therapies to augment islet regeneration during diabetes.

Functional β -cells secrete pro-angiogenic proteins responsible for recruiting circulating or tissue resident progenitor cells to islets after damage [33]. However, during autoimmunity or after islet isolation and transplantation these critical functions are likely to be dysregulated, resulting in transient ischemia that significantly impairs islet function [34]. Increased production of potent pro-angiogenic factors, such as FGF7, PDGF and VEGFA, by hMSC^R

underscores the functional capacity to generate a pro-angiogenic microenvironment. Collectively these proteins potently stimulate human islet vascularization *in vitro* [35]. To validate the functional relevance of pro-angiogenic secretory patterns, hMSC^R CM showed increased capacity to induce spontaneous tubule formation by HMVEC compared with hMSC^{NR} CM. Interestingly, hMSC^{NR} primarily secreted negative regulators of angiogenesis such as FLT1 and FGFR4, which have both been shown to inhibit the signal cascade mediated by VEGFA [18]. We have previously shown that intrapancreatic transplantation of pro-angiogenic hematopoietic progenitor cells induced islet revascularization and β -cell proliferation and augmented systemic insulin release in STZ-treated NOD/SCID mice [15]. Therefore, our data suggest hMSC^R may also formulate a pro-angiogenic microenvironment to support β -cell survival and function within endogenous or transplanted islets.

The prevention of pro-inflammatory states within damaged islets may also be relevant in the context of hMSC therapy for type 1 diabetes. The presence of central mediators of inflammation in CM from hMSC^{NR}, such as IL-1beta, IL-6 and IL-8, suggests that hMSC^{NR} may contribute to pro-inflammatory cascades. In people with type 1 diabetic, β -cell destruction is initiated by a combination of pro-inflammatory cytokines, including IL-1beta and IL-6 [36], and CXCL family chemokines, leading to recruitment of immune effectors that mediate β -cell destruction [37]. Furthermore, high levels of IL-8 have been linked to elevated non-essential fatty acids (NEFA), which can signal inflammatory cascades in the pancreas [38]. In contrast, these cytokines and chemokines were not secreted by hMSC^R. Rather, hMSC^R

secreted cytokines that could potentially reduce inflammation. For example, TGF-beta suppresses the secretion of various inflammatory cytokines/chemokines, and induces cytokine secretion patterns that balance local immunity [39]. Stromal cell-derived factor 1 (CXCL12), also upregulated by hMSC^R, has been shown to directly promote β -cell survival through the activation of AKT [40]. Collectively, we propose hMSC^R generate a niche with reduced inflammation, improving β -cell survival, while hMSC^{NR} contribute to a more deleterious pro-inflammatory microenvironment.

Inadequate β -cell mass leads to hyperglycemia in both type 1 and type 2 diabetes. Currently, there is significant interest in restoration of β -cell mass through induction of endogenous regenerative mechanisms in situ using cellular or protein therapies. Our previous transplantation studies suggested that human BM-derived hMSC stimulate an islet regeneration program with neogenic characteristics. Mice transplanted with hMSC^R, demonstrated improved glycemia control via the emergence of small β -cell clusters associated with the ductal epithelium [14]. Several identified effectors may act in synergy to mediate islet regenerative processes. First, hMSC^R showed increased secretion of EGF previously shown to increase β -cell mass in rodents by stimulating β -cell replication [41]. However, EGF receptor signaling was required for expansion of murine β -cell mass in response to a high-fat diet, but was not crucial for neo-islet formation after pancreatic ductal ligation [42]. Second, the CCN family of extracellular matrix-associated, heparin-binding proteins has been shown to modulate cell growth and repair in many tissues by increasing the bioavailability of BMPs, VEGF, Wnt and TGF ligands [43]. More specifically, connective tissue growth factor (CTGF) or CCN2 has

been widely studied during β -cell development [44]. Within our data set, hMSC^R exclusively secreted CCN5). Previously, we have identified WISP1 (encoding CCN4) and WISP2 (encoding CCN5) mRNA as being upregulated in hMSC^R [15]. Importantly, CCN4 and CCN5 secretion is directly linked to active Wnt-signaling. CCN5 also represents a link between insulin and IGF-I regulation in islet function, and CCN5 over expression leads to increased islet cell growth *in vitro* [45]. Interestingly, hMSC^{NR} exclusively secreted nephroblastoma overexpressed protein or NOV isoform (CCN3), which has been shown to impair β -cell proliferation and inhibit glucose-stimulated insulin secretion *in vitro* [44]. Thus, we predict modification of the ECM via Wnt-inducible CCN protein regulation is a critical step in islet regenerative processes.

One of the key differences between hMSC^R and hMSC^{NR} was the activation of Wnt-signaling. Wnt-signaling is highly conserved in primitive hMSC and is involved in multiple developmental processes, including cell proliferation, growth and fate determination. Aly and colleagues have shown that delivery of WNT3A and R-spondin to cultured islets increased the proliferation of adult human β -cells [46]. Our data suggests that hMSC^R propagate Wnt-signaling primarily by autocrine secretion of WNT5A/B ligands with potential regulation by SFRP1. In contrast, hMSC^{NR} expressed proteins that inhibit Wnt-signaling, namely DKK1 and DKK3. Although more research is required to determine potential effects of WNT5 signaling on human β -cells, it is clear that hMSC^R maintain active canonical Wnt-signaling and increase secretion of downstream effectors that promote β -cell regeneration. By inhibiting GSK3 activity using CHIR99201, we have shown that the activation

of canonical Wnt pathway signals in hMSC^{NR} can mimic Wnt-signaling allowing accumulation of nuclear β -catenin. Human pancreatic islets grown in media conditioned by hMSC^{NR} treated with CHIR99201 showed increased β -cell survival and proliferation during 7 days of culture. Manipulation of Wnt-signaling through the inhibition of GSK3 has been previously suggested to directly increase β -cell proliferation. One study treated diabetic neonates with LiCl, a known inhibitor of GSK3, and doubled β -cell mass in rat models of diabetes [47]. Others have inhibited GSK3 using small molecules to regulate islet cell survival and proliferation *in vitro* [48]. Although, the mechanisms by which inhibition of GSK3 affects β -cell survival and proliferation *in vivo* is still unclear, our results suggest that activation of Wnt-signaling in pancreas-resident stromal cells may have practical application in β -cell regenerative therapies. Nonetheless, activation of Wnt-signaling during hMSC culture increased the regenerative capacity of hMSC^{NR} by altering downstream secretory patterns.

In summary, our data outlines several dynamic and complementary pathways that formulate a regenerative microenvironment applicable to the development of islet expansion therapies for diabetes using hMSC or their secretory products. The proteomic data reported in this study will be used in future studies to characterize functional mechanisms relevant to islet regeneration, or as screening technology to select hMSC subpopulations that possess augmented capacity to regenerate islets *in situ*.

3.4 Experimental Methods

3.4.1 Transplantation of human derived hMSC

Human BM was obtained from healthy donors after informed consent at the London Health Sciences Centre (London, ON, Canada). All studies were approved by the Human Research Ethics Board at Western University (REB#12934, 12252E). The hyperglycemia-lowering capacity of six hMSC samples was assessed after tail vein injection of 500,000 cells into STZ-treated NOD/SCID mice as previously described [14]. Blood glucose concentrations were monitored weekly for 42 days and samples were segregated into regenerative (hMSC^R) or non-regenerative (hMSC^{NR}) based on the ability to reduce blood glucose compared with PBS-injected control mice.

3.4.2 hMSC culture and SILAC labeling

hMSC were expanded in AmnioMax media (Invitrogen). At passage 3, hMSC were switched to custom AmnioMax that contained no L-arginine or L-lysine. Heavy [¹³C₆, ¹⁵N₄] L-arginine and [¹³C₆, ¹⁵N₂] L-lysine were added into SILAC media at 87.8 mg/l and 52.2 mg/l, respectively (Silantes). Excess unlabelled L-proline was added to prevent conversion of heavy arginine into heavy proline [49]. hMSC were grown in SILAC media for 9 days to achieve >95% label incorporation.

3.4.3 Generation of labeled CM and proteomic workflows

After 9 days of labeling in SILAC media, hMSC were washed twice with PBS to remove residual growth factors and replated in basal AmnioMaxTM without supplement to collect proteins secreted by labeled hMSC for 24h.

Media conditioned by hMSC was collected, filtered and centrifuged at 450 x g to remove any cellular debris. Cell viability was assayed using trypan blue and >95% viability was used as a standard cut-off for secretome analyses. CM was generated in biological and technical duplicate for a total of 6 individual hMSC lines and was concentrated using 3 kDa molecular weight cut-off filter units (Millipore). Pelleted cells were harvested and lysed to determine isotopic label incorporation. Concentrated CM was lyophilized overnight and re-suspended in 8M urea, 50 mM ammonium bicarbonate, 10 mM dithiothreitol and 2% SDS solution prior to protein quantitation and fractionation. Protein concentration was measured using the Pierce 660 nm protein assay (ThermoFisher Scientific).

3.4.4 SDS-PAGE Fractionation and mass spectrometry

Protein samples generated from hMSC CM were subjected to 1D SDS-PAGE fractionation using in-house made 12% gels in technical duplicate. Briefly, 150 µg of total protein was loaded onto each gel generating 10 fractions. Each band was subsequently digested using an in-gel protocol with trypsin (Promega), as previously described. Fractions were quantified using the BCA assay (ThermoFisher Scientific) and approximately 1 µg of material was injected per fraction. Each fraction was injected and separated using a nanoAcquity system (Waters) on a 25 cm long x 75 µm inner diameter C18 column (Waters), maintained at 35°C. All samples were trapped for 5 min at 99% H₂O, 1% acetonitrile, and separated using a 5.0% to 37.5% acetonitrile gradient over 80 min, followed by 95% acetonitrile over 5 min, at a flow rate of 300 nL/min. Mass spectrometry was performed using a Q Exactive (ThermoFisher Scientific). Full MS parameters are outlined in Table A3.1.

3.4.5 Proteomic data analysis

Qualitative data analysis was performed using PEAKS 7.5 software (Bioinformatics Solutions Inc.). Briefly, raw data files were refined using correct precursor mass only and de novo sequencing was performed using the following parameters: parent mass tolerance 20 ppm; fragment ion tolerance 0.05 Da; enzyme was set to trypsin; fixed modifications, carbamidomethylation; and variable modifications included: deamidation (NQ), oxidation (M), +10 Da on arginine and +8 Da on lysine for SILAC labeling. Data were searched against the Uniprot human sequence database (updated May 2014, 20178 entries). Quantitative data analysis was performed using MaxQuant version 1.5.2.8 30. All parameters were set to as described above. Match between runs was enabled and all other parameters left at default. Data was analyzed using label free quantitation (LFQ) as described previously 30. Bioinformatic analysis was performed using Perseus version 1.5.0.8. Briefly, protein lists were loaded into Perseus. Proteins identified by site, reverse and contaminants were removed manually 20. Gene annotation was performed with the online software tool PANTHER version 9.0.

3.4.6 HMVEC tubule forming assay

To assess CM influence on endothelial cell function *in vitro*, 120,000 human microvascular endothelial cells (HMVECs) were cultured on growth factor-reduced Geltrex (Life Technologies) in endothelial basal media (EBM-2; Lonza) conditioned by hMSC^R and hMSC^{NR} for 24 h. As a positive control, HMVECs were also grown in Geltrex bathed in complete endothelial growth medium (EGM-2 = EBM-2 + 5% FBS + IGF, basic fibroblast growth factor [FGF], EGF, vascular endothelial growth factor [VEGF]). Tube formation was

quantified by counting the number of complete tubule branches in four fields of view using ImageJ software (NIH).

3.4.7 qRT-PCR of the Wnt-signaling pathway

RNA was purified in duplicate from three regenerative and three non-regenerative hMSC cell lines using the PerfectPureTM RNA Cultured Cell Kit according to the manufacturer instructions (5PRIME). RNA quality and quantity was assessed using NanoDrop. Subsequently, cDNA was synthesized using the High Capacity cDNA Reverse Transcription Kit with RNase inhibitor (Invitrogen). Real-time PCR was performed using SYBR[®] Green along with the human WNT-Signaling Pathway PCR Array, which contained 84 genes related to Wnt signal transduction using the 384 well formats (Qiagen). Samples were incubated at 50°C for 2 minutes followed by 10 min at 95°C. DNA was amplified at 95°C for 15 s followed by 1 min at 60°C for 40 cycles, using the Bio-Rad CFX384 Real-Time PCR Detection System (Bio-Rad). All samples were analyzed using the RT² Profiler PCR Array Data Analysis version 3.5 online (Qiagen). Samples were normalized using the geometric mean of three housekeeping genes.

3.4.8 Confocal microscopy for total β -catenin

hMSC were cultured in 6-well plates on glass cover slips and treated using the following concentrations of GSK3 inhibitor CHIR99021 (EMD Millipore): DMSO (vehicle control), (250 nM, 500 nM, 1 μ M, 5 μ M, 10 μ M) for 6, 12, 24, and 48 hrs in AmnioMaxTM media + supplement. hMSC were fixed in 10% formalin (Sigma), permeabilized in 1% triton X-100 and treated with goat block. Cells were incubated with rabbit anti-human β -catenin antibody

(1/200) (Abcam) and detected with goat anti-rabbit fluorescein antibody (Vector Laboratories). The cover slips were mounted using Vectashield with DAPI. Confocal microscopy was performed at the London Regional Confocal Microscopy Core Facility (London, ON) using the FV1000 microscope (Olympus).

3.4.9 Flow cytometry for total β -catenin

hMSC were treated for 24 h with 10 μ M of CHIR99021 inhibitor or DMSO (control). Cells were harvested and fixed using 10% formalin and permeabilized using Saponin buffer as indicated by manufacturer's instructions (Life Technologies). FITC conjugated β -catenin antibody was diluted into the cell suspension according to the manufacturer's instruction (EBioscience). Samples containing isotype controls for the primary antibody were used. All flow cytometry data were collected at the London Regional Flow Cytometry Facility (London, ON) using an LSR II flow cytometer (Beckton Dickinson) and analysis was performed using FACSDIVA software (BD Biosciences). Geometric mean fluorescent intensities (gMFI) were reported compared to isotype control.

3.4.10 Human islet culture with MSC CM

Human islets from five donors were obtained from the Integrated Islet Distribution Program (IIDP). Upon arrival, 200 islet equivalents were plated in RPMI media without serum (Invitrogen). hMSC CM was collected after 24 h from hMSC treated with DMSO (basal CM) or with 10 μ mol/l of CHIR99021 (GSK3i CM). CM was concentrated using 3 kDa molecular mass cut-off filters, and \sim 1.0 μ g/ μ l total protein was added to human islet culture for 1, 3 or 7 days

(Figure A3.2). After islet harvest and dissociation, β -cell content was estimated using FluoZin-3 (Flz3) (ThermoFisher Scientific) and apoptosis was quantified using 7AAD and Annexin-V. To detect islet cell proliferation, 500 nmol/l of 5-ethynyl-2'-deoxyuridine (EdU) was added to islet culture 24 h prior to harvest. Islets were fixed and permeabilized using 10% formalin and saponin buffer, stained for insulin using a PE-conjugated insulin antibody (R&D Systems), and nuclear EdU incorporation was detected using the Click-It flow cytometry assay (Life Technologies). Flow cytometry data were analyzed using FloJo software (Treestar).

3.4.11 Statistical analysis

Statistical analysis was performed using GraphPad Prism version 6.01 (GraphPad) by ANOVA with Tukey's post hoc test or by multiple t tests. Data are expressed as means (S.E.M).

3.5 References

- [1] A.B. Olokoba, O.A. Obateru, L.B. Olokoba, Type 2 Diabetes Mellitus: A Review of Current Trends, *Oman Med. J.* 27 (2012) 269–273. doi:10.5001/omj.2012.68.
- [2] E. a. Ryan, B.W. Paty, P. a. Senior, D. Bigam, E. Alfadhli, N.M. Kneteman, J.R.T. Lakey, a. M.J. Shapiro, Five-year follow-up after clinical islet transplantation, *Diabetes.* 54 (2005) 2060–2069. doi:10.2337/diabetes.54.7.2060.
- [3] a. M.J. Shapiro, E. a. Ryan, J.R.T. Lakey, Islet cell transplantation, *Lancet.* 358 (2001) S21. doi:10.1016/S0140-6736(01)07034-9.
- [4] C. Qi, X. Yan, C. Huang, A. Melerzanov, Y. Du, Biomaterials as carrier, barrier and reactor for cell-based regenerative medicine, *Protein Cell.* 6 (2015) 638–653. doi:10.1007/s13238-015-0179-8.
- [5] A.A. Pomeransky, I.B. Khriplovich, Equations of motion of spinning relativistic particle in external fields, *Surv. High Energy Phys.* 14 (1999) 145–173. doi:10.1080/01422419908228843.
- [6] R.H. Lee, M.J. Seo, R.L. Reger, J.L. Spees, A. a Pulin, S.D. Olson, D.J. Prockop, Multipotent stromal cells from human marrow home to and promote repair of pancreatic islets and renal glomeruli in diabetic NOD/scid mice, *Proc. Natl. Acad. Sci.* 103 (2006) 17438–17443. doi:10.1073/pnas.0608249103.
- [7] R.C. Lai, F. Arslan, M.M. Lee, N.S.K. Sze, A. Choo, T.S. Chen, M. Salto-Tellez, L. Timmers, C.N. Lee, R.M. El Oakley, G. Pasterkamp, D.P. V de Kleijn, S.K. Lim, Exosome secreted by MSC reduces myocardial ischemia/reperfusion injury, *Stem Cell Res.* 4 (2010) 214–222. doi:10.1016/j.scr.2009.12.003.
- [8] J.D. Anderson, H.J. Johansson, C.S. Graham, M. Vesterlund, M.T. Pham, C.S. Bramlett, E.N. Montgomery, M.S. Mellema, R.L. Bardini, Z. Contreras, M. Hoon, G. Bauer, K.D. Fink, B. Fury, K.J. Hendrix, F. Chedin, S. EL-Andaloussi, B. Hwang, M.S. Mulligan, J. Lehtiö, J.A. Nolte, Comprehensive Proteomic Analysis of Mesenchymal Stem Cell Exosomes Reveals Modulation of Angiogenesis via Nuclear Factor-KappaB Signaling, *Stem Cells.* 34 (2016) 601–613. doi:10.1002/stem.2298.
- [9] T. Meyerrose, S. Olson, S. Pontow, S. Kalomoiris, Y. Jung, G. Annett, G. Bauer, J.A. Nolte, Mesenchymal stem cells for the sustained *in vivo* delivery of bioactive factors, *Adv. Drug Deliv. Rev.* 62 (2010) 1167–1174. doi:10.1016/j.addr.2010.09.013.
- [10] A.M. Madec, R. Mallone, G. Afonso, E. Abou Mrad, A. Mesnier, A. Eljaafari, C. Thivolet, Mesenchymal stem cells protect NOD mice from

- diabetes by inducing regulatory T cells, *Diabetologia*. 52 (2009) 1391–1399. doi:10.1007/s00125-009-1374-z.
- [11] D.M. Berman, M. a Willman, D. Han, G. Kleiner, N.M. Kenyon, O. Cabrera, J. a Karl, R.W. Wiseman, D.H. O'Connor, A.M. Bartholomew, N.S. Kenyon, Mesenchymal Stem Cells Enhance Allogeneic Islet Engraftment in Nonhuman Primates, *Diabetes*. 59 (2010) 2558–2568. doi:10.2337/db10-0136.
- [12] O. Karnieli, Y. Izhar-Prato, S. Bulvik, S. Efrat, Generation of insulin-producing cells from human bone marrow mesenchymal stem cells by genetic manipulation., *Stem Cells*. 25 (2007) 2837–2844. doi:10.1634/stemcells.2007-0164.
- [13] V.S. Urbán, J. Kiss, J. Kovács, E. Gócza, V. Vas, E. Monostori, F. Uher, Mesenchymal stem cells cooperate with bone marrow cells in therapy of diabetes., *Stem Cells*. 26 (2008) 244–253. doi:10.1634/stemcells.2007-0267.
- [14] G.I. Bell, H.C. Broughton, K.D. Levac, D.A. Allan, A. Xenocostas, D.A. Hess, Transplanted Human Bone Marrow Progenitor Subtypes Stimulate Endogenous Islet Regeneration and Revascularization, *Stem Cells Dev*. 21 (2012) 97–109. doi:10.1089/scd.2010.0583.
- [15] G.I. Bell, M.T. Meschino, J.M. Hughes-Large, H.C. Broughton, A. Xenocostas, D.A. Hess, Combinatorial Human Progenitor Cell Transplantation Optimizes Islet Regeneration Through Secretion of Paracrine Factors, *Stem Cells Dev*. 21 (2012) 1863–1876. doi:10.1089/scd.2011.0634.
- [16] S.-E. Ong, Stable Isotope Labeling by Amino Acids in Cell Culture, SILAC, as a Simple and Accurate Approach to Expression Proteomics, *Mol. Cell. Proteomics*. 1 (2002) 376–386. doi:10.1074/mcp.M200025-MCP200.
- [17] S.C. Bendall, C. Hughes, M.H. Stewart, B. Doble, M. Bhatia, G. a Lajoie, Prevention of amino acid conversion in SILAC experiments with embryonic stem cells., *Mol. Cell. Proteomics*. 7 (2008) 1587–97. doi:10.1074/mcp.M800113-MCP200.
- [18] D. Hess, L. Li, M. Martin, S. Sakano, D. Hill, B. Strutt, S. Thyssen, D. a Gray, M. Bhatia, Bone marrow-derived stem cells initiate pancreatic regeneration., *Nat. Biotechnol*. 21 (2003) 763–770. doi:10.1038/nbt841.
- [19] M. Shibuya, Vascular Endothelial Growth Factor (VEGF) and Its Receptor (VEGFR) Signaling in Angiogenesis: A Crucial Target for Anti- and Pro-Angiogenic Therapies, *Genes Cancer*. 2 (2011) 1097–1105. doi:10.1177/1947601911423031.

- [20] M.D. Gordon, R. Nusse, Wnt signaling: Multiple pathways, multiple receptors, and multiple transcription factors, *J. Biol. Chem.* 281 (2006) 22429–22433. doi:10.1074/jbc.R600015200.
- [21] Y. Yang, Wnt5a and Wnt5b exhibit distinct activities in coordinating chondrocyte proliferation and differentiation, *Development.* 130 (2003) 1003–1015. doi:10.1242/dev.00324.
- [22] B. Bakondi, I.S. Shimada, B.M. Peterson, J.L. Spees, SDF-1 α secreted by human CD133-derived multipotent stromal cells promotes neural progenitor cell survival through CXCR7., *Stem Cells Dev.* 20 (2011) 1021–1029. doi:10.1089/scd.2010.0198.
- [23] Z. Huang, S.D. Bao, Roles of main pro- and anti-angiogenic factors in tumor angiogenesis, *World J. Gastroenterol.* 10 (2004) 463–470.
- [24] M. Aziz, A. Jacob, W.-L. Yang, A. Matsuda, P. Wang, Current trends in inflammatory and immunomodulatory mediators in sepsis., *J. Leukoc. Biol.* 93 (2013) 329–42. doi:10.1189/jlb.0912437.
- [25] J. Cox, M.Y. Hein, C. a Luber, I. Paron, Accurate proteome-wide label-free quantification by delayed normalization and maximal peptide ratio extraction, termed MaxLFQ, *Mol. Cell.* 13 (2014) 2513–2526. doi:10.1074/mcp.M113.031591.
- [26] M.G. Rohani, W.C. Parks, Matrix remodeling by MMPs during wound repair, *Matrix Biol.* 44–46 (2015) 113–121. doi:10.1016/j.matbio.2015.03.002.
- [27] S. Vadon-Le Goff, D.J.S. Hulmes, C. Moali, BMP-1/tolloid-like proteinases synchronize matrix assembly with growth factor activation to promote morphogenesis and tissue remodeling., *Matrix Biol.* 44–46 (2015) 14–23. doi:10.1016/j.matbio.2015.02.006.
- [28] R. a. Boomsma, D.L. Geenen, Mesenchymal Stem Cells Secrete Multiple Cytokines That Promote Angiogenesis and Have Contrasting Effects on Chemotaxis and Apoptosis, *PLoS One.* 7 (2012) e35685. doi:10.1371/journal.pone.0035685.
- [29] T.K. Ho, J. Tsui, S. Xu, P. Leoni, D.J. Abraham, D.M. Baker, Angiogenic effects of stromal cell-derived factor-1 (SDF-1/CXCL12) variants *in vitro* and the *in vivo* expressions of CXCL12 variants and CXCR4 in human critical leg ischemia, *J. Vasc. Surg.* 51 (2010) 689–699. doi:10.1016/j.jvs.2009.10.044.
- [30] M.S. Pepper, Positive and negative regulation of angiogenesis: from cell biology to the clinic, *Vasc. Med.* 1 (1996) 259–266.
- [31] C. Blanpain, W.E. Lowry, H.A. Pasolli, E. Fuchs, Canonical notch signaling functions as a commitment switch in the epidermal lineage, *Genes Dev.* 20 (2006) 3022–3035. doi:10.1101/gad.1477606.

- [32] N. Yokoyama, D. Yin, C.C. Malbon, Abundance, complexation, and trafficking of Wnt/ β -catenin signaling elements in response to Wnt3a, *J. Mol. Signal.* 2 (2007) 11. doi:10.1186/1750-2187-2-11.
- [33] L. Meijer, M. Flajolet, P. Greengard, Pharmacological inhibitors of glycogen synthase kinase 3, *Trends Pharmacol. Sci.* 25 (2004) 471–480. doi:10.1016/j.tips.2004.07.006.
- [34] D.K. Jin, K. Shido, H. Kopp, I. Petit, S. V Shmelkov, L.M. Young, A.T. Hooper, H. Amano, S.T. Avecilla, B. Heissig, K. Hattori, F. Zhang, D.J. Hicklin, Y. Wu, Z. Zhu, A. Dunn, H. Salari, Z. Werb, N.R. Hackett, R.G. Crystal, D. Lyden, S. Rafii, Cytokine-mediated deployment of SDF-1 induces revascularization through recruitment of CXCR4+ hemangiocytes, *Nat. Med.* 12 (2006) 557–567. doi:10.1038/nm1400.
- [35] M. Brissova, A. Shostak, M. Shiota, P.O. Wiebe, G. Poffenberger, J. Kantz, Z. Chen, C. Carr, W.G. Jerome, J. Chen, H.S. Baldwin, W. Nicholson, D.M. Bader, T. Jetton, M. Gannon, A.C. Powers, Pancreatic islet production of vascular endothelial growth factor-A is essential for islet vascularization, revascularization, and function, *Diabetes.* 55 (2006) 2974–2985. doi:10.2337/db06-0690.
- [36] J.Z.Q. Luo, F. Xiong, a S. Al-Homsi, T. Roy, L.G. Luo, Human BM stem cells initiate angiogenesis in human islets *in vitro.*, *Bone Marrow Transplant.* 46 (2011) 1128–1137. doi:10.1038/bmt.2010.278.
- [37] M. Blandino-Rosano, G. Perez-Arana, J.M. Mellado-Gil, C. Segundo, M. Aguilar-Diosdado, Anti-proliferative effect of pro-inflammatory cytokines in cultured β -cells is associated with extracellular signal-regulated kinase 1/2 pathway inhibition: protective role of glucagon-like peptide -1., *J. Mol. Endocrinol.* 41 (2008) 35–44. doi:10.1677/JME-07-0154.
- [38] D.L. Eizirik, M.L. Colli, F. Ortis, The role of inflammation in insulinitis and β -cell loss in type 1 diabetes., *Nat. Rev. Endocrinol.* 5 (2009) 219–226. doi:10.1038/nrendo.2009.21.
- [39] H. Shi, M. V Kokoeva, K. Inouye, I. Tzamelis, H. Yin, J.S. Flier, TLR4 links innate immunity and fatty acid – induced insulin resistance, *J. Clin. Invest.* 116 (2006) 3015–3025. doi:10.1172/JCI28898.TLRs.
- [40] S. Sanjabi, L.A. Zenewicz, M. Kamanaka, R.A. Flavell, Anti-inflammatory and pro-inflammatory roles of TGF-??, IL-10, and IL-22 in immunity and autoimmunity, *Curr. Opin. Pharmacol.* 9 (2009) 447–453. doi:10.1016/j.coph.2009.04.008.
- [41] T. Yano, Z. Liu, J. Donovan, M.K. Thomas, J.F. Habener, Stromal Cell-Derived Factor-1 (SDF-1)/CXCL12 Attenuates Diabetes in Mice and Promotes Pancreatic β -cell Survival by Activation of the Prosurvival Kinase Akt, *Diabetes.* 56 (2007) 2946–2957. doi:10.2337/db07-0291.Additional.

- [42] I. Rooman, L. Bouwens, Combined gastrin and epidermal growth factor treatment induces islet regeneration and restores normoglycaemia in C57Bl6/J mice treated with alloxan, *Diabetologia*. 47 (2004) 259–265. doi:10.1007/s00125-003-1287-1.
- [43] E. Hakonen, J. Ustinov, I. Mathijs, J. Palgi, L. Bouwens, P.J. Miettinen, T. Otonkoski, Epidermal growth factor (EGF)-receptor signaling is needed for murine β -cell mass expansion in response to high-fat diet and pregnancy but not after pancreatic duct ligation, *Diabetologia*. 54 (2011) 1735–1743. doi:10.1007/s00125-011-2153-1.
- [44] G.W. Zuo, C.D. Kohls, B.C. He, L. Chen, W. Zhang, Q. Shi, B.Q. Zhang, Q. Kang, J. Luo, X. Luo, E.R. Wagner, S.H. Kim, F. Restegar, R.C. Haydon, Z.L. Deng, H.H. Luu, T.C. He, Q. Luo, The CCN proteins: Important signaling mediators in stem cell differentiation and tumorigenesis, *Histol. Histopathol.* 25 (2010) 795–806. doi:10.1111/j.1365-2958.2010.07165.x.Characterization.
- [45] R. Paradis, N. Lazar, P. Antinozzi, B. Perbal, J. Buteau, Nov/Ccn3, a Novel Transcriptional Target of FoxO1, Impairs Pancreatic β -Cell Function, *PLoS One*. 8 (2013) 1–8. doi:10.1371/journal.pone.0064957.
- [46] S. Chowdhury, X. Wang, C.B. Srikant, Q. Li, M. Fu, Y.J. Gong, G. Ning, J.L. Liu, IGF-I stimulates CCN5/WISP2 gene expression in pancreatic β -cells, which promotes cell proliferation and survival against streptozotocin, *Endocrinology*. 155 (2014) 1629–1642. doi:10.1210/en.2013-1735.
- [47] H. Aly, N. Rohatgi, C.A. Marshall, T.C. Grossenheider, H. Miyoshi, T.S. Stappenbeck, S.J. Matkovich, M.L. McDaniel, A Novel Strategy to Increase the Proliferative Potential of Adult Human β -Cells While Maintaining Their Differentiated Phenotype, *PLoS One*. 8 (2013). doi:10.1371/journal.pone.0066131.
- [48] F. Figeac, B. Uzan, M. Faro, N. Chelali, B. Portha, J. Movassat, Neonatal growth and regeneration of β -cells are regulated by the Wnt/ β -catenin signaling in normal and diabetic rats, *AJP Endocrinol. Metab.* 298 (2010) E245–E256. doi:10.1152/ajpendo.00538.2009.
- [49] R. Mussmann, M. Geese, F. Harder, S. Kegel, U. Andag, A. Lomow, U. Burk, D. Onichtchouk, C. Dohrmann, M. Austen, Inhibition of GSK3 promotes replication and survival of pancreatic β -cells, *J. Biol. Chem.* 282 (2007) 12030–12037. doi:10.1074/jbc.M609637200.

Chapter 4

Predicting the Therapeutic Potential of Human Multipotent Stromal Cells Using Quantitative Proteomics¹

4.1 Introduction

Multipotent stromal cells (MSC) have been described as one of the most versatile cell types for use in regenerative medicine applications. Since their initial discovery in bone marrow, MSC have been identified and isolated from several adult and fetal tissues [1]. The use of donor-matched MSC or autologous MSC greatly increases therapeutic potential in the clinical setting, bypassing host-versus-graft disease requirement for long-term immunosuppression that normally arise during cell based therapies [2]. In addition, MSC have the capacity to respond to injury, infection or diseases in all vascularized tissues within the body [3]. MSC harvested from multiple anatomical locations are equivalent in terms of surface marker expression and differentiation potential [4]. However, MSC harvested from different sites may express very different genes, which may have an impact on their function as well as clinical relevance in cellular therapies [5]. For example, MSC harvested from amniotic fluid have been shown to have neonatal defense properties while MSC harvested from bone marrow play functional roles in blood and bone formation [6].

¹ This chapter contains excerpts with permission from the following paper:

Kuljanin M, Bell GI, Hess DA, Lajoie GA. (2017) "Predicting the Therapeutic Potential of Human Multipotent Stromal Cells Conditioned Media using Quantitative Proteomics". (In preparation)

One of the most useful properties that MSC possess is ample secretion of various regenerative cytokines and immunomodulatory factors. MSC secrete a wide variety of growth factors and cytokines/chemokines that can induce cell proliferation and angiogenesis [7]. It has been well documented that MSC secrete pro-angiogenic cytokines, such as HGF, EGF, and VEGF, that increase fibroblast, epithelial and endothelial cell division as well as chemokines, such as stromal derived factor-1 (SDF-1 or CXCL12), that increase accessory cell recruitment to sites of injury [8]. MSC have also been shown to secrete a wide variety of extracellular vesicles to package peptides, proteins, membrane lipids and nucleic acids, that impact regenerative processes at distant sites via the blood stream [9,10]. In addition to having pro-angiogenic effects, MSC have also been implemented in anti-inflammatory, immunomodulatory, anti-apoptotic, anti-microbial and most recently β -cell regeneration applications [7,11,12].

Although MSC have been safely and successfully used in many clinical applications, direct characterization of trophic factors secreted by MSC is still lacking and could lead to optimization of their therapeutic potential [13]. The therapeutic potential of each MSC line isolated is directly related to what they secrete and how much of each factor they secrete. For example, the vascular regenerative capacity of BM-derived MSC can be enriched by subset selection based on high aldehyde dehydrogenase activity [14]. In addition, the heterogeneous nature of MSC populations isolated from different donors, and expanded in culture, has been shown to impact β -cell regenerative potential using *in vivo* mouse models [15]. Interestingly, the β -cell therapeutic potential of MSC has also been shown to diminish with age, or with prolonged passage

in culture [16]. Both of the above mentioned studies relied on lengthy *in vivo* evaluations to characterize MSC that have angiogenic and β -cell regenerative properties. This process is inherently ineffective at screening a large number of donor derived MSC lines for therapeutic efficacy relevant to cellular therapies. Therefore, thorough examination of protein secretion by MSC using high throughput technologies are needed to improve existing therapies, to tailoring each MSC line isolated for a specific function.

Extensive proteomic characterization of human MSC (hMSC) that possess the ability to decrease blood glucose levels in hyperglycemia mouse models have revealed key protein signature that could be used for future screening techniques [17]. These include: the increased secretion of pro-angiogenic, cell growth supportive factors and reduced secretion of common pro-inflammatory signals that were found highly expressed in non-regenerative hMSC. However, due to the relatively small sample sized used, more in depth analysis is required to determine a protein signature that can be used to predict which hMSC lines possess the ability to initiate islet regeneration after transplantation into streptozotocin (STZ)-treated mice *in vivo*.

Herein, we present a quantitative proteomic approach that can be used to predict the therapeutic potential of hMSC lines in terms of angiogenesis and β -cell regeneration inducing capacity (Figure 4.1). By using previously characterized hMSC lines, we were able to develop a surrogate assay using human islets to assess the β -cell regenerative effects of hMSC conditioned media (CM) *in vitro*. Quantitative label-free proteomics was used to generate a training data set. Next, using machine learning algorithms, we are able to

determine an unbiased protein signature of islet regenerative hMSC samples that are in turn quantitatively validated by using targeted proteomics. In addition, the secreted proteins from 16 uncharacterized cells lines were tested against this protein signature to predict the therapeutic potential of each hMSC line. Lastly, results are were validated using the aforementioned *in vitro* co-culture human islet assay coupled with multiparametric flow cytometry as well as quantitative recovery from hyperglycemia in STZ-treated mice. For the first time, we describe a protein signature that can be used to screen hMSC lines selected for use in β -cell regenerative applications.

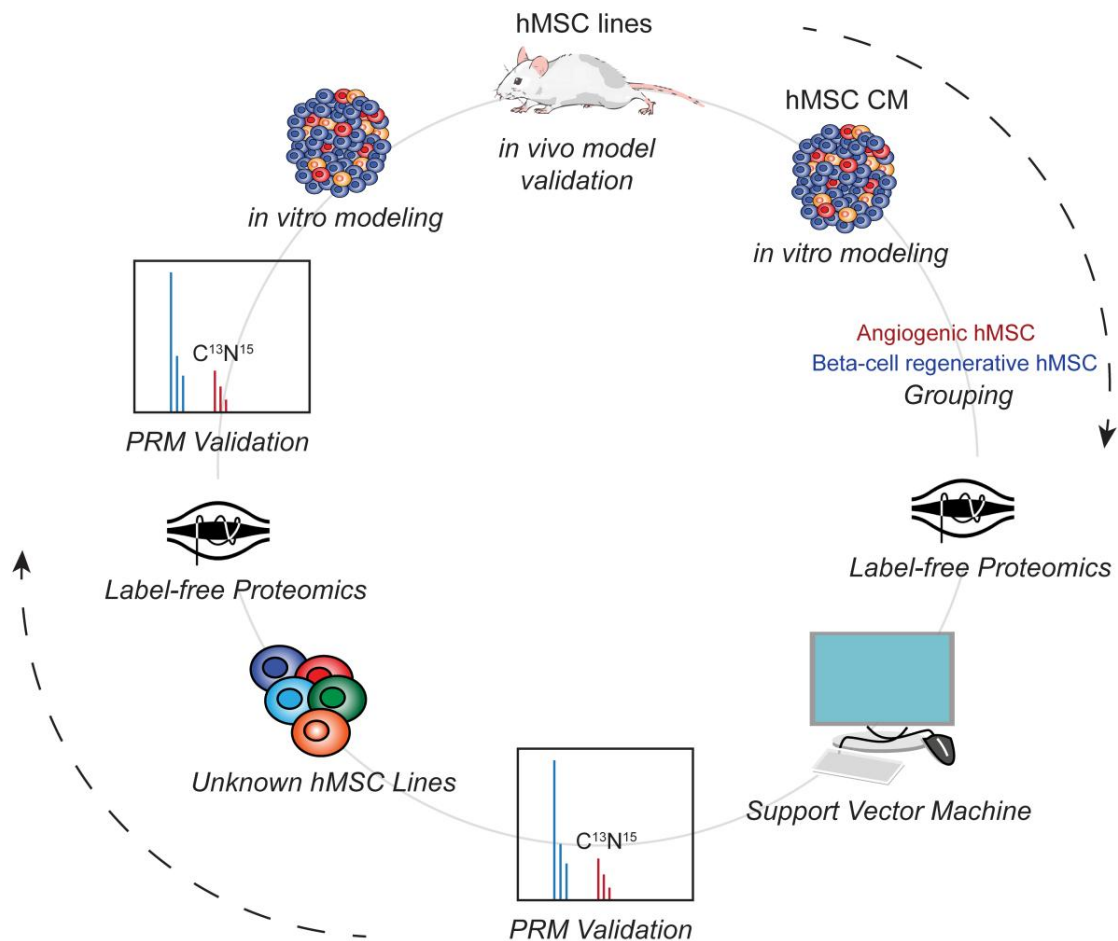


Figure 4.1 Predictive assay workflow. hMSC lines previously characterized were used to recapitulate angiogenic or β -cell regenerative potential using *in vitro* models. Label-free quantitative proteomics was performed on secreted proteins from 10 different hMSC lines to build a training data set. Protein signatures were obtained using machine learning and validated with targeted proteomics. The predictive power of the assay was tested using 10 previously uncharacterized hMSC lines and their regenerative properties were validated using proteomics and *in vitro* / *in vivo* models.

4.2 Results

4.2.1 Angiogenic capacity of hMSC CM

To determine the angiogenic potential of hMSC CM, spontaneous tubular formation was assessed *in vitro* using human microvascular endothelial cells (HMVEC). HMVEC were cultured on growth factor reduced Geltrex™ bathed in endothelial basal media (EBM) without growth factors, endothelial growth media (EGM) supplemented with bFGF, EGF, IGF, VEGF or ~ 50 µg of secreted protein from hMSC CM for 20 hours. The total number of tubes formed was numerated and angiogenic capacity was quantified (Figure 4.2a-d). In total, 10 different hMSC CM samples, generated by 10 different hMSC lines, were evaluated for the capacity to increase tubule formation in biological triplicate. A significant increase in the tubule formation was observed for three out of 10 hMSC lines. hMSC lines that possessed significant tubule formation capacity compared to EBM were grouped and deemed angiogenic and those that failed to augment tubule formation grouped and deemed non-angiogenic (Figure 4.2e). Collectively, angiogenic hMSC showed significantly increased number of tubules formed compared to non-angiogenic hMSC (Figure 4.2f, *** $p < 0.001$). Quantitative label-free proteomics was used to determine relative expression levels of all proteins identified in hMSC CM, in biological triplicate. In addition, quantitative assessment of the proteins was used to identify signatures that could be implemented in predicting the angiogenic potential of hMSC CM.

In total ~ 2500 proteins were identified and gene ontology cellular component (GOCC) analysis was used to determine proteins that were associated with extracellular localization (752). Protein lists were further filtered to only include

proteins that were quantified in > 6 out of 10 hMSC lines, and missing values were imputed [18,19]. Protein lists were cross-compared using Gene Set Enrichment Analysis (GSEA) to hallmark gene sets for angiogenesis and in total 32 proteins were selected for subsequent analysis [20]. In addition, the two groups were compared using hierarchical clustering with Euclidean distances in Perseus, with z-scoring to determine directional changes in protein abundances (Figure 4.2g) [21]. Unfortunately, protein changes were very heterogeneous between samples and showed no distinct correlations that could be used to predict angiogenic potential of hMSC CM. However, the top two and bottom two hMSC CM could be predicted using the expression levels of four proteins. The top two angiogenic hMSC lines were predictable by high relative abundance of two potent pro-angiogenic proteins, stem cell factor (KITLG) and angiogenin (ANG), while the least angiogenic hMSC lines showed low relative abundance. Conversely, platelet factor 4 variant (PF4V1) and vascular endothelial factor C (VEGFC) were highly expressed in the least angiogenic hMSC lines. In summary, these data suggested that proteomic assessment of angiogenic capacity could not be reliably achieved for each sample using the current screening strategy. However, the angiogenic potential of the top 20% and the bottom 20% of hMSC samples could be predicted by the relative expression levels of four angiogenic proteins.

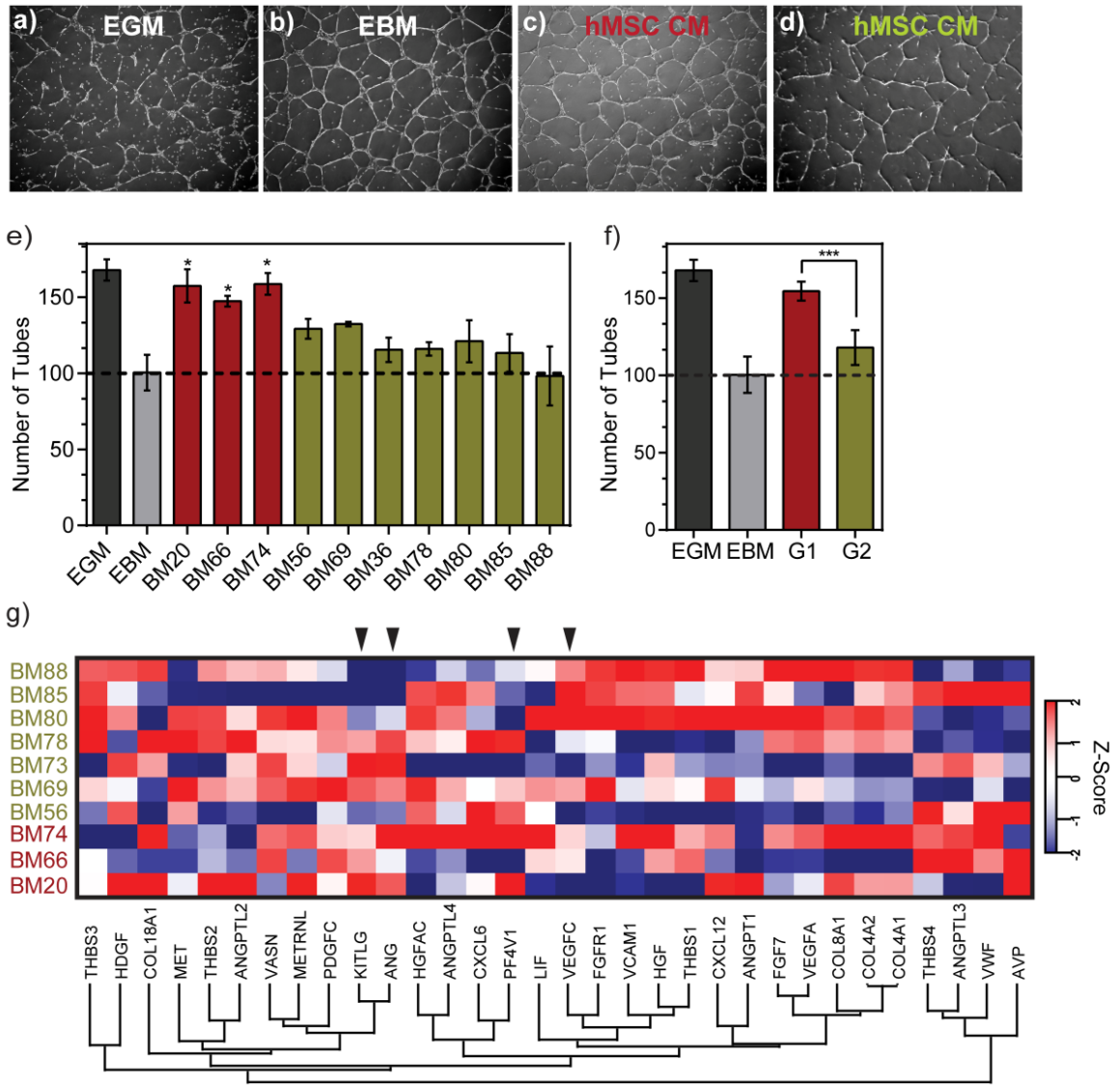


Figure 4.2 Angiogenic potential of hMSC CM. (a) HMVEC were grown on growth factor reduced Matrigel and spontaneous tubular formation was assessed using (a) EGM, (b) EBM, (c-d) CM from hMSC samples. (e) Average number of tubules formed was quantified in triplicate and three hMSC lines showed significantly increased tubular formation compared to EBM control. (f) hMSC lines were grouped and angiogenic hMSC (red) showed significantly higher number of tubules formed compared to non-angiogenic hMSC. (g) Label-free quantitative proteomic clustering using Euclidean distances and z-scoring did not show a distinct angiogenic protein secretion pattern that could be used to predict angiogenic potential of hMSC. Data is represented as mean \pm S.E.M. (* $p < 0.05$, *** $p < 0.001$).

4.2.2 β -cell regenerative capacity of hMSC CM

We have previously shown that hMSCs can be used to initiate regeneration of endogenous β -cells after transplantation into STZ-treated NOD/SCID mice. However, hMSC represented a heterogeneous population and the extent of regenerative capacity was cell line specific [15]. In addition, hMSC that possessed the capacity to induce islet regeneration after transplantation were rare, with only ~10-20% of hMSC samples able to reverse established hyperglycemia after transplantation. To determine whether hMSC possessed β -cell regenerative capacity, a lengthy 42 day *in vivo* experiment needed to be performed, making it too inefficient to be used as a screening modality. Similar to the angiogenesis screen performed above, we sought to identify a quantitative proteomic signature that could be used to predict β -cell regenerative capacity using hMSC CM. A training data set was constructed using two known regenerative hMSC lines and two non-regenerative hMSCs lines that were previously characterized using the *in vivo* transplantation model [15]. In addition, 6 previously uncharacterized hMSC lines were added to the training data set, for a total of 10 hMSC lines. To group hMSC lines, human islet culture assays were performed using CM to assess which hMSC lines could improve β -cell survival *in vitro* after 7 days of culture, using multiparametric flow cytometry for beta cell survival and proliferation (Figure 4.3a-b). CM from two islet regenerative hMSC lines showed significantly higher total live β -cell numbers compared to CM generated from the two known non-regenerative hMSC lines, as previously shown (Figure 4.3c) [17]. The remaining hMSC lines were used for test validation and none of the samples showed significant improvement over

negative controls (RPMI) and were thus classified as non-regenerative. When grouped, regenerative hMSC showed a significant increase in the total number of viable β -cells compared to non-regenerative hMSC (Figure 4.3d), therefore validating our *in vitro* functional assay.

Quantitative proteomics was used to determine what factors could best identify and place unknown hMSC lines into either regenerative or non-regenerative classes. Unbiased mining and protein marker selection of label-free quantitative proteomic data was achieved using the R package “geNetClassifier support vector machine (SVM)” [22]. Data mining was performed using the training data set mentioned above, where two regenerative lines and 8 non-regenerative lines were used to train the SVM. The posterior probability of each gene was assessed and, in total, 20 genes that met a threshold of 0.90 could be used to reliably segregate the two classes (Figure 4.3e). A full list of all proteins and their corresponding posterior probabilities can be found in Table A4.1. The top 10 proteins, which included: six inflammatory markers, one Wnt-signaling protein and three proteases, were chosen to perform further prospective validation.

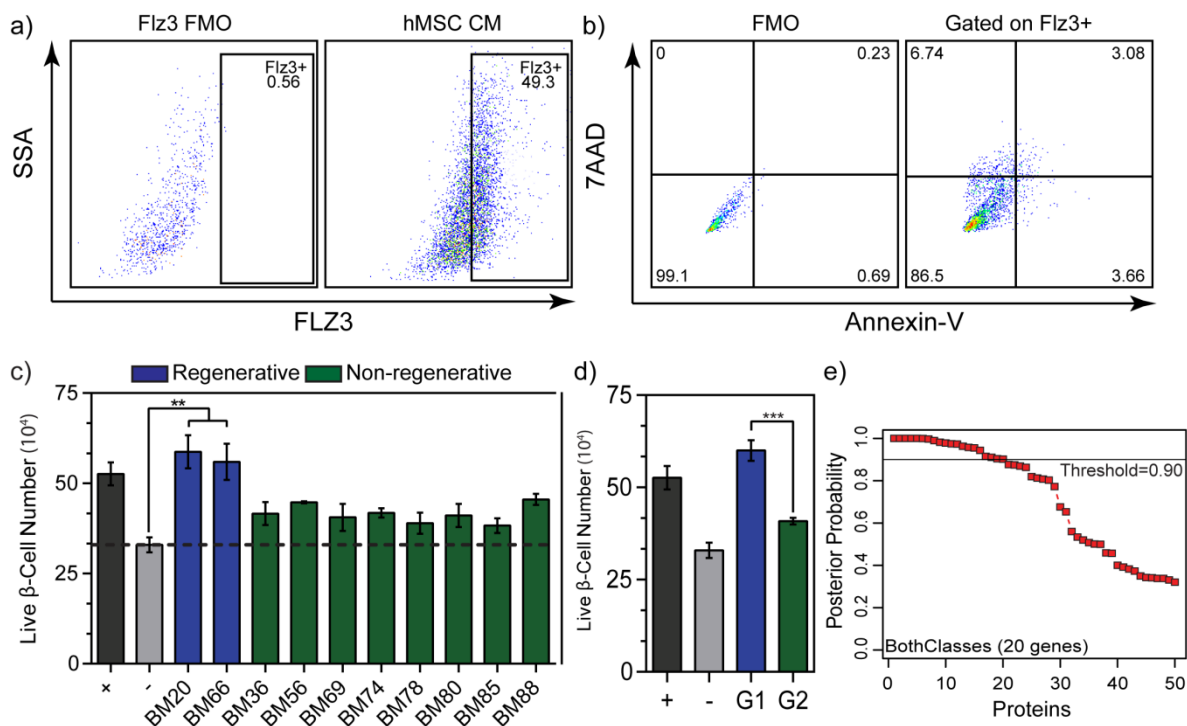


Figure 4.3 Predictive protein signatures for β -cell regenerative hMSC.

(a) Multiparametric flow analysis of human islets cultured for 7 days bathed in hMSC CM. Assessment of β -cell content was achieved with FluoZin-3. (b) Survival rate of β -cell was assessed by looking at the frequency of 7AAD and Annexin-V. (c) Total live β -cell number was used to assess regenerative potential of two regenerative and two non-regenerative hMSC lines. Regenerative hMSC lines showed significantly increased total live β -cell numbers compared to RPMI. Non-regenerative hMSC lines were not significantly different from RPMI. Six additional hMSC lines were characterized as non-regenerative. (d) Regenerative hMSC lines were grouped and showed significantly increased live β -cell numbers compared to non-regenerative hMSC lines. (e) Unbiased machine learning was performed using label free quantitative values and 20 proteins could be used accurately segregate regenerative and non-regenerative hMSC lines. Data is represented as mean \pm S.E.M. ** $p < 0.01$, *** $p < 0.001$.

4.2.3 Validation of regenerative signature using targeted proteomics

Proteins obtained from the SVM suggested that regenerative hMSC lines secreted three proteins in significantly higher abundance than non-regenerative hMSC, while 7 proteins were secreted in significantly lower abundance compared to non-regenerative hMSC. To confirm these findings, label-free quantitation (LFQ) for each of the top 10 proteins was assessed across classes (Figure 4.4a). Indeed, the three proteins chosen by SVM showed elevated relative expression levels in regenerative hMSC ranging from 16-32-fold higher compared to non-regenerative hMSC. In contrast, the 7 proteins chosen as highly expressed in non-regenerative hMSC showed relative expression levels in non-regenerative hMSC ranging from 4-32-fold higher compared to regenerative hMSC. These results confirmed that the classification performed by the SVM algorithm was accurate.

To further quantify the relative abundance of the candidate proteins obtained from SVM, parallel reaction monitoring (PRM) was performed using an in-house made, stable isotope labeled (SIL) peptide spike-in (glu-1-fibrinopeptide B: EGVNDNEEGFFSAR) that was purified using HPLC (>95%). Endogenous light peptide levels were first assessed in hMSC CM and were determined to be below the detection limit. Next, a five point standard curve, spanning 3 orders of magnitude (50amol-50fmol), was constructed using the ratio of light to heavy peptides within the hMSC CM to account for matrix effects (Figure 4.4b) [23]. To assess the relative abundance of each protein, three highly abundant peptides were chosen per target (where applicable) (Table A4.2), and five transitions were used for total area integrations in Skyline [24]. Each sample was spiked with 1fmol/uL of SIL peptide and 1 µg

of total protein was injected onto the column and analyzed by PRM-LC-MSMS in duplicate. The total integrated fragment area for each target was normalized to the spike-in SIL peptide, and the relative abundance (fmol) for each target was determined using a standard curve (Figure 4.4c). Proteins ranged from ~ 0.20-18 fmol and could be reliably quantified using the targeted parameters. Proteins that were classified as overexpressed by the SVM in regenerative hMSC were once again confirmed using our PRM approach. Proteins such as SFRP1 were found to be 7.7 fold higher in regenerative hMSC, while classifiers of non-regenerative hMSC, such as CXCL6, were found to be 17.5-fold lower in regenerative hMSC. In addition, the inter-coefficient of variance (CV) for each protein target was assessed (Figure 4.4d-e). In general, CV was found to be very low (<20%) for the majority of hMSC samples tested. One cell line showed consistently high CV for each protein investigated and was removed from further analysis. Samples that did not meet CV standards were not used in averaging in assigning relative abundance cut-offs.

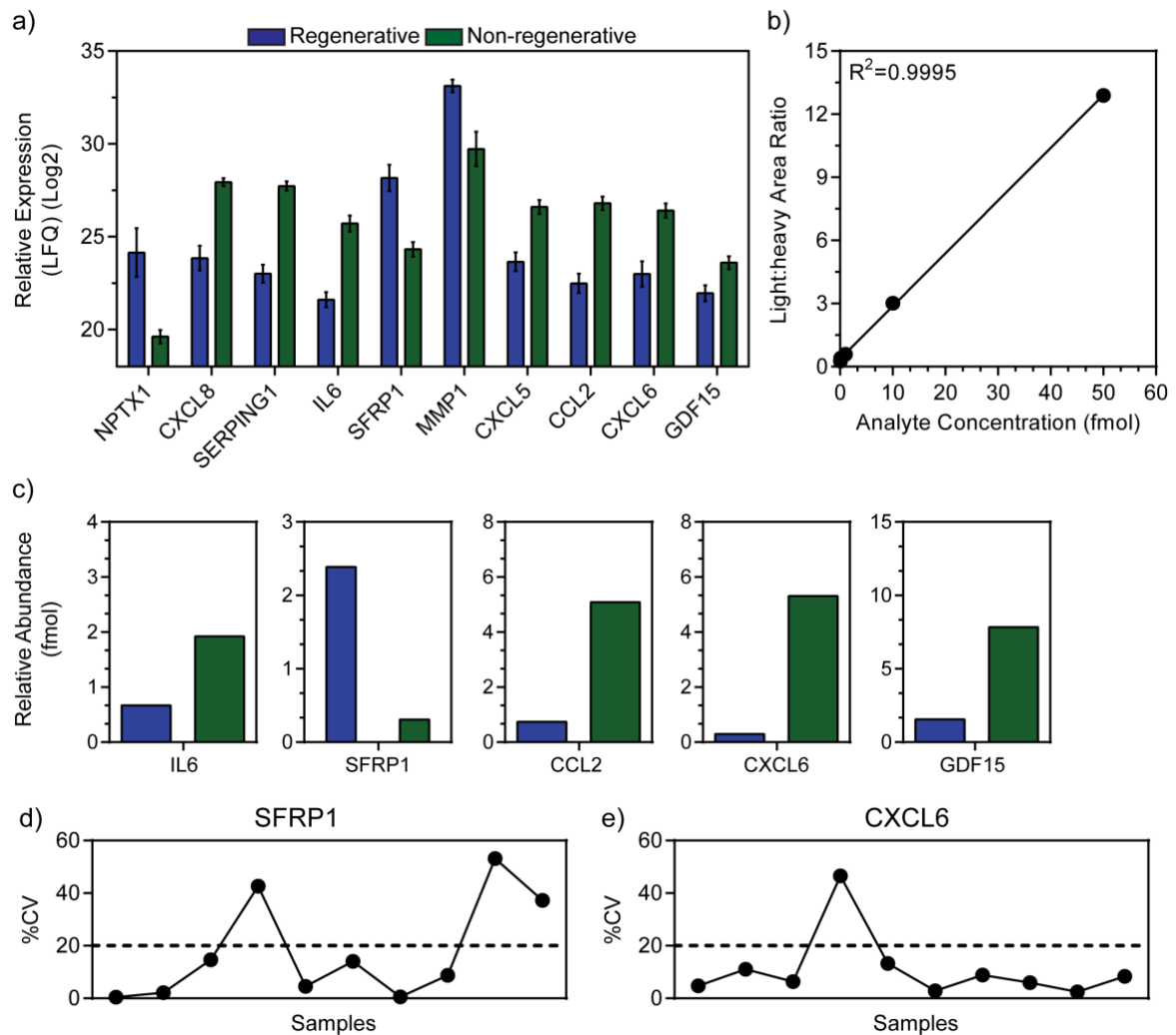


Figure 4.4 Quantitative validation of regenerative hMSC protein signature. (a) Label-free quantitative values for the top 10 proteins identified by the SVM as regenerative discriminators. (b) A 5-point standard curve was constructed using light and heavy isotope labeled peptide spanning 3 orders of magnitude. (c) The relative abundance (fmol) of each protein selected by the SVM was assessed using PRM and the generated standard curve. Concentrations ranged from 0.2-18 fmol. The inter-coefficient of variance was assessed for each targeted protein, as shown for (d) SFRP1 and (e) CXCL6. Samples with consistently high CV (>20%) were discarded in subsequent analysis. Data is represented as mean \pm S.D.

4.2.4 Characterization of unknown hMSC lines using proteomic classifier

To determine if accurate assessment of unknown hMSC lines could be achieved using the top 10 proteins within the classifier, 10 unknown hMSC lines were grown in biological triplicate, and CM was collected after 24 hours of culture. Concentrated CM was first assessed using label-free quantitative proteomics, representing the test data set. Each protein target in the training data set was quantified and relative label-free expression levels were compared. Relative expression levels from the training data set were used to create cut-off that must be met by unknown samples to be classified as regenerative or non-regenerative. For example, the relative expression levels of proteins that were highly expressed, such as SFRP1 minus the standard error of the mean (S.E.M) was used to determine what the lowest value an unknown hMSC line must have to be considered regenerative (Figure 4.5a-b). In this fashion, a score system could be constructed. Samples that reached set cut-offs that were representative of a regenerative samples (shaded area) received a score of +1 and those that did not received a score of -1. The sum of the score was used to assign an unknown sample into either the regenerative or non-regenerative cohorts. Unknown hMSC samples that achieved a score of ≥ 6 were termed as regenerative and samples that achieved a combined score of ≤ 5 were termed as non-regenerative (Table 4.1). In total one unknown hMSC line was determined to be regenerative with a score of 8, the remaining unknown hMSC lines were determine to be non-regenerative (ranging from -5 to -10). In addition, quantitative validation of candidate proteins obtained from the SVM was performed using PRM as mentioned above (Figure 4.5c). In general the relative abundance of each

protein correlated well with the LFQ expression levels reported earlier. However, noticeable variability was associated with some proteins, such as CCL2, suggesting that it was a poor candidate for targeted proteomic applications. The hMSC line that was classified as regenerative by LFQ scoring also met many of the cut-off assigned by using the relative abundance quantification obtained from the training data set.

To assess the efficiency of our scoring metrics, all LFQ data obtained from the unknown samples was tested against the SVM created using the training data set. Each sample was tested against the SVM and the probability of assigning each unknown cell line to either regenerative or non-regenerative class was calculated (Table 4.2). Using this approach, we obtained a call rate accuracy of 100%, meaning that all unknown cell lines could be assigned with confidence to one category or the other. Again, only one uncharacterized hMSC line could be assigned to the regenerative class with a 97.6% probability. The remaining hMSC lines were assigned to the non-regenerative class ranging from 77.5%-93% probabilities.

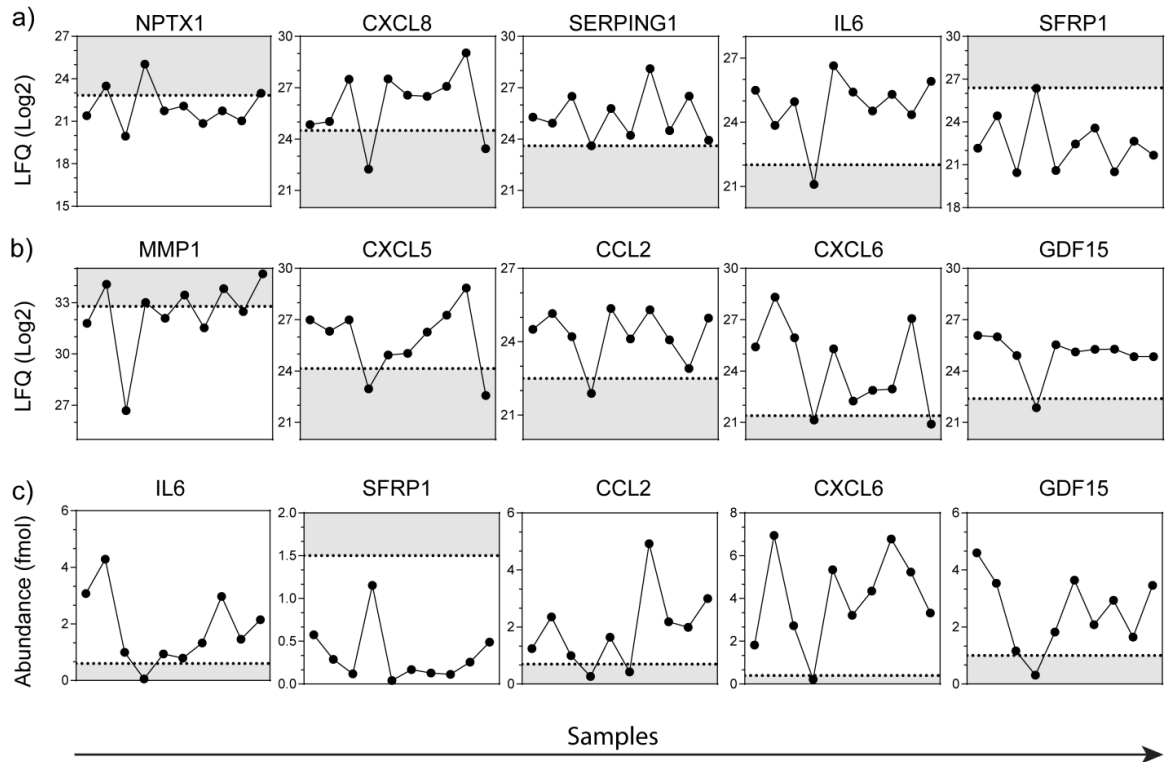


Figure 4.5 Quantitative proteomic assessments of unknown hMSC lines. (a-b) Label-free quantitation for the top 10 proteins identified by the SVM as regenerative discriminators was used to assess scoring of each unknown hMSC cell lines. Training data set cut-offs were shown in the shaded area. For each protein, samples that met cut-offs (were within the shaded area) received a score of +1, those that did not meet the cut-offs received a score of -1. (c) The abundance of each protein target was also assessed using targeted proteomics and a standard curve generated using SIL peptide. Abundance cut off for regenerative samples are shown in shaded area. Data is represented as mean.

Table 4.1 Score metric for regenerative capacity of unknown hMSC lines. A table outlining the score system used to place each unknown hMSC line based on the relative expression level of each protein obtained from the SVM.

Cell Line	NPTX1	CXCL8	SERPING1	IL6	SFRP1	MMP1	CXCL5	CCL2	CXCL6	GDF15	Total Score	Class
BM34	-1	-1	-1	-1	-1	-1	-1	-1	-1	-1	-10	NR
BM67	1	-1	-1	-1	-1	1	-1	-1	-1	-1	-8	NR
BM71	-1	-1	-1	-1	-1	-1	-1	-1	-1	-1	-10	NR
BM73	1	1	-1	1	-1	1	1	1	1	1	8	R
BM75	-1	-1	-1	-1	-1	-1	-1	-1	-1	-1	-10	NR
BM77	-1	-1	-1	-1	-1	1	-1	-1	-1	-1	-9	NR
BM82	-1	-1	-1	-1	-1	-1	-1	-1	-1	-1	-10	NR
BM83	-1	-1	-1	-1	-1	1	-1	-1	-1	-1	-9	NR
BM86	-1	-1	-1	-1	-1	-1	-1	-1	-1	-1	-10	NR
BM89	1	1	-1	-1	-1	1	1	-1	1	-1	-5	NR

* Regenerative score ≥ 6 , non-regenerative score ≤ 5 .

Table 4.2 Support vector machine scoring metric for regenerative capacity of unknown hMSC lines. A table outlining the posterior probability of each unknown hMSC line being assigned to a regenerate or non-regenerative class.

Cell Line	Probability R	Probability NR	Class
BM34	0.191	0.809	NR
BM67	0.255	0.775	NR
BM71	0.07	0.93	NR
BM73	0.976	0.024	R
BM75	0.107	0.893	NR
BM77	0.093	0.907	NR
BM82	0.183	0.817	NR
BM83	0.128	0.872	NR
BM86	0.159	0.841	NR
BM89	0.163	0.837	NR

4.2.5 Biological validation of unknown hMSC lines

Validation of each of the uncharacterized cell lines was performed using the human islet culture with CM *in vitro* screen described above. The total live β -cell number was once again used to determine which hMSC lines had the ability to increase β -cell survival. We found that only one out of 10 uncharacterized hMSC cell lines had significantly increased total number of live β -cell compared to our negative control, and that the remaining hMSC samples were not statistically different from control (Figure 4.6a). Again, these results highlight the predictive power of the quantitative screen. To further validate and β -cell regenerative potential of our unknown cell lines assigned by our system, one non-regenerative hMSC lines was assessed by transplantation *in vivo*. STZ-treated (35 mg/kg/day, days 1-5), hyperglycemic (15-25mmol/l) NOD/SCID mice were intravenously (IV) injected on day 10 with BM-derived hMSC (5.0×10^5 cells), and blood glucose levels were monitored for 42 days (Figure 4.6b). Compared with PBS-injected control mice ($n=3$) that remained severely hyperglycemic ($>25\text{mmol/l}$), mice transplanted with the non-regenerative hMSC line ($n=3$) remained severely hyperglycemic and showed no improvement compared to PBS-injected mice over the 42 day time course (Figure 4.6c). Thus, the predictive proteomic screen presented here efficiently identified both regenerative and non-regenerative hMSC validated by both *in vitro* and *in vivo* functional testing. Lastly, to demonstrate the potential utility of the screen, donor information, including age, sex, weight and BMI, was correlated with islet regenerative classification to determine whether any general trends could be observed with patient characteristics. In total, 10 female and 10 male donors were used in

our studies that ranged in age from 21-66 years (Figure 4.6d). Surprisingly, no direct correlation between the regenerative capacity of the hMSC and the age of the donor could be determined. Conversely, when donor BMI was considered, there was an apparent trend between BMI and islet regenerative classification, with 15/17 non-regenerative lines had BMI>25 and 7/7 hMSC donors with BMI>30 were classified as non-regenerative (Figure 4.6e). In contrast all hMSC lines (3/3) classified as regenerative were within healthy BMI range (18-24.9).

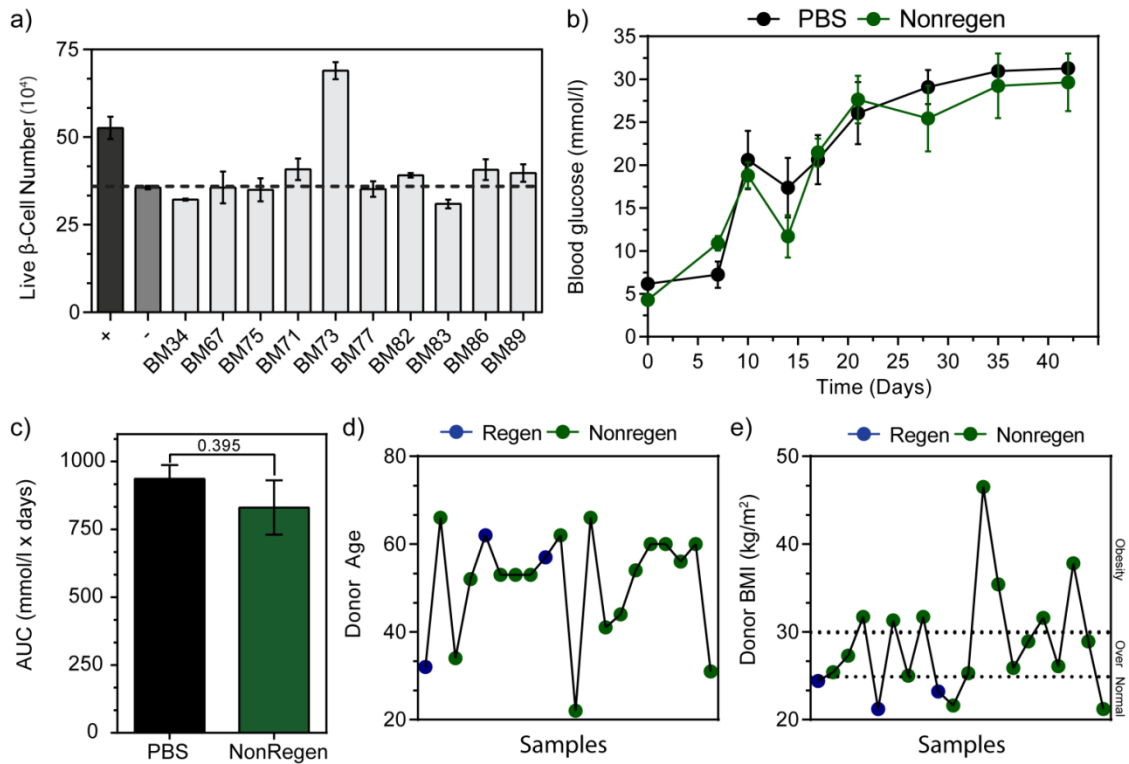


Figure 4.6 Biological validation of the predictive assay. (a) Multiparametric flow analysis of human islets cultured for 7 days bathed in hMSC CM. (b) hMSC from one non-regenerative and one regenerative line was transplanted into STZ-treated (35 mg/kg per day, days 1–5) NOD/SCID mice on day 10, and blood glucose was monitored weekly until 42 days compared with PBS-injected control mice. Blood glucose concentrations remained equal compared to PBS-injected mice. (c) Blood glucose AUC was not significantly reduced with non-regenerative hMSC ($n = 3$) compared to PBS-controls ($n = 3$). (d) No correlation with donor age was observed for islet regenerative potential. (e) All hMSC line classified as regenerative were obtained from donors that had healthy BMI, while the majority (15/17) of non-regenerative hMSC samples were from donors with BMI > 25. Data is represented as mean \pm S.E.M. (* $p < 0.05$).

4.3 Discussion

Our study demonstrates that CM derived from hMSC can be used to predict the therapeutic potential for the paracrine induction of regeneration by corresponding hMSC lines. Importantly, using a quantitative proteomics approach, we showed that each hMSC line could be efficiently placed into a regenerative or non-regenerative class based on hMSC secretory profiling. Employing the current proteomics strategy, the angiogenic potential of the top 20% and the bottom 20% of hMSC samples could be predicted by the relative expression levels of four angiogenic proteins. In addition, using machine learning algorithms, an unbiased protein signature of β -cell regenerative hMSC could be efficiently determined. Impressively, a panel of 10 proteins and their expression levels within hMSC CM could reliably predict the β -cell regenerative potential of 16 uncharacterized hMSC samples. Further validation using targeted proteomics confirmed our findings providing a high throughput assay that could be used to efficiently screen up to 10 uncharacterized hMSC lines within 24hours. Lastly, using patient information including donor age or BMI for 20 screened hMSC samples; we identify a trend correlating BMI to β -cell regenerative capacity, which could be used as a prescreening approach, in conjunction with our targeted proteomics approach, to identify the most regenerative hMSC lines selected for clinical applications.

Protein signatures were used to predict the angiogenic potential of uncharacterized hMSC samples relied on the ability to distinguish two different classifications, hMSC that possessed angiogenic capacity and those that did not. In an attempt to determine the pro-angiogenic classification of

hMSC samples, HMVEC tubule forming assays were performed, and perhaps were not a reliable predictor of paracrine hMSC CM pro-angiogenic functions. Tubule forming assays are commonly used as a surrogate assay for vessel formation *in vitro* but may not necessarily be the best predictors of angiogenic potential *in vivo* [25]. In addition to tube forming assays, directed *in vivo* angiogenesis assays (DIVAA) are commonly performed to assess angiogenic capacity [26]. We have used DIVAA inserts to assess angiogenic induction by hMSC CM and has provided evidence for secretome variability between hMSC samples [14]. However, DIVAA was not used as a screening modality in the current study but could represent a possible solution to the poor assignment of angiogenic versus non-angiogenic hMSC. Nonetheless, the use of two potent angiogenic proteins, kit ligand (or SCF) and angiogenin [27] could be used as potential prescreening tools, to assess hMSC lines with promise towards angiogenesis secretory patterns. In combination, prescreening hMSC CM to determine which hMSC lines possessed the highest levels of angiogenic factors, in combination with DIVAA could potentially improve the accuracy of characterization with unknown hMSC lines.

Combining previously characterized hMSC lines, a surrogate *in vitro* human islet survival assay, and our high-throughput proteomic screening techniques, we successfully demonstrate that hMSC CM could be used to determine a subset of 10 secretory proteins that predict β -cell regenerative capacity by hMSC. Within this list of proteins, we identified neuronal pentraxin 1 (NPTX1) to be highly upregulated in β -cell regenerative hMSC. NPTX1 decreases apoptotic and oxidative stress pathways shown previously to

impair insulin secretion and β -cell failure using rat models [28]. These results could be predicted with the islet survival culture assay, and hMSC lines classified as regenerative consistently showed increased β -cell survival compared to non-regenerative hMSC. In addition, expression of SFRP1, a Wnt-signaling modulator, was consistently upregulated in β -cell regenerative hMSC. Wnt-signaling has been previously characterized as an important pathway modulating β -cell functions including cell proliferation and survival [17,29,30]. Lastly, the expression of matrix metalloproteinase 1 (MMP1) was also found to be consistently upregulated in islet regenerative hMSC. Although matrix metalloproteinases (MMPs) have not been thoroughly studied in the context of diabetes and β -cells, evidence has suggested that MMPs are important in modulating inflammation and innate immunity (reviewed in [31]). Thus β -cell regenerative hMSC lines secreted several proteins consistent with the modulation of β -cell survival, proliferation and innate immunity.

hMSC samples characterized as non-regenerative represented 85% of samples screened, and showed elevated levels of 5 pro-inflammatory markers. Firstly, upregulated secretion of C-X-C motif chemokine 8 (CXCL8/IL8) and 6 (CXCL6) has been linked to increased inflammatory responses within islets that can lead to down regulation of pancreas-specific transcription factors and upregulation of pancreatic progenitor cell specific factors, suggesting transformation of mature β -cells towards a more immature endocrine cell phenotype, a phenomenon referred to as dedifferentiation [32]. Secondly, upregulated of interleukin 6 (IL6) within β -cells has been shown to decrease GLUT2-expression, implicated in the loss of glucose sensing ability,

as well as increased T-cell responses and reduced regulatory T-cell function [33]. Thirdly, C-C motif chemokine ligand 2 (CCL2) is involved in the recruitment of inflammatory monocytes towards islet or β -cell populations [34]. In addition, CCL2 plays a critical role in the clinical outcome of islet transplantation in patients with type one diabetes (T1D) by increasing macrophage recruitment, increasing destruction of β -cells and negatively impacting long-lasting insulin independence [35]. Finally, the increased serum expression of CXCL5 is linked to obesity and the onset of type two diabetes (T2D) by impairing insulin secretion in response to glucose stimulation [36]. Taken together, these data suggested that non-regenerative hMSC establish a pro-inflammatory microenvironment not permissive of β -cell regeneration in murine models *In vivo*.

Recently, growth differentiated factor 15 (GDF15) has been described as a novel marker of conditions associated with T2D. A commonly used glucose-lowering drug metformin is used to alleviate complications associated with T2D, and the concentration of GDF15 can be used as a biomarker that directly correlates with dosage amount and duration of metformin [37]. In addition, levels of GDF15 serum concentrations have been used as a valuable clinical marker for predicting transitions in albuminuria stages in patients with T2D [38], as well as cardiovascular risk in newly diagnosed T2D [39] and most recently involvement in body weight management [40,41]. Lastly, GDF15 can be accurately used to predict future insulin resistance and impaired glucose control in obese non-diabetic individuals [42].

There are two possible reasons for the elevated levels of GDF15 observed in non-regenerative hMSC. Firstly, in agreement with the pro-

inflammatory microenvironment established by non-regenerative hMSC, GDF15 represented yet another protein responsible for mediating chronic islet inflammation [43]. Secondly, elevated levels of GDF15 in non-regenerative hMSC could be directly correlated to the BMI of the donors that the cell lines were derived from. As mentioned previously, (>88%) of the non-regenerative hMSC lines were derived from donors that had BMIs > 25. Increased BMI is correlated with increased inflammation as well as increased risk of diabetes [44]. Patients at risk or with long-term exposure to T2D related inflammation may have altered hMSC function [45]. Specifically, in mouse models of T2D, the therapeutic potential of endogenous bone marrow-derived MSC was impaired [46]. Also, hMSC derived from patients with T2D showed gene expression profiles that were significantly different in terms of cytokine secretion, immunomodulatory ability, suggesting states of “disease memory” within hMSC samples [47]. Taking all these considerations together, hMSC derived from patients that are outside of the healthy BMI range, or are considered ‘pre-diabetic’ can generate altered secretory profiles that warrant further investigation in eventual disease progression.

In summary, our proteomic analyses of hMSC CM revealed that the most and least angiogenic hMSC lines could be predicted by using the expression values of four angiogenesis modulating proteins. In addition, our analysis demonstrated the rarity of finding a hMSC with islet regenerative capacity without prior *ex vivo* manipulations. Also, for the first time, quantitative proteomic analysis has determined an hMSC sample-specific protein secretion signature that can be used, in a high-throughput fashion, to

pre-determine the β -cell regenerative potential of previously uncharacterized hMSC lines.

4.4 Experimental Methods

4.4.1 Generation of CM for co-culture and proteomic analysis

After 4 days of culture (~80% confluency), hMSC were washed twice with PBS to remove residual growth factors and replated in basal AmnioMax™ without supplement to collect proteins secreted by hMSC for 24 hrs. Media conditioned by hMSC was collected, filtered and centrifuged at 450 x g to remove any cellular debris. Cell viability was assayed using trypan blue and >95% viability was used as a standard cut-off for co-culture and secretome analyses. CM was generated in triplicate for a total of 20 individual MSC lines and was concentrated using 3 kDa molecular weight cut-off filter units (Millipore). For co-culture assays, CM was quantified and the protein amount was normalized (~50 μ g total). For proteomic analysis, concentrated CM was lyophilized overnight and re-suspended in 8M urea, 50 mM ammonium bicarbonate, 10 mM dithiothreitol and 2% SDS solution prior to protein quantitation. Protein concentration was measured using the Pierce 660nm protein assay (ThermoFisher Scientific).

4.4.2 HMVEC tubule forming assay

To assess CM influence on endothelial cell function *in vitro*, 120,000 human microvascular endothelial cells (HMVECs) were cultured on growth factor-reduced Geltrex (Life Technologies) in endothelial basal media (EBM-2; Lonza) conditioned by hMSC CM for 20 hrs. As a positive control, HMVECs were also grown in Geltrex bathed in complete endothelial growth medium (EGM-2 = EBM-2 + 5% FBS + IGF, basic fibroblast growth factor [FGF], EGF,

vascular endothelial growth factor [VEGF]). Tube formation was quantified by counting the number of complete tubule branches in four fields of view using ImageJ software (NIH).

4.4.3 Human islet culture with hMSC CM

Human islets from 6 donors were obtained from the Integrated Islet Distribution Program (IIDP). Upon arrival, 200 islet equivalents were plated in RPMI media without serum (Invitrogen). CM was concentrated using 3 kDa molecular mass cut-off filters, and ~50 µg total protein was added to human islet culture for 7 days. After islet harvest and dissociation, β-cell content was estimated using FluoZin-3 (Flz3) (ThermoFisher Scientific) and apoptosis was quantified using 7AAD and Annexin-V. Flow cytometry data were analyzed using FloJo software (Treestar).

4.4.4 Chloroform/Methanol Precipitation and Protein Digestion

Protein extracts from hMSC CM samples were reduced in 10 mM DTT for 30 min and alkylated with 100 mM iodoacetamide (IAA) for 30 min at room temperature in the dark. Next, to facilitate the removal of incompatible detergents, reducing and alkylating reagents, the proteins were precipitated using chloroform/methanol according to the Wessel and Flügge protocol [48]. Briefly, 30 µg of protein extracted from each sample was diluted to a total volume of 150 µL with 50 mM ammonium bicarbonate (ABC), and 600 µL of ice cold methanol was added to each sample, followed by 150 µL of chloroform, with thorough vortexing. 450 µL of ice-cold DIH₂O was added before additional vortexing and centrifugation at 14,000 x g for 5 min at room temperature. The upper/aqueous methanol phase was removed and 450 µL

of ice-cold methanol was added to each sample, followed by vigorous vortexing and centrifugation at 14,000 x g for 5 min. The remaining chloroform/methanol was discarded and the precipitated protein pellet was air dried before protein digestion.

For on-pellet protein digestion, 100 μ L of 50 mM ABC (pH 8.0) with LysC (Wako) (1:100) solution was added to each precipitated sample and incubated in a ThermoMixer at 37°C for 4 hrs at 1000 RPM, followed by trypsin/LysC (1:50 ratio of enzyme: sample) (Promega) solution was added to each precipitated sample and incubated in a water bath shaker at 37°C overnight at 400 RPM. The next day, an additional aliquot of trypsin (1:100 ratio) was added for ~ 4 hrs, prior to acidifying with 10% formic acid (FA) (pH 3-4). The peptide concentrations were estimated using a Pierce BCA assay (ThermoFisher Scientific).

4.4.5 Liquid Chromatography-Tandem Mass Spectrometry (LC-MS/MS)

Approximately 1 μ g of each sample was injected onto a Waters M-Class nanoAcquity HPLC system (Waters) coupled to an ESI ion-trap/Orbitrap mass spectrometer (Q Exactive Plus). Buffer A consisted of mass spec. grade water/0.1% FA and Buffer B consisted of ACN/0.1% FA. All samples were trapped for 5 min at a flow rate of 5 μ L/min using 99% Buffer A and 1% Buffer B on a Symmetry BEH C18 Trapping Column (5 μ m, 180 μ m x 20 mm, Waters). Peptides were separated using a Peptide BEH C18 Column (130 Å, 1.7 μ m, 75 μ m x 250 mm) operating at a flow rate of 300 nL/min at 35°C (Waters). Samples were separated using a non-linear gradient consisting of 1-7% Buffer B over 1 min, 7-23% Buffer B over 135 min and 23-35% Buffer B

over 45 min, before increasing to 98% Buffer B and washing. Settings for data acquisition on the Q Exactive Plus for both LFQ and PRM are outlined in Table A4.3.

4.4.6 Label-free proteomic data analysis

All MS raw files were searched in MaxQuant version 1.5.8.30 using the Human Uniprot database (updated May 2015 with 20, 264 entries) [49,50]. For all database searches, missed cleavages were set to 3, cysteine carbamidomethylation was set as a fixed modification and Oxidation (M), N-terminal Acetylation (protein) and Deamidation (NQ) were set as a variable modifications (max. number of modifications per peptide = 5). Precursor mass deviation was left at 20 ppm and 4.5 ppm for first and main search, respectively. Fragment mass deviation was left at 20 ppm. Protein and peptide FDR was left to 0.01 (1%) and decoy database was set to revert. Match between runs was enabled and all other parameters left at default. Bioinformatics analysis was performed using Perseus version 1.5.8.5. Briefly, protein lists were loaded into Perseus and proteins identified by site reverse and contaminants were removed. When using the match between runs feature, datasets were filtered for proteins containing a minimum of 1 unique peptide in at least two of three biological replicates, as well as 6 out of 10 different hMSC lines.

4.4.7 Support vector machine learning

Data mining and protein marker selection of label-free quantitative proteomic data was achieved using the R package “geNetClassifier support vector machine (SVM)”. Briefly, a text document was constructed that

included all secreted proteins identified within the initial training data set. In additions, classification (regenerative versus non-regenerative) was assigned using human islet co-culture assays mentioned above. The posterior probability, or the predictive power, of each protein within the data set was determined and exported. Proteins that achieved a posterior probability of >0.90 were further evaluated. Uncharacterized hMSC lines were assessed against the classifier in the same manor. LFQ data for each uncharacterized hMSC line was imported into the SVM constructed from the training data set, and the probability of assigning each cell line was determined.

4.4.8 Peptide Synthesis

Solid phase peptide synthesis was achieved using the 96-well format on the MultiPep RS (Intavis). Peptides were synthesized using fmoc-chemistry on heavy ($^{13}\text{C}^{15}\text{N}$) labeled arginine preloaded chlorotriyl chloride resin (Cambridge Isotopes). Crude peptides were purified using an Agilent 1100 pump systems on a C18 column. Peptide purify was assessed using LC-MSMS.

4.4.9 Targeted proteomic data analysis

Parallel reaction monitors (PRM) data sets were analyzed using Skyline V3.7.0.11317. A spectral library was constructed from combining data-dependent acquisition runs using each cell line. Protein lists were filtered to only include proteins that had posterior probabilities of >0.80. In addition, missed cleavages were set to zero, and peptide length was limited to 16 amino acids. Peptides were chosen for targeting by order of pick intensity, meaning the three most abundant peptides for each target were measured for

a total of 28 targets corresponding to 208 peptides. A scheduled list was exported using a retention time window of ± 10 min. For each PRM sample, 20 μg of peptide was lyophilized and resuspended in 1 fmol/ μL solution of “heavy gfp”. PRM raw files were processed using skyline and total fragment area, which corresponded to the 5 most intense fragment ions (not including y1), were chosen for automatic integration. The total integrated fragment area of each peptide was determined and the ratio of target: heavy gfp was used to determine the relative abundance of each protein using a standard curve.

4.4.10 Transplantation of hMSC

Human BM was obtained from healthy donors after informed consent at the London Health Sciences Centre (London, ON, Canada). All studies were approved by the Human Research Ethics Board at Western University (REB# 12934, 12252E). The hyperglycemia-lowering capacity of one non-regenerative hMSC cell line classified using the SVM was assessed after tail vein injection of 500,000 cells into STZ-treated NOD/SCID mice as previously described [15]. Blood glucose concentrations were monitored weekly for 42 days and samples were segregated into regenerative or non-regenerative hMSC based on the ability to reduce blood glucose compared with PBS-injected control mice.

4.4.11 Statistical analysis

Statistical analysis was performed using GraphPad Prism version 6.01 (GraphPad) by ANOVA with Tukey’s post hoc test or by multiple t tests.

4.5 References

- [1] A.G. Via, A. Frizziero, F. Oliva, Biological properties of mesenchymal Stem Cells from different sources., *Muscles. Ligaments Tendons J.* 2 (2012)154–62.
- [2] R. Henschler, E. Deak, E. Seifried, Homing of mesenchymal stem cells, *Transfus. Med. Hemotherapy.* 35 (2008) 306–312. doi:10.1159/000143110.
- [3] A.I. Caplan, D. Correa, The MSC: An injury drugstore, *Cell Stem Cell.* 9 (2011) 11–15. doi:10.1016/j.stem.2011.06.008.
- [4] L. Zazzeroni, G. Lanzoni, G. Pasquinelli, C. Ricordi, Considerations on the harvesting site and donor derivation for mesenchymal stem cells-based strategies for diabetes, *5* (2017) 1–13.
- [5] A. El-Badawy, N. El-Badri, Clinical efficacy of stem cell therapy for diabetes mellitus: A meta-analysis, *PLoS One.* 11 (2016) 1–16. doi:10.1371/journal.pone.0151938.
- [6] M.-S. Tsai, S.-M. Hwang, K.-D. Chen, Y.-S. Lee, L.-W. Hsu, Y.-J. Chang, C.-N. Wang, H.-H. Peng, Y.-L. Chang, A.-S. Chao, S.-D. Chang, K.-D. Lee, T.-H. Wang, H.-S. Wang, Y.-K. Soong, Functional Network Analysis of the Transcriptomes of Mesenchymal Stem Cells Derived from Amniotic Fluid, Amniotic Membrane, Cord Blood, and Bone Marrow, *Stem Cells.* 25 (2007) 2511–2523. doi:10.1634/stemcells.2007-0023.
- [7] M.B. Murphy, K. Moncivais, A.I. Caplan, Mesenchymal stem cells: environmentally responsive therapeutics for regenerative medicine, *Exp. Mol. Med.* 45 (2013) e54. doi:10.1038/emm.2013.94.
- [8] L. Chen, E.E. Tredget, P.Y.G. Wu, Y. Wu, Y. Wu, Paracrine factors of mesenchymal stem cells recruit macrophages and endothelial lineage cells and enhance wound healing, *PLoS One.* 3 (2008). doi:10.1371/journal.pone.0001886.
- [9] R.C. Lai, S.S. Tan, R.W.Y. Yeo, A.B.H. Choo, A.T. Reiner, Y. Su, Y. Shen, Z. Fu, L. Alexander, S.K. Sze, S.K. Lim, MSC secretes at least 3 EV types each with a unique permutation of membrane lipid, protein and RNA, *J. Extracell. Vesicles.* 5 (2016) 29828. doi:10.3402/jev.v5.29828.
- [10] D. Todorova, S. Simoncini, R. Lacroix, F. Sabatier, F. Dignat-George, Extracellular vesicles in angiogenesis, *Circ. Res.* 120 (2017) 1658–1673. doi:10.1161/CIRCRESAHA.117.309681.
- [11] X. Gao, L. Song, K. Shen, H. Wang, M. Qian, W. Niu, X. Qin, Bone marrow mesenchymal stem cells promote the repair of islets from diabetic mice through paracrine actions, *Mol. Cell. Endocrinol.* 388

(2014) 41–50. doi:10.1016/j.mce.2014.03.004.

- [12] H. Hao, J. Liu, J. Shen, Y. Zhao, H. Liu, Q. Hou, C. Tong, D. Ti, L. Dong, Y. Cheng, Y. Mu, J. Liu, X. Fu, W. Han, Multiple intravenous infusions of bone marrow mesenchymal stem cells reverse hyperglycemia in experimental type 2 diabetes rats, *Biochem. Biophys. Res. Commun.* 436 (2013) 418–423. doi:10.1016/j.bbrc.2013.05.117.
- [13] S.H. Ranganath, O. Levy, M.S. Inamdar, J.M. Karp, Harnessing the mesenchymal stem cell secretome for the treatment of cardiovascular disease, *Cell Stem Cell*. 10 (2012) 244–258. doi:10.1016/j.stem.2012.02.005.
- [14] S.E. Sherman, M. Kuljanin, T.T. Cooper, D.M. Putman, G.A. Lajoie, D.A. Hess, High Aldehyde Dehydrogenase Activity Identifies a Subset of Human Mesenchymal Stromal Cells with Vascular Regenerative Potential, *Stem Cells*. 35 (2017). doi:10.1002/stem.2612.
- [15] G.I. Bell, H.C. Broughton, K.D. Levac, D.A. Allan, A. Xenocostas, D.A. Hess, Transplanted Human Bone Marrow Progenitor Subtypes Stimulate Endogenous Islet Regeneration and Revascularization, *Stem Cells Dev.* 21 (2012) 97–109. doi:10.1089/scd.2010.0583.
- [16] G.I. Bell, M.T. Meschino, J.M. Hughes-Large, H.C. Broughton, A. Xenocostas, D.A. Hess, Combinatorial Human Progenitor Cell Transplantation Optimizes Islet Regeneration Through Secretion of Paracrine Factors, *Stem Cells Dev.* 21 (2012) 1863–1876. doi:10.1089/scd.2011.0634.
- [17] M. Kuljanin, G.I. Bell, S.E. Sherman, G.A. Lajoie, D.A. Hess, Proteomic characterisation reveals active Wnt-signalling by human multipotent stromal cells as a key regulator of beta cell survival and proliferation, *Diabetologia*. (2017). doi:10.1007/s00125-017-4355-7.
- [18] J. Cox, M.Y. Hein, C. a Luber, I. Paron, Accurate proteome-wide label-free quantification by delayed normalization and maximal peptide ratio extraction, termed MaxLFQ, *Mol. Cell*. 13 (2014) 2513–2526. doi:10.1074/mcp.M113.031591.
- [19] S. Tyanova, T. Temu, P. Sinitcyn, A. Carlson, M.Y. Hein, T. Geiger, M. Mann, J. Cox, The Perseus computational platform for comprehensive analysis of (prote)omics data., *Nat. Methods*. 13 (2016) 731–40. doi:10.1038/nmeth.3901.
- [20] A. Subramanian, P. Tamayo, V.K. Mootha, S. Mukherjee, B.L. Ebert, M. a Gillette, A. Paulovich, S.L. Pomeroy, T.R. Golub, E.S. Lander, J.P. Mesirov, Gene set enrichment analysis: a knowledge-based approach for interpreting genome-wide expression profiles., *Proc. Natl. Acad. Sci. U. S. A.* 102 (2005) 15545–50. doi:10.1073/pnas.0506580102.
- [21] S. Tyanova, T. Temu, A. Carlson, P. Sinitcyn, M. Mann, J. Cox,

Visualization of LC-MS/MS proteomics data in MaxQuant, *Proteomics*. 15 (2015) 1453–1456. doi:10.1002/pmic.201400449.

- [22] C. Devi Arockia Vanitha, D. Devaraj, M. Venkatesulu, Gene expression data classification using Support Vector Machine and mutual information-based gene selection, *Procedia Comput. Sci.* 47 (2014) 13–21. doi:10.1016/j.procs.2015.03.178.
- [23] A. Cappiello, G. Famigliani, P. Palma, E. Pierini, V. Termopoli, H. Trufelli, U. Carlo, S. Chimiche, F.B. Urbino, Overcoming Matrix Effects in Liquid Chromatography - Mass Spectrometry, 80 (2008) 9343–9348.
- [24] B. MacLean, D.M. Tomazela, N. Shulman, M. Chambers, G.L. Finney, B. Frewen, R. Kern, D.L. Tabb, D.C. Liebler, M.J. MacCoss, Skyline: An open source document editor for creating and analyzing targeted proteomics experiments, *Bioinformatics*. 26 (2010) 966–968. doi:10.1093/bioinformatics/btq054.
- [25] K.L. DeCicco-Skinner, G.H. Henry, C. Cataisson, T. Tabib, J.C. Gwilliam, N.J. Watson, E.M. Bullwinkle, L. Falkenburg, R.C. O'Neill, A. Morin, J.S. Wiest, Endothelial Cell Tube Formation Assay for the &em;In Vitro&em; Study of Angiogenesis, *J. Vis. Exp.* 10 (2014) 1–8. doi:10.3791/51312.
- [26] L. Guedez, A.M. Rivera, R. Salloum, M.L. Miller, J.J. Diegmüller, P.M. Bungay, W.G. Stetler-Stevenson, Quantitative assessment of angiogenic responses by the directed in vivo angiogenesis assay., *Am. J. Pathol.* 162 (2003) 1431–9. doi:10.1016/S0002-9440(10)64276-9.
- [27] A. Tello-Montoliu, J. V. Patel, G.Y.H. Lip, Angiogenin: A review of the pathophysiology and potential clinical applications, *J. Thromb. Haemost.* 4 (2006) 1864–1874. doi:10.1111/j.1538-7836.2006.01995.x.
- [28] D. Schvartz, Y. Couté, Y. Brunner, C.B. Wollheim, J.-C. Sanchez, Modulation of Neuronal Pentraxin 1 Expression in Rat Pancreatic β -Cells Submitted to Chronic Glucotoxic Stress, *Mol. Cell. Proteomics*. 11 (2012) 244–254. doi:10.1074/mcp.M112.018051.
- [29] M.S. Islam, The islets of Langerhans. Preface., 2010. doi:10.1007/978-90-481-3271-3_1.
- [30] I.C. Rulifson, S.K. Karnik, P.W. Heiser, D. ten Berge, H. Chen, X. Gu, M.M. Taketo, R. Nusse, M. Hebrok, S.K. Kim, Wnt signaling regulates pancreatic beta cell proliferation, *Proc. Natl. Acad. Sci. U. S. A.* 104 (2007) 6247–6252. doi:10.1073/pnas.0701509104.
- [31] M.G. Rohani, W.C. Parks, Matrix remodeling by MMPs during wound repair, *Matrix Biol.* 44–46 (2015) 113–121. doi:10.1016/j.matbio.2015.03.002.
- [32] S. Negi, A. Jetha, R. Aikin, C. Hasilo, R. Sladek, S. Paraskevas, Analysis of Beta-Cell gene expression reveals inflammatory signaling

and evidence of dedifferentiation following human islet isolation and culture, *PLoS One*. 7 (2012) 1–11. doi:10.1371/journal.pone.0030415.

- [33] T.L. van Belle, P.P. Pagni, J. Liao, S. Sachithanatham, A. Dave, A. Bel Hani, Y. Manenkova, N. Amirian, C. Yang, B. Morin, H. Zhang, I.L. Campbell, M.G. von Herrath, Beta-cell specific production of IL6 in conjunction with a mainly intracellular but not mainly surface viral protein causes diabetes, *J. Autoimmun.* 55 (2015) 24–32. doi:10.1016/j.jaut.2014.02.002.
- [34] S.J. Burke, M.R. Goff, B.L. Updegraff, D. Lu, P.L. Brown, S.C. Minkin, J.P. Biggerstaff, L. Zhao, M.D. Karlstad, J.J. Collier, Regulation of the CCL2 Gene in Pancreatic β -Cells by IL-1 β and Glucocorticoids: Role of MKP-1, *PLoS One*. 7 (2012). doi:10.1371/journal.pone.0046986.
- [35] L. Piemonti, B.E. Leone, R. Nano, A. Sacconi, P. Monti, P. Maffi, G. Bianchi, A. Sica, G. Peri, R. Melzi, L. Aldrighetti, A. Secchi, V. Di Carlo, P. Allavena, F. Bertuzzi, Human pancreatic islets produce and secrete MCP-1/CCL2: Relevance in human islet transplantation, *Diabetes*. 51 (2002) 55–65. doi:10.2337/diabetes.51.1.55.
- [36] C.S. Nunemaker, H.G. Chung, G.M. Verrilli, K.L. Corbin, A. Upadhye, P.R. Sharma, Increased serum CXCL1 and CXCL5 are linked to obesity, hyperglycemia, and impaired islet function, *J. Endocrinol.* 222 (2014) 267–276. doi:10.1530/JOE-14-0126.
- [37] H.C. Gerstein, G. Pare, S. Hess, R.J. Ford, J. Sjaarda, K. Raman, M. McQueen, S.F. Lee, H. Haenel, G.R. Steinberg, Growth differentiation factor 15 as a novel biomarker for metformin, *Diabetes Care*. 40 (2017) 280–283. doi:10.2337/dc16-1682.
- [38] M.E. Hellemons, M. Mazagova, R.T. Gansevoort, R.H. Henning, D. De Zeeuw, S.J.L. Bakker, H.J. Lambers-Heerspink, L.E. Deelman, Growth-differentiation factor 15 predicts worsening of albuminuria in patients with type 2 diabetes, *Diabetes Care*. 35 (2012) 2340–2346. doi:10.2337/dc12-0180.
- [39] M.Y. Shin, J.M. Kim, Y.E. Kang, M.K. Kim, K.H. Joung, J.H. Lee, K.S. Kim, H.J. Kim, B.J. Ku, M. Shong, Association between growth differentiation factor 15 (GDF15) and cardiovascular risk in patients with newly diagnosed type 2 diabetes mellitus, *J. Korean Med. Sci.* 31 (2016) 1413–1418. doi:10.3346/jkms.2016.31.9.1413.
- [40] P.J. Emmerson, F. Wang, Y. Du, Q. Liu, R.T. Pickard, M.D. Gonciarz, T. Coskun, M.J. Hamang, D.K. Sindelar, K.K. Ballman, L.A. Foltz, A. Muppidi, J. Alsina-Fernandez, G.C. Barnard, J.X. Tang, X. Liu, X. Mao, R. Siegel, J.H. Sloan, P.J. Mitchell, B.B. Zhang, R.E. Gimeno, B. Shan, X. Wu, The metabolic effects of GDF15 are mediated by the orphan receptor GFRAL, *Nat. Med.* 23 (2017). doi:10.1038/nm.4393.
- [41] S.E. Mullican, X. Lin-Schmidt, C.-N. Chin, J.A. Chavez, J.L. Furman,

- A.A. Armstrong, S.C. Beck, V.J. South, T.Q. Dinh, T.D. Cash-Mason, C.R. Cavanaugh, S. Nelson, C. Huang, M.J. Hunter, S.M. Rangwala, GFRAL is the receptor for GDF15 and the ligand promotes weight loss in mice and nonhuman primates, *Nat. Med.* 23 (2017). doi:10.1038/nm.4392.
- [42] T. Kempf, A. Guba-Quint, J. Torgerson, M.C. Magnone, C. Haefliger, M. Bobadilla, K.C. Wollert, Growth differentiation factor 15 predicts future insulin resistance and impaired glucose control in obese nondiabetic individuals: Results from the XENDOS trial, *Eur. J. Endocrinol.* 167 (2012) 671–678. doi:10.1530/EJE-12-0466.
- [43] S.N. Breit, H. Johnen, A.D. Cook, V.W.W. Tsai, M.G. Mohammad, T. Kuffner, H.P. Zhang, C.P. Marquis, L. Jiang, G. Lockwood, M. Lee-Ng, Y. Husaini, L. Wu, J.A. Hamilton, D.A. Brown, The TGF- β superfamily cytokine, MIC-1/GDF15: A pleiotropic cytokine with roles in inflammation, cancer and metabolism, *Growth Factors.* 29 (2011) 187–195. doi:10.3109/08977194.2011.607137.
- [44] H.E. Bays, R.H. Chapman, S. Grandy, The relationship of body mass index to diabetes mellitus, hypertension and dyslipidaemia: Comparison of data from two national surveys, *Int. J. Clin. Pract.* 61 (2007) 737–747. doi:10.1111/j.1742-1241.2007.01336.x.
- [45] S.M. Phadnis, S.M. Ghaskadbi, A.A. Hardikar, R.R. Bhonde, Mesenchymal stem cells derived from bone marrow of diabetic patients portrait unique markers influenced by the diabetic microenvironment, *Rev. Diabet. Stud.* 6 (2009) 260–270. doi:10.1900/RDS.2009.6.260.
- [46] L. Shin, D.A. Peterson, Impaired Therapeutic Capacity of Autologous Stem Cells in a Model of Type 2 Diabetes, *Stem Cells Transl. Med.* 1 (2012) 125–135. doi:10.5966/sctm.2012-0031.
- [47] K.A. de Lima, G.L. V de Oliveira, J.N.U. Yaochite, D.G. Pinheiro, J.T.C. de Azevedo, W.A. Silva, D.T. Covas, C.E.B. Couri, B.P. Simões, J.C. Voltarelli, M.C. Oliveira, K.C.R. Malmegrim, Transcriptional profiling reveals intrinsic mRNA alterations in multipotent mesenchymal stromal cells isolated from bone marrow of newly-diagnosed type 1 diabetes patients., *Stem Cell Res. Ther.* 7 (2016) 92. doi:10.1186/s13287-016-0351-y.
- [48] D. Wessel, U.I. Flügge, A method for the quantitative recovery of protein in dilute solution in the presence of detergents and lipids, *Anal. Biochem.* 138 (1984) 141–143. doi:10.1016/0003-2697(84)90782-6.
- [49] J. Cox, M. Mann, MaxQuant enables high peptide identification rates, individualized p.p.b.-range mass accuracies and proteome-wide protein quantification, *Nat. Biotechnol.* 26 (2008) 1367–1372.
- [50] T.U. Consortium, UniProt: a hub for protein information, *Nucleic Acids Res.* 43 (2014) D204–D212. doi:10.1093/nar/gku989.

Chapter 5

Wnt-Activated hMSC Conditioned Media Mediates Islet Cell Regeneration *in vivo*¹

5.1 Introduction

Both type 1 (T1D) and type 2 diabetes (T2D) are characterized by a deficiency in insulin due to β -cell failure. Therefore curative strategies for diabetes treatment must begin with renewal of functional β -cell mass [1]. Even with modern exogenous insulin therapy, dysregulated glucose homeostasis results in devastating complications, and current therapeutic approaches to replace lost β -cells have included whole pancreas transplantation or intraportal delivery of isolated islets [2]. Unfortunately, implementation of these replacement strategies is limited due to an extreme shortage of donor tissue, and therapy is associated with eventual graft failure despite chronic immunosuppression [3,4].

In recent years, considerable progress has been made in the development of strategies to replace β -cell mass via *ex vivo* production of insulin-secreting, beta-like cells from pluripotent stem cells. Human embryonic stem cells (hESC) possess the potential to generate an unlimited number of β -cells for diabetes therapy [5].

¹ This chapter contains excerpts with permission from the following paper:

Kuljanin M, Elgamal RM, Bell GI, Lajoie GA, Hess DA. (2017) "Wnt-pathway stimulated hMSC-secreted effectors mediate islet cell regeneration ". Cell Stem Cell. (Submitted, November 2017)

However, hESC must be guided through various stages of development to form pancreatic endoderm and then endocrine precursors that ultimately acquire the ability to release insulin after pro-longed residence *in vivo* [6]. Recently, functionally matured beta-like cells have been generated *in vitro* through strict differentiation regimes to produce cells that secrete insulin in response to elevated glucose, and can revert hyperglycemia after implantation into STZ-treated NOD/SCID mice [7,8]. Like hESC, human induced pluripotent stem cells (iPSC) have also been used to generate insulin secreting cells. Most recently, the direct differentiation of multiple iPSC lines using small molecules, has been shown to produce insulin secreting cells that co-express PDX1 and NKX6.1 at varying frequencies [9,10]. Although the aforementioned studies represent impressive advances in the field of β -cell replacement, the cells generated secreted insulin at variable efficiencies and a deeper understanding of the genetic programs that govern β -cell genesis is still required to efficiently produce fully differentiated, glucose-responsive β -cells.

β -cell replacement can also be achieved by regeneration of β -cells within the pancreas itself. Interestingly, patients with long-standing T1D (Joslin Medalists) have preserved C-peptide production after >50 years of diabetes [11]. This has led to the notion that recovery of β -cell function *in situ* represents a feasible strategy for T1D treatment. Furthermore, recent evidence has shown that regulation of β -cell mass is more dynamic than previously understood. Human β -cells are capable of undergoing massive replication during obesity and pregnancy [12]. Two mechanisms controlling β -cell regeneration have been proposed. The first, suggests pre-existing β -cells

can undergo proliferation to generate greater β -cell mass [13,14]. The second suggests that β -cell regeneration is initiated from within islets or the ductal epithelial niche through the activation of facultative endocrine precursors via β -cell neogenesis [15–17]. In addition, α - β -cell conversion can occur in human islets [18], and recapitulates a developmental pattern elegantly demonstrated in lineage-tracing studies in mice [19]. Importantly, α - β -cell transition is accompanied by epithelial to mesenchymal transition (EMT) in the ductal epithelium, which subsequently convert to endocrine cell types that expand to generate new islets through a neogenic cascade. Currently, the specific stimuli that control these multi-factorial regenerative processes are unknown and remain the key to harnessing β -cell neogenesis *in situ* as a therapeutic option for T1D.

In a series of publications, elucidating the mechanisms of islet regeneration stimulated by the transplantation of human bone marrow-derived stem cells into STZ-treated mice, we have show that human multipotent stromal cells (hMSC) stimulate the emergence of small, recipient-derived islet-like structures associated with the ductal epithelial niche, [20–22]. Detailed proteomic analysis of secretory factors deposited into the regenerative niche have revealed Wnt-signaling to be an important pathway in hMSC regulation of this secretory pattern [23]. Indeed, activation of Wnt-signaling resulted in the production of a conditioned media (CM) cocktail that increased the proliferation rate of adult human β -cells and more than doubled the β -cell mass in rodent models [24,25]. Collectively, these findings suggested that activation of endogenous islet regenerative mechanisms could be achieved via protein-based therapies derived from hMSC.

The use of protein factors or media conditioned by hMSC to treat diabetes has recently gained traction. Multiple intravenous injections of CM in experimental T2D rats effectively reduced systemic blood glucose levels by stimulating the proliferation of residual β -cells [26]. In addition, Gao *et. al.* demonstrated the CM could initiate recovery of T1D mice through the activation of pAKT pathways, and successfully demonstrated that harvested islets bathed in CM can undergo β -cell proliferation *in vitro* [27]. Both studies used intravenous-injection as their mode of delivery and did not investigate whether direct delivery to the pancreas would increase the therapeutic effect of the CM. Other modes of delivery have been investigated. Intraperitoneal and intra-ductal injection of periostin, a protein produced by pancreatic stellate cells and found in high levels in hMSC CM, resulted in an increased number of islets and augmented glucose homeostasis *in vivo* [28].

Herein, we investigate the direct delivery of hMSC CM into the pancreas of STZ-treated mice and show for the first time that islet regeneration is efficient and robust after CM delivery. The regenerative response could be modulated by protein dose and activation of Wnt-signaling *in vitro* augmented the regenerative potency of CM generated. We also show that the regenerative mechanism for the restoration of glucose homeostasis involved the paracrine activation of multiple regenerative pathways consistent with ductal tree associated α to beta-like cell neogenesis followed by β -cell replication and functional maturation. Finally, key effectors secreted during Wnt-pathway stimulation were identified using quantitative proteomics and provided a list of potential targets for further investigation.

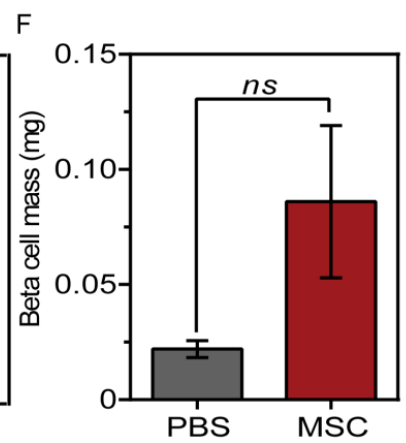
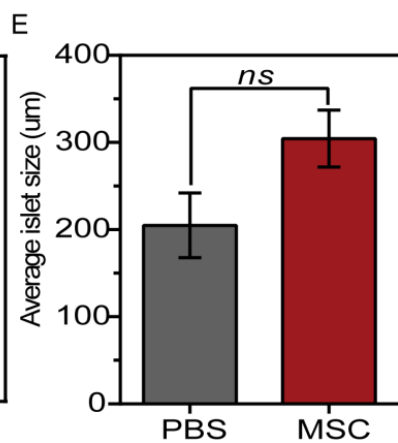
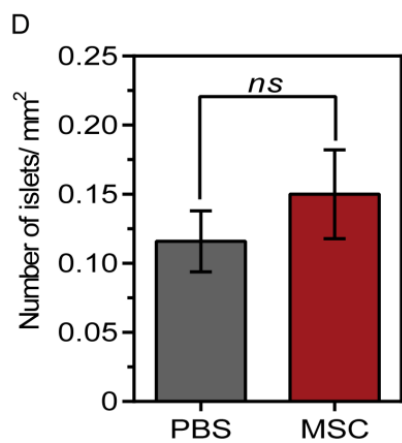
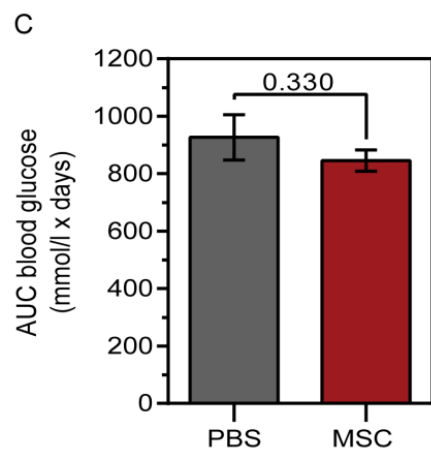
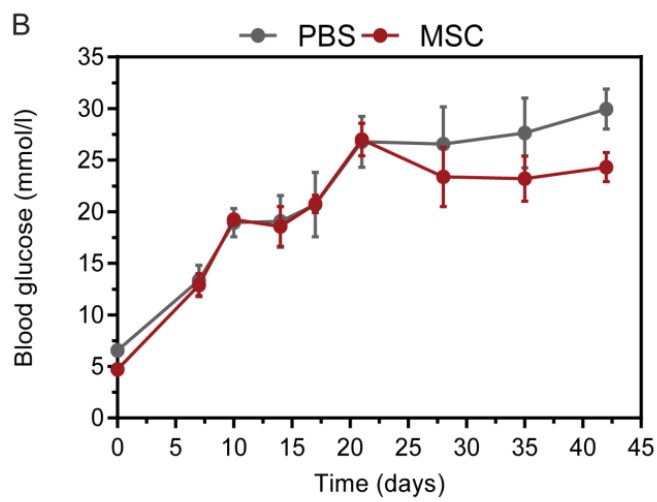
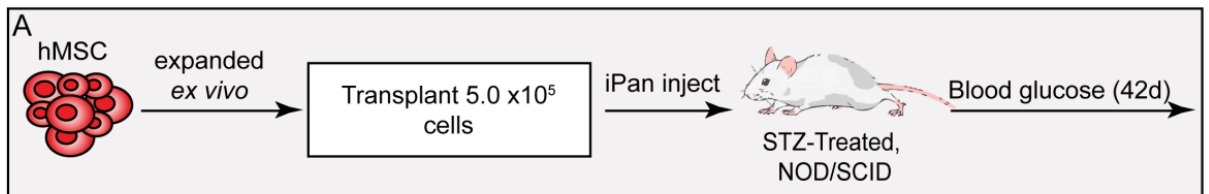
5.2 Results

5.2.1 *Intrapancreatic hMSC injection induced emergence of single insulin⁺ cells*

STZ-treated (35 mg/kg/day, days 1-5) and hyperglycemic (15-25 mmol/l) NOD/SCID mice were intrapancreatically (iPan) injected on day 10 with BM-derived hMSC (5.0×10^5 cells), and blood glucose levels were monitored for 42 days (Figure 5.1a). Compared with PBS-injected control mice ($n=6$) that remained severely hyperglycemic (>25 mmol/l), hMSC injection ($N=3$, $n=8$) led to slightly reduced systemic glycemia from days 28-42 (Figure 5.1b). Although blood glucose stabilized after hMSC transplantation, glucose levels plateaued at 22.5 ± 2.5 mmol/l (Figure 5.1b) indicating transplantation did not significantly reduce established hyperglycemia (AUC) over the full time course (Figure 5.1c). To better characterize endogenous mechanisms by which transplanted hMSC showed improved glycemia, the pancreas of transplanted mice were stained for murine insulin and analyzed for islet number (Figure 5.1d), islet size (Figure 5.1e) and β -cell mass (Figure 5.1f). Although histological sections at day 42 did not reveal any differences in islet number or structure between PBS (Figure 5.2a) or hMSC (Figure 5.2b) transplanted mice, we observed a trend towards increased islet size and total β -cell mass, but these differences were not significant by student's T-test. However, all mice transplanted with hMSC showed the emergence of single insulin⁺ cells at early (D14) time points (Figure 5.2c, d). To rule out whether hMSC were differentiating into insulin⁺ cells, human cell engraftment (HLA) and co-expression of insulin was assessed. Mice transplanted with hMSC show high levels of engraftment at day 14 (Figure 5.2e), which was diminished by day 42 (Figure 5.2f). Although hMSC never co-expressed

insulin, hMSC were commonly found adjacent to single murine insulin⁺ cells, suggesting that endogenous regenerative mechanisms were activated in a paracrine fashion. Thus, iPan transplantation of hMSC seemed to induce regenerative effects consistent with the activation of putative islet neogenic mechanisms.

Figure 5.1 Intrapancreatic delivery of ex vivo expanded hMSC cells does not augment the recovery of blood glucose in STZ-treated NOD/SCID mice. (a) hMSC were expanded *ex vivo* and transplanted (5.0×10^5 cells) directly into the pancreas and systemic blood glucose was monitored for 42 days. (b) Compared with PBS injected controls, mice transplanted with hMSC showed a slight reduction in blood glucose at D28-D42. (c) Total AUC after 42 days was not significantly different from PBS. Mice injected with hMSC did not show a significant increase in (d) number of islets/mm² (e) or average islet size and β -cell mass (f). Data is represented as mean \pm S.E.M.



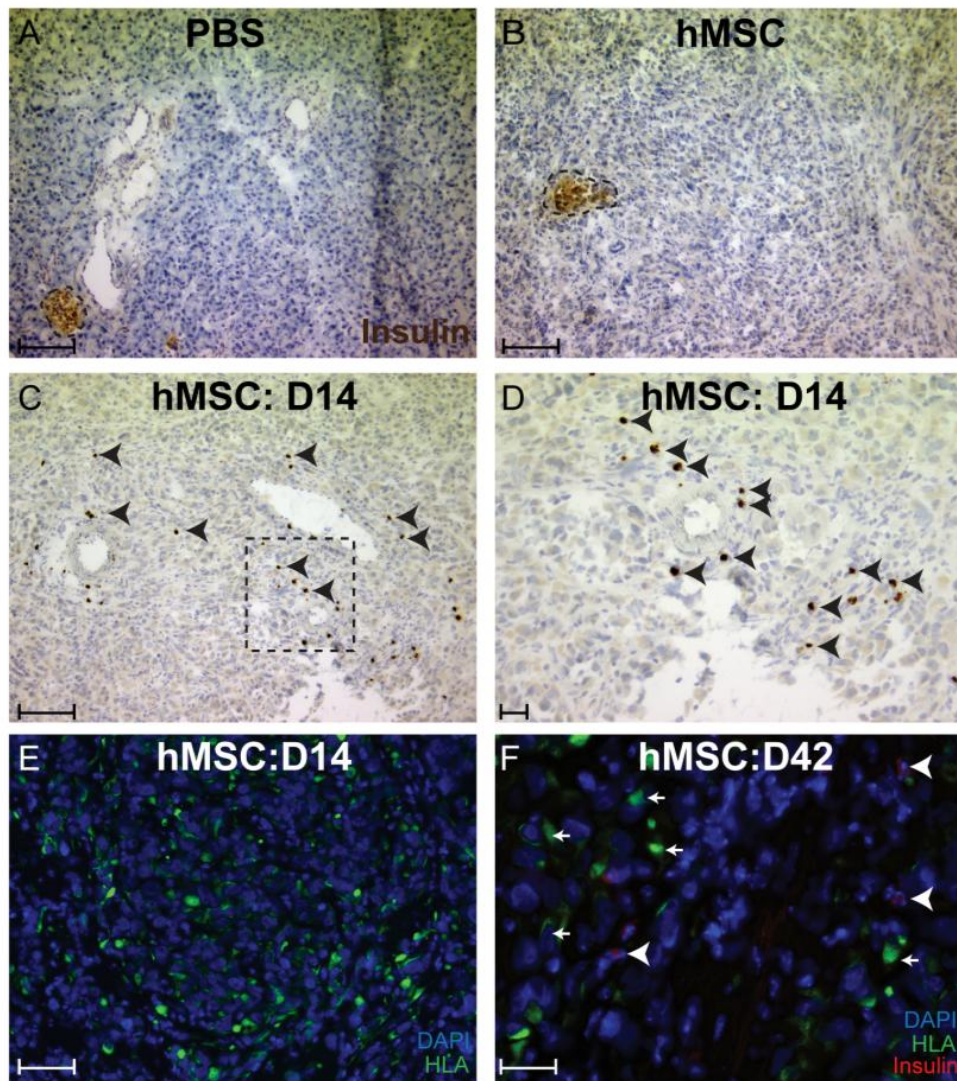


Figure 5.2 Intrapancreatic transplanted hMSC are present in the pancreas at D42 and give rise to single insulin positive murine cells. Representative photomicrographs of insulin+ islets at D42 injected with (a) PBS and (b) hMSC. (c) Mice injected with hMSC give rise to single insulin+ cells (arrow heads), not observed in PBS controls. (d) Magnified view of box found in (c). (d) Transplantation of hMSC resulted in consistent and high-frequency cell engraftment in the mouse pancreas at D14. (e) At D42 human HLA A,B,C+ (arrows) surrounding murine cells that do not co-express insulin are present (arrow heads). Scale bars= 200 μ m.

5.2.2 *Intrapancreatic hMSC CM injection reduced hyperglycemia*

hMSC were grown to ~80% confluency and switched to serum free media for 24 hours when CM was collected, concentrated and quantified. Hyperglycemic (15-25 mmol/l), STZ-treated NOD/SCID mice were iPan injected on day 10 with hMSC CM with either 4 µg or 8 µg of total protein (in 20 µl) and blood glucose levels were monitored for 42 days (Figure 5.3a). Normoglycemic control mice were injected with citric acid buffer (CAB) instead of STZ from days 1-5, or STZ-treated mice were injected with basal media concentrated without conditioning (unconditioned media). Compared to mice injected with unconditioned media ($n=11$) that remained severely hyperglycemic or mice injected with the lower dose of 4 µg hMSC CM ($n=7$), mice injected with higher dose of 8 µg CM ($n=7$) showed significantly improved systemic glycemia as early as 4 days post injection (Figure 5.3b). Overall, injection of 8 µg CM significantly reduced AUC for systemic blood glucose levels over the full 42 days (Figure 5.3c). At day 42, serum insulin levels were quantified. STZ-injected, media control mice, or mice injected with 4 µg CM showed ≈5-fold reduced serum insulin concentrations compared to CAB controls (Figure 5.3d). However, mice transplanted with 8 µg CM showed significantly increased serum insulin compared to mice injected with unconditioned media or 4 µg CM. Residual insulin levels within concentrated basal CM samples were below the detectable limit of the assay (<0.0025 ng/ml).

Glucose tolerance was also performed at day 42 to assess whether transplanted mice could respond to a glucose challenge. Compared with CAB-injected mice that were normoglycemic (4.4 ± 1.0 mmol/l) and showed

strong biphasic glucose reduction, while mice injected with unconditioned media or 4 μg CM showed little response to glucose bolus and prolonged hyperglycemia that never returned to starting concentrations (Figure 5.3e). In contrast, mice injected with 8 μg CM showed glucose levels that peaked at 30 min (22.7 ± 2.5 mmol/l) and eventually returned back down to initial concentration (13.5 ± 2.3 mmol/l) at 90 minutes. The AUC for mice injected with 8 μg CM was significantly lower than both mice injected with unconditioned media or mice injected with 4 μg CM (Figure 5.3f). In addition, the weight of each mouse was monitored for the full 42 days to ensure weight loss did not contribute to glucose readings (Figure 5.3g). There was no significant reduction in weight for any of the treated mouse groups. Taken together, mice transplanted with hMSC CM demonstrated significant recovery of endocrine function and improved glycemia was observed in a concentration-dependent manner.

5.2.3 *Active Wnt-signaling generated CM with augmented glucose lowering capacity*

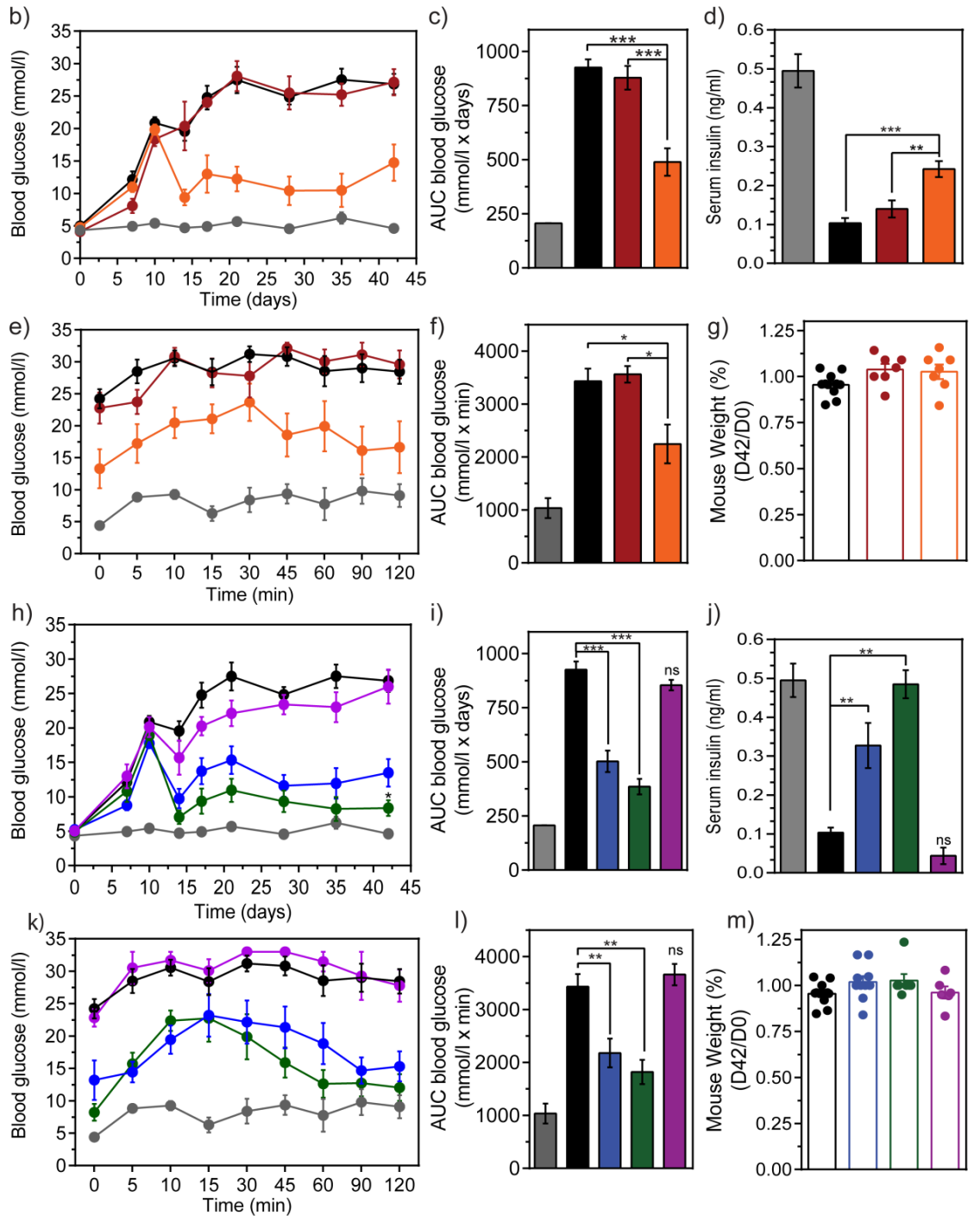
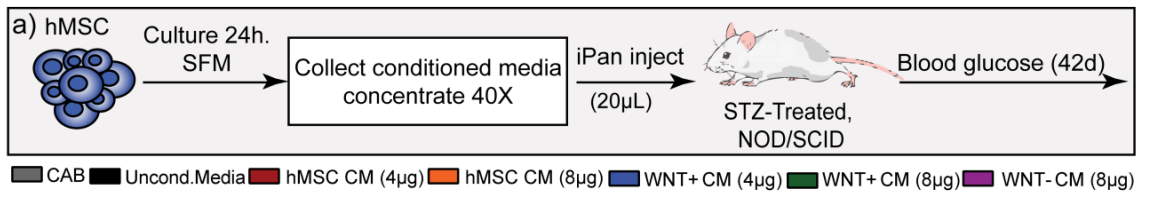
We have previously shown that active Wnt-signaling is an important component of the islet regenerative niche established by hMSC, and activation of Wnt-signaling using GSK-inhibition during hMSC CM generation increased cultured human β -cell survival and proliferation *in vitro* [23]. To determine how modulation of Wnt-signaling during hMSC CM generation would impact systemic blood glucose levels after iPan injection of CM, we sought to activate and inhibit Wnt-signaling using small molecules (CHIR99201 and IWR-1) respectively [29,30]. To determine the optimal concentration for Wnt-pathway activation, qPCR was performed on two

downstream Wnt-signaling genes, *BCL9* (Figure 5.4a) and *MYC* (Figure 5.4b). A significant (>2 fold) increase was observed in both genes upon treatment of hMSC with 10 μ M of CHIR99201. In addition, we also quantified total β -catenin levels, the master regulator of Wnt-signaling pathway [31], by flow cytometry. Treatment with 10 μ M of CHIR99201 increased β -catenin protein levels \sim 1.9 fold (Figure 5.4c). The optimal concentration for inhibition of Wnt-signaling with IWR-1 was determined using the same approach. Treatment of hMSC with 20 μ M of IWR-1 showed a significant (>two fold) decrease in both *BCL9* (Figure 5.4d) and *MYC* (Figure 5.4e). Treatment with 20 μ M of IWR-1 also decreased β -catenin protein levels by \sim 1.5 fold (Figure 5.4f).

To generate Wnt-activated (WNT+) or inhibited (WNT-) media, hMSC were grown to \sim 80% confluency, switched to serum free media and cultured with 10 μ M CHIR99201 or 20 μ M of IWR-1, for 24 hours. CM was collected and concentrated as described above and hyperglycemic mice were injected with WNT+ CM (20 μ l) at either \sim 4 or \sim 8 μ g total protein or \sim 8 μ g WNT- CM. Compared to mice injected with unconditioned media, mice injected with 4 μ g WNT+ CM (13.5 ± 1.6 mmol/l) or 8 μ g WNT+ CM (8.3 ± 1.1 mmol/l) showed significantly reduced systemic glycemia post injection (Figure 5.3h). In contrast, 8 μ g WNT- CM did not significantly reduce systemic glycemia post injection (29.7 ± 2.2 mmol/l). Overall, injection of either 4 or 8 μ g WNT+ CM significantly reduced the AUC for blood glucose levels over the full 42 days compared to media controls and 8 μ g WNT- CM (Figure 5.3i). The total recovery was not significantly different between 4 and 8 μ g WNT+ CM over the full time course ($p=0.10$), but was found to be significantly different at day 42. Mice injected with 4 or 8 μ g WNT+ CM showed significantly increased

serum insulin levels at day 42, compared to unconditioned media controls (3.2-fold and 4.7-fold increase, respectively), while WNT- CM did not alter serum insulin (Figure 5.3j). Most notably, mice injected with 8 μ g WNT+ CM had circulating serum insulin levels equivalent to CAB controls (0.485 ng/ml). Again, residual insulin levels within concentrated CM were below the detectable limit of the assay (<0.0025 ng/ml). Finally glucose tolerance was also performed at day 42 to assess response to a glucose challenge. Mice injected with 4 μ g WNT+ CM showed blood glucose levels that peaked at 15 min (22.7 ± 3.1 mmol/l) and gradually decreased to (15.3 ± 2.2 mmol/l) (Figure 5.3k). Furthermore, mice injected with 8 μ g WNT+ CM showed blood glucose levels that spiked at 10 min (22.3 ± 1.5 mmol/l) and rapidly returning back down to initial conditions (11.5 ± 2.1 mmol/l). In contrast, mice injected with 8 μ g WNT- CM showed blood glucose levels that spiked at 30 min to maximal levels (>33 mmol/l) remained high (26.2 ± 4.5 mmol/l) for 120 minutes. The AUC for mice that were injected with 4 or 8 μ g of WNT+ CM were significantly lower compared to unconditioned controls or 8 μ g of WNT- CM injected mice (Figure 5.3l). A ratio of the starting weight (D0) and the final weight (D42) showed that there was no significant reduction in weight (Figure 5.3m). Taken together, mice that were injected with 4 μ g WNT+ CM demonstrated significant, although partial, recovery of endocrine function in response to glucose challenge, while mice that were injected with 8 μ g WNT+ CM demonstrated full recovery of endocrine function. Thus activation of Wnt-signaling during CM generation augmented glucose control, and inhibition of Wnt-signaling reversed this beneficial effect.

Figure 5.3 Intrapancreatic-injection of Wnt-activated hMSC CM improved glucose control. (a) hMSC CM was generated for 24h, concentrated (40X), and iPan-injected at 4 μ g or 8 μ g total protein. (b-f) Mice injected with 8 μ g hMSC CM showed reduced blood glucose, increased serum insulin, and improved glucose tolerance compared to mice injected with 4 μ g hMSC CM or unconditioned media. (g) Mouse weight was not changed by injection of hMSC CM. (h-l) Mice injected with 4 μ g or 8 μ g WNT+ CM showed reduced blood glucose, increased serum insulin, and improved glucose tolerance compared to mice injected with 8 μ g WNT- CM or unconditioned media. (m) Mouse weight was not changed by injection of WNT+ or WNT- CM. Data is represented as mean \pm S.E.M. (* p <0.05, ** p <0.01, *** p <0.001).



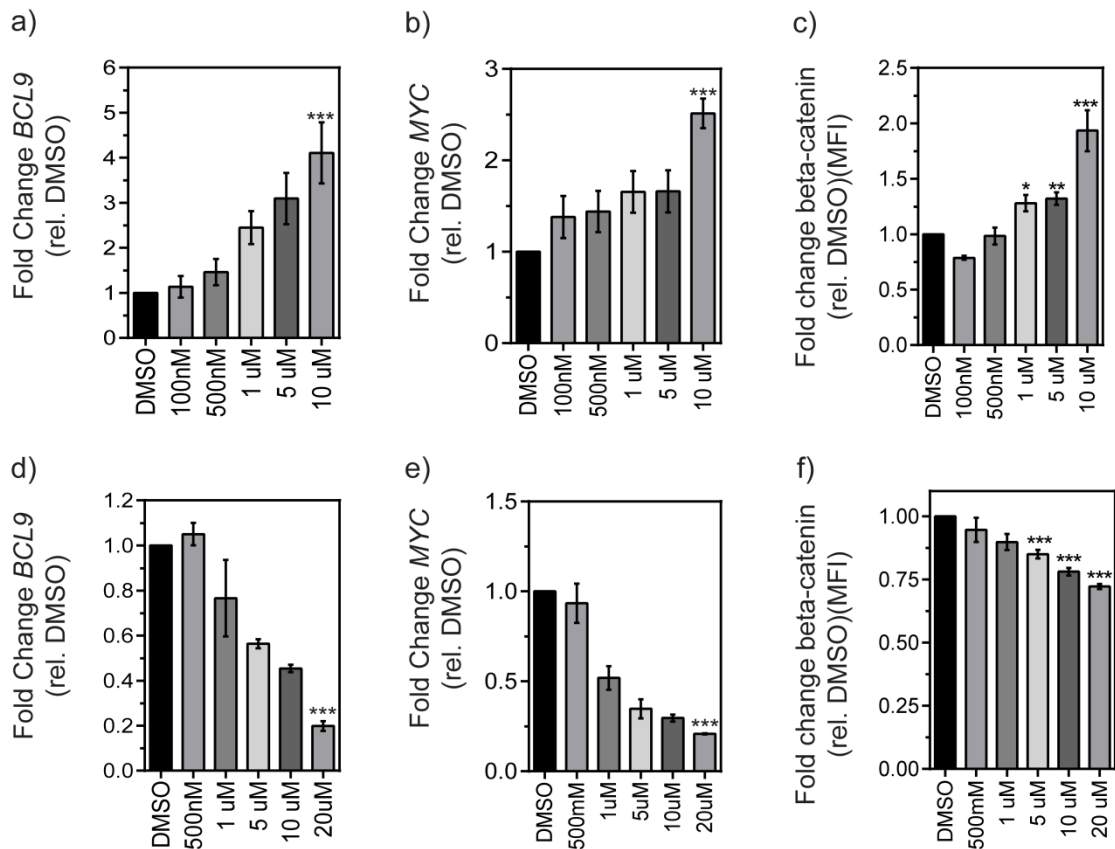


Figure 5.4 hMSC show robustly stimulation and inhibition of Wnt-signaling by CHIR99201 and IWR-1, respectively. hMSC stimulated with CHIR99201 at (0.1, 0.5, 1, 5 and 10 μ M) show increased transcript expression of downstream products of Wnt-signaling (a) BCL9 and (b) MYC. (c) hMSC stimulated with CHIR99201 also show increased expression of β -catenin at the protein level. hMSC inhibited with IWR-1 at (0.5, 1, 5, 10 and 20 μ M) show decreased expression of downstream products of Wnt-signaling (d) BCL9 and (e) MYC. (f) hMSC inhibited with IWR-1 also show decreased expression of β -catenin at the protein level. Transcript data was normalized to housekeep gene (ACTB). Data is represented as mean \pm S.D. (* p <0.05, *** p <0.01, **** p <0.001).

5.2.4 *hMSC CM loses glucose lowering capacity after heat denaturing*

Wnt-activated CM was generated and concentrated as described above and CM was denatured via heating at 90°C for 20 min. After heating, mice were injected with an equivalent dose (4 µg) of denatured CM (dWNT+) ($n=3$) and compared to 4 µg of WNT+ CM. Overall, transplantation of 4µg WNT+ CM significantly reduced systemic blood glucose levels over the full 42 days compared to media controls and injection of 4 µg dWNT+ CM did not reduce blood glucose levels (Figure 5.5a). AUC measurements confirmed a significant reduction in hyperglycemia (Figure 5.5b). In addition, serum insulin concentrations in mice injected with dWNT+ CM were 6.8-fold lower than WNT+ CM (data not shown). To determine what factors in the CM were degraded during heating, native PAGE was performed to confirm proteins present in the CM were fully denatured (Figure 5.5c). Proteins within the dWNT+ CM migrated differently on native PAGE due to disruption of the overall charge state [32], and serum albumin shifted (lane 2), along with other faint bands, signifying denaturation of proteins has occurred.

Generation of CM was achieved using MWCO filters (3 kDa) that are also known to concentrate extracellular vesicles containing protein, long-non-coding RNA and micro-RNAs [33]. To investigate residual RNA content within dWNT+ CM samples, RNA integrity analysis was performed using picoRNA chip technology (Figure 5.5d-e). Upon heating, there was a drastic decrease in the total RNA content observed in the CM. However, the quality of the RNA, interpreted by using the RNA Integrity Number (RIN), was extremely low in both the WNT+ (1.9) and the dWNT+ (1.0) CM, suggesting that residual RNA in the CM was severely degraded during collection and concentration of the

media without RNase inhibition (Figure 5.5f) [34] . In summary, heating CM reversed the blood glucose lowering capacity through denaturing of proteins within the CM. Although the effect of residual miRNA was not directly investigated, only 6.1-12.2 pg of mostly degraded RNA was injected into each mouse, making the glucose lowering contribution of RNA within the CM samples highly unlikely.

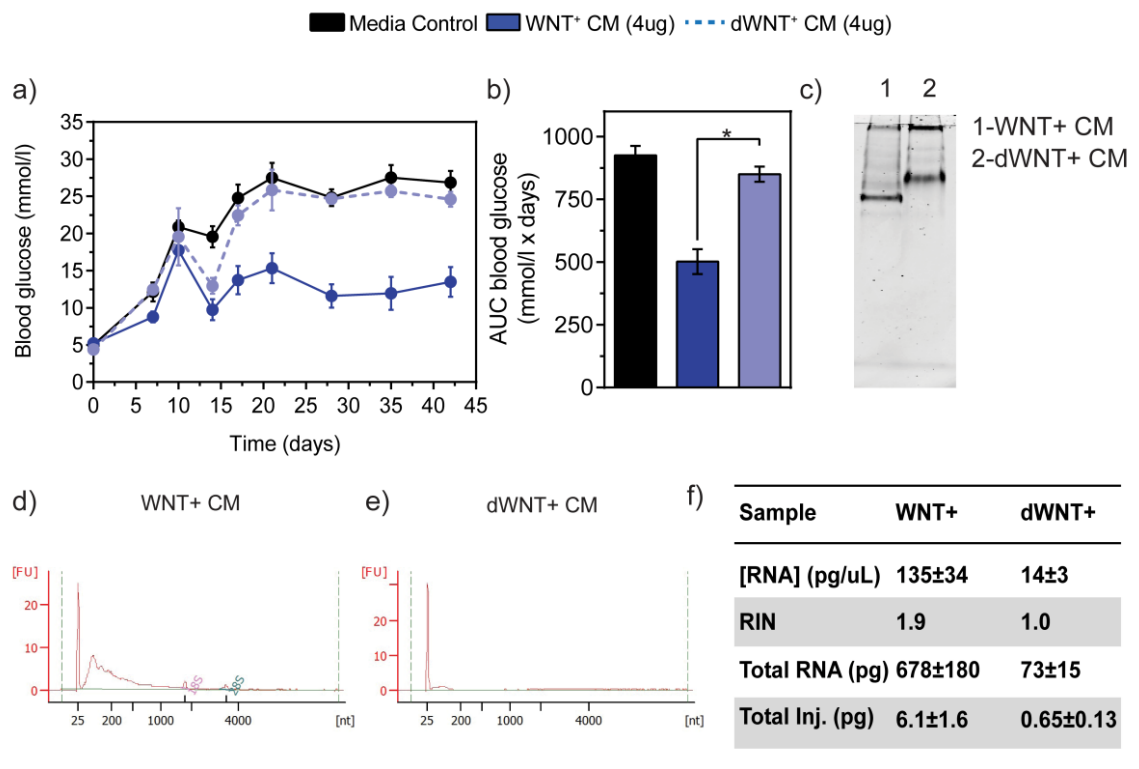


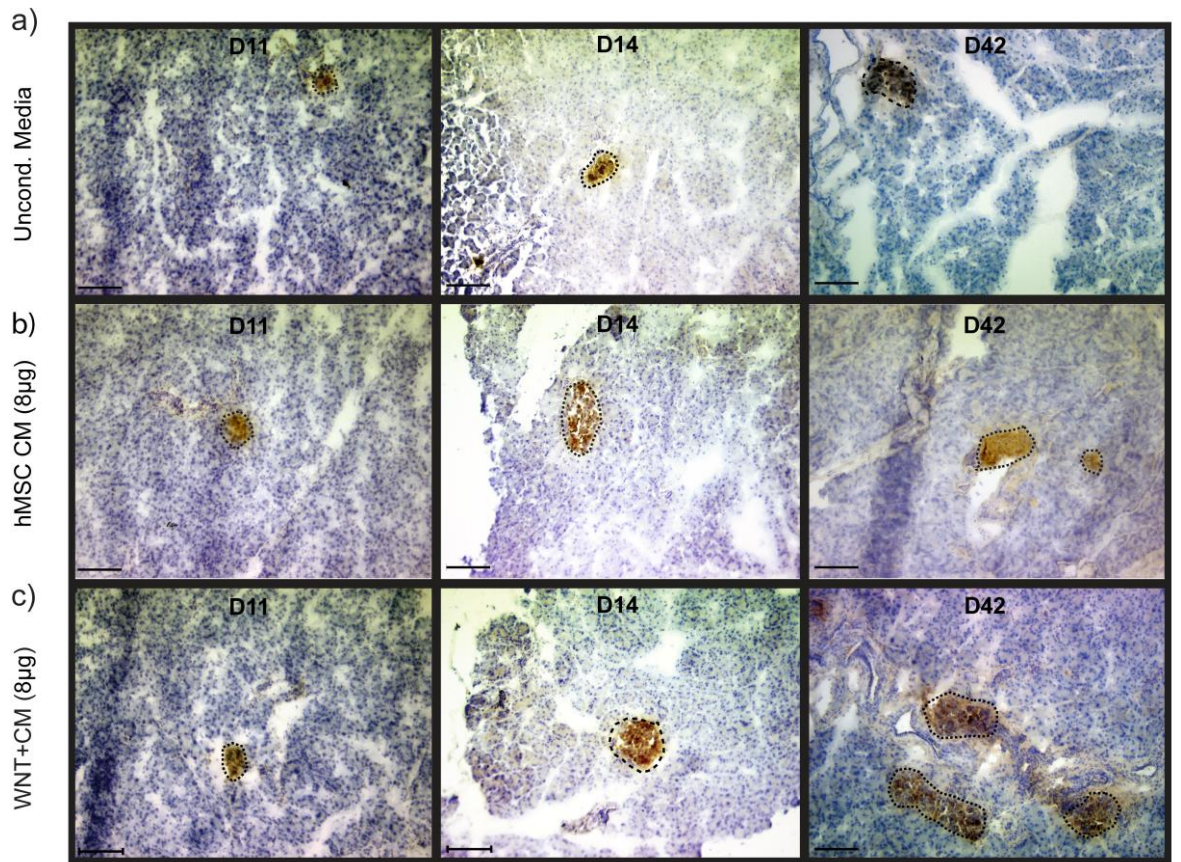
Figure 5.5 Islet Regenerative CM loses capacity to lower blood glucose levels after heating. (a) hMSC CM generated by stimulation with 10 μ M of CHIR99201 was heated to 90°C for 20 min and injected into STZ-treated NOD/SCID mouse. Glucose lowering capacity was abrogated upon denaturation of the components in the CM. (b) Blood glucose concentrations were significantly higher after injection of denatured CM compared to native CM. (c) WNT+ CM was assessed using Native PAGE to determine if proteins were denatured. Lane 1 contains native CM, while lane 2 is heated to 90°C. (d-e) PicoRNA analysis revealed that RNA content was severely degraded during CM generation and concentration. (f) Total amount of RNA injected per condition.

5.2.5 *Islet regeneration resulted in increased β -cell mass*

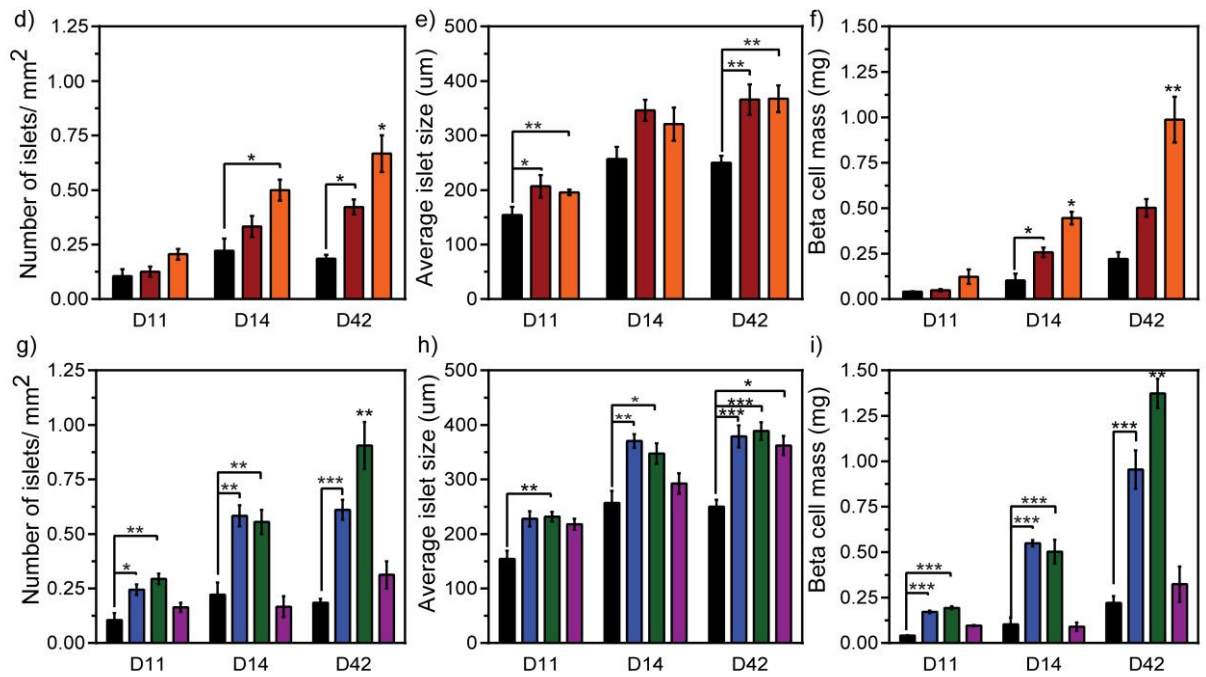
To characterize the mechanisms and dynamics by which injection of hMSC CM augmented islet regeneration, pancreata of injected mice euthanized at day 11 (D11), 14 (D14) and 42 (D42), were first stained for murine insulin (Figure 5.6a-c). As a general observation, the number of islets, mean islet size and total β -cell mass were increased over time in each condition tested (D11-D42). Compared to mice injected with unconditioned media, mice that received 8 μ g hMSC CM had significantly increased islet number (Figure 5.6d), islet size (Figure 5.6e), and total β -cell mass (Figure 5.6f) at each time point tested. Importantly, mice that received 4 μ g hMSC CM also showed significantly increased islet size compared to unconditioned controls at D42. In addition, the increase in both islet number and islet size after WNT+ CM injection occurred within 4 days after transplantation (between D10-D14), eventually plateauing between D14-D42. Mice injected with 4 μ g or 8 μ g WNT+ CM also demonstrated significantly increased islet number (Figure 5.6g), islet size (Figure 5.6h), and total β -cell mass (Figure 5.6i). Interestingly, 4 μ g WNT+ CM showed islet regenerative capacity similar to 8 μ g hMSC CM. In contrast, when Wnt-signaling was inhibited during CM generation, islet number, islet size and β -cell mass were similar to media controls (Figure 5.6g-i). As an overall indication of endocrine recovery, transplantation of 8 μ g hMSC CM or 8 μ g WNT+ CM maximally increased β -cell mass (Figure 5.6f,i), and the kinetics of β -cell mass increased steadily over time. Finally, injection of 8 μ g WNT+ CM initiated islet regeneration within one day post-injection and β -cell mass continued to increase over 42 days. Overall, these data confirm that hMSC CM can stimulate the recovery of

β -cell mass and that active Wnt-signaling during CM generation is an important contributor for β -cell recovery.

Figure 5.6 Intrapancreatic-injection of Wnt-activated hMSC CM increased islet number, size, and β -cell mass. (a-c) Representative photomicrographs of insulin expression in islets at days 11, 14 and 42 in mice injected with unconditioned media, or 8 μ g hMSC CM, or 8 μ g WNT+ CM. (d-f) Mice injected with 8 μ g hMSC CM showed increased islet number, islet size, and β -cell mass compared to mice injected with 4 μ g hMSC CM or unconditioned media. (g-i) Mice injected with 4 μ g or 8 μ g WNT+ CM showed increased islet number, islet size, and β -cell mass compared to mice injected with 8 μ g WNT- CM or unconditioned media. Data is represented as mean \pm S.E.M. (* p <0.05, ** p <0.01, *** p <0.001).



■ Uncond. Media ■ hMSC CM (4 μ g) ■ hMSC CM (8 μ g) ■ WNT+CM (4 μ g) ■ WNT+CM (8 μ g) ■ WNT-CM (8 μ g)



5.2.6 Regenerated islets showed increased vascularization

Immunofluorescent staining for murine insulin in combination with vWF or CD31, to mark larger vessels, and intra-islet capillaries respectively, was used to investigate islet vascularization at D42 (Figure A5.1a-f). Because we observed differences in islet size between treatments, total CD31⁺ vessels and capillaries within islets were normalized to islet area. Compared with unconditioned media injected controls, mice that were injected with 8 µg hMSC CM or 4/8 µg WNT+ CM showed significantly increased vWF⁺ vessels associated with islets (Figure A5.1g) and total CD31⁺ cells found within islets (Figure A5.1h-i). Notably, these cohorts showed no difference in vessel density compared to CAB injected mice, suggesting newly formed islet were highly vascularized. Injection of WNT- CM showed vessel densities equivalent to unconditioned media control injected mice. Thus, transplantation of hMSC CM promoted re-vascularization of regenerated islets, thereby improving insulin release into circulation.

5.2.7 Regenerative CM increased islet association with the ductal epithelium

Transplantation of hMSC has been shown to increase the number of islets associated with the ductal epithelium, suggesting developmental islet neogenesis was activated [21,22]. To investigate whether islet formation was initiated in ductal regions after hMSC CM injection, co-staining for insulin and ck19, to mark ductal epithelial cells, was performed at each time points (Figure 5.7a-c). As a general observation, the ductal association of islet clusters decreased over time under each condition tested. Interestingly, unconditioned media injected mice showed increased ductal associated islets at early time points (40%), suggesting that STZ-treatment alone stimulated

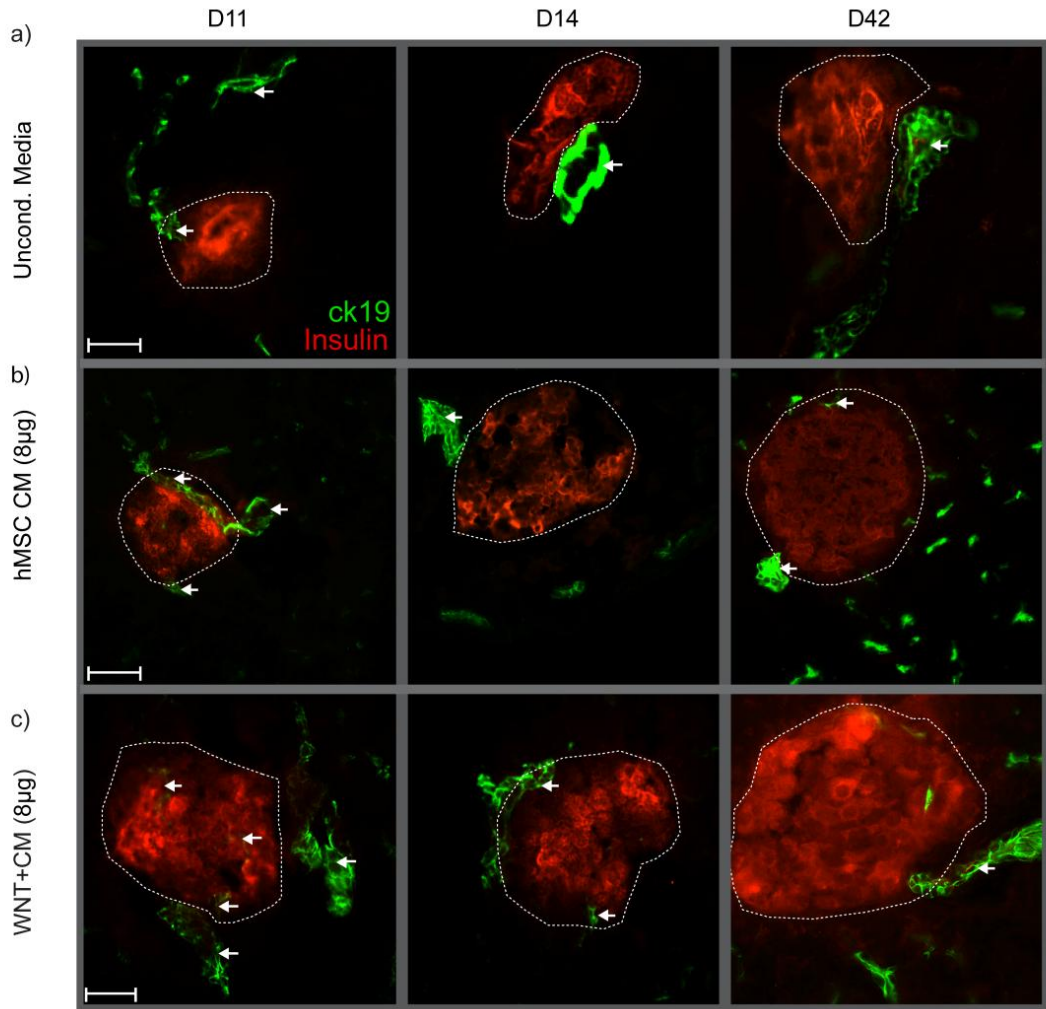
endogenous islet regeneration in the ductal epithelial niche. Mice that received 8 μ g hMSC CM showed significantly increased ductal association at early and late time points (D11 and D42) (Figure 5.7d). However, activation of Wnt-signaling during CM generation significantly increased ductal association for 4 μ g or 8 μ g WNT+ CM injected mice at each time point tested (Figure 5.7e). Finally, injection of WNT- CM showed ductal association of islets similar to unconditioned media injected mice across each time point. These data suggested the ductal epithelial niche as a site for hMSC CM-mediated islet regeneration.

5.2.8 Regenerative CM stimulated β -cell proliferation

To further investigate the mechanisms of islet expansion induced after CM injection, we analyzed EdU incorporation into proliferating β -cell within islets labeled for 24 hours prior to euthanasia at D11, D14 and D42 (Figure 5.8a-c). As a general observation, the frequency of islets that contained proliferating β -cells were decreased over time under each condition tested (D11-D42). In mice injected with unconditioned media, proliferating insulin⁺ β -cells were extremely rare, with approximately 1 in 5 islets containing a proliferating β -cell, indicating a slow turnover of β -cells after STZ-treatment. Mice that received 8 μ g hMSC CM showed proliferation rates that were more than 2-fold higher compared 8 μ g hMSC CM and unconditioned media at D14 (Figure 5.8d). Mice that received WNT+ (either 4 or 8 μ g) CM showed significantly higher proliferation rates at D11, D14 and D42 (Figure 5.8e). In all conditions that showed significantly increased proliferation rates at D14, the frequency of proliferating islets was maintained at D42, suggesting that restoration of basal proliferative levels was achieved. These data suggest that

hMSC CM induced β -cell proliferation leading to increased β -cell mass. In addition, Wnt-pathway activation during CM generation increased the frequency of proliferating β -cells maximally within 1 day post-injection.

Figure 5.7 Intrapancreatic-injection of Wnt-activated hMSC CM increased islet ductal association. (a-c) Representative photomicrographs of ck19⁺ cells (arrows) associated with islets at day 11, 14, and 42 in mice injected with unconditioned media, or 8 µg hMSC CM, or 8 µg WNT+ CM. (d) Mice injected with 8 µg hMSC CM showed an increased frequency of islets associated with ducts compared to mice injected with 4µg hMSC CM or unconditioned media. (e) Mice injected with 4 µg or 8 µg WNT+ CM showed an increased frequency of islets associated with ducts compared to mice injected with 8 µg WNT- CM or unconditioned media. Scale bar=200µm. Data is represented as mean ± S.E.M. (*p<0.05, **p<0.01, ***p<0.001).



Uncond. Media
 hMSC CM (4µg)
 hMSC CM (8µg)
 WNT+ CM (4µg)
 WNT+ CM (8µg)
 WNT- CM (8µg)

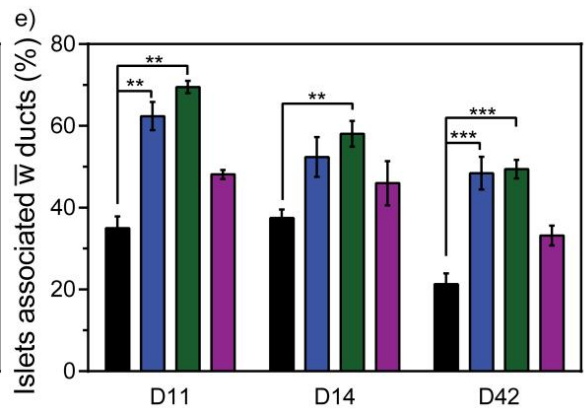
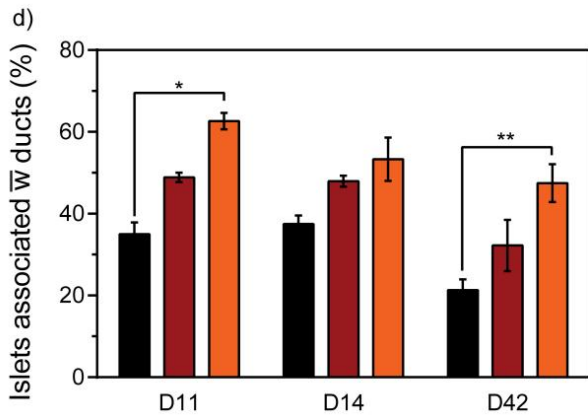
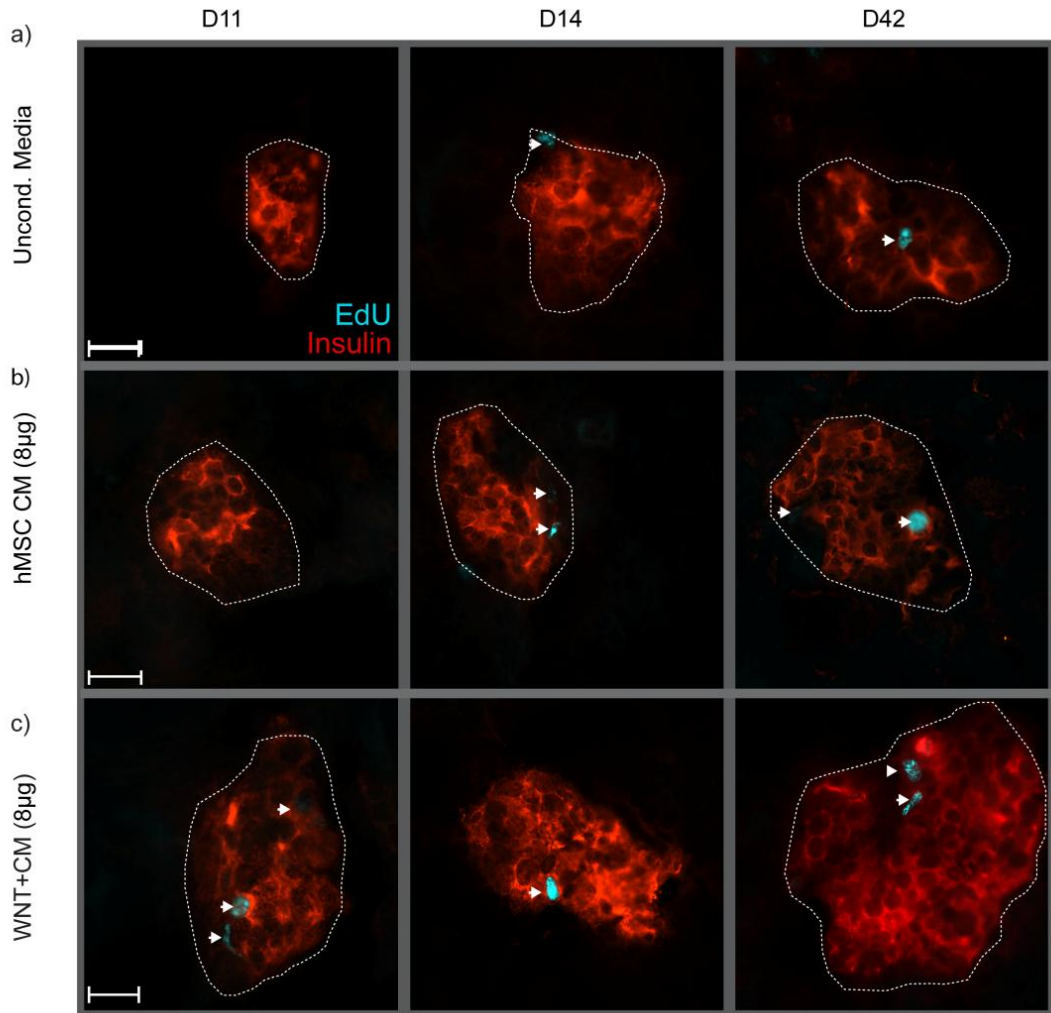
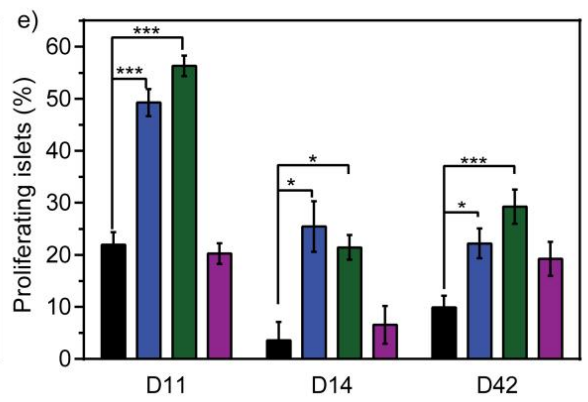
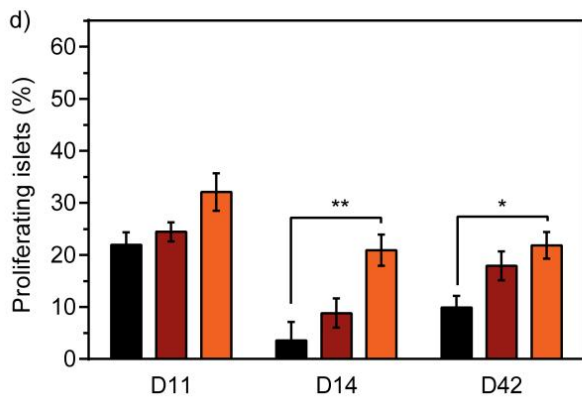


Figure 5.8 Intrapancreatic-injection of Wnt-Activated hMSC CM increased β -cell proliferation. (a-c) Representative photomicrographs of EdU⁺ β -cells (arrows) within islets at day 11, 14, and 42 in mice injected with unconditioned media, or 8 μ g hMSC CM, or 8 μ g WNT+ CM. (d) Mice injected with 8 μ g hMSC CM showed an increased number of proliferating islets compared to mice injected with 4 μ g hMSC CM or unconditioned media at late time points. (e) Mice injected with 4 μ g or 8 μ g WNT+ CM showed an increased number of proliferating islets at all time points compared to mice injected with 8 μ g WNT- CM or unconditioned media. Scale bar=200 μ m. Data is represented as mean \pm S.E.M. (* p <0.05, ** p <0.01, *** p <0.001).



Uncond. Media
 hMSC CM (4µg)
 hMSC CM (8µg)
 WNT+ CM (4µg)
 WNT+ CM (8µg)
 WNT- CM (8µg)



5.2.9 *hMSC CM induce α - β -cell conversion and maturation of new β -cells*

The homeodomain transcription factor NKX2.2 is required for cell fate decisions in pancreatic islets and has been implicated in the prevention of α - β -cell reprogramming [35]. In addition, NKX6.1 expression has been shown to be vital in the final stages of β -cell differentiation and maturation [9,10]. Therefore, to further characterize the mechanism of islet formation after injection of hMSC CM, we investigated the presence of both NKX2.2 and NKX6.1 in newly formed islets at D11, D14 and D42. Representative photomicrographs show that nuclear localization of NKX2.2 (Figure A5.2a-c) was present in similar frequencies (~80%) across all conditions tested at all time points, including CAB injected mice (Figure A5.2d-e). Interestingly, the expression of NKX6.1 varied drastically between conditions but not between different time points (Figure 5.9a-c). Compared to unconditioned media injected mice, mice injected with 8 μ g of hMSC CM and 4 or 8 μ g WNT+ CM showed significantly higher frequencies of nuclear localization of NKX6.1 at D14-D42 (Figure 5.9d-e). Mice that were injected with 4 μ g of hMSC CM or WNT- CM did not show significantly increased NKX6.1 expression. It has been estimated that adult mice contain approximately 60% β -cells in their islets, and in turn have about 60% expression of NKX6.1 [36]. Mice that were CAB injected had an expression of ~ 58%, supporting this hypothesis. Taken together, these data suggest that hMSC CM is capable of inducing both β -cell regeneration and maturation.

In addition, hMSC CM has the ability to initiate conversion of α -cells to β -cells. Therefore, to characterize these mechanisms, the total number of glucagon⁺ cells was investigated (Figure 5.10a-c). The total number of

glucagon⁺ cells was found to be elevated in each condition at early time points. However, only mice injected with 8 µg hMSC CM or WNT+ CM showed significantly reduced levels of glucagon⁺ cells by D14-42 that eventually returned to physiological level (Figure 5.10d-e). More importantly, the misexpression of mature β-cell marker NKX6.1 was observed in significantly higher frequencies at early time points. Mice that were injected with 8 µg hMSC CM or WNT+ CM showed significantly higher misexpression glucagon⁺ cells at early time points that decreased over time compared to unconditioned media injected mice (Figure 5.10f-g). Interestingly, this decrease directly correlated with the total decrease in glucagon⁺ cells. Thus hMSC CM has the ability to induce α-β-cell conversion to increase total β-cell mass. Finally, confocal z-stacking was used to confirm these findings and illustrated the presence of glucagon⁺ cells, glucagon⁺ NKX6.1⁺ cells, insulin⁺ NKX6.1⁺ cells and finally insulin⁺ glucagon⁺ cells (Figure 5.11a-c).

Figure 5.9 Intrapancreatic-injection of Wnt-activated hMSC CM increased β -cell maturation. (a-c) Representative photomicrographs of NKX6.1⁺ cells within islets at day 11, 14, and 42 in mice injected with unconditioned media, or 8 μ g hMSC CM, or 8 μ g WNT+ CM. (d) Mice injected with 8 μ g hMSC CM showed an increased frequency of NKX6.1⁺ cells per islet compared to mice injected with 4 μ g hMSC CM or unconditioned media. (e) Mice injected with 4 μ g or 8 μ g WNT+ CM showed an increased frequency of NKX6.1⁺ cells per islet compared to mice injected with 8 μ g WNT- CM or unconditioned media. Scale bar=200 μ m. Data is represented as mean \pm S.E.M. (*p<0.05, **p<0.01, ***p<0.001).

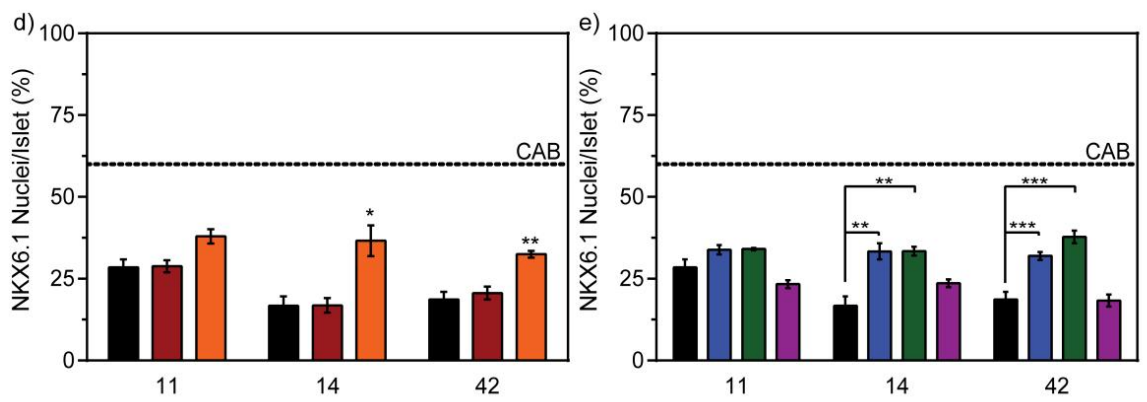
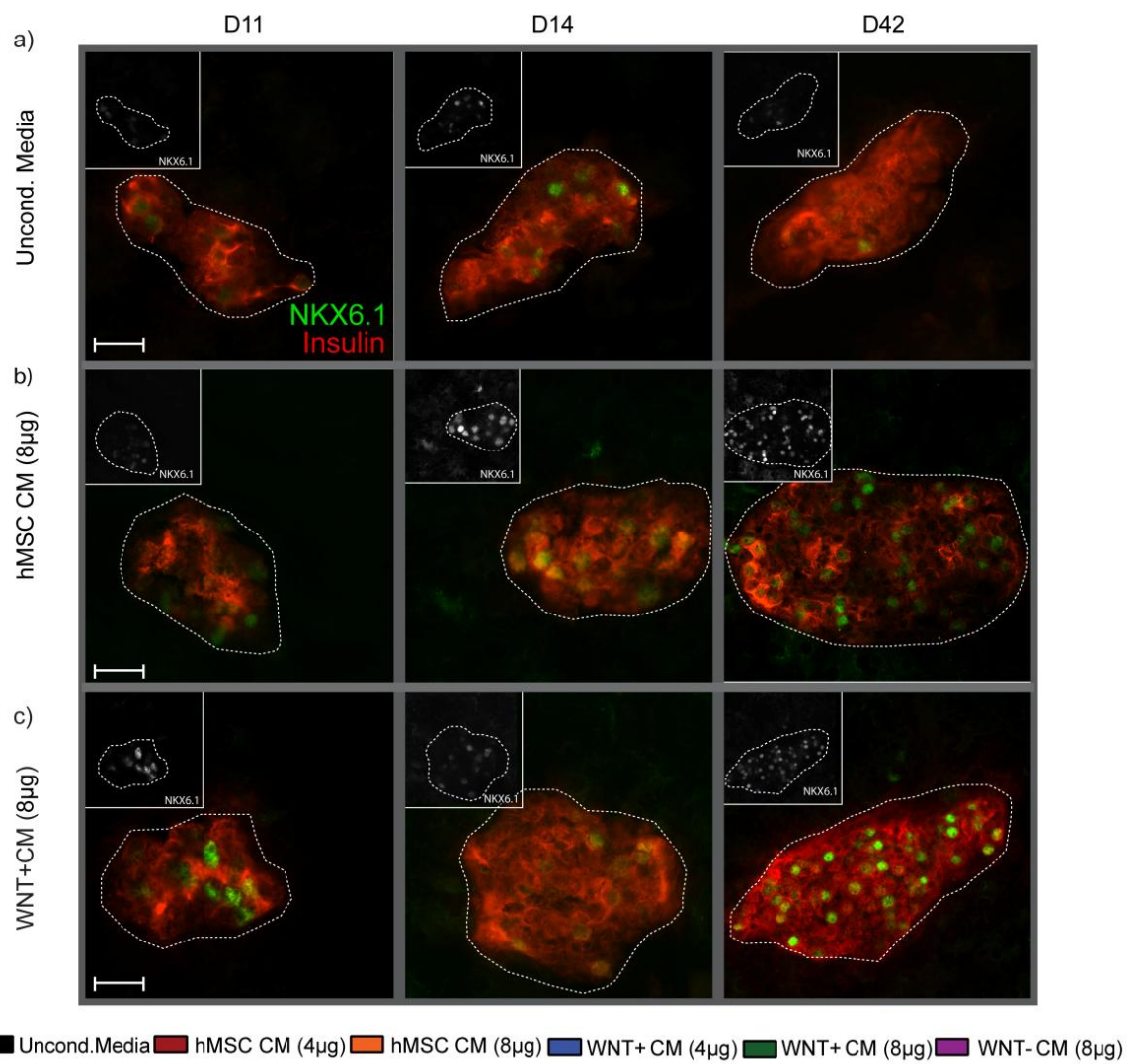
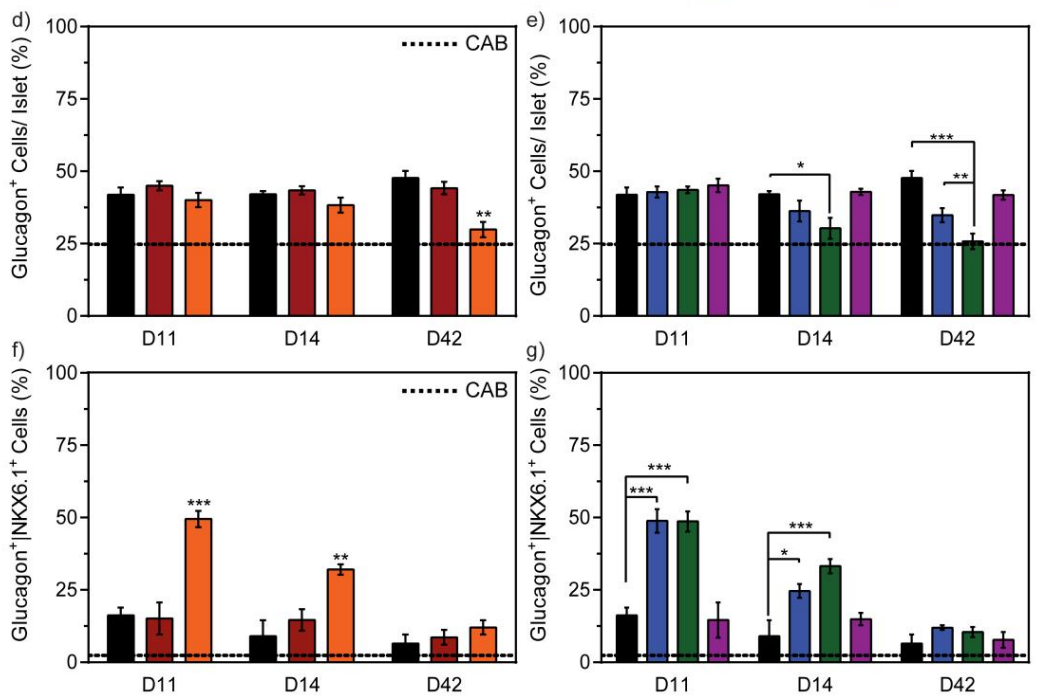
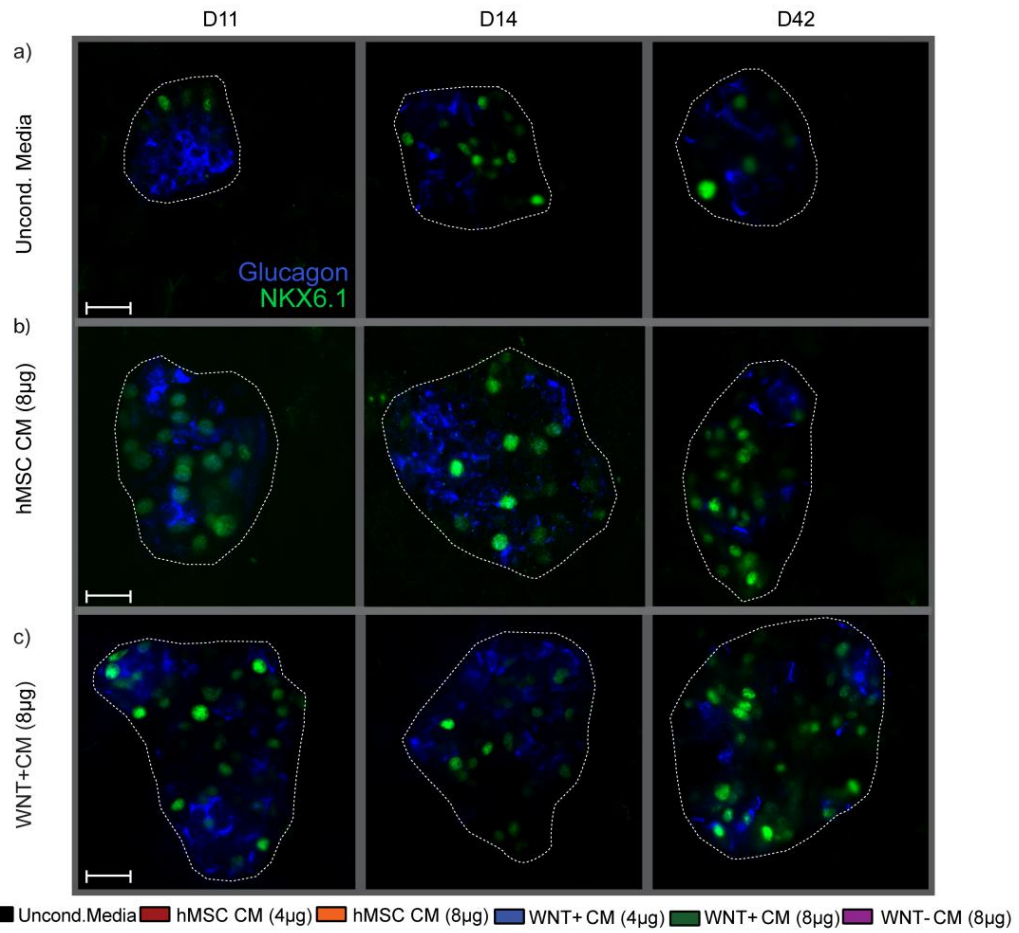


Figure 5.10 Intrapancreatic-injection of Wnt-activated hMSC CM increased α - β -cell conversion. (a-c) Representative photomicrographs of glucagon⁺ NKX6.1⁺ cells within islets at day 11, 14, and 42 in mice injected with unconditioned media, or 8 μ g hMSC CM, or 8 μ g WNT+ CM. (d-e) Mice injected with 8 μ g hMSC CM showed a decreased frequency of glucagon⁺ and glucagon⁺ NKX6.1⁺ cells per islet compared to mice injected with 4 μ g hMSC CM or unconditioned media. (f-g) Mice injected with 4 μ g or 8 μ g WNT+ CM showed an increased decreased frequency of glucagon⁺ and glucagon⁺ NKX6.1⁺ cells per islet compared to mice injected with 8 μ g WNT- CM or unconditioned media. Scale bar=200 μ m. Data is represented as mean \pm S.E.M. (*p<0.05, **p<0.01, ***p<0.001).



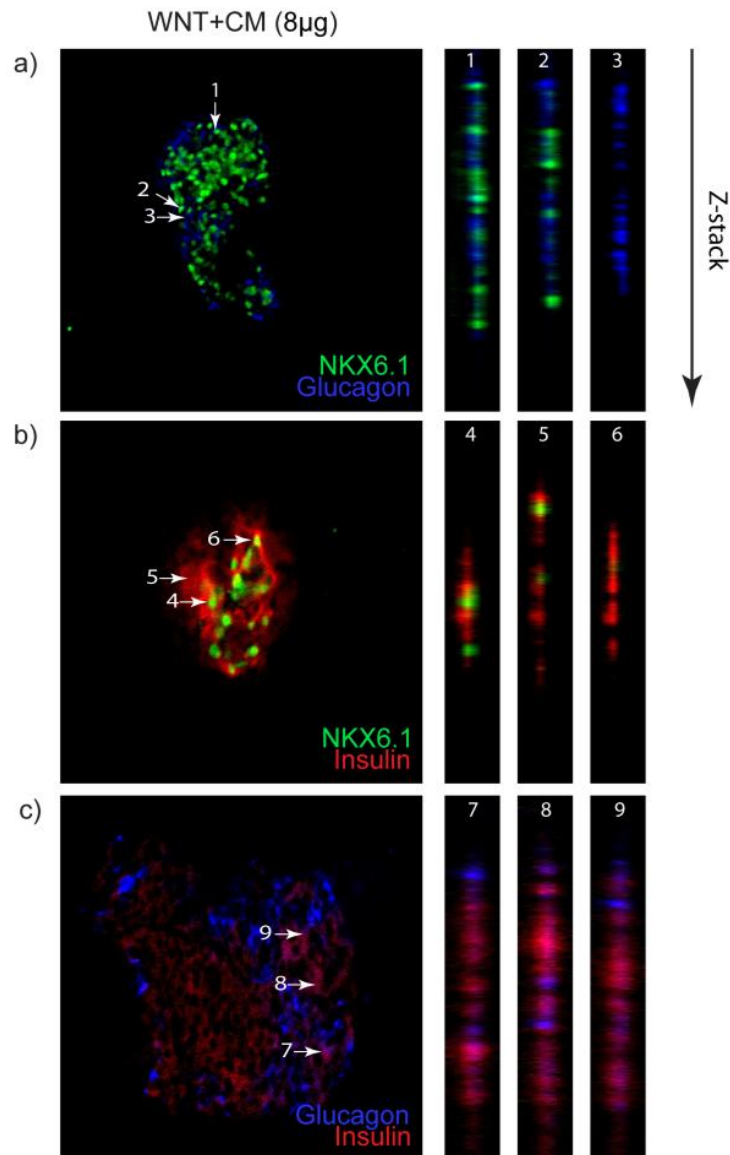


Figure 5.11 Intrapancreatic-injection of Wnt-activated hMSC CM displays α - β -cell transition. (a) [(1), (2), (3)] Represent individual cells that co-express nuclear transcription factor Nkx6.1 and cytosolic hormone, glucagon . (Right) Z-stack showing NKX6.1⁺ nuclei surrounded by glucagon. (b) [(4), (5), (6)] represent individual cells that co-express nuclear transcription factor NKX6.1 and cytosolic hormone, insulin. (Right) Z-stack showing NKX6.1⁺ nuclei surrounded by insulin. (c) [(7), (8), (9)] represent individual cells that co-express cytosolic hormones insulin and glucagon. (Right) Z-stack showing insulin and glucagon co-staining (magenta). Z-stack reconstructions were created from a tissue depth of 20 μ m.

5.2.10 *Proteomic analyses of WNT+ CM identified pro-islet regenerative proteins*

To identify proteins secreted by hMSC and associated with increased β -cell mass, we performed global quantitative proteomic analysis on hMSC CM generated under untreated conditions (hMSC CM), Wnt-activated conditions (WNT+) and Wnt-inhibited conditions (WNT-), in biological triplicate (Figure 5.12a). Protein lists were filtered to include only those identified in at least two biological replicates in a single condition and missing values were imputed using a normal distribution [37]. Gene ontology using cellular component (GOCC) analysis was used to filter proteins to only include extracellular proteins. In total 434 proteins were found to be secreted in hMSC CM (ESM Table 5.1). Label-free quantitation was used to investigate what proteins were differentially expressed upon treatment of hMSC by CHIR99201 (WNT+) or IWR-1 (WNT-). Investigation of proteins differentially expressed compared to WNT+ CM were highlighted (Figure 5.12b) (Table A5.1). Proteins that were upregulated in WNT+ CM included those associated with regulation of Wnt-signaling such as LRP1, and WNT5A. Conversely, negative regulators of Wnt-signaling, such as DKK1-3, were observed in decreased amounts in WNT+ CM, confirming robust Wnt-activation occurred during CM generation. Down-regulated proteins also included biomarkers of pancreatic cancer (VNN1) [38], negative regulators of insulin secretion (CFD) [39], as well as connective-tissue growth factor (CTGF), which has been shown previously to be a regulator of β -cell regeneration [40–42]. Of most importance, we observed upregulation of key β -cell pro-survival and proliferative proteins, such as IGF-1, TGF β 2 and LIF, in WNT+ CM [43–45].

Many proteins were not differentially expressed between the three conditions, and included extracellular matrix scaffolding proteins, and angiogenic factors such as angiopoietin like protein 2 (ANGPTL2) and VEGFA.

To determine whether murine islets could receive the signals found in WNT+ CM, we probed murine islets for receptors corresponding to TGFB2, IGF1 and LIF (Figure 5.12c-e). Murine islets showed robust signals for both TGF β 2 and LIFR, and modest expression of IGFR1. Nonetheless, these findings confirmed that murine islets could putatively respond to these β -cell survival and proliferative cues generated by hMSC CM. Next, we sought to investigate whether culturing of human-derived islets using recombinant proteins for TGF β 2, IGF-1 and LIF could increase survival and proliferation *in vitro* compared to full hMSC CM. Human islets were obtained from the IIDP and cultured for three days in hMSC CM (hMSC CM, WNT+ CM and WNT-CM), along with each recombinant ligand alone, or in combination. Concentration ranges of each ligand were determined by using the average total detector intensity (raw intensity) across all three conditions (data not shown) [46]. Each ligand was matched to the average concentration found in the hMSC CM and β -cell survival and proliferation was assessed using multiparametric flow cytometry. Although we did not observe any differences in the proliferation rates of human β -cells after three-days of culture, a significant increase in the frequency of live β -cells (Figure 5.12f) and total live β -cells (Figure 5.12g) was observed for the WNT+ CM conditions and for TGF β 2, IGF-1 and LIF used in combination. Interestingly, ligands in combination achieved β -cell survival rates equivalent to WNT+ CM.

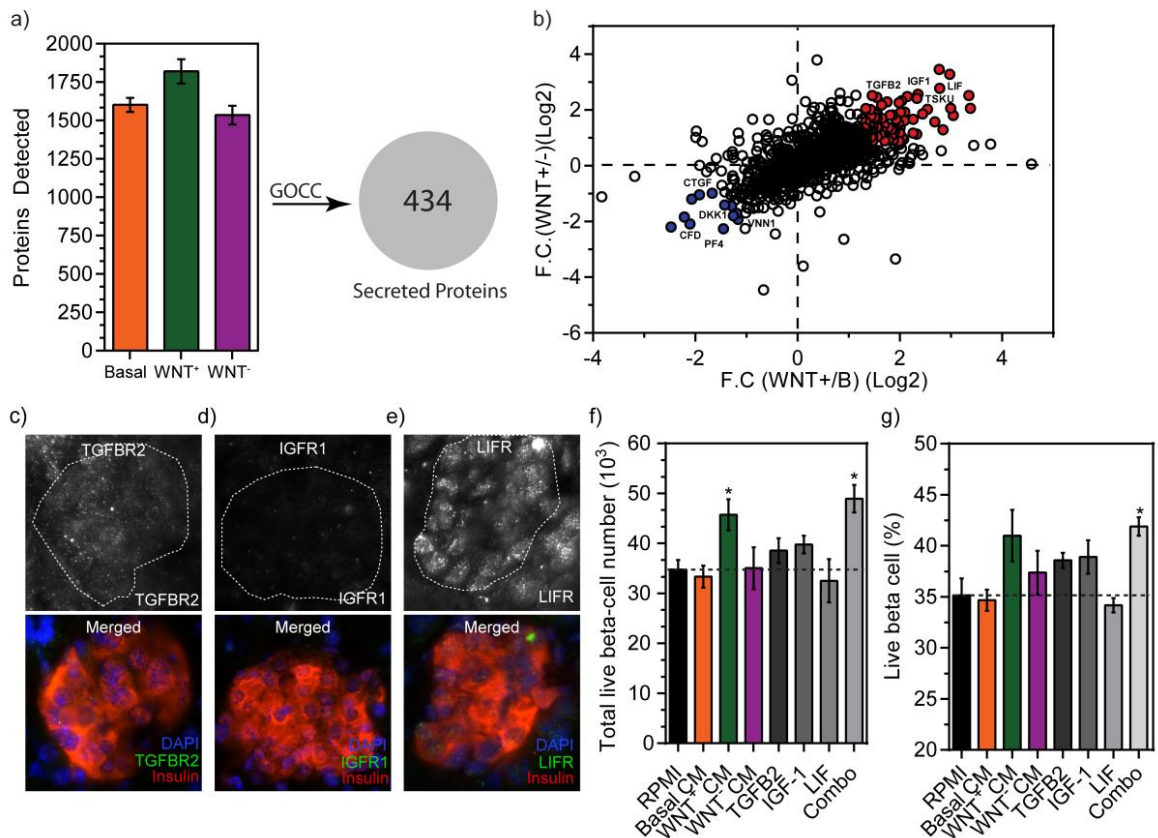


Figure 5.12 Proteomic analyses of WNT+ CM identified pro-islet regenerative proteins. (a) Quantitative proteomic of secreted proteins found in hMSC CM, WNT+ and WNT- CM. Total quantified proteins were filtered using GOCC to only include extracellular proteins. (b) Scatter plot showing the fold change of WNT+CM compared to hMSC CM and WNT- CM. Significantly changing proteins are highlighted. Representative photomicrographs of (c) TGF β 2, (d) IGFR1 and (e) LIFR on murine islets. (f) WNT+ CM and recombinant proteins used in combination show increases in total live β -cell numbers, while (g) only recombinant proteins used in combination show increases in live β -cell frequency. Data is represented as mean \pm S.E.M. (* $p < 0.05$).

5.3 Discussion

Our study demonstrates that secreted products contained in hMSC CM can stimulate endogenous islet regeneration without cell transfer. Importantly, regenerated β -cells were functionally mature, and secreted insulin in response to elevated blood glucose to reverse chemically-induced hyperglycemia *in vivo*. In addition, the extent glucose control was dependent on the concentration of secreted proteins delivered to the pancreas, and stimulation of Wnt-signaling during CM generation augmented regenerative capacity. Impressively, mice injected with Wnt-activated hMSC CM showed full recovery of endocrine function, resulting from increased β -cell mass and accelerated β -cell maturation via α - β -cell conversion accompanied by increased β -cell proliferation. Misexpression of NKX6.1 within glucagon⁺ cells suggested that hMSC CM stimulated initial conversion of α -cells into β -like cells, and these mechanisms occurred within a four day therapeutic window after a single dose hMSC CM. Finally, using quantitative proteomic screening techniques, we were able to identify a subset of 3 proteins, IGF-1, TGF- β 2 and LIF, upregulated during CM generation, that directly stimulated β -cell survival and proliferation using human islet preparations, suggesting that targeted protein based therapies may be developed to restore β -cell mass in patients with diabetes.

Although administration of hMSC directly into the pancreas had minimal effect on overall hyperglycemic recovery, the emergence of single insulin⁺ cells found adjacent to the ductal epithelium at early time points suggested that hMSC were capable of initiating β -cell neogenesis *in situ*. Thus, poor hMSC survival in the pancreas after injection, alteration in the

secretory profile of cells *in vivo* and insufficient accumulation of regenerative factors resulted in a truncated or partial regenerative response *in vivo*. After transplantation, hMSC are met with a harsh environment coupled with activation of detachment-induced apoptotic signals and inadequate adhesion caused by a lack of matrix supports [47], that may drastically limit hMSC engraftment and function within the injured pancreas [48]. Indeed, detection of viable hMSC by HLA-A, B, C-expression was drastically reduced at the site of injection between days 14 and 42. However, direct administration of hMSC CM, is not limited by the same complications associated with cellular transfer, we were able to demonstrate the immediate emergence of functional islets as early as one day after a single CM injection. Interestingly, an increase in islet number was observed when sufficient total protein was administered, and appeared to plateau at approximately four days post transplantation only when delivered at a lower dose of 4 μ g hMSC CM. In contrast, this plateau was not observed for mice that received 8 μ g hMSC CM, or when CM was generated under Wnt-pathway stimulated conditions suggesting that CM-delivery triggered endogenous regenerative programs, partially dependent on protein concentration. In addition, a single dose of 4 μ g WNT+ CM sequential increases in islet size, islet number and β -cell mass suggesting protein content was also important for the extent of islet regeneration observed. Finally, a single injection of 12 μ g WNT+ CM was also investigated and showed no difference over 8 μ g WNT+ CM, suggesting maximum therapeutic recovery was achieved. Further insights on how to extend this therapeutic window could lead to improved protein based therapies designed to stimulate β -cell regeneration.

Exploring the components within the hMSC CM that stimulate endogenous regeneration also suggested protein as opposed to microvesicles-encapsulated miRNA, as the major signaling moiety contributing to islet regeneration. However, CM generation and concentration process will collect content within the microvesicle fraction, and miRNA content analyses as well as metabolite profiling within hMSC-secreted fraction may represent an additional avenue for future investigation for potential islet regenerative stimuli. Recently, gamma-aminobutyric acid (GABA) has been shown to induce islet hyperplasia in STZ-treated mouse models [18,49]. Although the impact of GABA was also not assessed herein, hMSC possess the ability to produce GABA [50], that may contribute to the therapeutic effect. However, in experiments performed by the Collombat group administration of GABA was >1 month in duration before islet hyperplasia was observed. In contrast, in our experimental design, mice only received a single dose of CM and responded with new islet formation within 4 days, making it unlikely that GABA could be solely responsible for β -cell mass recovery. In addition, the involvement of miRNA in the regulation of β -cell function during islet development had been documented [51]. Therefore, hMSC may influence cellular processes through extracellular vesicles shuttling miRNA [52]. Microarray analysis on harvested extracellular vesicles from hMSC has revealed high expression of miR-21, miR-146a, and miR-181, linked to downstream products important in immune response [53], but did not identify any miRNA directly implicated in insulin homeostasis. Nonetheless, only a small amount of already degraded RNA was injected in the current study,

making it improbable that miRNA was the main contributor to islet regeneration.

The endogenous mechanisms underlining the induction of β -cell regeneration by hMSC CM were multi-factorial. Increased ductal association with newly formed islets suggests the ductal epithelial niche as a potential source of β -cell renewal. *In vitro* cultivation of ductal tissue preparations has provided evidence that ductal cells can be directed to differentiate into glucose responsive β -cells [54,55]. However, we did not observe direct evidence for ck19⁺ ductal epithelial conversion to cells that expressed endocrine specific genes, such as NKX2.2, or insulin or glucagon. However, we observed increased representation of ck19⁺ cells within islets suggesting the involvement of the epithelial niche as a site of active regeneration. In addition, periductal vimentin⁺ cell hyperplasia was associated with the emergence of glucagon⁺ cell clusters as early as one day post-transplantation. Activation of β -cell proliferation was also predominant at early time points in mice that received Wnt-activated CM. Wnt-ligands have been well documented to play a key role in initiating β -cell proliferation both *in vitro* and *vivo* [23,24]. However, the short burst of β -cell proliferation in our study suggested that alternative mechanisms of β -cell conversion were likely to account for the large increases in β -cell mass observed.

Although lineage tracing needs to be performed to conclusively demonstrate endocrine cell conversion, several observations support α to β -cell conversion as the primary mechanism for the recovery of β -cell mass after CM injection. First, as β -cell mass gradually increased with time after WNT+ CM injection, the frequency of glucagon⁺ cells was diminished. Second, using

NKX6.1 as a marker of functionally matured β -cells, WNT+ CM accelerated the maturation of β -cells as early as 24 hours post injection. While the expression of endocrine marker NKX2.2 remained constant across all time points and conditions, the frequency of NKX6.1⁺ cells / islet was significantly increased in mice that received WNT+ CM, but failed to reach the 60% benchmark observed in healthy, CAB-treated islets. The outcome of this was confirmed in glucose tolerance tests, where the recovery from hyperglycemia after glucose bolus was present but delayed compared to CAB controls. Third, glucagon⁺ cell that expressed NKX6.1 were consistently detected at early time points under conditions that induced regeneration of β -cells. Indeed, the expression of mature β -cell transcription factor NKX6.1 was detected in ~50% of glucagon⁺ cells at day 11 in mice treated with WNT+ CM. As expected the frequency of Glucagon⁺ / NKX6.1⁺ cells decreased with time post-CM injection. Finally, presence of islet cells that expressed both glucagon and insulin further supports the hypothesis that hMSC CM efficiently induced α - β -cell conversion [19,56].

Combining quantitative proteomic analysis comparing the secreted protein composition of various hMSC treatments, human islet co-culture experiments and multiparametric flow cytometer analysis, we identified a shortlist of proteins (IGF-1, TGF β 2, LIF) within hMSC CM as our top secreted candidates to modulate β -cell survival and proliferation *in vitro*. As proof of concept, these recombinant proteins were equivalent, if not better than Wnt-activated CM at preserving β -cell survival. The effective range of each ligand was determined using the average detector intensity to equally compare back to CM. Therefore, further optimization is needed to determine the optimal

concentration needed elicit islet regeneration. Proteins known to negatively alter the secretion of insulin (CFD, VNN1) were found in hMSC CM that decreased during Wnt-activation. Importantly, deleterious proteins are present in all hMSC CM, potentially decreasing the therapeutic effects. Nonetheless, we provide a list of protein targets that can be used to design protein-based strategies to stimulate endogenous islet regeneration that offer one step closer towards a potential peptide treatment for diabetes.

In summary, our analyses of hMSC CM directly injected into STZ-treated hyperglycemic mice demonstrates that: (1) hMSC CM can induce endogenous regeneration of murine islet without transferring cells; (2) newly formed islets are mature and functional; (3) regeneration of β -cell mass is multi-factorial involving both β -cell maturation and proliferation; (4) regenerating β -cells are primarily derived from α - β -cell conversion; and lastly (5) hMSC CM contains pro- β -cell effectors that can potentially be administered in combination to reduce hyperglycemia. Based on these findings, we believe that injection of Wnt-pathway stimulated hMSC-derived CM or peptide effectors represents a promising approach as a novel therapy for T1D.

5.4 Experimental Methods

5.4.1 Animal Maintenance and Manipulations

Mouse protocols were reviewed and approved by the Institutional Ethical committee at the University of Western Ontario and all colonies were maintained following Canadian animal research guidelines. NOD/SCID mice obtained from Jackson Laboratories were housed and used according to the

guidelines of the Animal Use Protocol (AUB#2015-033). To induce hyperglycemia, STZ (Sigma) was dissolved in 0.1M sodium citrate buffer (CAB) (pH 4.5), and 5 doses (Days 1-5) were administered intraperitoneally (35 mg/kg/day) within 15 minutes of dissolving. Hyperglycemia progression (>15 mmol/l) was assessed by monitoring the blood glucose levels of mice on transplant day (day 10). For intrapancreatic (iPan) injections, mice were anesthetized; the pancreas and spleen exposed; cells (5×10^5) or CM (~4 or 8 μ g) was microinjected (20 μ l) into the splenic portion of the pancreas. Negative control mice were injected with unconditioned basal media that was used to collect secreted hMSC proteins. Positive control mice received CAB instead of STZ for five days. In addition CAB mice were intrapancreatically injected with unconditioned basal media on day 10. To assess cell proliferation, mice were intraperitoneally injected (100 μ l) with EdU (2 μ g/ μ l) 24 hrs prior to sacrifice. Cells that had incorporated EdU were detected by immunohistochemistry (ThermoFisher Scientific).

5.4.2 Human Subjects

Human bone marrow was obtained from healthy donors after informed consent at the London Health Science Centre (London, ON, Canada). All studies were approved by the Human Research Ethics board at the University of Western Ontario (REB#12934, 12252E). Human pancreatic islets were provided by the National Institute of Diabetes and Digestive and Kidney Diseases (NIDDK) funded Integrated Islet Distribution Program (IIDP) at the City of Hope (California, USA), NIH Grant # 2UC4DK098085-02.

5.4.3 Generation of hMSC CM for injection and proteomics

After 4 days of culture (~80% confluency), hMSC were washed twice with PBS to remove residual growth factors and replated in basal AmnioMax™ without supplement to collect proteins secreted by hMSC for 24 hrs. Media conditioned by hMSC was collected, filtered and centrifuged at 450 x g to remove any cellular debris. Cell viability was assayed using trypan blue and >95% viability was used as a standard cut-off for co-culture and secretome analyses. CM was generated fresh and concentrated the morning of each *in vivo* experiment. For proteomics CM was generated in triplicate and all CM was concentrated using 3 kDa molecular weight cut-off filter units (Millipore). For *in vivo* assays, CM was quantified and the protein amount was normalized to either 0.2 or 0.4 µg/µL. For proteomic analysis, concentrated CM was lyophilized overnight and re-suspended in 8M urea, 50mM ammonium bicarbonate, 10mM dithiothreitol and 2% SDS solution prior to protein quantitation. Protein concentration was measured using the Pierce 660 nm protein assay (ThermoFisher Scientific) or by NanoDrop (A280). For Wnt-modulated hMSC CM, cells were treated with 10 µM of CHIR99201 or 20 µM of IWR-1 for 24 hrs during media generation.

5.4.4 Glucose Tolerance Test

For challenge purposes, mice were fasted for 4-6hrs and were injected intraperitoneally with glucose (2.0 g/kg). Blood glucose levels were measured at the indicated time points for 2 hrs using a FreeStyle Lite glucometer (Abbott).

5.4.5 Serum insulin and glucagon ELISA

On day 42, after cervical dislocation, blood was collected from the left ventricle from serum insulin and glucagon quantification by ELISA. Approximately 25 ul of serum was used to assay circulating insulin by ultra-sensitive ELISA according to manufacturer's specifications (Alpco). Approximately 50 ul of serum was used to assay circulating glucagon levels according to manufacturer's specifications (Alpco). Each mouse was measured in duplicate.

5.4.5 RNA isolation, qPCR and integrity analysis

RNA was purified in triplicate from CHIR99201 or IWR-1 treated hMSC cell using the RNeasy™ RNA extraction kit according to the manufacturer instructions (Qiagen). RNA quality and quantity was assessed using NanoDrop. Subsequently, cDNA was synthesized using the High Capacity cDNA Reverse Transcription Kit with RNase inhibitor (Invitrogen). Real-time PCR was performed using SYBR® Green along with BCL9 and c-MYC primers (Genecopoeia). Samples were incubated at 50°C for 2 minutes followed by 10min at 95°C. DNA was amplified at 95°C for 15 s followed by 1 min at 60°C for 40 cycles, using the Bio-Rad CFX384 Real-Time PCR Detection System (Bio-Rad). Samples were normalized using the geometric mean of three housekeeping genes. For RNA integrity, 4 uL of extracted RNA analyzed using the Agilent RNA 6000 pico kit coupled to the 2100 bioanalyzer system (Agilent). Total chromatographic area integration was performed using the 2100 Expert software package.

5.4.6 *Immunohistochemistry and Immunofluorescent analysis*

Pancreata were frozen in optimal cutting temperature media and sectioned at 10 μm such that each slide contained 3 sections each 150 μm apart. Sections were fixed in 10% buffered formalin and blocked with mouse serum, incubated with mouse insulin antibody (1/1000) and were detected with peroxidase-labeled rabbit anti-mouse antibody and DAB (Vector). Size and number of islets were quantified by using light microscopy and analyzing four areas (1 mm^2) selected at random per section for a total of three sections/mouse. β -cell mass was calculated by β -cell area/(total area- β -cell area) \times pancreas weight. Frozen pancreas sections were also stained for Immunofluorescent analysis to detect murine insulin, glucagon, human cell engraftment (HLA), blood vessel density (vWF, CD31), proliferation (EdU), islet transcription factors (NKX2.2, 6.1), ductal association (ck19), and vimentin. Concentration and manufacture information for all antibodies used for immunofluorescent analysis are found in Table A5.2

5.4.7 *Quantification of islet blood vessel density*

Von Willebrand factor (vWF) and CD31 were used to detected large vessels and small capillaries respectively. Briefly, intra-islet blood vessel densities were quantified by counting vWF⁺ vessels/ islet by randomly selecting four islets/section for three section/mouse. In addition the total numbers of CD31⁺ cells were counted for within the total insulin area for each islet and the number of CD31⁺ cells was normalized by using the area of each islet.

5.4.8 Quantification of proliferating cells and ductal association

EdU⁺ cells were detected using the Click-iT™ EdU imaging kit (Invitrogen) and co-stained for insulin to identify proliferating β -cells and every islet in three sections for each mouse was used from quantification. Islets that contained ≥ 1 proliferating β -cell were counted and divided by the total number of β -cells per mouse. Cytokeratin-19 (ck19) was used to label ductal structures within the pancreas. Each islet in three pancreatic sections per mouse was designated as not associated with, or in direct contact with, ck19⁺ ducts.

5.4.9 Quantification of transcription factor expression

Pan-endocrine marker NKX2.2 and β -cell specific NKX6.1 were used to assess β -cell maturity. Each marker was co-stained with insulin to determine the total frequency within 12 islets per section per mouse. The total frequency of each transcription factor was calculated by counting the total number of NKX2.2 or 6.1 positive nuclei/ the total number of nuclei per islet.

5.4.10 Quantification of glucagon+ cells with NKX6.1

Glucagon was co-stained with NKX6.1 and insulin as just described. The frequency of glucagon positive cells was calculated by counting the total number of glucagon⁺ cells/ the total number of cells per islet for 12 islets per section per mouse. The frequency of glucagon⁺ cells expression NKX 6.1 was calculated by counting the total number of glucagon⁺ cells NNK6.1⁺ cells/ total number of NKX6.1⁺ cells per islet for 12 islets per section per mouse.

5.4.11 Confocal Microscopy

Immunohistochemistry was performed on 20 μm pancreas cryosections for confocal imaging. Tissue was fixed with 10% buffered formalin for 20 min and permeabilized with 1% Triton X-100 for 10 min. Prior to incubation with antibodies, tissue samples were blocked in 10% heat inactivated FBS for 90 min. Tissue samples were incubated with the following primary antibodies for 60 min at room temperature: mouse monoclonal anti-glucagon, rabbit monoclonal anti-insulin, and goat polyclonal Nkx6.1. Tissue samples were washed 2 times with PBS prior to incubation with the following secondary antibodies for 30 min at room temperature: horse anti-mouse IgG fluorescein, goat anti-rabbit IgG AlexaFluor 647 and bovine anti-goat IgG AlexaFluor 594 . Tissue samples were washed 2 times with PBS and incubated for 5 min with DAPI. Images were acquired using the LSM 510 confocal laser scanning microscope (Zeiss) running Zeiss ZEN 2009 imaging software (Zeiss). Images were captured using a 20x objective lens. Z-stack optimization was performed using Zeiss Zen 2009 imaging software to determine optimal slice thickness and Z-projections were constructed and analyzed using ImageJ software (NIH).

5.4.12 Chloroform/methanol precipitation and protein digestion

Protein extracts from hMSC CM samples were reduced in 10 mM DTT for 30 min and alkylated with 100 mM iodoacetamide (IAA) for 30 min at room temperature in the dark. Next, to facilitate the removal of incompatible detergents, reducing and alkylating reagents, the proteins were precipitated using chloroform/methanol. Briefly, 25 μg of protein extracted from each sample was diluted to a total volume of 150 μL with 50 mM ammonium

bicarbonate (ABC), and 600 μL of ice cold methanol was added to each sample, followed by 150 μL of chloroform, with thorough vortexing. 450 μL of ice-cold DIH_2O was added before additional vortexing and centrifugation at 14,000 $\times g$ for 5 min at room temperature. The upper/aqueous methanol phase was removed and 450 μL of ice-cold methanol was added to each sample, followed by vigorous vortexing and centrifugation at 14,000 $\times g$ for 5 min. The remaining chloroform/methanol was discarded and the precipitated protein pellet was air dried before protein digestion. For on-pellet protein digestion, 100 μL of 50 mM ABC (pH 8.0) with LysC (Wako) (1:100) solution was added to each precipitated sample and incubated in a ThermoMixer at 37°C for 4 hrs at 1000 RPM, followed by trypsin/LysC (1:50 ratio of enzyme: sample) (Promega) solution was added to each precipitated sample and incubated in a water bath shaker at 37°C overnight at 400 RPM. The next day, an additional aliquot of trypsin (1:100 ratio) was added for ~ 4 hrs, prior to acidifying with 10% formic acid (FA) (pH 3-4). The peptide concentrations were estimated using a Pierce BCA assay (ThermoFisher Scientific).

5.4.13 Liquid Chromatography-Tandem Mass Spectrometry (LC-MS/MS)

Approximately 1 μg of each sample was injected onto a Waters M-Class nanoAcquity HPLC system (Waters) coupled to an ESI ion-trap/Orbitrap mass spectrometer (Q Exactive Plus). Buffer A consisted of mass spec. grade water/0.1% FA and Buffer B consisted of ACN/0.1% FA. All samples were trapped for 5 min at a flow rate of 5 $\mu\text{L}/\text{min}$ using 99% Buffer A and 1% Buffer B on a Symmetry BEH C18 Trapping Column (5 μm , 180 μm \times 20 mm, Waters). Peptides were separated using a Peptide BEH C18 Column (130 \AA , 1.7 μm , 75 μm \times 250 mm) operating at a flow rate of 300 nL/min at 35°C

(Waters). Samples were separated using a non-linear gradient consisting of 1-7% Buffer B over 1 min, 7-23% Buffer B over 135 min and 23-35% Buffer B over 45 min, before increasing to 98% Buffer B and washing. Settings for data acquisition on the Q Exactive Plus are outlined in Table A4.3.

5.4.14 Label-free proteomic data analysis

All MS raw files were searched in MaxQuant version 1.5.8.30 using the Human Uniprot database (updated May 2015 with 20,264 entries). For all database searches, missed cleavages were set to 3, cysteine carbamidomethylation was set as a fixed modification and Oxidation (M), N-terminal Acetylation (protein) and Deamidation (NQ) were set as a variable modifications (max. number of modifications per peptide = 5). Precursor mass deviation was left at 20 ppm and 4.5 ppm for first and main search, respectively. Fragment mass deviation was left at 20 ppm. Protein and peptide FDR was left to 0.01 (1%) and decoy database was set to revert. Match between runs was enabled and all other parameters left at default. Bioinformatics analysis was performed using Perseus version 1.5.8.5. Briefly, protein lists were loaded into Perseus and proteins identified by site reverse and contaminants were removed. When using the match between runs feature, datasets were filtered for proteins containing a minimum of 1 unique peptide in at least two of three biological replicates.

5.4.15 Human islet culture with hMSC CM and recombinant ligands

Human islets from 4 donors were obtained from the Integrated Islet Distribution Program (IIDP). Upon arrival, 200 islet equivalents were plated in RPMI media without serum (Invitrogen). CM was concentrated using 3 kDa

molecular mass cut-off filters, and ~50 µg total protein was added to human islet culture for 7 days. After islet harvest and dissociation, β-cell content was estimated using FluoZin-3 (Flz3) (ThermoFisher Scientific) and apoptosis was quantified using 7AAD and Annexin-V. Recombinant proteins were added at concentrations estimated by proteomics. Flow cytometry data were analyzed using FloJo software (Treestar).

5.4.16 Cell Counts

Quantitative analyses were performed by manually counting of cells and nuclei on immunostained section of the mouse pancreas in a blinded fashion. Specifically, every tenth section was counted and photographs were taken at random by three different people. For islet size and beta cell mass quantification, colorimetric insulin was used to define regions on interest. Circumferences and area calculation were made by using AxioVision microscope software

5.4.17 Statistical analysis

All values are represented as mean ±S.E.M, unless otherwise stated in the figure legend, and were considered significant if $p < 0.05$ using ANOVA with Tukey's post hoc test. Data were analyzed using Prism software (Graphpad Version 6.01). Proteomic data analysis was conducted using build in multiple sample t-tests using Perseus. Fold changes were considered significant if they were >2-fold higher and $p < 0.05$ using Permutation based FDR test.

5.5 References

- [1] J.J. Meier, B-cell mass in diabetes: A realistic therapeutic target?, *Diabetologia*. 51 (2008) 703–713. doi:10.1007/s00125-008-0936-9.
- [2] R.F.O.R. The, R. Of, I Slet T Ransplantation for the T Reatment of T Ype 1 D labetes, (2013) 289–297.
- [3] E. a. Ryan, B.W. Paty, P. a. Senior, D. Bigam, E. Alfadhli, N.M. Kneteman, J.R.T. Lakey, a. M.J. Shapiro, Five-year follow-up after clinical islet transplantation, *Diabetes*. 54 (2005) 2060–2069. doi:10.2337/diabetes.54.7.2060.
- [4] R.P. Robertson, Islet Transplantation as a Treatment for Diabetes — A Work in Progress, *N. Engl. J. Med.* 350 (2004) 694–705. doi:10.1056/NEJMra032425.
- [5] J.J. Meier, A. Bhushan, P.C. Butler, The potential for stem cell therapy in diabetes, *Pediatr. Res.* 59 (2006). doi:10.1203/01.pdr.0000206857.38581.49.
- [6] K. a D'Amour, A.G. Bang, S. Eliazer, O.G. Kelly, A.D. Agulnick, N.G. Smart, M.A. Moorman, E. Kroon, M.K. Carpenter, E.E. Baetge, Production of pancreatic hormone-expressing endocrine cells from human embryonic stem cells., *Nat. Biotechnol.* 24 (2006) 1392–401. doi:10.1038/nbt1259.
- [7] A. Rezanian, J.E. Bruin, P. Arora, A. Rubin, I. Batushansky, A. Asadi, S. O'Dwyer, N. Quiskamp, M. Mojibian, T. Albrecht, Y.H.C. Yang, J.D. Johnson, T.J. Kieffer, Reversal of diabetes with insulin-producing cells derived *in vitro* from human pluripotent stem cells, *Nat. Biotechnol.* 32 (2014) 1121–1133. doi:10.1038/nbt.3033.
- [8] F.W. Pagliuca, J.R. Millman, M. Gürtler, M. Segel, A. Van Dervort, J.H. Ryu, Q.P. Peterson, D. Greiner, D.A. Melton, Generation of functional human pancreatic β cells *in vitro*, *Cell*. 159 (2014) 428–439. doi:10.1016/j.cell.2014.09.040.
- [9] M.P. Walczak, A.M. Drozd, E. Stoczynska-Fidelus, P. Rieske, D.P. Grzela, Directed differentiation of human iPSC into insulin producing cells is improved by induced expression of PDX1 and NKX6.1 factors in IPC progenitors, *J. Transl. Med.* 14 (2016) 341. doi:10.1186/s12967-016-1097-0.
- [10] M.C. Nostro, F. Sarangi, C. Yang, A. Holland, A.G. Elefanty, E.G. Stanley, D.L. Greiner, G. Keller, Efficient generation of NKX6-1+ pancreatic progenitors from multiple human pluripotent stem cell lines, *Stem Cell Reports*. 4 (2015) 591–604. doi:10.1016/j.stemcr.2015.02.017.
- [11] H. a Keenan, J.K. Sun, J. Levine, A. Doria, L.P. Aie, Residual Insulin

- Production and Pancreatic [Beta] -Cell Turnover After 50 Year ..., *Diabetes*. 59 (2010) 2846–2853. doi:10.2337/db10-0676.
- [12] A.E. Butler, J. Janson, W.C. Soeller, P.C. Butler, Increased Beta -Cell Apoptosis Prevents Adaptive Increase in Beta -Cell Mass in Mouse Model of Type 2 Diabetes, *Diabetes*. 52 (2003) 2304–2314. doi:10.2337/diabetes.52.9.2304.
- [13] Y. Dor, J. Brown, O.I. Martinez, D. a Melton, Adult pancreatic β -cells are formed by self-duplication rather than stem-cell differentiation., *Nature*. 429 (2004) 41–46. doi:10.1038/nature02520.
- [14] L. Bouwens, D.G. Pipeleers, Extra-insular β -cells associated with ductules are frequent in adult human pancreas, *Diabetologia*. 41 (1998) 629–633. doi:10.1007/s001250050960.
- [15] F. Delaspre, R.L. Beer, M. Rovira, W. Huang, G. Wang, S. Gee, M. Del Carmen Vitery, S.J. Wheelan, M.J. Parsons, Centroacinar cells are progenitors that contribute to endocrine pancreas regeneration, *Diabetes*. 64 (2015) 3499–3509. doi:10.2337/db15-0153.
- [16] R.L. Beer, M.J. Parsons, M. Rovira, Centroacinar cells: At the center of pancreas regeneration, *Dev. Biol.* 413 (2016) 8–15. doi:10.1016/j.ydbio.2016.02.027.
- [17] S. Afelik, M. Rovira, Pancreas β -cell regeneration: Facultative or dedicated progenitors?, *Mol. Cell. Endocrinol.* 445 (2016). doi:http://dx.doi.org/10.1016/j.mce.2016.11.008.
- [18] N. Ben-Othman, A. Vieira, M. Courtney, F. Record, E. Gjernes, F. Avolio, B. Hadzic, N. Druelle, T. Napolitano, S. Navarro-Sanz, S. Silvano, K. Al-Hasani, A. Pfeifer, S. Lacas-Gervais, G. Leuckx, L. Marroquí, J. Thévenet, O.D. Madsen, D.L. Eizirik, H. Heimberg, J. Kerr-Conte, F. Pattou, A. Mansouri, P. Collombat, Long-Term GABA Administration Induces Alpha Cell-Mediated Beta-like Cell Neogenesis, *Cell*. 168 (2017) 73–85.e11. doi:10.1016/j.cell.2016.11.002.
- [19] K. Al-Hasani, A. Pfeifer, M. Courtney, N. Ben-Othman, E. Gjernes, A. Vieira, N. Druelle, F. Avolio, P. Ravassard, G. Leuckx, S. Lacas-Gervais, D. Ambrosetti, E. Benizri, J. Hecksher-Sorensen, P. Gounon, J. Ferrer, G. Gradwohl, H. Heimberg, A. Mansouri, P. Collombat, Adult duct-lining cells can reprogram into β -like cells able to counter repeated cycles of toxin-induced diabetes, *Dev. Cell*. 26 (2013) 86–100. doi:10.1016/j.devcel.2013.05.018.
- [20] G.I. Bell, M.T. Meschino, J.M. Hughes-Large, H.C. Broughton, A. Xenocostas, D.A. Hess, Combinatorial Human Progenitor Cell Transplantation Optimizes Islet Regeneration Through Secretion of Paracrine Factors, *Stem Cells Dev.* 21 (2012) 1863–1876. doi:10.1089/scd.2011.0634.

- [21] G.I. Bell, H.C. Broughton, K.D. Levac, D.A. Allan, A. Xenocostas, D.A. Hess, Transplanted Human Bone Marrow Progenitor Subtypes Stimulate Endogenous Islet Regeneration and Revascularization, *Stem Cells Dev.* 21 (2012) 97–109. doi:10.1089/scd.2010.0583.
- [22] D. Hess, L. Li, M. Martin, S. Sakano, D. Hill, B. Strutt, S. Thyssen, D. a Gray, M. Bhatia, Bone marrow-derived stem cells initiate pancreatic regeneration., *Nat. Biotechnol.* 21 (2003) 763–770. doi:10.1038/nbt841.
- [23] M. Kuljanin, G.I. Bell, S.E. Sherman, G.A. Lajoie, D.A. Hess, Proteomic characterisation reveals active Wnt-signalling by human multipotent stromal cells as a key regulator of β -cell survival and proliferation, *Diabetologia.* (2017). doi:10.1007/s00125-017-4355-7.
- [24] H. Aly, N. Rohatgi, C.A. Marshall, T.C. Grossenheider, H. Miyoshi, T.S. Stappenbeck, S.J. Matkovich, M.L. McDaniel, A Novel Strategy to Increase the Proliferative Potential of Adult Human β -Cells While Maintaining Their Differentiated Phenotype, *PLoS One.* 8 (2013). doi:10.1371/journal.pone.0066131.
- [25] R. Mussmann, M. Geese, F. Harder, S. Kegel, U. Andag, A. Lomow, U. Burk, D. Onichtchouk, C. Dohrmann, M. Austen, Inhibition of GSK3 promotes replication and survival of pancreatic β -cells, *J. Biol. Chem.* 282 (2007) 12030–12037. doi:10.1074/jbc.M609637200.
- [26] H. Hao, J. Liu, J. Shen, Y. Zhao, H. Liu, Q. Hou, C. Tong, D. Ti, L. Dong, Y. Cheng, Y. Mu, J. Liu, X. Fu, W. Han, Multiple intravenous infusions of bone marrow mesenchymal stem cells reverse hyperglycemia in experimental type 2 diabetes rats, *Biochem. Biophys. Res. Commun.* 436 (2013) 418–423. doi:10.1016/j.bbrc.2013.05.117.
- [27] X. Gao, L. Song, K. Shen, H. Wang, M. Qian, W. Niu, X. Qin, Bone marrow mesenchymal stem cells promote the repair of islets from diabetic mice through paracrine actions, *Mol. Cell. Endocrinol.* 388 (2014) 41–50. doi:10.1016/j.mce.2014.03.004.
- [28] J.K. Smid, S. Faulkes, M.A. Rudnicki, Periostin induces pancreatic regeneration, *Endocrinology.* 156 (2015) 824–836. doi:10.1210/en.2014-1637.
- [29] L. Meijer, M. Flajolet, P. Greengard, Pharmacological inhibitors of glycogen synthase kinase 3, *Trends Pharmacol. Sci.* 25 (2004) 471–480. doi:10.1016/j.tips.2004.07.006.
- [30] B. Chen, M.E. Dodge, W. Tang, J. Lu, Z. Ma, C.-W. Fan, S. Wei, W. Hao, J. Kilgore, N.S. Williams, M.G. Roth, J.F. Amatruda, C. Chen, L. Lum, Small molecule-mediated disruption of Wnt-dependent signaling in tissue regeneration and cancer, *Nat. Chem. Biol.* 5 (2009) 100–107. doi:10.1038/nchembio.137.
- [31] M.D. Gordon, R. Nusse, Wnt signaling: Multiple pathways, multiple

- receptors, and multiple transcription factors, *J. Biol. Chem.* 281 (2006) 22429–22433. doi:10.1074/jbc.R600015200.
- [32] A.B. Nowakowski, W.J. Wobig, D.H. Petering, Native SDS-PAGE: high resolution electrophoretic separation of proteins with retention of native properties including bound metal ions, *Metallomics*. 6 (2014) 1068–1078. doi:10.1039/C4MT00033A.
- [33] T. Baranyai, K. Herczeg, Z. Onódi, I. Voszka, K. Módos, N. Marton, G. Nagy, I. Mäger, M.J. Wood, S. El Andaloussi, Z. Pálkás, V. Kumar, P. Nagy, Á. Kittel, E.I. Buzás, P. Ferdinandy, Z. Giricz, Isolation of exosomes from blood plasma: Qualitative and quantitative comparison of ultracentrifugation and size exclusion chromatography methods, *PLoS One*. 10 (2015) 1–13. doi:10.1371/journal.pone.0145686.
- [34] A. Schroeder, O. Mueller, S. Stocker, R. Salowsky, M. Leiber, M. Gassmann, S. Lightfoot, W. Menzel, M. Granzow, T. Ragg, The RIN: an RNA integrity number for assigning integrity values to RNA measurements., *BMC Mol. Biol.* 7 (2006) 3. doi:10.1186/1471-2199-7-3.
- [35] J.B. Papizan, R.A. Singer, S.I. Tschen, S. Dhawan, J.M. Friel, S.B. Hipkens, M.A. Magnuson, A. Bhushan, L. Sussel, Nkx2.2 repressor complex regulates islet -cell specification and prevents -to- -cell reprogramming, *Genes Dev.* 25 (2011) 2291–2305. doi:10.1101/gad.173039.111.breakthrough.
- [36] Y. Suissa, J. Magenheim, M. Stolovich-Rain, A. Hija, P. Collombat, A. Mansouri, L. Sussel, B. Sosa-Pineda, K. McCracken, J.M. Wells, R.S. Heller, Y. Dor, B. Glaser, Gastrin: A Distinct Fate of Neurogenin3 Positive Progenitor Cells in the Embryonic Pancreas, *PLoS One*. 8 (2013) 2–11. doi:10.1371/journal.pone.0070397.
- [37] J. Cox, M.Y. Hein, C. a Luber, I. Paron, Accurate proteome-wide label-free quantification by delayed normalization and maximal peptide ratio extraction, termed MaxLFQ, *Mol. Cell.* 13 (2014) 2513–2526. doi:10.1074/mcp.M113.031591.
- [38] M. Kang, W. Qin, M. Buya, X. Dong, W. Zheng, W. Lu, J. Chen, Q. Guo, Y. Wu, VNN1, a potential biomarker for pancreatic cancer-associated new-onset diabetes, aggravates paraneoplastic islet dysfunction by increasing oxidative stress, *Cancer Lett.* 373 (2016) 241–250. doi:10.1016/j.canlet.2015.12.031.
- [39] G.L. Stahl, Y. Xu, L. Hao, M. Miller, J.A. Buras, M. Fung, H. Zhao, Role for the alternative complement pathway in ischemia/reperfusion injury, *Am.J.Pathol.* 162 (2003) 449–455. doi:10.1016/S0002-9440(10)63839-4.
- [40] M. Brissova, A. Shostak, M. Shiota, P.O. Wiebe, G. Poffenberger, J. Kantz, Z. Chen, C. Carr, W.G. Jerome, J. Chen, H.S. Baldwin, W. Nicholson, D.M. Bader, T. Jetton, M. Gannon, A.C. Powers, Pancreatic

islet production of vascular endothelial growth factor-A is essential for islet vascularization, revascularization, and function, *Diabetes*. 55 (2006) 2974–2985. doi:10.2337/db06-0690.

- [41] M.A. Guney, C.P. Petersen, A. Boustani, M.R. Duncan, U. Gunasekaran, R. Menon, C. Warfield, G.R. Grotendorst, A.L. Means, A.N. Economides, M. Gannon, Connective tissue growth factor acts within both endothelial cells and β cells to promote proliferation of developing β cells., *Proc. Natl. Acad. Sci. U. S. A.* 108 (2011) 15242–15247. doi:10.1073/pnas.1100072108.
- [42] K.G. Riley, R.C. Pasek, M.F. Maulis, J. Peek, F. Thorel, D.R. Brigstock, P.L. Herrera, M. Gannon, Connective tissue growth factor modulates adult β -cell maturity and proliferation to promote β -cell regeneration in mice, *Diabetes*. 64 (2015) 1284–1298. doi:10.2337/db14-1195.
- [43] T.W. Van Haeften, T.B. Twickler, Insulin-like growth factors and pancreas β -cells, *Eur. J. Clin. Invest.* 34 (2004) 249–255. doi:10.1111/j.1365-2362.2004.01337.x.
- [44] B. Han, S. Qi, B. Hu, H. Luo, J. Wu, TGF- β Promotes Islet β -Cell Function and Regeneration, *J. Immunol.* 186 (2011) 5833–5844. doi:10.4049/jimmunol.1002303.
- [45] L. Baeyens, S. De Breuck, J. Lardon, J.K. Mfopou, I. Rooman, L. Bouwens, *In vitro* generation of insulin-producing β -cells from adult exocrine pancreatic cells, *Diabetologia*. 48 (2005) 49–57. doi:10.1007/s00125-004-1606-1.
- [46] J.R. Wiśniewski, D. Rakus, Multi-enzyme digestion FASP and the “Total Protein Approach”-based absolute quantification of the *Escherichia coli* proteome, *J. Proteomics*. 109 (2014) 322–331. doi:10.1016/j.jprot.2014.07.012.
- [47] H. Song, M.J. Cha, B.W. Song, I.K. Kim, W. Chang, S. Lim, E.J. Choi, O. Ham, S.Y. Lee, N. Chung, Y. Jang, K.C. Hwang, Reactive oxygen species inhibit adhesion of mesenchymal stem cells implanted into ischemic myocardium via interference of focal adhesion complex, *Stem Cells*. 28 (2010) 555–563. doi:10.1002/stem.302.
- [48] W. Chang, B.W. Song, S. Lim, H. Song, Y.S. Chi, M.J. Cha, H.A. Dong, Y.G. Jung, D.H. Lee, H.C. Ji, K.D. Choi, S.K. Lee, N. Chung, S.K. Lee, Y. Jang, K.C. Hwang, Mesenchymal stem cells pretreated with delivered Hph-1-Hsp70 protein are protected from hypoxia-mediated cell death and rescue heart functions from myocardial injury, *Stem Cells*. 27 (2009) 2283–2292. doi:10.1002/stem.153.
- [49] E. Berishvili, T. Harkany, D. Meyer, P. Collombat, J. Klughammer, M. Farlik, S. Sdelci, P. Májek, F.M. Pauler, T. Penz, A. Stukalov, M. Gridling, K. Parapatics, J. Colinge, K.L. Bennett, C. Bock, G. Superti-Furga, S. Kubicek, Artemisinins Target GABAA Receptor Signaling and

Impair α Cell Identity, *Cell*. 168 (2017) 86–100.e15. doi:10.1016/j.cell.2016.11.010.

- [50] M. Urrutia, S. Fernández, M. González, R. Vilches, P. Rojas, M. Vásquez, M. Kurte, A.M. Vega-Letter, F. Carrión, F. Figueroa, P. Rojas, C. Irrarázabal, R.A. Fuentealba, Overexpression of glutamate decarboxylase in mesenchymal stem cells enhances their immunosuppressive properties and increases GABA and nitric oxide levels, *PLoS One*. 11 (2016) 1–29. doi:10.1371/journal.pone.0163735.
- [51] M.N. Poy, L. Eliasson, J. Krutzfeldt, S. Kuwajima, X. Ma, P.E. MacDonald, S. Pfeffer, T. Tuschl, N. Rajewsky, P. Rorsman, M. Stoffel, A pancreatic islet-specific microRNA regulates insulin secretion, *Nature*. 432 (2004) 226–230. doi:10.1038/nature03076.
- [52] D.G. Phinney, M. Di Giuseppe, J. Njah, E. Sala, S. Shiva, C.M. St Croix, D.B. Stolz, S.C. Watkins, Y.P. Di, G.D. Leikauf, J. Kolls, D.W.H. Riches, G. Deiuliis, N. Kaminski, S. V. Boregowda, D.H. McKenna, L.A. Ortiz, Mesenchymal stem cells use extracellular vesicles to outsource mitophagy and shuttle microRNAs, *Nat. Commun*. 6 (2015) 8472. doi:10.1038/ncomms9472.
- [53] D. Ti, H. Hao, X. Fu, W. Han, Mesenchymal stem cells-derived exosomal microRNAs contribute to wound inflammation, *Sci. China Life Sci*. 59 (2016) 1305–1312. doi:10.1007/s11427-016-0240-4.
- [54] S. Bonner-Weir, M. Taneja, G.C. Weir, K. Tatarkiewicz, K.-H. Song, A. Sharma, J.J. O’Neil, *In vitro* cultivation of human islets from expanded ductal tissue, *Proc. Natl. Acad. Sci*. 97 (2000) 7999–8004. doi:10.1073/pnas.97.14.7999.
- [55] R. Gao, J. Ustinov, M. -a. Pulkkinen, K. Lundin, O. Korsgren, T. Otonkoski, Characterization of endocrine progenitor cells and critical factors for their differentiation in human adult pancreatic cell culture, *Diabetes*. 52 (2003) 2007–2015. doi:10.2337/diabetes.52.8.2007.
- [56] Z. Li, F.A. Karlsson, S. Sandler, Islet loss and alpha cell expansion in type 1 diabetes induced by multiple low-dose streptozotocin administration in mice, *J. Endocrinol*. 165 (2000) 93–99. doi:10.1677/joe.0.1650093.

Chapter 6

Discussion

6.1 Summary

Proteomic characterization by mass spectrometry has emerged as one of the most powerful tools for studying biological systems. Large-scale analysis of complex biological systems has been obscured by an increase in available proteomic techniques. Central to the success of applying proteomic characterizations to investigate both qualitative and quantitative changes is inherent in method selection. Due to the complex nature of the human proteome, both in terms of protein number as well as dynamic concentration range, fractionation is often needed to maximize visibility. However, choosing the appropriate fractionation strategies to answer the biological questions at hand are not always apparent. To this end, the work in this thesis has provided insight into method selection as well highlights trade-offs, such as cost and time, which need to be considered when performing large-scale mass spectrometry based proteomics (Chapter 2) [1]. Ultimately, all fractionation techniques offer investigators a deeper view into biological systems. When combined with the analysis of human multipotent stromal cells (hMSC) to probe for novel secreted proteins, we discovered an unprecedented number of growth factors which serve as signals for endogenous regeneration of β -cell mass (Chapter 3) [2]. In doing so, we established the concept that Wnt-signaling was essential for optimized islet regeneration, based on protein expression levels observed in hMSC that possessed the ability to augment blood glucose using *in vivo* models. In

addition, we recognized the clinical applicability of determining protein signatures that could be used to screen hMSC that possessed the ability to induce islet regeneration. Therefore, a robust quantitative proteomics method was developed to predict, or screen, hMSC that could be used in downstream clinical applications for β -cell regeneration (Chapter 4). The adapted quantitative method not only proved that a protein signature obtained from hMSC conditioned media (CM) could be used to reliably characterize many hMSC lines in a high throughput fashion, but it also highlighted the rarity of identifying hMSC lines that possessed regenerative potential. To circumvent this challenge, we applied concepts borrowed from earlier proteomic analyses (Chapter 3) to increase the regenerative potential of hMSC that were classified as non-regenerative by activating Wnt-signaling during expansion (Chapter 5). Applying these methodologies, we proved that Wnt-activation during CM generation reliably increased the regenerative potential of non-regenerative hMSC and potentially initiated regeneration of β -cell mass through previously undocumented mechanisms. Taken together, these observations into hMSC trophic factors that mediate β -cell regeneration will aid in the development of potential cell, protein or drug therapies for the treatment of diabetes.

6.2 A new model for hMSC regulated β -cell regeneration

Research focused on recovery of β -cell mass has mostly been achieved using transplantation of pre-differentiated β -like cells from pluripotent stem cells or by the induction of endogenous islet regenerative programs after intravenous infusion of hMSC [3–5]. Although, both methods have shown tremendous promise, recoveries achieved by these methods

have been suboptimal and further understanding of relevant mechanisms is required to harness the potential of these cell types for islet regenerative applications. Parallel to this need, is to cultivate the ability to induce islet regeneration without transplantation of foreign cells potentially rejected by the immune system. Currently, there are only a few examples of stimulated endogenous recoveries achieved by delivery of proteins or metabolites [6–8]. However, many of these studies struggle to produce potential targets that contribute to regeneration as well as detailed understanding of regenerative mechanisms. As we have shown in this thesis, the compilation of signals secreted by hMSC can be used to induce regeneration in mice, without the transfer of cells, and ultimately coordinate in order to promote two critical events in β -cell neogenesis: (1) initiating conversion of α -cells to β -like cells, and (2) promoting the survival and proliferation of newly formed β -cells. In hMSC CM, the specific factors upregulated during Wnt-activation, in addition to other supportive factors constitutively present in hMSC CM, have been characterized as playing a central role in homeostatic regulation of pancreatic

6.2.1 Insulin like growth factors (IGFs) and β -cell mass

Many protein-based studies have been conducted to identify factors important in regeneration of β -cell mass. As part of our own efforts to characterize signals secreted by islet regenerative hMSC (Chapter 3), we identified a number of components belonging to the insulin like growth factor (IGF) family, mainly IGF1 and IGF2 [2]. Interestingly, the expression of IGF2 was only found in measurable quantities in hMSC lines that possessed the ability to augment hyperglycemia recovery after transplantation. IGF2 has many important roles in maintaining “stemness” of multiple cell types including

hMSC [9]. Of particular interest, IGF2 has been shown to regulate β -cell mass both in development and the adult pancreas [10]. Using spontaneous models of type 2 diabetes (T2D), defective IGF2 production within the embryonic pancreas was directly responsible for anomalies in β -cell mass [11]. In the adult pancreas, using IGF2 knockout mice, Modi *et. al.* showed that adult β -cells actively secreted IGF2 to regulate β -cell mass after pancreatic damage and during pregnancy [12]. Additionally, the re-expression of IGF2 in adult mice increased endogenous β -cell regeneration after STZ-damage *in vivo* [13]. High levels of IGF2 produced by hMSC could act on endogenous β -cells to increase proliferation and maintenance. In contrast, IGF1 protein was not differentially expressed by regenerative and non-regenerative hMSC. However, after Wnt-activation, the secreted levels of IGF1 were also significantly increased (Chapter 4). IGF1 can also influence β -cell mass using similar mechanisms discussed for IGF2, but also has been implicated in the regulation of β -cell apoptosis [14]. These results can be directly observed in human co-culture assay in which exposure of human islets to recombinant human IGF1 promoted the survival of β -cells over 7 days (Figure 5.10). Conversely, IGF1 does not participate in controlling β -cell development, but has been directly linked to defective glucose stimulated insulin secretion and impaired glucose tolerance [15]. Lastly, distribution of IGF1 within pancreatic biopsies harvested from T2D patients showed significantly reduced levels, again cementing an important role for IGF1 in maintaining both β -cell mass and regulation of insulin secretion [16]. Finally, the expression of IGF1 has been shown to protect β -cells against apoptosis, by an autocrine loop established by glucagon-like peptide 1 (GLP1) [17].

6.2.2 Transforming growth factor β and β -cell mass

Further proteomic analysis of secreted growth factors derived from hMSC revealed the presence of multiple members belonging to the transforming growth factor β (TGF β) superfamily (Chapter 3) [2]. In particular two TGF β family members, TGF β 1 and TGF β i were upregulated in hMSC that possessed the ability to reduce hyperglycemia after transplantation (Figure 3.3). Exogenous administration of TGF β i to islets *in vitro*, or over expression of TGF β i in mice, both resulted in increased β -cell proliferation rates and better glucose tolerance, suggesting TGF β i was necessary for islet regeneration and function [18]. On the other hand, the role of TGF β 1 in islet function is less clear with conflicting results suggesting it may act both as a negative or positive regulator of β -cell genesis. Inhibition of TGF β 1 signaling after partial pancreatectomy significantly decreased β -cell mass recovery resulting directly from increased β -cell apoptosis[19]. Similarly, independent reports also suggested that inhibition of TGF β 1 reduced β -cell proliferation by interfering with cell cycle check points [20,21]. TGF β 1 involvement in the mechanisms elicited by hMSC was not further investigated and could be of future interest. The proteomic data obtained after activation of Wnt-signaling could offer some insight into unanswered questions regarding TGF β involvement. Upon Wnt-activation, the secreted levels of TGF β 1 were found to be equivalent across all conditions. However, TGF β 2 protein levels in Wnt-activated CM were more than 4-fold higher compared to untreated CM or Wnt-inhibited CM. Human islet co-cultures exposed to recombinant human TGF β 2 showed significantly increased survival rates compared to islets exposed to untreated or Wnt-inhibited media (Figure 5.10). Recently, TGF β 2

signaling was reported to be involved in β -cell proliferation under increased inflammation and increased β -cell workloads [22]. We believe this is strong evidence that TGF β pathway plays an important role in inducing or maintaining the islet regenerative niche created by hMSC.

6.2.3 *Wnt-signals formulate a regenerative niche*

Throughout this thesis, much focus has been put on characterization of Wnt-signaling, both in terms of hMSC secretory profiles in relation to β -cell biology. Wnt-signaling plays a vital role in regulating proliferation and differentiation of hMSC [23]. Although not investigated, multiple studies have suggested that the inhibition or low levels of Wnt-signaling could be responsible for cell senescence [24]. Indeed, studies previously conducted by our lab have suggested, at the transcriptional level, that Wnt-signaling was important in maintaining regenerative capacity as cells were passaged in culture [25]. Preliminary unpublished proteomic investigation confirmed these results as inhibitors of Wnt-signaling were increased at later passages. Within the data set presented in Chapter 3, low levels of Wnt-signaling in non-regenerative hMSC may predict premature hMSC senescence. In addition, the establishment of a deleterious pro-inflammatory microenvironment by non-regenerative hMSC (Chapter 4) may be potentially be linked to senescence-associated secretory phenotypes [26]. Thus, we used the activation of Wnt-signaling during hMSC culture to increase the therapeutic potential of non-regenerative hMSC CM (Chapter 5). Further proteomic characterization of the secretory changes upon Wnt-activation have also revealed decreased levels of pro-inflammatory cytokines (Table 5.1). This would suggest that a prevention of hMSC senescence was potentially involved in decreasing a deleterious

secretory microenvironment contributed by non-regenerative hMSC, although further investigations are needed to confirm these findings. If the niche established by hMSC could be further optimized to exclude these deleterious proteins, and translated *in vivo* via delivery of CM, the therapeutic potential on β -cell regenerative pathways could be greatly increased. Overall these observations combine to highlight that multiple factors secreted by hMSC both *in vitro* and *in vivo* need to work in synergy to optimize β -cell proliferation and survival within newly formed islets (Figure 6.1).

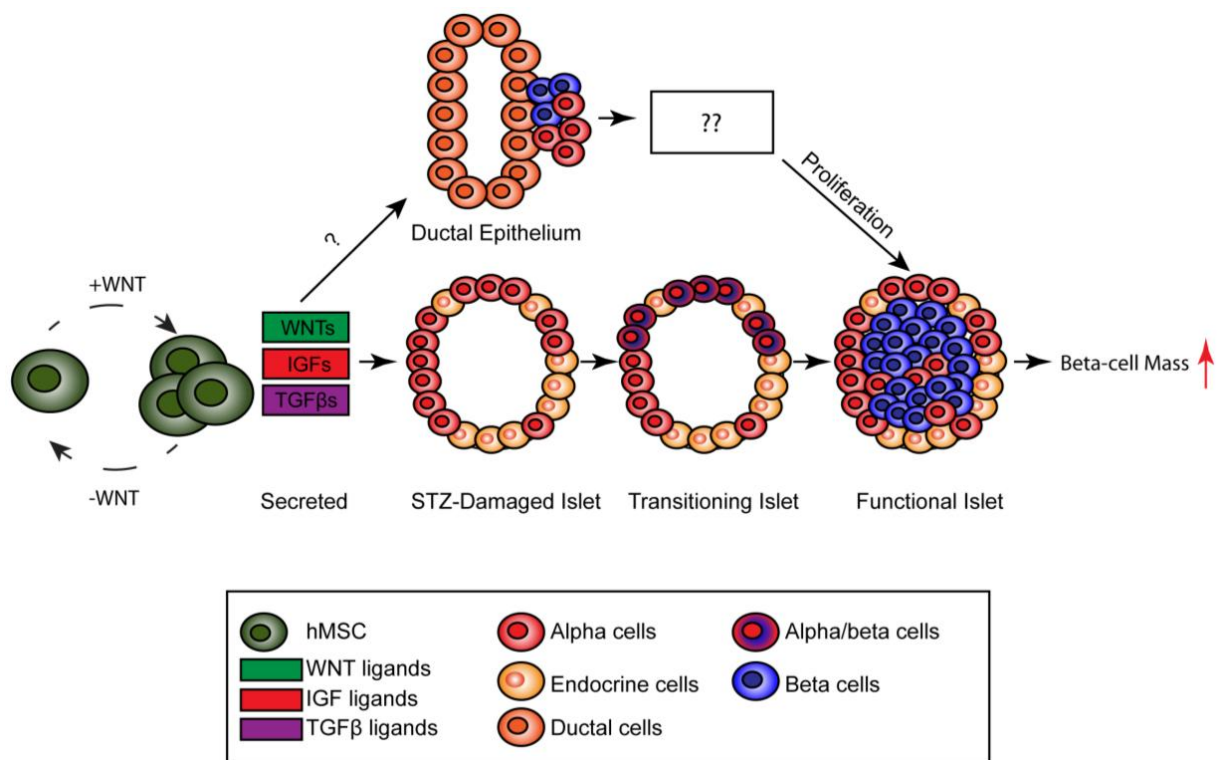


Figure 6.1 New model for hMSC induced β-cell regeneration. A schematic of potential ligands secreted by hMSC that act synergistically to activate neogenic mechanisms and convert residual α-cells into β-like cells and finally into fully functional β-cells.

6.3 α -to- β -cell conversion

The islets of Langerhans are multi-cellular structures that regulate glucose metabolism within the body [27]. During type 1 diabetes (T1D) the destruction of β -cells by the immune systems occurs through auto-antibodies against specific epitomes only found on β -cells [28]. However, other cells types within the islets, such as α -cells, remain largely unaffected. Recent, genetic analyses of endocrine cells within the islet reveal a high degree of cellular plasticity (reviewed in [29]). An overwhelming amount of recent evidence in animal models has emerged suggesting α -cells can be converted into functional β -cells and represent a means to increase β -cell mass after islet damage [30]. Epigenomic analysis of human islets also supports the hypothesis that α -to- β -cell conversion is also possible [31]. Lineage-tracing experiments using chemically induced β -cell damage have demonstrated that a large fraction of regenerated β -cells were derived from α -cells [32]. These findings represent previously unexplored avenues for β -cell regeneration. With this in mind, most efforts to direct α - β -cell conversion have relied on genetic manipulation of transcription factors found within α -cells, such as Pax-4 [33–35]. Only recently, has work been performed to determine exogenous factors that can initiate conversion of α - β -cells. As mentioned previously, the long-term administration of GABA has been well characterized in the recovery of β -cell mass via the conversion of α -cells [36]. In addition, the use of small molecule compounds can initiate similar processes and increase β -cell mass [37]. Within this thesis, for the first time we provide evidence that the secretory products generated during hMSC culture can be harnessed to initiate regeneration of β -cell mass via the conversion of α -cells that survive STZ-

treatment (Chapter 5). In addition, using proteomic techniques we have provided a list of potential factors that could mediate initiation of conversion. Although these findings still premature, we feel these data may be extended to the potential development of new therapies for the treatment of diabetes.

6.4 Clinical Applications

The findings presented in this thesis provide substantial pre-clinical justification for further investigation of islet regenerative strategies using hMSC as well as their secretory products for the treatment of diabetes. The clinical feasibility of using hMSC transfer to treat diabetes have been previously investigated (reviewed in [38]), but the advantages of transferring protein cocktails generated from hMSC, rather than hMSC themselves has been presented here for the first time. One of the biggest advantages of using protein cocktails over cells is that autologous sources are not required. As we have exemplified in Chapter 4, the rarity of acquiring islet regenerative hMSC represented a potential setback for clinical applications. In addition, donor-specific characteristics should be taken into account, such as BMI, to maximize therapeutic potential of transplanting cell lines also hinder progression towards clinic. Preliminary data not presented here, has shown that injection of regenerative hMSC CM has increased β -cell regenerative potential compared to non-regenerative hMSC and did not need additional manipulation, such as Wnt-activation. However, because regenerative hMSC lines are less accessible, we presented an alternative approach to increase the potency of any bone marrow derived hMSC lines, through the activation of Wnt-signaling (Chapter 5). The scalability of hMSC culture has already been proven using batch culture systems [39]. In theory, generation of hMSC CM in

large quantities, using xeno-free serum-free approaches, can be achieved by applying these methodologies. Therefore it is realistic to predict that many diabetic patients could be treated using hMSC CM. However, certain considerations that were not investigated within this thesis must be taken into account.

6.4.1 Directed delivery of hMSC CM

One avenue that needs to be addressed before injection of hMSC CM can become a potential treatment for T1D patients is how to deliver CM using a clinically applicable modality. It has been largely accepted that one of the main factors reducing the regenerative efficacy of hMSC after transplantation, at least in mouse models, is that cells often get trapped in the lungs and are not directly targeted to the site of tissue damage [40]. As we have also shown in Chapter 5, transplanted cell do not survive long when directly delivered to pancreas. Also, delivery of hMSC CM intravenously would hypothetically encounter similar problems. Trophic factors responsible for initiating endogenous recovery may never make it to the site of injury and those that do may not be found within concentrations needed for regeneration. Although not presented in this thesis, preliminary assessment of hMSC CM delivered intravenously was attempted. Initial results were promising in which mice that were injected with Wnt-activated CM showed signs of recovery that quickly dissipated and never reached levels observed with direct delivery into the pancreas. Importantly, 12.5X more CM was needed to elicit fractional results. One of the major hurdles met with injection of hMSC CM into the pancreas is that it is very invasive and as the data presented in this thesis suggests, multiple injection of CM directly to the site of injury could potentially increase

recovery. In addition, only very small volumes (20 μ L in mice) were used to deliver CM, limiting the dose available for delivery. Others have delivered proteins factor throughout the pancreas using the common bile duct [7]. Although this is still an invasive procedure it could offer a larger volume range for CM delivery. Another potential solution to increase the therapeutic effects of CM could include a combination of delivery systems. Initial delivery directly into the pancreas could be superseded with infusion of CM, either once or multiple times, intravenously. Finding the least invasive way, while retaining the therapeutic benefits of the CM-injection would be the first step towards commercialization of CM based therapies for diabetes.

6.4.2 Autoimmunity after regeneration

One major concern that all therapies aimed at increasing β -cell mass face is the concomitant destruction of newly formed islets by the immune system that have retained memory of β -cell antigens. In addition, dealing with potential insulin resistance and co-morbidities common in T2D may also represent a hurdle to therapeutic application. Although not investigated, multiple solutions to this problem might already exist in the current study. Firstly, the autoimmune-mediated β -cell loss is a slow progressing condition [41]. Therefore, regeneration of newly formed β -cells could occur at a faster rate than destruction if an attempt to curb ongoing autoimmunity can be established. This is exemplified in the data presented in this thesis by highlighting the very fast therapeutic response to CM injection with significant recovery of β -cell function observed within 1-4 days of CM-injection. Therefore if multiple rounds of CM delivery prove feasible, the eventual deletion of β -cell mass by the immune system could be combated. Secondly, since the

mechanisms responsible for restoring β -cell mass are via α -cell conversion, newly formed β -cells could contain surface antigens that are specific to α -cells, rendering them undetected by immune surveillance. Complete profiling for surface antigens that are known to be involved in β -cell destruction, such as zinc transporter 8, could be conducted to determine if newly formed β -cells have autoantibody antigens [42]. Lastly, a combinatorial approach that involves immunosuppressive treatment with regeneration mediated by hMSC CM could be a viable strategy. Screening hMSC lines that possess a high degree of immuno-suppressive secreted ligands, using the proteomic techniques developed in Chapter 4 could represent one approach that would allow mix-and-matching of targeted CMs, with islet regenerative and immunosuppressive capacity that someday may be possible to achieve both regeneration and induce immune tolerance.

6.5 Future Directions

Despite the extensive analysis of growth factors secreted by islet regenerative hMSC (Chapter 3) and growth factors upregulated during Wnt-activation (Chapter 5), relatively few of those that were identified have yet to be characterized in islet culture assays or *in vivo*. For example, we identified members of the IGF and TGF β families, found in regenerative and Wnt-activated CM, have only been shown briefly in this thesis to enhance survival of human islet *in vitro*. When used in combination, these ligands performed equivalently, if not better, than CM generated from hMSC. While these ligands were investigated, their optimal dose was not determined and would require additional *in vitro* characterization using the methods described in this thesis (Chapter 3 and 5). In addition, direct delivery of each ligand or in combination

need to be performed using *in vivo* mouse models to determine whether they can induce endogenous islet regeneration. Using any of these approaches, growth factors identified in islet regenerative hMSC could be studied in the context of β -cell regeneration.

While both islet regenerative and non-regenerative hMSC were investigated in this thesis, it is clear that the majority of samples received for clinical application may not be useful for islet regeneration. Although successful, our screening approaches aimed at identify secreted proteins that could predict the islet regenerative potential of hMSC could be improved by acquiring more samples. Since the majority of samples used in this assay were classified as non-regenerative, more samples that are regenerative are needed to better assign classes using the support vector machine algorithm. In particular, one of the proposed future directions should include further characterization of donor BMI and regenerative capacity. As it has been presented in this thesis, the donor BMI was correlative with islet regenerative capacity. Obtaining more samples from donors in health <25 BMI ranges could further strength this observation and allow for further optimization of the predictive assay. In theory, donor BMI information could be used as a prerequisite for assessing regenerative capacity in conjunction with the quantitative proteomic assays developed in Chapter 4. As mentioned previously, one major question left to answer if hMSC CM is to be used as a therapeutic, is whether endogenous regeneration can occur in the face of autoimmunity. Thus, to answer some of these questions hMSC CM injection needs to be performed using NOD mice. NOD mice develop diabetes spontaneously with many similarities to human autoimmune T1D [43]. A

promising feature of the methodologies presented here is that CM used to induce endogenous regeneration may simultaneously contain a wide variety of effectors known to regulate and often suppress immune responses [2]. Nonetheless, transplantation of hMSC CM into NOD mice may induce islet regeneration and/or delay insulinitis progression by modulating regulatory T-cell functions [44]. Finally, the transplantation of bone marrow derived hMSC into patients with new onset T1D has been shown to preserve β -cell function for up to 2 years, [45]. Therefore, combining the immunomodulatory properties inherent to hMSC, as well as the β -cell regenerative properties shown here within hMSC CM, represents an extremely attractive option for the potential development of a cell-free regenerative treatment designed to tip the balance in favor of islet regeneration versus autoimmune destruction.

6.6 References

- [1] M. Kuljanin, D.Z. Dieters-Castator, D.A. Hess, L.-M. Postovit, G.A. Lajoie, Comparison of sample preparation techniques for large-scale proteomics, *Proteomics*. 17 (2017). doi:10.1002/pmic.201600337.
- [2] M. Kuljanin, G.I. Bell, S.E. Sherman, G.A. Lajoie, D.A. Hess, Proteomic characterisation reveals active Wnt-signalling by human multipotent stromal cells as a key regulator of beta cell survival and proliferation, *Diabetologia*. (2017). doi:10.1007/s00125-017-4355-7.
- [3] M.P. Walczak, A.M. Drozd, E. Stoczynska-Fidelus, P. Rieske, D.P. Grzela, Directed differentiation of human iPSC into insulin producing cells is improved by induced expression of PDX1 and NKX6.1 factors in IPC progenitors, *J. Transl. Med.* 14 (2016) 341. doi:10.1186/s12967-016-1097-0.
- [4] F.W. Pagliuca, J.R. Millman, M. Gürtler, M. Segel, A. Van Dervort, J.H. Ryu, Q.P. Peterson, D. Greiner, D.A. Melton, Generation of functional human pancreatic β cells in vitro, *Cell*. 159 (2014) 428–439. doi:10.1016/j.cell.2014.09.040.
- [5] G.I. Bell, H.C. Broughton, K.D. Levac, D.A. Allan, A. Xenocostas, D.A. Hess, Transplanted Human Bone Marrow Progenitor Subtypes Stimulate Endogenous Islet Regeneration and Revascularization, *Stem Cells Dev.* 21 (2012) 97–109. doi:10.1089/scd.2010.0583.
- [6] G.C. Weir, S. Bonner-Weir, GABA Signaling Stimulates β Cell Regeneration in Diabetic Mice, *Cell*. 168 (2017) 7–9. doi:10.1016/j.cell.2016.12.006.
- [7] J.K. Smid, S. Faulkes, M.A. Rudnicki, Periostin induces pancreatic regeneration, *Endocrinology*. 156 (2015) 824–836. doi:10.1210/en.2014-1637.
- [8] X. Gao, L. Song, K. Shen, H. Wang, M. Qian, W. Niu, X. Qin, Bone marrow mesenchymal stem cells promote the repair of islets from diabetic mice through paracrine actions, *Mol. Cell. Endocrinol.* 388 (2014) 41–50. doi:10.1016/j.mce.2014.03.004.
- [9] A. Youssef, D. Aboalola, V.K.M. Han, The Roles of Insulin-Like Growth Factors in Mesenchymal Stem Cell Niche, *Stem Cells Int.* 2017 (2017) 1–12. doi:10.1155/2017/9453108.
- [10] A. Casellas, C. Mallol, A. Salavert, V. Jimenez, M. Garcia, J. Agudo, M. Obach, V. Haurigot, L. Vilà, M. Molas, R. Lage, M. Morró, E. Casana, J. Ruberte, F. Bosch, Insulin-like growth factor 2 overexpression induces β -Cell dysfunction and increases beta-cell susceptibility to damage, *J. Biol. Chem.* 290 (2015) 16772–16785. doi:10.1074/jbc.M115.642041.
- [11] S. Calderari, M.N. Gangnerau, M. Thibault, M.J. Meile, N. Kassis, C.

- Alvarez, B. Portha, P. Serradas, Defective IGF2 and IGF1R protein production in embryonic pancreas precedes beta cell mass anomaly in the Goto-Kakizaki rat model of type 2 diabetes, *Diabetologia*. 50 (2007) 1463–1471. doi:10.1007/s00125-007-0676-2.
- [12] H. Modi, C. Jacovetti, D. Tarussio, S. Metref, O.D. Madsen, F.P. Zhang, P. Rantakari, M. Poutanen, S. Nef, T. Gorman, R. Regazzi, B. Thorens, Autocrine action of IGF2 regulates adult β -cell mass and function, *Diabetes*. 64 (2015) 4148–4157. doi:10.2337/db14-1735.
- [13] L. Zhou, S. Pelengaris, S. Abouna, J. Young, D. Epstein, J. Herold, T.W. Nattkemper, H. Nakhai, M. Khan, Re-Expression of IGF-II Is Important for Beta Cell Regeneration in Adult Mice, *PLoS One*. 7 (2012) 1–8. doi:10.1371/journal.pone.0043623.
- [14] C.J. Rhodes, IGF-I and GH post-receptor signaling mechanisms for pancreatic β -cell replication, *J. Mol. Endocrinol.* 24 (2000) 303–311. doi:10.1677/jme.0.0240303.
- [15] R.N. Kulkarni, M. Holzenberger, D.Q. Shih, U. Ozcan, M. Stoffel, M.A. Magnuson, C.R. Kahn, β -cell-specific deletion of the Igf1 receptor leads to hyperinsulinemia and glucose intolerance but does not alter β -cell mass, *Nat. Genet.* 31 (2002) 111–115. doi:10.1038/ng872.
- [16] S. Al-Salam, R. Hameed, H. Parvez, E. Adeghate, Pattern of distribution of IGF-1 and EGF in pancreatic islets of type 2 diabetic patients., *Islets*. 1 (2009) 102–105. doi:10.4161/isl.1.2.9273.
- [17] M. Cornu, H. Modi, D. Kawamori, R.N. Kulkarni, M. Joffraud, B. Thorens, Glucagon-like peptide-1 increases β -cell glucose competence and proliferation by translational induction of insulin-like growth factor-1 receptor expression, *J. Biol. Chem.* 285 (2010) 10538–10545. doi:10.1074/jbc.M109.091116.
- [18] B. Han, S. Qi, B. Hu, H. Luo, J. Wu, TGF- β Promotes Islet β -Cell Function and Regeneration, *J. Immunol.* 186 (2011) 5833–5844. doi:10.4049/jimmunol.1002303.
- [19] C. Lei, X. Zhou, Y. Pang, Y. Mao, X. Lu, M. Li, J. Zhang, TGF- β signalling prevents pancreatic beta cell death after proliferation, *Cell Prolif.* 48 (2015) 356–362. doi:10.1111/cpr.12183.
- [20] T. Suzuki, P. Dai, T. Hatakeyama, Y. Harada, H. Tanaka, N. Yoshimura, T. Takamatsu, TGF- β Signaling Regulates Pancreatic β -Cell Proliferation through Control of Cell Cycle Regulator p27 Expression, *Acta Histochem. Cytochem.* 46 (2013) 51–58. doi:10.1267/ahc.12035.
- [21] S. Dhawan, E. Dirice, R.N. Kulkarni, A. Bhushan, Inhibition of TGF- β signaling promotes human pancreatic β -cell replication, *Diabetes*. 65 (2016) 1208–1218. doi:10.2337/db15-1331.
- [22] X. Xiao, J. Wiersch, Y. El-Gohary, P. Guo, K. Prasad, J. Paredes, C.

- Welsh, C. Shiota, G.K. Gittes, TGF β receptor signaling is essential for inflammation-induced but not β -cell workload-induced β -cell proliferation, *Diabetes*. 62 (2013) 1217–1226. doi:10.2337/db12-1428.
- [23] L. Ling, V. Nurcombe, S.M. Cool, Wnt signaling controls the fate of mesenchymal stem cells, *Gene*. 433 (2009) 1–7. doi:10.1016/j.gene.2008.12.008.
- [24] Z. Varecza, K. Kvell, G. Talabér, G. Miskei, V. Csongei, D. Bartis, G. Anderson, E.J. Jenkinson, J.E. Pongracz, Multiple suppression pathways of canonical Wnt signalling control thymic epithelial senescence, *Mech. Ageing Dev.* 132 (2011) 249–256. doi:10.1016/j.mad.2011.04.007.
- [25] G.I. Bell, M.T. Meschino, J.M. Hughes-Large, H.C. Broughton, A. Xenocostas, D.A. Hess, Combinatorial Human Progenitor Cell Transplantation Optimizes Islet Regeneration Through Secretion of Paracrine Factors, *Stem Cells Dev.* 21 (2012) 1863–1876. doi:10.1089/scd.2011.0634.
- [26] J.-P. Coppé, P.-Y. Desprez, A. Krtolica, J. Campisi, The Senescence-Associated Secretory Phenotype: The Dark Side of Tumor Suppression, *Annu. Rev. Pathol. Mech. Dis.* 5 (2010) 99–118. doi:10.1146/annurev-pathol-121808-102144.
- [27] M.S. Islam, The islets of Langerhans. Preface., 2010. doi:10.1007/978-90-481-3271-3_1.
- [28] V. Öling, H. Reijonen, O. Simell, M. Knip, J. Ilonen, Autoantigen-specific memory CD4 + T cells are prevalent early in progression to Type 1 diabetes, *Cell. Immunol.* 273 (2012) 133–139. doi:10.1016/j.cellimm.2011.12.008.
- [29] A. Migliorini, E. Bader, H. Lickert, Islet cell plasticity and regeneration, *Mol. Metab.* 3 (2014) 268–274. doi:10.1016/j.molmet.2014.01.010.
- [30] C.H. Chung, F. Levine, Adult pancreatic alpha cells: A new source of cells for beta-cell regeneration, *Rev. Diabet. Stud.* 7 (2010) 120–127. doi:10.1900/RDS.2010.7.120.
- [31] N.C. Bramswig, L.J. Everett, J. Schug, C. Dorrell, C. Liu, Y. Luo, P.R. Streeter, a Najji, M. Grompe, K.H. Kaestner, Epigenomic plasticity enables human pancreatic alpha to beta cell reprogramming, *J Clin Invest.* 123 (2013) 1275–1284. doi:10.1172/JCI66514.
- [32] F. Thorel, V. Népote, I. Avril, K. Kohno, R. Desgraz, S. Chera, P.L. Herrera, Conversion of adult pancreatic α -cells to β -cells after extreme β -cell loss, *Nature*. 464 (2010) 1149–1154. doi:10.1038/nature08894.
- [33] P. Collombat, A. Mansouri, J. Hecksher-sørensen, P. Serup, J. Krull, G. Gradwohl, P. Gruss, Opposing actions of Arx and Pax4 in endocrine pancreas development Opposing actions of Arx and Pax4 in endocrine

pancreas development, 4 (2003) 2591–2603. doi:10.1101/gad.269003.

- [34] P. Collombat, The simultaneous loss of Arx and Pax4 genes promotes a somatostatin-producing cell fate specification at the expense of the δ - and ϵ -cell lineages in the mouse endocrine pancreas, *Development*. 132 (2005) 2969–2980. doi:10.1242/dev.01870.
- [35] K. Al-Hasani, A. Pfeifer, M. Courtney, N. Ben-Othman, E. Gjernes, A. Vieira, N. Druelle, F. Avolio, P. Ravassard, G. Leuckx, S. Lacas-Gervais, D. Ambrosetti, E. Benizri, J. Hecksher-Sorensen, P. Gounon, J. Ferrer, G. Gradwohl, H. Heimberg, A. Mansouri, P. Collombat, Adult duct-lining cells can reprogram into β -like cells able to counter repeated cycles of toxin-induced diabetes, *Dev. Cell*. 26 (2013) 86–100. doi:10.1016/j.devcel.2013.05.018.
- [36] N. Ben-Othman, A. Vieira, M. Courtney, F. Record, E. Gjernes, F. Avolio, B. Hadzic, N. Druelle, T. Napolitano, S. Navarro-Sanz, S. Silvano, K. Al-Hasani, A. Pfeifer, S. Lacas-Gervais, G. Leuckx, L. Marroquí, J. Thévenet, O.D. Madsen, D.L. Eizirik, H. Heimberg, J. Kerr-Conte, F. Pattou, A. Mansouri, P. Collombat, Long-Term GABA Administration Induces Alpha Cell-Mediated Beta-like Cell Neogenesis, *Cell*. 168 (2017) 73–85.e11. doi:10.1016/j.cell.2016.11.002.
- [37] E. Berishvili, T. Harkany, D. Meyer, P. Collombat, J. Klughammer, M. Farlik, S. Sdelci, P. Májek, F.M. Pauler, T. Penz, A. Stukalov, M. Gridling, K. Parapatics, J. Colinge, K.L. Bennett, C. Bock, G. Superti-Furga, S. Kubicek, Artemisinin Target GABAA Receptor Signaling and Impair α Cell Identity, *Cell*. 168 (2017) 86–100.e15. doi:10.1016/j.cell.2016.11.010.
- [38] N. Kim, S.-G. Cho, Clinical applications of mesenchymal stem cells, *Korean J. Intern. Med.* 28 (2013) 387. doi:10.3904/kjim.2013.28.4.387.
- [39] P.J. Hanley, Z. Mei, M.G. Cabreira-hansen, M. Klis, W. Li, Manufacturing mesenchymal stromal cells for phase I clinical trials, 15 (2014) 416–422. doi:10.1016/j.jcyt.2012.09.007.Manufacturing.
- [40] S. Schrepfer, T. Deuse, H. Reichenspurner, M.P. Fischbein, R.C. Robbins, M.P. Pelletier, Stem Cell Transplantation: The Lung Barrier, *Transplant. Proc.* 39 (2007) 573–576. doi:10.1016/j.transproceed.2006.12.019.
- [41] M. Cnop, N. Welsh, J.C. Jonas, a Jorns, S. Lenzen, D.L. Eizirik, Mechanisms of pancreatic beta-cell death in type 1 and type 2 diabetes: many differences, few similarities, *Diabetes*. 54 Suppl 2 (2005) S97–107. doi:10.2337/diabetes.54.suppl_2.S97.
- [42] H. Skärstrand, E. Krupinska, T.J.K. Haataja, F. Vaziri-Sani, J.O. Lagerstedt, Å. Lernmark, Zinc transporter 8 (ZnT8) autoantibody epitope specificity and affinity examined with recombinant ZnT8 variant proteins in specific ZnT8R and ZnT8W autoantibody-positive type 1

diabetes patients, *Clin. Exp. Immunol.* 179 (2015) 220–229. doi:10.1111/cei.12448.

- [43] J.A. Pearson, F.S. Wong, L. Wen, The importance of the Non Obese Diabetic (NOD) mouse model in autoimmune diabetes, *J. Autoimmun.* 66 (2016) 76–88. doi:10.1016/j.jaut.2015.08.019.
- [44] A.M. Madec, R. Mallone, G. Afonso, E. Abou Mrad, A. Mesnier, A. Eljaafari, C. Thivolet, Mesenchymal stem cells protect NOD mice from diabetes by inducing regulatory T cells, *Diabetologia.* 52 (2009) 1391–1399. doi:10.1007/s00125-009-1374-z.
- [45] L. Li, H. Hui, X. Jia, J. Zhang, Y. Liu, Q. Xu, D. Zhu, Infusion with Human Bone Marrow-derived Mesenchymal Stem Cells Improves β -cell Function in Patients and Non-obese Mice with Severe Diabetes, *Sci. Rep.* 6 (2016) 37894. doi:10.1038/srep37894.

Appendix I

Supporting datasets for proteomic characterization of conditioned media generated from human multipotent stromal cells (hMSC).

Table A2.1 Proteomic performance across different fractionation workflows. The total number of converted MSMS scans, unique peptides, unique proteins and average number of proteins identified per hour for: in-solution, SDS-PAGE, GELFrEE, SCX, HpH and all data sets combined.

Method	In-solution	SDS-PAGE	GELFrEE	SCX	HpH	Comb.
MS/MS Scans	318K	2.96M	2.90M	2.55M	2.68M	11.4M
PSMs	182K	557K	830K	769K	653K	2.97M
Unique Peptides	52.5K	85.9K	71.7K	104K	111K	165K
Proteins	5189	6959	5919	7655	8470	8710
Pep/Pro Ratio	10.1	12.3	12.1	13.5	13.1	18.9
Gradient Time ^a	4.0h	40h	40h	40h	40h	492h
Proteins/hr ^b	1298	173	148	191	212	n/a

a Total amount of time per LC MS gradient excluding washing and equilibration

b Average proteins per hour identified for one biological replicate

Table A2.2 Acquisition parameters for the Q Exactive. Overview of the parameters used for data acquisition on a Q Exactive for large scale sample preparation.

Parameter	Q Exactive
Mass Range (m/z)	400-1500
Isolation Window (m/z)	1.2
MS resolution	70K @ 200m/z
MSMS Resolution	17.5K
MS Injection Time (ms)	250
MSn Injection Time (ms)	64
AGC Target (MS)	3E6
AGC Target (MSn)	2E5
Preview Scan	n/a
Threshold (counts)	3.1E4
Minimum AGC Target	2.0E3
Data Dependent Acquisition	Top12
Dynamic Exclusion (s)	30
Exclusion Mass Width (m/z)	n/a
Exclude Isotopes/ Monoisotopic precursor Selection	Enabled
Fragmentation Type	HCD
Normalized Collision Energy	25
Lock Mass (445.120025m/z)	Best
Charge State Rejection	Unassigned, +1, 7,>8
Default Charge State	+2

Table A3.1 Acquisition parameters for the Q Exactive. Overview of the parameters used for data acquisition on a Q Exactive for secreted proteins from hMSC.

Parameter	Q Exactive
Mass Range (m/z)	400-1450
Isolation Window (m/z)	2.0
MS resolution	70K @ 200m/z
MSMS Resolution	17.5K
MS Injection Time (ms)	250
MSn Injection Time (ms)	120
AGC Target (MS)	1E6
AGC Target (MSn)	2E5
Preview Scan	n/a
Threshold (counts)	5.0E4
Minimum AGC Target	6.0E3
Data Dependent Acquisition	Top15
Dynamic Exclusion (s)	30
Exclusion Mass Width (m/z)	n/a
Exclude Isotopes/ Monoisotopic precursor Selection	Enabled
Fragmentation Type	HCD
Normalized Collision Energy	25
Lock Mass (445.120025m/z)	Best
Charge State Rejection	Unassigned, +1,>8
Default Charge State	+2

Table A4.1 Posterior probabilities generated using SVM. Posterior probability of each protein used to identify a protein signature that could segregate regenerative and non-regenerative hMSC.

Accession Number	Gene Name	Posterior Probability	Direction
Q15818	NPTX1	1	DOWN
P12111	COL6A3	1	UP
P01210	PENK	1	UP
P10145	CXCL8	0.99989	UP
P05155	SERPING1	0.99989	UP
P05231	IL6	0.99928	UP
Q8N474	SFRP1	0.99713	DOWN
P03956	MMP1	0.98958	DOWN
P42830	CXCL5	0.98215	UP
P13500	CCL2	0.97828	UP
P10915	HAPLN1	0.97428	UP
P80162	CXCL6	0.97341	UP
Q99988	GDF15	0.96315	UP
Q05707	COL14A1	0.95743	DOWN
P41271	NBL1	0.95535	UP
P36222	CHI3L1	0.94348	UP
P23142	FBLN1	0.91515	DOWN
P35556	FBN2	0.91069	DOWN
P05120	SERPINB2	0.90423	UP
P35318	ADM	0.90229	UP
P31947	SFN	0.8768	UP
Q00888	PSG4	0.87446	UP
Q9NZU1	FLRT1	0.86897	DOWN
P26583	HMGB2	0.86321	DOWN
Q71DI3	HIST2H3A	0.81959	DOWN
P09341	CXCL1	0.81228	UP
P20742	PZP	0.80745	DOWN
P43121	MCAM	0.8029	UP
Q9BUD6	SPON2	0.77233	DOWN
Q9H5V8	CDCP1	0.6761	UP
P19876	CXCL3	0.65295	UP
O00622	CYR61	0.56003	UP
P10451	SPP1	0.53353	UP
O60565	GREM1	0.51981	DOWN
P11464	PSG1	0.50732	UP
P12107	COL11A1	0.50057	DOWN
O75094	SLIT3	0.4996	UP
P00749	PLAU	0.45896	UP
P0C0L4	C4A	0.45695	DOWN
P58215	LOXL3	0.40034	DOWN
Q04756	HGFAC	0.39176	UP
P30533	LRPAP1	0.383	UP
Q14515	SPARCL1	0.37279	DOWN
O94907	DKK1	0.34996	UP
P05156	CFI	0.34264	UP

P55268	LAMB2	0.34133	UP
Q16352	INA	0.33821	DOWN
P01185	AVP	0.33801	DOWN
Q8IW75	SERPINA12	0.33079	UP
P69905	HBA1	0.32042	UP
P02790	HPX	0.31057	DOWN
P39060	COL18A1	0.30654	DOWN
Q99470	SDF2	0.29463	UP
P35443	THBS4	0.29269	DOWN
P07093	SERPINE2	0.27079	DOWN
Q13219	PAPPA	0.23725	UP
P21583	KITLG	0.2343	DOWN
P24043	LAMA2	0.23247	UP
P62328	TMSB4X	0.23026	UP
O94813	SLIT2	0.22586	DOWN
P62805	HIST1H4A	0.22213	DOWN
P26927	MST1	0.2178	DOWN
P02751	FN1	0.21377	DOWN
Q13753	LAMC2	0.20698	UP
P19320	VCAM1	0.20395	UP
Q8TB73	NDNF	0.20354	DOWN
P14618	PKM	0.20082	DOWN
P01040	CSTA	0.19951	UP
Q99880	HIST1H2BL	0.19624	DOWN
Q9BX67	JAM3	0.18673	UP
P12643	BMP2	0.17129	UP
P04114	APOB	0.16782	DOWN
P02753	RBP4	0.16063	DOWN
Q02388	COL7A1	0.15448	UP
P47929	LGALS7	0.15433	UP
A8K2U0	A2ML1	0.1476	UP
Q99985	SEMA3C	0.14525	UP
P05089	ARG1	0.13376	UP
P03952	KLKB1	0.13201	DOWN
Q13361	MFAP5	0.13088	DOWN
P48307	TFPI2	0.12743	UP
Q06828	FMOD	0.12607	DOWN
P22692	IGFBP4	0.123	UP
P0DML3	CSH2	0.11377	DOWN
P05090	APOD	0.10707	UP
Q15063	POSTN	0.106	UP
Q9BZM5	ULBP2	0.103	UP
Q8IX30	SCUBE3	0.096418	DOWN
Q14574	DSC3	0.094911	UP
P18065	IGFBP2	0.093993	UP
P00750	PLAT	0.093536	UP
P55145	MANF	0.088626	UP
Q6UXH1	CRELD2	0.08812	UP
P48594	SERPINB4	0.087681	UP
Q07092	COL16A1	0.084733	DOWN
P55001	MFAP2	0.083819	DOWN
Q8WZ42	TTN	0.082636	DOWN

Table A4.2 Proteins and peptides used for targeted proteomics. The proteins and peptides chosen for parallel reaction monitoring (PRM) based on the list obtained from the SVM.

Protein	Peptide	Precursor m/z	Precursor Charge
MMP1	IENYTPDLPR	609.3117	2
	MIAHDFPGIGHK	441.5607	3
	VDAVFMK	405.2149	2
SFRP1	FYTKPPQCVDIPADLR	640.661	3
	MVLPNLLHETMAEVK	618.6548	3
	WLCEAVR	467.2342	2
NPTX1	FQLTFPLR	511.2951	2
	TNYMYAK	445.7075	2
	LPFVINDGK	501.7846	2
IL6	YILDGISALR	560.8217	2
	FESSEEQAR	541.7411	2
	VLIQFLQK	494.8131	2
CXCL5	CVCLQTTQGVHPK	509.9184	3
	MISNLQVFAIGPQCSK	896.9579	2
	EICLDPEAPFLK	716.3631	2
CXCL6	LQVFPAGPQCSK	666.3425	2
	VEVVASLK	422.7606	2
	QVCLDPEAPFLK	708.8632	2
GDF15	ILTPEVR	414.2529	2
	AALPEGLPEASR	605.825	2
	LKPDTVPAPCCVPASYNPMVLIQK	900.1304	3
CCL2	EICADPK	416.6971	2
	WVQDSMDHLDK	458.5433	3
CXCL8	VIESGPHCANTEIIVK	589.6147	3
	ELCLDPK	437.7206	2
	ENWVQR	416.209	2
SERPING1	LLDSLPSDTR	558.7984	2
	VPMMNSK	403.6989	2
	FQPTLLTLPR	593.3531	2

Table A4.3 Acquisition parameters for the Q Exactive Plus. Overview of the parameters used for data acquisition on a Q Exactive Plus for label-free and targeted proteomics.

Parameter	Q Exactive Plus	PRM
Mass Range (m/z)	400-1500	395-1500
Isolation Window (m/z)	2.0	1.2
MS resolution	70K @ 200m/z	70K @ 200m/z
MSMS Resolution	17.5K	35.0K
MS Injection Time (ms)	250	250
MSn Injection Time (ms)	64	120
AGC Target (MS)	3E6	3E6
AGC Target (MSn)	2E5	1E6
Preview Scan	n/a	n/a
Threshold (counts)	2.0E3	n/a
Minimum AGC Target	3.1E4	n/a
Data Dependent Acquisition	Top12	Loop Count 30
Dynamic Exclusion (s)	30	Inclusion List
Exclusion Mass Width (m/z)	n/a	n/a
Exclude Isotopes/ Monoisotopic precursor Selection	Enabled	Enabled
Fragmentation Type	HCD	HCD
Normalized Collision Energy	25	25
Lock Mass (445.120025m/z)	Best	Best
Charge State Rejection	Unassigned, +1,7,8,>8	n/a
Default Charge State	+2	+2

Table A5.1 Fold change of proteins during Wnt-modulation. All secreted proteins differentially expressed between Wnt-activated, Wnt-inhibited and untreated hMSC CM.

Accession Number	Gene Name	F.C (Wnt+/hMSC)	F.C (Wnt+/Wnt-)
P27487	DPP4	4.579510	0.054511
Q8WZ78	TUBB8	3.775380	0.769514
Q16778	HIST2H2BE	3.448830	0.720582
P10606	COX5B	3.383160	2.056420
Q99985	SEMA3C	3.351510	2.515130
P20674	COX5A	3.047730	1.792340
P05161	ISG15	2.997400	2.049760
P61026	RAB10	2.975210	3.269350
B4DKM5	VDAC2	2.848110	1.280320
P39026	RPL11	2.811480	0.532597
P15018	LIF	2.781470	2.763490
P08195	SLC3A2	2.773380	3.447360
Q9H0B8	CRISPLD2	2.685340	1.567540
B3KUF5	TOM1	2.541680	2.020100
A1L4P6	AKR1D1	2.447030	1.853950
B4DW94	RAP1B	2.446660	0.380342
Q6UVK1	CSPG4	2.397310	0.549941
Q3SXN8	NEDD8	2.357050	2.558250
A0A024R5J8	TSKU	2.335850	2.410870
B3KXM0	PIN4	2.331660	1.130390
Q96QL0	RPL3	2.273780	0.610528
A8K538	DDX3X	2.261690	1.159570
Q16641	LAMP2	2.261320	1.661700
Q96C49	SLC25A6	2.242380	0.391869
A8K4I2	HIST1H1C	2.209940	0.297064
Q9HD42	CHMP1A	2.192860	0.078407
Q9UGJ9	PGRMC1	2.162670	0.121006
Q9UP99	CSE1L	2.148670	2.472240
Q01813	PFKP	2.097090	1.914970
A6NKY0	H2AFV	2.090800	1.612350
Q6IB98	EIF3H	2.078410	0.941184
B7Z1N7	ATP1B3	2.051660	1.001310
A0A024R4D1	COPS8	2.046190	0.110893
Q14467	CYFIP1	2.037050	2.320730
Q5TEE6	MARCKSL1	2.030850	0.616287
D3DUT6	CLSTN3	2.019180	1.904560
A8K879	NAPA	2.007760	1.358000
B7Z5K8	CUL4B	2.006380	0.020088
Q504S5	CKAP4	2.005710	0.817987
B7Z6V1	EIF4E	2.000910	1.167210
B2RC19	DKK1	-1.243730	-1.000200
Q5TZY5	GSTM2	-1.251380	0.271942
Q8WWI9	TNFAIP6	-1.253530	-1.795970
Q96JJ0	CXCL1	-1.266380	-0.367760
Q9BWC4	PTX3	-1.266680	-0.480790

Q96A79	KIAA0319L	-1.272620	0.495421
P98160	JUP	-1.273010	0.380095
P48669	CTGF	-1.280530	-1.083540
O43479	HSPG2	-1.289480	-1.442840
Q9HB01	KRT6B	-1.302050	-0.796300
Q68D21	RBP4	-1.303350	-1.054570
P10645	DSC1	-1.359340	0.365096
Q9UNA0	MASP1	-1.416630	-0.943110
Q04756	CHGA	-1.446660	-2.263450
P49746	ADAMTS5	-1.475220	-0.706500
O94955	HGFAC	-1.586710	0.260090
C7S7T9	THBS3	-1.665760	-0.992860
Q99806	RHOBTB3	-1.695530	-0.066970
P19883	SSC5D	-1.778390	-0.222490
E9PBV3	VWF	-1.912120	0.011694
Q5T749	FST	-1.918420	-1.047180
Q149N0	SBSN	-1.975900	1.233270
Q7Z2X9	KPRP	-1.987160	1.008220
P00746	COL11A1	-2.067740	-1.199500
Q96KY1	CEP164	-2.101500	-2.087610
C9JAB2	CFD	-2.211990	-1.840850
P27487	C1QTNF3	-2.470000	-2.198390
Q8WZ78	SRSF7	-3.183980	-0.385980

Table A5.2 Antibody concentration and manufacture information. All antibodies used in immunohistochemistry and immunofluorescence analysis of mouse pancreatic tissue.

Reagent	Source	Identifier	Concentration
Mouse anti-insulin	Sigma	I2018	1/500
Guinea pig anti-insulin	Abcam	AB7842	1/40
Rabbit anti-insulin	Abcam	AB181547	1/500
Mouse β -catenin	ThermoFisher	53-2567-42	1/67
Mouse anti-glucagon	Abcam	AB10988	1/500
Rat anti-CD31	BD	550274	1/100
Rabbit anti-vWF	Millipore Sigma	AB7356	1/200
Rabbit anti-ck19	Abcam	AB52625	1/400
Rabbit anti-NKX2.2	Abcam	AB191077	1/1000
Rabbit anti-NKX6.1	Abcam	AB221549	1/2000
Goat anti-NKX6.1	R&D Systems	AF5857	1/80
Mouse anti-NKX2.2	Novus Biologicals	NBP2-29432	1/400
Rabbit anti-LIFR	Abcam	AB101228	1/2000
Rabbit anti-IGFR1	Abcam	AB39675	1/1000
Rabbit anti-TGFBR1	Abcam	AB31013	1/200
Guinea pig anti-vimentin	Antibodiesonline	ABIN126094	1/200
Horse anti-igG (H+L)	MJS Biolynx	VECTPI2000	1/250
DAB peroxidase	MJS Biolynx	VECTSK4105	1/33
DAPI solution	ThermoFisher	62248	1/1000
Goat fluorescein	MJS Biolynx	VECTFI1000	1/400
Horse Texas red	MJS Biolynx	VECTFI2000	1/400
Goat Texas red	MJS Biolynx	VECTTI1000	1/400
Donkey cy5	Cedarlane	706-175-148	1/400
EdU Alexa 488	ThermoFisher	C10637	n/a
Vectashield DAPI	MJS Biolynx	VECTH1200	1/667

Appendix II

Supporting figures for proteomic characterization of conditioned media generated from human multipotent stromal cells (hMSC).

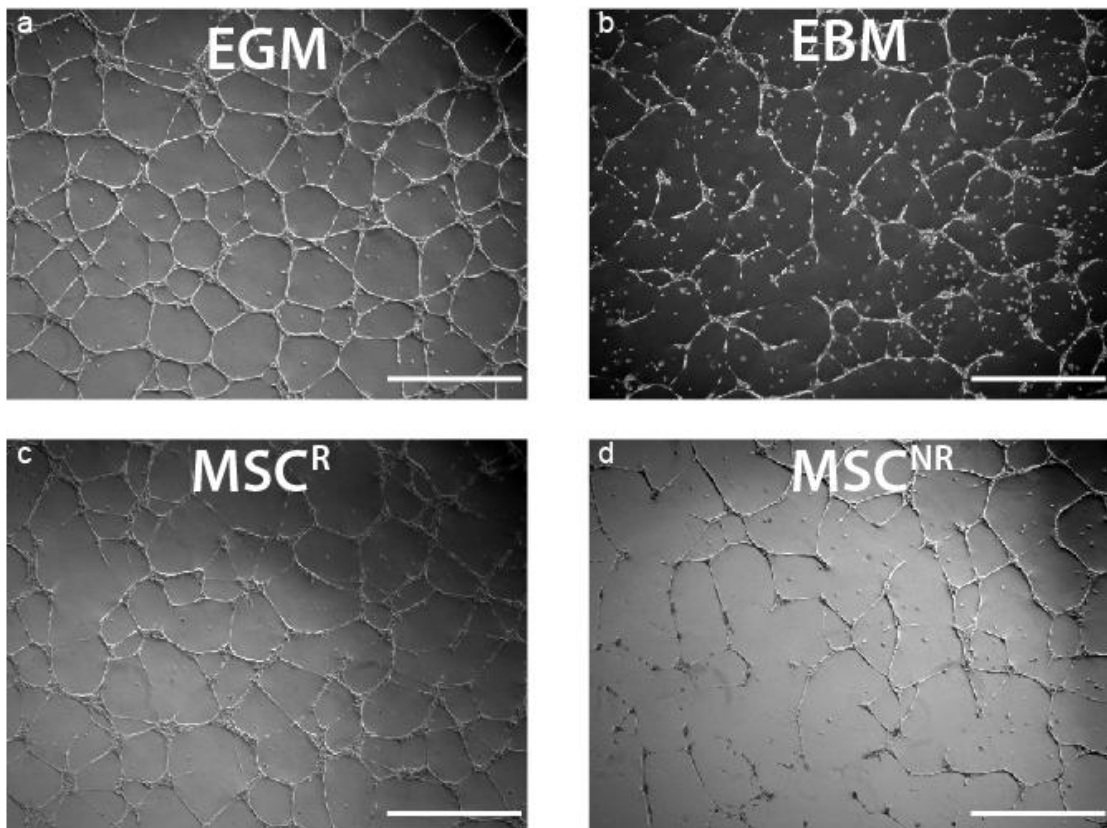


Figure A3.1 Condition media generated by hMSC^R augments spontaneous HMVEC tube formation after 24 hrs in vitro. Representative photomicrographs of HMVEC tube formation after 24 hrs on growth factor reduced Geltrex™ supplemented with (a) EGM-2, (b) EBM-2, (c) condition media generated by hMSC^R and (d) condition media generated by hMSC^{NR}. Scale bar, 100 μ m.

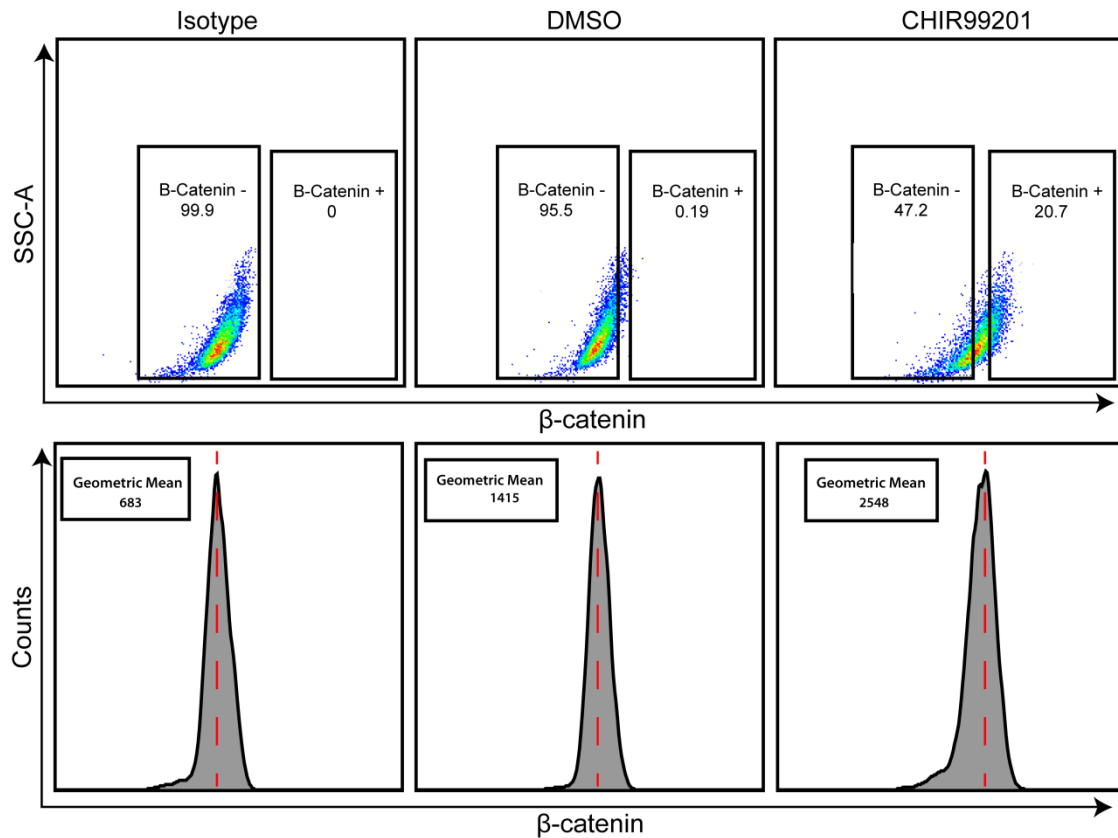


Figure A3.2 Total β -catenin levels in hMSC treated with CHIR99201 quantified using flow cytometry. Flow representative dot plots showing intracellular levels of β -catenin in hMSC treated with DMSO (control) or 10 μ M of CHIR99201. hMSC were treated for 24 h prior to analysis by flow cytometry. Cells were fixed using 1% formalin and permeabilized using Saponin buffer. Cells were incubated with an isotype control (left) or with a FITC conjugated antibody. hMSCs treated with CHIR99201 showed a significant increased in total β -catenin (top panel). To quantify total levels of β -catenin, the geometric mean fluorescence intensity was calculated and normalized to the isotype control.

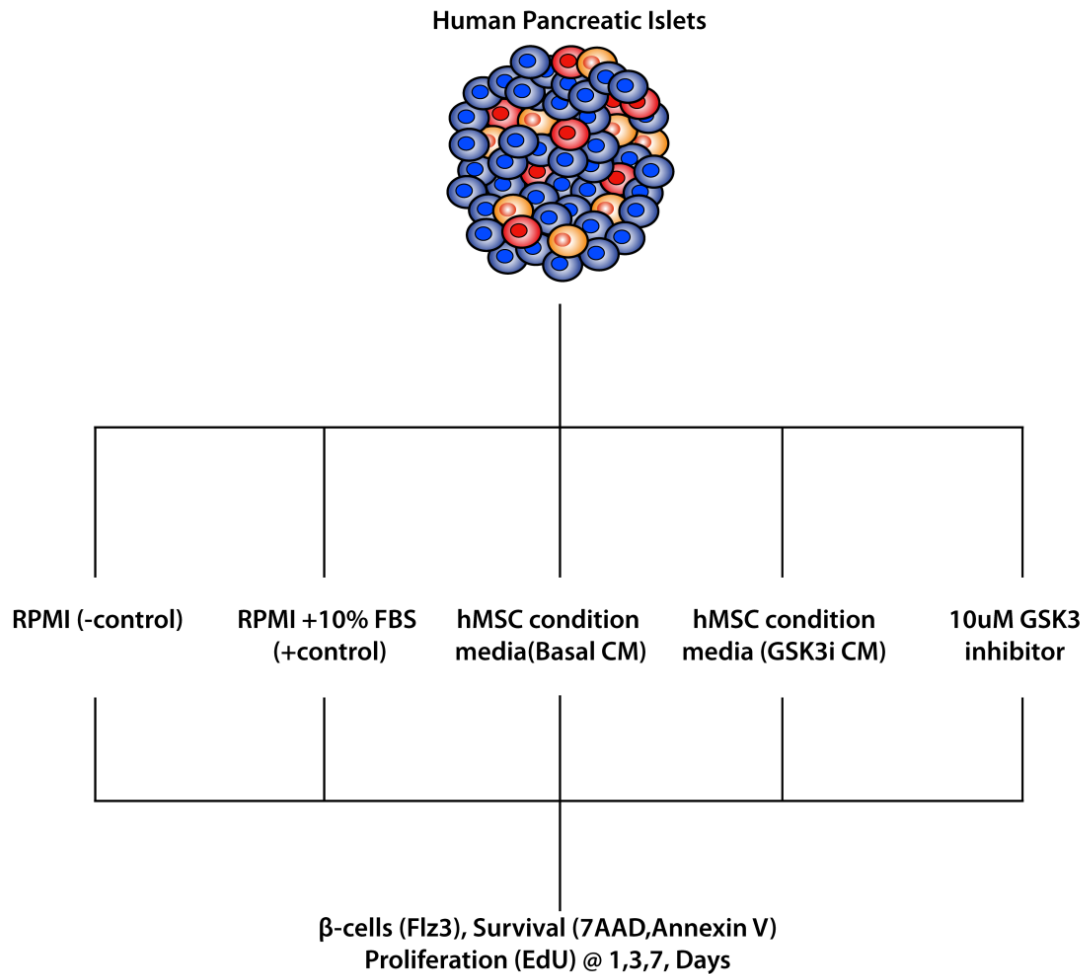


Figure A3.3 Culture conditions for human pancreatic islets using condition media generated by hMSC samples. Human islets were plated at 200 islets equivalence (IEQ) in 3 mL of RPMI media (6-well plate). A total of five different conditions were tested. Islets grown in RPMI media served as a negative control, RPMI supplemented with 10% FBS served as a positive control to ensure islet survival and growth. Concentrated condition media from hMSC treated with DMSO (drug control) are labeled as basal CM, hMSC treated with CHIR99201 are labeled as GSK3i CM. Also 10 μ M of CHIR99201 was directly added to one culture condition. β -cell survival and proliferation was quantified using flow cytometry after 1, 3, 7 days of culture.

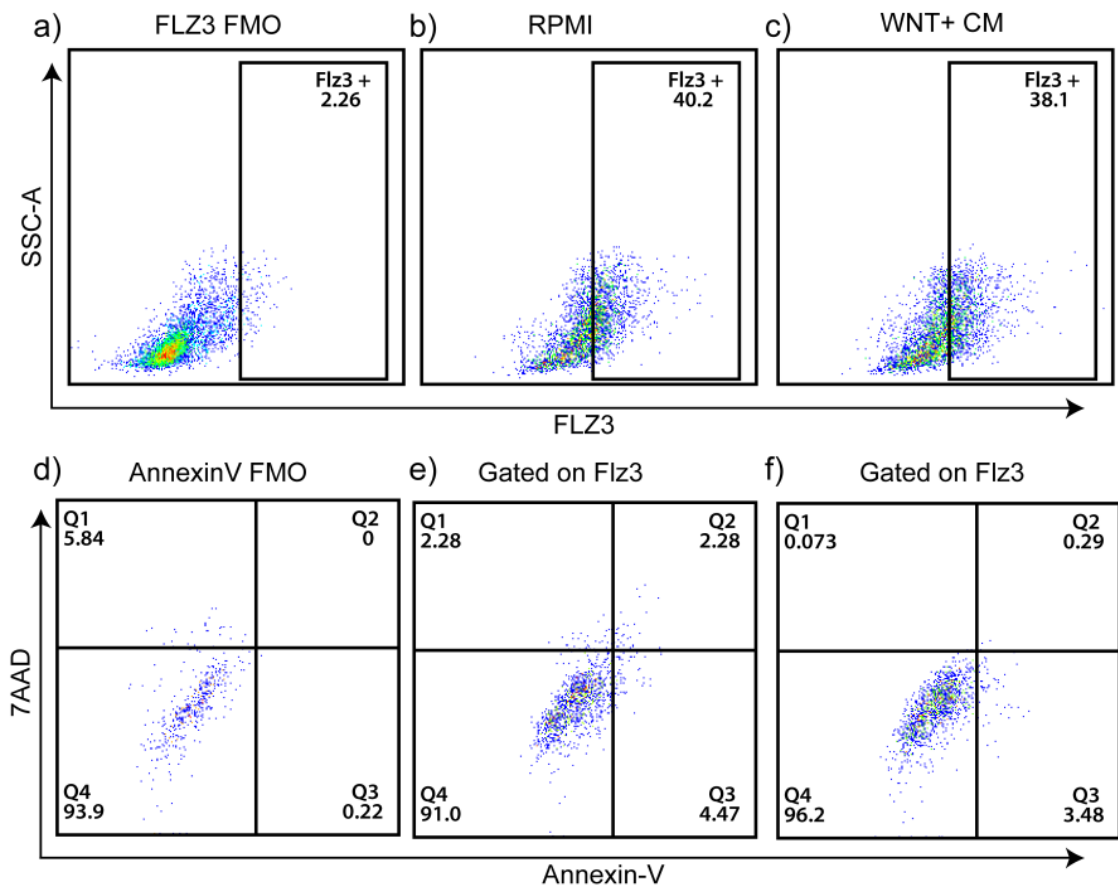


Figure A3.4 Flow cytometry analysis of human pancreatic islets for β -cell content and survival. Human pancreatic islets preparations were obtained from the IIDP. Before analysis using flow cytometry, islet preparations were dissociated using trypsin and stained using Fluozin3 for β -cell content. (a) Representative dot plots for β -cell content using Fluozin3 gating and corresponding FMO. Islets were cultured using RPMI alone (b) and condition media from CHIR99201 treated hMSC (WNT+ CM) (c). Survival was quantified using 7AAD and AnnexinV. Representative dot plots gated on Fluozin3 positive cells for survival using corresponding FMO (d), RPMI alone (e), WNT+ CM (f). Total parent frequencies are shown inside each gate.

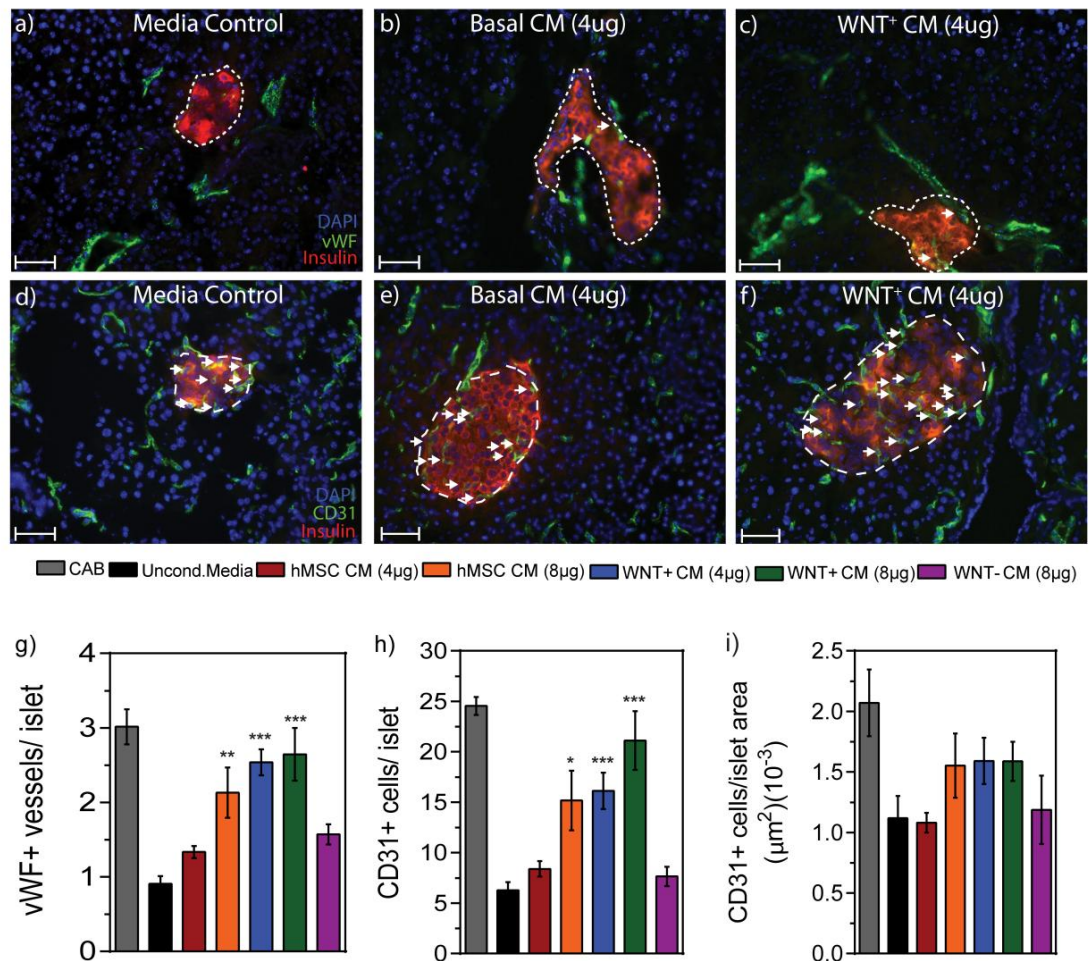


Figure A5.1 hMSC conditioned media transplanted increased islet vascularization. Representative photomicrographs of vWF+ blood vessels (green) associated with insulin+ islets (red) at day 42 after injection of (a) media control, (b) basal CM (4 μg), (c) WNT+ CM (4 μg). Arrows mark vWF+ vessels within islets (outlined with dashed lines). Representative photomicrographs of CD31+ (green) within insulin+ islets (red) at day 42 after injection of (d) media control, (e) basal CM (4 μg), (f) WNT+ CM (4 μg). Arrows mark CD31+ microvessels within islets (outlined with dashed lines). Compared to media control, mice injected with 8μg of basal CM or mice injected with WNT+CM (4 or 8 μg) showed increased vWF islet vascularization (g) and total number of CD31+ capillaries (h). No significant difference was observed in the normalized (for size) microvasculature. Scale bar=200 μm. Data is represented as mean ± S.E.M. (**p<0.01, ***p<0.001)

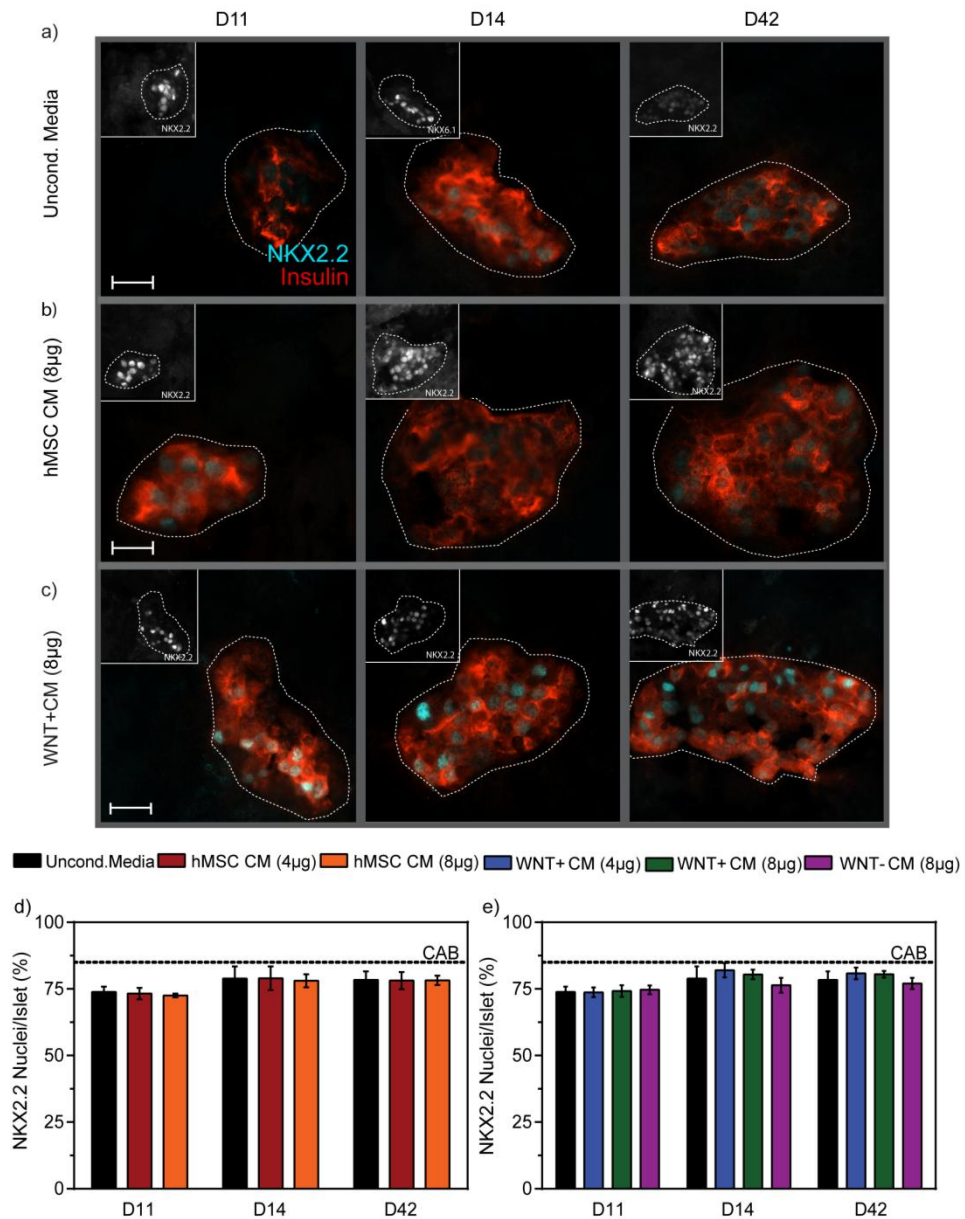


Figure A5.2 Intrapancreatic-injection of Wnt-activated hMSC CM shown no difference in endocrine marker NKX2.2. (a-c) Representative photomicrographs of NKX2.2⁺ cells within islets at day 11, 14, and 42 in mice injected with unconditioned media, or 8 µg hMSC CM, or 8 µg WNT+ CM. (d) Mice injected with hMSC CM showed no difference in frequency of NKX2.2⁺ cells per islet compared to mice injected with r unconditioned media. (e) Mice injected with WNT+ CM showed no difference in frequency of NKX2.2⁺ cells per islet compared to mice injected with WNT- CM or unconditioned media. Scale bar=200 µm. Data is represented as mean ± S.E.M.

Appendix III

Copyright Permission

From: Proteomics-Wiley

License Number	4211450091037
License date	Oct 17, 2017
Licensed Content Publisher	John Wiley and Sons
Licensed Content Publication	Proteomics
Licensed Content Title	Comparison of sample preparation techniques for large-scale proteomics
Licensed Content Author	Miljan Kuljanin, Dylan Z. Dieters-Castator, David A. Hess, Lynne-Marie Postovit, Gilles A. Lajoie
Licensed Content Date	Jan 18, 2017
Licensed Content Pages	1
Type of use	Dissertation/Thesis
Requestor type	Author of this Wiley article
Format	Electronic
Portion	Full article
Will you be translating?	No
Title of your thesis / dissertation	Proteomic Characterization of Human Multipotent Stromal Cells Secreted Proteins with Therapeutic Potential for B-cell Regeneration
Expected completion date	Dec 2017
Expected size (number of pages)	250
Requestor Location	Western University 1400 Western Road London, ON N6H 4R5 Canada Attn: Western University
Publisher Tax ID	EU826007151
Billing Type	Invoice
Billing Address	Western University 1400 Western Road London, ON N6H 4R5 Canada Attn: Western University
Total	0.00 USD

From: Diabetologia-Springer

License Number	4211441382260
License date	Oct 17, 2017
Licensed Content Publisher	Springer
Licensed Content Publication	Diabetologia
Licensed Content Title	Proteomic characterisation reveals active Wnt-signalling by human multipotent stromal cells as a key regulator of β -cell survival and proliferation
Licensed Content Author	Miljan Kuljanin, Gillian I. Bell, Stephen E. Sherman et al
Licensed Content Date	Jan 1, 2017
Licensed Content Volume	60
Licensed Content Issue	10
Type of Use	Thesis/Dissertation
Portion	Excerpts
Author of this Springer article	Yes and you are the sole author of the new work
Order reference number	
Title of your thesis / dissertation	Proteomic Characterization of Human Multipotent Stromal Cells Secreted Proteins with Therapeutic Potential for B-cell Regeneration
Expected completion date	Dec 2017
Estimated size(pages)	250
Requestor Location	Western University 1400 Western Road London, ON N6H 4R5 Canada Attn: Western University
Billing Type	Invoice
Billing Address	Western University 1400 Western Road London, ON N6H 4R5 Canada Attn: Western University
Total	0.00 USD

Curriculum Vitae

Miljan Kuljanin

- Education**
- Sept. 2012-Dec. 2017
University of Western Ontario
PhD. Biochemistry
Biological Mass Spectrometry & Human Multipotent Stromal Cell Biology
- Sept.2008-April.2012
Wilfrid Laurier University
B.Sc. Hon. Biochemistry/Biotechnology
Thesis Student: Biophysical Chemistry & Antimicrobial Peptide Synthesis
- Relevant Experience**
- PhD. Candidate-** Mass spectrometry & Diabetes
2012-2017
University of Western Ontario
London, ON, Canada
- Research Assistant-** Biophysical Chemistry
April 2011-Sept. 2012
Wilfrid Laurier University
Waterloo, ON, Canada
- Research Assistant-** Antimicrobial peptide Design
April 2009-Sept. 2011
Wilfrid Laurier University
Waterloo, ON, Canada
- Referred Publications**
- (8) **Kuljanin, M**, Elgamal RM, Bell GI, Lajoie GA, and Hess DA. Wnt-pathway stimulated hMSC-secreted effectors mediate islet cell regeneration. Cell Stem Cell. (Submitted **November 2017**)
- (7) **Kuljanin M**, Brown CFC, Raleigh MJ, Lajoie GA, Flynn LE. (2017) Collagenase Treatment Enhances Proteomic Coverage of Low-Abundance Proteins In Decellularized Matrix Bioscaffolds. Biomaterials. **144**: 130-143.

(6) **Kuljanin M**, Bell GI, Sherman SE, Lajoie AG, Hess DA. (2017) Proteomic Characterisation Reveals Active Wnt-signaling by Human Multipotent Stromal Cells as a Key Regulator of B-cell Survival and Proliferation. *Diabetologia*. **10**: 1987-1998.

(5) Sherman SE, **Kuljanin M**, Cooper TT, Putman DM, Lajoie GA, Hess DA. (2017) High Aldehyde Dehydrogenase Activity Identifies a Subset of Human Mesenchymal Stromal Cells with Vascular Regenerative Potential. *Stem Cells*. **6**: 1542-1553.

(4) **Kuljanin M** *, Dieters-Castator DZ *, Hess DA, Postovit LM, Lajoie GA. (2017) Comparison of Sample Preparative Techniques for Large-Scale Proteomics. *Proteomics*. **17**:1-9.

(3) Sun W, **Kuljanin M**, Pittcock P, Ma B, Zhang K, Lajoie GA. (2016) An Effective Approach for Glycan Structure De Novo Sequencing from HCD Spectra. *IEEE Trans Nanobioscience*. **15**: 177-84.

(2) Hoang T, **Kuljanin M**, Smith MD, Jelokhani-Niaraki M. (2015) A biophysical Study on Molecular physiology of the Uncoupling Proteins of the Central Nervous System. *Bioscience Reports*. **35**:1-15.

(1) Nichols M, **Kuljanin M**, Nategholeslam M, Hoang T, Vafaei S, Tomberli B, Gray CG, DeBruin L, Jelokhani-Niaraki M. (2013) Dynamic Turn Conformation of a Short Tryptophan-rich Cationic Antimicrobial peptide and its Interaction with Phospholipid Membranes. *Journal of Physical Chemistry B*. **47**: 14697-708.

**Selected
Refereed
Presentation**

Kuljanin M, Hess Da, Lajoie GA. (2016): Proteomic Investigation of Paracrine Signals from Multipotent Stromal Cells that Augment Islet Regenerative Capacity. Poster. Till & McCulloch 6th Annual Meeting, Whistler, Canada, 2016

Kuljanin M, Hess Da, Lajoie GA. (2016): Proteomic Investigation of Paracrine Signals from Multipotent Stromal Cells that Augment Islet Regenerative Capacity.

Poster. Canadian National Proteomics Network 6th Annual Meeting, Montreal, Canada, 2016

Kuljanin M, Hess Da, Lajoie GA. (2015): Human bone Marrow Derived Multipotent Stromal Cells Augment Islet Regenerative Capacity Through Secretion of Wnt-signaling proteins. Poster. International Society for Stem Cell Research 13th Annual Meeting, Stockholm, Sweden, 2015

Kuljanin M, Hess Da, Lajoie GA. (2014): Secretome Analyses of Human Bone Marrow Derived Multipotent Stromal Cells with Islet Regenerative Capacity. Poster. International Society for Stem Cell Research 12th Annual Meeting, Vancouver, Canada, 2014

Kuljanin M, Hess Da, Lajoie GA. (2014): Analysis of Bone Marrow Derived Multipotent Stromal Cell Secretome. Poster. American Society for Mass Spectrometry 62th Annual Meeting, Baltimore, Maryland, 2014

Awards & Scholarships

2012-2017: University of Western Ontario: Graduate Scholarship (\$22 500)

2017: Ontario Institute of Regenerative Medicine (OIRM) Travel Award (\$ 2000)

2017: Canadian National Proteomics Network (CNP) Travel Award (\$ 1000)

2017: American Society for Mass Spectrometry (ASMS) Travel Award (\$ 500)

2016: Stem Cell Network (SCN) Travel Award (\$1500)

2016: Canadian National Proteomics Network (CNP) Travel Award (\$ 1000)

2015: Ontario Institute of Regenerative Medicine (OIRM) Travel Award (\$ 2000)

2014: Ontario Institute of Regenerative Medicine (OIRM) Travel Award (\$ 2000)

2013: Max Planck Society Summer School Munich Travel Award (\$500)

2012: Wilfrid Laurier University: In Course Scholarship (Honor Role) (\$ 1500)

2010-2011: Wilfrid Laurier University: In Course Scholarship (Honor Role) (\$ 3000)